AD_____

Award Number:

W81XWH-11-1-0803

TITLE:

Muscle Stem Cell Therapy for the Treatment of DMD Associated Cardiomyopathy

PRINCIPAL INVESTIGATOR:

Johnny Huard, PhD

CONTRACTING ORGANIZATION:

**University of Pittsburgh
Pittsburgh, PA 15260**

REPORT DATE:

October 2013

TYPE OF REPORT:

Annual Report

PREPARED FOR:

**U.S. Army Medical Research and Materiel Command
Fort Detrick, Maryland 21702-5012**

DISTRIBUTION STATEMENT:

Approved for Public Release; Distribution Unlimited

The views, opinions and/or findings contained in this report are those of the author(s) and should not be construed as an official Department of the Army position, policy or decision unless so designated by other documentation.

REPORT DOCUMENTATION PAGE		*Form Approved* *OMB No. 0704-0188*
Public reporting burden for this collection of information is estimated to average 1 hour per response, including the time for reviewing instructions, searching existing data sources, gathering and maintaining the data needed, and completing and reviewing this collection of information. Send comments regarding this burden estimate or any other aspect of this collection of information, including suggestions for reducing this burden to Department of Defense, Washington Headquarters Services, Directorate for Information Operations and Reports (0704-0188), 1215 Jefferson Davis Highway, Suite 1204, Arlington, VA 22202-4302. Respondents should be aware that notwithstanding any other provision of law, no person shall be subject to any penalty for failing to comply with a collection of information if it does not display a currently valid OMB control number. **PLEASE DO NOT RETURN YOUR FORM TO THE ABOVE ADDRESS.**		

1. REPORT DATE	2. REPORT TYPE	3. DATES COVERED
October 2013	Annual Report	30 September 2012-29 September 2013

4. TITLE AND SUBTITLE	5a. CONTRACT NUMBER
Muscle Stem Cell Therapy for the Treatment of DMD Associated Cardiomyopathy **Subproject 1:** Muscle Stem Cell Therapy for the Treatment of DMD Associated Cardiomyopathy **Subproject 2**: Human hepatocytes for treatment of life-threatening liver injury	
	5b. GRANT NUMBER W81XWH-11-1-0803
	5c. PROGRAM ELEMENT NUMBER

6. AUTHOR(S)	5d. PROJECT NUMBER
Johnny Huard, Ph.D. – Principle Investigator PI: Sub-Project 1 Ira Fox, M.D. Co-PI: Sub-Project 2 David Perlmutter, M.D. Co-PI: Sub-Project 2	
	5e. TASK NUMBER
E-Mail: jhuard@pitt.edu	5f. WORK UNIT NUMBER

7. PERFORMING ORGANIZATION NAME(S) AND ADDRESS(ES)	8. PERFORMING ORGANIZATION REPORT NUMBER
University of Pittsburgh Pittsburgh, PA 15219	

9. SPONSORING / MONITORING AGENCY NAME(S) AND ADDRESS(ES)	10. SPONSOR/MONITOR'S ACRONYM(S)
U.S. Army Medical Research and Materiel Command Fort Detrick, Maryland 21702-5012	
	11. SPONSOR/MONITOR'S REPORT NUMBER(S)

12. DISTRIBUTION / AVAILABILITY STATEMENT
Approved for Public Release; Distribution Unlimited

13. SUPPLEMENTARY NOTES

14. ABSTRACT

Project 1:

Dilated cardiomyopathy affects approximately 1 in 2,500 individuals in the United States and is the 3rd most common cause of heart failure and the most frequent cause of heart transplantation. Patients that suffer from various muscle diseases, including Duchenne muscular dystrophy (DMD), develop progressive cardiomyopathy. Cellular cardiomyoplasty, which involves the transplantation of exogenous cells into the heart, is a possible approach by which to repair diseased or injured myocardium and improve cardiac function. Though there are a number of drugs prescribed to treat dilated cardiomyopathy, there is no cure and individuals eventually require a heart transplant; therefore the use of cardiomyoplasty to repair the hearts of individuals suffering from cardiomyopathy could possibly be an effective alternative to heart transplantation.

Technical Objective #1: To investigate the effect of cell survival, proliferation, and differentiation on the regeneration/repair capacity of various human MDSC populations implanted into the heart of mdx/SCID mice.

Technical Objective #2: To investigate the role that angiogenesis plays in the regeneration/repair capacity of human MDSCs injected into the hearts of mdx/SCID mice.

Project 2:

This project will determine the extent to which novel sources of hepatocytes can be used for regeneration and repair of injuries to the liver and liver failure. A more complete understanding of the extent to which donor liver cells can be resuscitated from non-traditional sources and expanded for application to reduce liver injury and toxin and/or cancer risk should enhance the number of areas where hepatic stem cell transplantation might be effectively applied.

Technical Objective #1: To characterize and expand hepatocytes from patients with cirrhosis and end-stage liver disease in immune deficient hosts whose livers permit extensive repopulation with donor cells.

Technical Objective #2: To determine the extent to which transplantation with human hepatocytes can reverse hepatic failure in a clinically relevant non-human primate model of this process.

15. SUBJECT TERMS

Project 1: Duchenne muscular dystrophy, Cardiomyopathy, Cell Therapy, Cellular cardiomyoplasty, Pericytes, myo-endothelial cells, Angiogenesis,

Project 2: Liver disease, Cirrhosis, Hepatocyte isolation, Hepatocyte transplantation, Induced Pluripotent Stem (iPS) cells

16. SECURITY CLASSIFICATION OF:			17. LIMITATION OF ABSTRACT	18. NUMBER OF PAGES	19a. NAME OF RESPONSIBLE PERSON USAMRMC
a. REPORT U	**b. ABSTRACT** U	**c. THIS PAGE** U	UU	107	**19b. TELEPHONE NUMBER** *(include area code)*

Investigator: Huard, Johnny

Table of Contents

Sub-project 1: Muscle Stem Cell Therapy for the Treatment of DMD Associated Cardiomyopathy

PI: Johnny Huard

INTRODUCTION:

Cardiomyopathy is a serious disease of the heart muscle that can lead to congestive heart failure, a condition in which the heart can no longer effectively pump blood. Dilated cardiomyopathy affects approximately 1 in 2,500 individuals in the United States and is the 3rd most common cause of heart failure and the most frequent cause of heart transplantation. Patients that suffer from some diseases of the cytoskeleton, such as the progressive muscular dystrophies, often develop cardiomyopathy. Duchenne muscular dystrophy (DMD), one of the progressive muscular dystrophies, is an X-linked muscle disease caused by mutations in the dystrophin gene. This devastating disease is characterized by progressive muscle weakness due to a lack of dystrophin expression at the sarcolemma of muscle fibers. DMD patients usually develop symptoms of dilated cardiomyopathy in their early teens, and these symptoms steadily progress with age. This dilated cardiomyopathy is characterized by an enlarged ventricular chamber, wall thinning, and systolic dysfunction. Histological examination of a human DMD cardiomyopathic heart reveals fibrosis, degeneration, and fatty infiltration. The lack of dystrophin has consequently been linked to the cardiomyopathy that develops in DMD. In the hearts of mdx, dystrophin-deficient, mice (a murine model of DMD), especially in aged mdx mice, fibrosis and degeneration of the myocardium are evident upon histological examination. Because the mammalian heart possesses only a limited capacity to regenerate new cardiac muscle after injury and disease, noncontractile scar tissue eventually replaces the injured and diseased myocardium. Cellular cardiomyoplasty, which involves the transplantation of exogenous cells into the heart, is a possible approach by which to repair diseased or injured myocardium and improve cardiac function. Though there are a number of drugs prescribed to treat dilated cardiomyopathy, there is no cure and individuals eventually require a heart transplant; therefore the use of cardiomyoplasty to repair the hearts of individuals suffering from cardiomyopathy could possibly be an effective alternative to heart transplantation.

Technical Objectives

Technical Objective #1: To investigate the effect of cell survival, proliferation, and differentiation on the regeneration/repair capacity of various human muscle derived cell populations implanted into the heart of aged mdx/SCID mice and/or dystrophin/utrophin double knock-out mice.
Hypothesis: After implantation into the heart, the human muscle derived cells abilities to survive and undergo long-term proliferation play a role in their efficient regeneration and repair of diseased cardiac tissue.

Technical Objective #2: To investigate the role that angiogenesis plays in the regeneration/repair capacity of human muscle derived cell populations injected into the hearts of aged mdx/SCID mice and/or dystrophin/utrophin double knock-out mice.
Hypothesis: Enhancing angiogenesis will increase the regeneration/repair capacity of human muscle derived cells injected into the hearts of dystrophic mice.

Technical Objective #3: To investigate the potential beneficial effect that creating a parabiotic pair between dystrophin/utrophin double knock-out (dKO) mice and normal mice might have on preventing the progression of cardiomyopathy in the dKO animals.

Hypothesis: Parabiosis between dKO and normal mice will slow the progression of cardiomyopathy in the dKO mice.

Technical Objective #4: To investigate the role that RhoA signaling plays in the cardiac dysfunction observed in dKO mice and determine if inactivating RhoA might have a beneficial effect on improving the dystrophic cardiac phenotype observed in the dKO mice

Hypothesis: RhoA inactivation will improve the dystrophic cardiac phenotype observed in the dKO mice.

BODY:

Progress made from: 10-1-12 to 9-30-13

1) ***Intraperitoneal injection of hMDSCs prevents progressive heart failure and promotes angiogenesis in the aging dystrophic hearts of mdx SCID mice.***
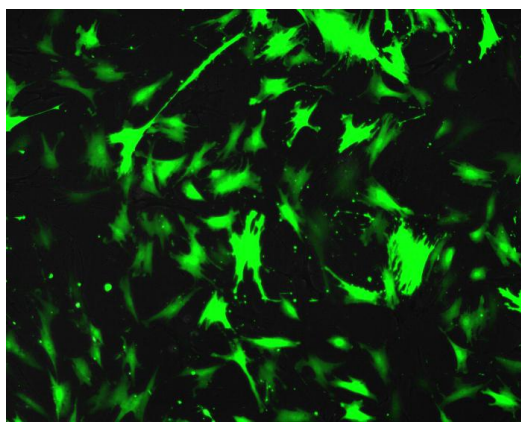
Cell isolation and labeling

Figure 1: Sorted GFP+ hMDSCs

Human muscle-derived stem cells (hMDSCs) were isolated using the modified pre-plate technique as previously described by our group (Okada, et al. Mol Ther 2012). hMDSCs were expanded in MDSC proliferation medium (MDSC-PM) containing high-glucose DMEM (Gibco), 10% fetal bovine serum (FBS, Invitrogen), 10% horse serum (HS, Invitrogen), 1% chicken embryo extract (CEE, Accurate Chemical), and 1% penicillin and streptomycin (P/S, Invitrogen). Cells were transduced with lentiviral vectors encoding GFP at MOI of 1:10 in the presence of 8µg/ml polybrene for 16hrs. After transduction, the cells were washed and expanded in MDSC-PM. Though a high transduction efficiency was achieved (~80%), the lentiviral-GFP transduced hMDSCs were further subjected to fluorescence-activated cell sorting (FACS) based on GFP signal positivity. The sorted GFP+ hMDSCs (>95% GFP positivity) were cultured and maintained in MDSC-PM following FACS (**Figure 1**).

Intraperitoneal injection and echocardiography in the dystrophic mouse model

To examine whether the intraperitoneal injection of hMDSCs could benefit the hearts of dystrophic mice, we used senile mdx/SCID mice (16-18 month old) that displayed symptoms of DMD. All mdx/SCID mice (total 10 mice) were randomly assigned to each group (N=5/group) before the start of the study. The experimental group received a single injection of 1×10^6 cells resuspended in 50ul of PBS in the lower abdomen while the control group received an equal amount of PBS in the same region. Cardiac function was assessed by echocardiography performed repeatedly immediately before (baseline) and after injection at 1 and 2 months. Animals that died prior to 2 month post-injection were excluded from the study. A total of 4 mice in the experimental group and 3 mice in the control group survived the 2-month experiment. Student's t-test was used for statistical analyses.
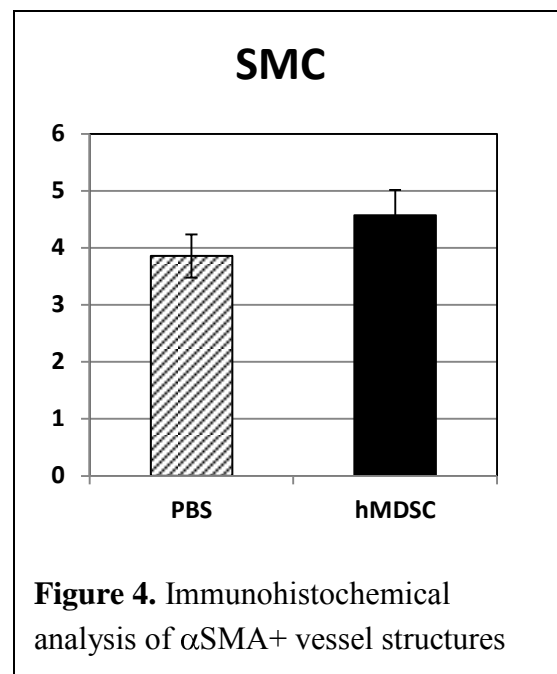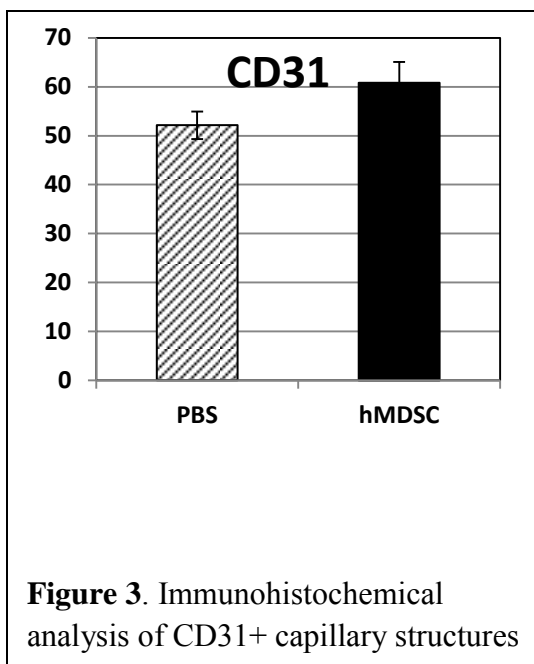
Intraperitoneal injection of hMDSCs prevented progressive heart failure

Left ventricular (LV) chamber size was measured by LV end-diastolic area (LVEDA, **Figure 2A**) and end-systolic area (LVESA, **Figure 2B**), whereas LV contractility was evaluated by LV fraction shortening (LVFS, Figure 2C), LV fractional area change (LVFAC, Figure 2D), and LV ejection fraction (LVEF, Figure 2E). Echocardiographic analyses showed notable enlargement in LV chamber dimension in the sham injected control group (Figure 2A-B), suggesting progressive LV dilatation and ultimately, heart failure. In the hMDSC-injected group, significantly smaller LV chamber sizes were observed at 2 month post-injection (LVEDA, *p*=0.024 and LVESA, *p*=0.008), indicating the prevention of progressive cardiac remodeling. Similarly, cardiac contractile function dramatically deteriorated in the control group over time (**Figure 2C-E**). Cardiac contractility was notably sustained following hMDSC injection for up to 2 months, including LVFS (*p*=0.054), LVFAC (*p*≦0.001) and LVEF (*p*=0.004). Overall, these data suggest beneficial effects of intraperitoneal injection of MDSCs in aging dystrophic hearts, not only preventing progressive LV dilatation but also sustaining cardiac contractility.


Figure 2. Echocardiographic analyses of LV chamber dimension and contractility
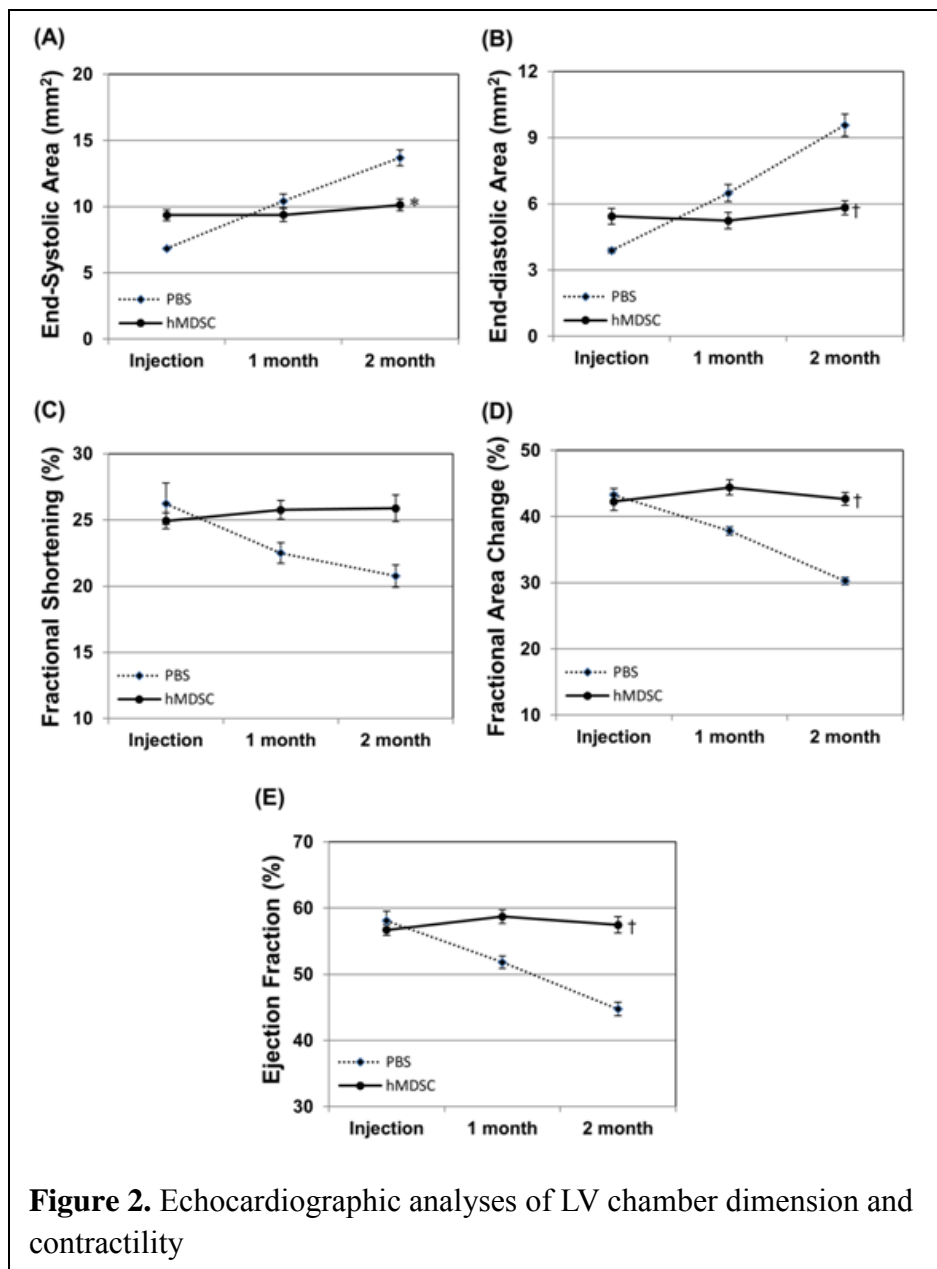
Intraperitoneal injection of hMDSCs promoted angiogenesis in the aging dystrophic heart of the mdx/SCID mice.

Immunohistochemical analysis revealed increased CD31+ capillary structures in the myocardium of hMDSC-injected mice (60.86±8.45/HPF) when compared with control mice (52.14±4.86/HPF) (Figure 3). Similarly, an increased number of alpha-smooth muscle actin (αSMA)-positive vessel structure was observed in hMDSC-injected mice (4.57±0.89/HPF) when compared with control mice (3.86±0.65/HPF) (Figure 4). Together these data suggest the promotion of angiogenesis and/or vasculogenesis in the myocardium following hMDSC intraperitoneal injection. Currently we hypothesize that this is due to the production of angiogenic and/or vasculogenic signaling molecules by the injected hMDSCs that subsequently travel to the heart via systemic circulation.

Figure 3. Immunohistochemical analysis of CD31+ capillary structures

Figure 4. Immunohistochemical analysis of αSMA+ vessel structures

*2) Potential benefit of parabiosis for cardiac repair in dKO mice*

Based on the positive effect of RhoA inactivation in cardiac muscle of dKO mice, we proposed that the parabiotic pairing of dKO mice with normal mice could help repress the activation of RhoA signaling in the cardiac muscles of dKO mice, and therefore improve their defective muscle phenotype.
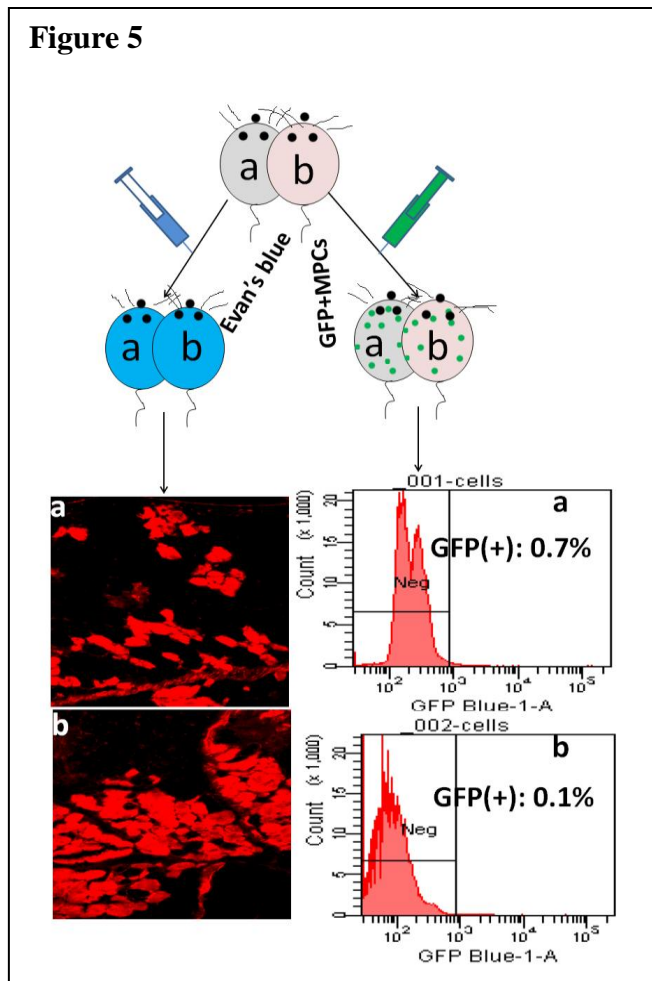
Figure 5

As a proof of concept and to verify the development of cross-circulation between the animals, we examined the distribution of an intravascular dye (Evan's Blue) across the joining wounds (**Figure 5**). After injection into one animal of the pair, the Evan's Blue dye immediately flushed the same animal (**a**) and progressively spread through the common vascular tree at the junction to its partner (**b**). We also found that MPCs could travel from mouse (**a**) to the parabiotic partner (**b**) when GFP positive MPCs are injected intravenously (**Figure 5**).

Next we preformed heterochronic parabiotic pairings between old dKO-hetero mice and young mdx mice and tested whether the cardiac muscle histopathology could be improved by blood-borne factors in vivo which created a constant exchange of peripheral blood between the mice. We performed parabiosis between young mdx mice (3-5 months) and old dKO- hetero mice (12-14 months)**.** These heterochronic pairs were compared to the control isochronic pairs of two old dKO-hetero mice (12-14 months). H&E was performed to determine whether the cardiac muscles were more greatly improved in their histopathological appearance in the old dKO-hetero mice sutured with young mdx mice. Trichrome staining was also performed according to the manufacturer's

instructions to determine whether less fibrosis formed in the old mice sutured with young mice. Intramyocardial lipid accumulation, which is a precursor of myocardial degradation and can cause myocardial toxicity and heart failure, was also determined via AdipoRed staining. We found that there was decreased fibrosis and an improvement in the histology of the cardiac muscle, and a decrease in intramyocardial lipid accumulation in the cardiac muscle of old dKO-hetero mice after they were sutured together with young mdx mice for 3 months (**Figure 6**). The results suggest that the defect in the MPCs might be related to the dystrophic microenvironment or some circulating factors. These observations suggest that changes in the dystrophic microenvironment could be a new approach to improve cardiac muscle weakness in DMD patients, despite the continued lack of dystrophin expression.

Figure 6

9
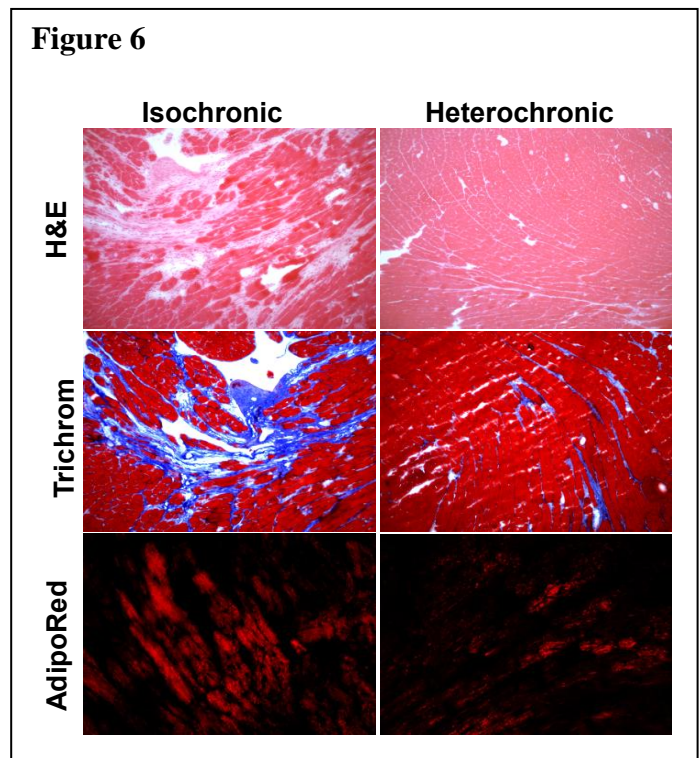
3) Myocardial Calcification and Fibrosis in Dystrophic Mice is Reduced by RhoA Inactivation

Myocardial calcification refers to the excessive deposition of calcium in the cardiac muscle and is usually observed in the aging population as-well-as long-term survivors of substantial myocardial infarctions (1-2). Myocardial calcification could either be the result of chronic degeneration or reflect ongoing pathologic processes (2); h*owever, the cellular and molecular mechanisms leading to* myocardial calcification *remains largely unknown.* We have recently reported the observation of extensive skeletal muscle calcification/heterotopic ossification in the dystrophin/utrophin double knockout (dKO) mouse model of Duchenne muscular dystrophy (3), which could be mediated by the over-activation of the RhoA signaling in muscle stem cells (MSCs) (4). RhoA is a small GTPase protein that regulates cell morphology and migration in response to extracellular signaling and stresses. RhoA activation in MSCs induces their osteogenesis potential, inhibits their adipogenic potential, mediates BMP-induced signaling, and promotes osteoblastic cell survival (5). The involvement of RhoA in mediating inflammatory processes and myocardial fibrosis has previously been described (6). In addition, previous studies have indicated that the sustained activation of the RhoA pathway can block the differentiation of muscle cells by inhibiting myoblast fusion (7). Cardiac involvement is the leading cause of early death in DMD patients, and the current study was performed to elucidate the role of RhoA in mediating fibrosis and calcification in the cardiac muscle of dystrophic mice.

Methods:

1. Animals: WT, mdx and dKO mice were used in this experiment **2. RhoA inactivation with Y-27632:** dKO mice from 3 weeks of age received either an intraperitoneal (IP) injection of Y-27632 [5mM in Phosphate Buffered Saline (PBS), 10mg/kg per mouse], which is a systematic inhibitor of RhoA signaling or PBS only (control). IP injections were conducted 3 times a week for 4 weeks. **3. Histology:** Mice were sacrificed and 10µm cryostat sections were prepared from the cardiac muscles of the mice. Alizarin red stain was conducted to stain calcium deposition in the cardiac muscle. **4. Statistics**: N >=6 for each group. Student's T-test was used to evaluate for significance.

Results:

a) *Cardiac muscle of dKO mice featured increased fibrosis and calcification when compared to mdx and WT mice.*

Trichrome staining of the cardiac muscles from 8-week old WT, mdx, and dKO mice was conducted to characterize ECM collagen deposition, which revealed that fibrosis formation was generally severe in the dKO mice, mild in the mdx mice, and absent in WT mice (**Figure 7A**). Alizarin red staining of the cardiac muscle revealed that calcification occurred in the dKO mice (**Figure 7B**), but not in the WT or mdx mice.

b) **Up-regulation of RhoA in the cardiac muscle of the dKO mice.**

Semi-quantitative PCR showed that, compared to the WT and mdx mice, the expression of RhoA and the inflammation signaling genes, TNF-α and IL-6, was up-regulated in the dKO cardiac muscle, while the expression of the anti-inflammation gene Klotho was down-regulated (**Figure 7C**). We suggest that the activation of RhoA and inflammatory mediators are involved in the cardiac fibrosis and calcification seen in dKO mice.
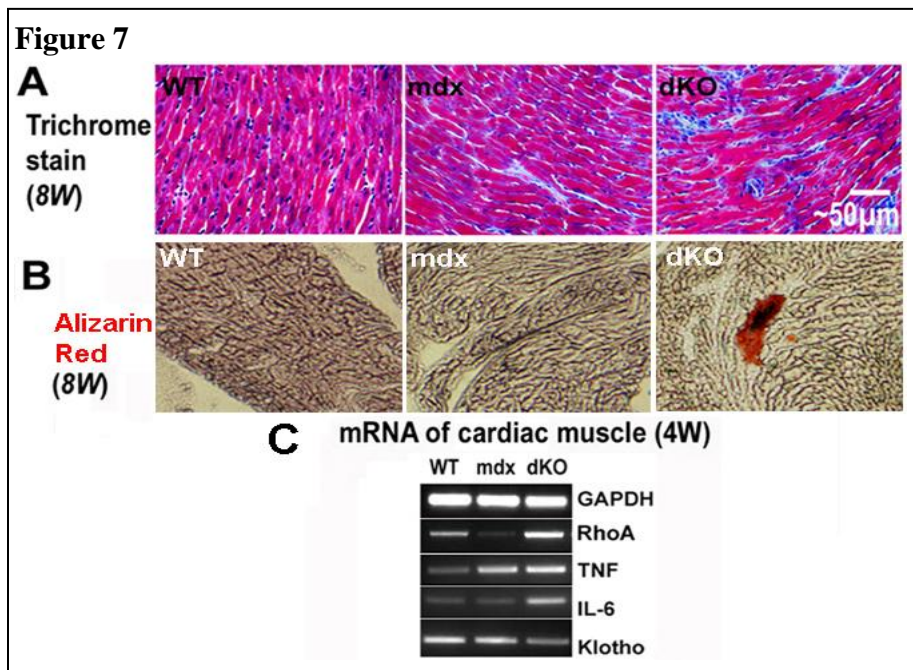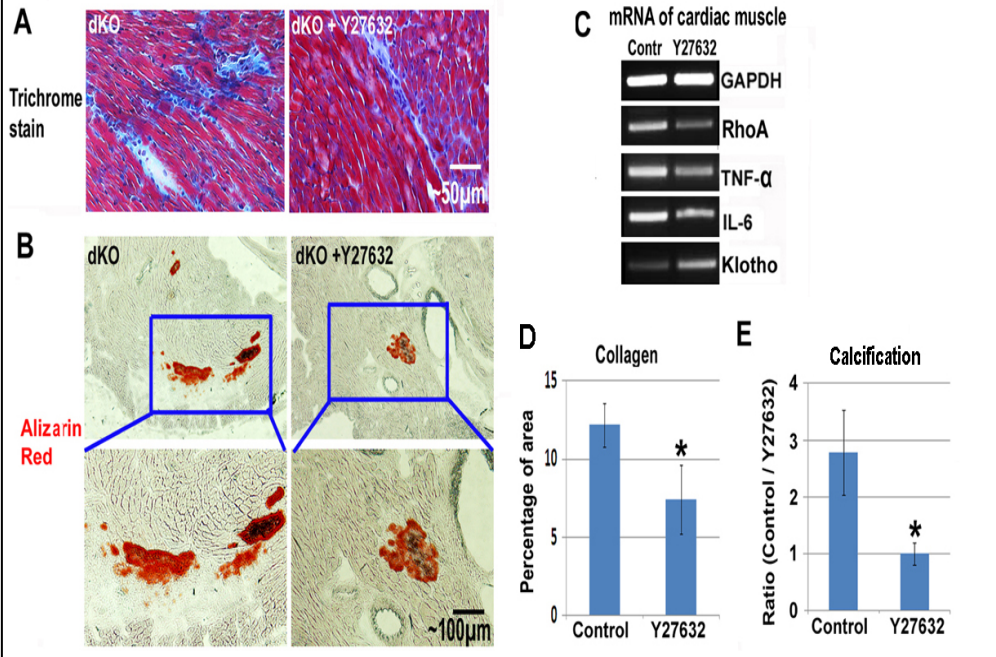

Figure 7
A Trichrome stain (8W)
B Alizarin Red (8W)
C mRNA of cardiac muscle (4W)

Figure 8

c) **Systemic RhoA inactivation via intraperitoneal injection (IP) of Y-27632 reduced fibrosis and HO in dKO cardiac muscle.**

We hypothesized that RhoA inactivation could reduce fibrosis and calcification in the cardiac muscles of the dKO mice. To confirm this hypothesis, Y-27632 was injected intraperitoneally (IP) to achieve the systemic inhibition of RhoA signaling in 3-week old dKO mice. As expected, after 4 weeks of continuous injection. Semi-quantitative PCR revealed that the expression of RhoA, TNF-α and IL-6 was down-regulated with Y-27632 administration, while the expression of Klotho was up-regulated (**Figure 8E**). Fibrosis and calcification in the cardiac muscles of dKO mice was decreased compared to non-treated mice (**Figure 8A-D**).

Discussion:

Our data reveals the involvement of RhoA signaling in regulating calcification and fibrosis of cardiac muscle, and indicates RhoA may serve as a potential target for repressing injury-induced and congenital cardiac muscle calcification and fibrosis in humans.
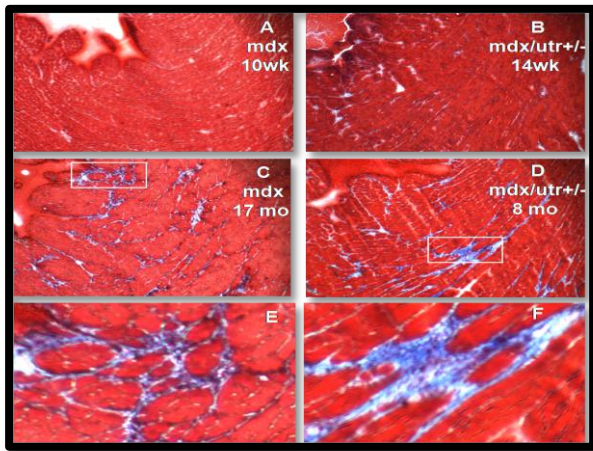
Both calcification and fibrosis in cardiac muscle is typically the result of a pathologic process. Our current results revealed that the RhoA signaling pathway may mediate the calcification and fibrosis processes in the cardiac muscles of dKO mice. RhoA seems to be co-activated with inflammatory signaling in severely dystrophic cardiac muscle, and the inactivation of RhoA signaling could repress this signaling. Therefore, our results indicate that the involvement of RhoA signaling in the therapeutic prevention of calcification and fibrosis in cardiac muscle should be further investigated as a potential target for treating DMD patients and other pathologic conditions of the heart.

Progress made from: 10-1-11 to 9-30-12

1) Double Utrophin/dystrophin knockout mice (dKO mice) develop a more severe cardiomyopathy than the mdx mice.

DMD patients die of cardiac or respiratory failure in their 3rd decade (8). The *Mdx* mouse model has near-normal cardiac function until very late in life; therefore, we aimed to determine if dystrophin-/- utrophin+/- (double knock-out, DKO het) mice might represent a superior model of DMD associated cardiomyopathy, and test it to see if we could eventually treat DMD associated heart failure via cell therapy. Some hallmarks of cardiomyopathy include inflammation and fibrosis which leads to decreased contractility and thus dysfunction of the heart. Left ventricle dilation and wall thinning which leads to a decreased ability to pump blood

Figure 1

Figure 2

Fibrosis in DKO het hearts

Figure 3

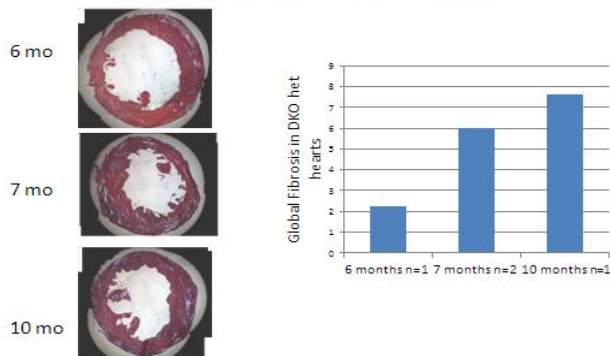LV dilation of DKO hets

Figure 4

DKO het ECHO analysis

(contractile dysfunction), decreased angiogenesis, which leads to greater cell death due to a of lack of appropriate nutrients and oxygen , and arrhythmias (9). First we assayed and compared the amount of fibrosis in the hearts of mdx and DKO het mice at the ages of 10 weeks to 17 months. We found similar levels of fibrosis in mdx mice at 10 weeks and DKO het mice at 14 weeks (**Figure 1A and B**); however, the DKO het mice appeared to accumulate cardiac fibrosis more rapidly than mdx mice. The DKO het mice at 8 months had similar fibrosis levels to mdx mice at 17 months (**Figure 1C -F**).

Therefore we went on to further characterize the hallmarks of cardiomyopathy in DKO het mice aged 6-10 months. First we looked at global fibrosis from 6-10 months and found rapidly increasing fibrosis levels (**Figure 2**). Next, we characterized the cardiac function looking at end diastolic area and fractional area change. Dilation of the hearts increased with the age of the mice which is shown in **Figure 3** and quantified in **Figure 4** as end diastolic area. Correspondingly, the cardiac functional parameter fractional area change decreases from 6-10 months (**Figure 4**).
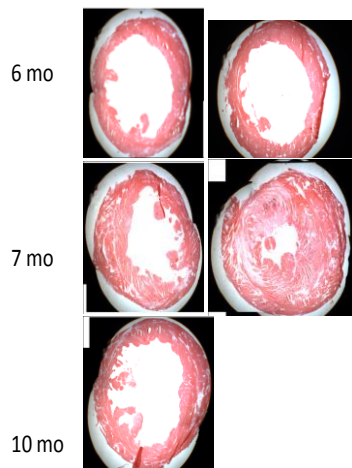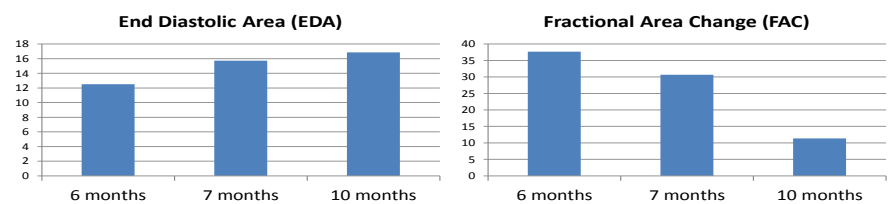
12

Finally, we examined angiogenesis in the DKO het hearts and found that the percent area of CD31+ endothelial cells increased at 10 months; however, the number of alpha smooth muscle actin positive cells, which marks more mature vascular structures, decreased from 6-7 months and then remained fairly constant through to 10 months (**Figure 5**).

Figure 5

Angiogenesis: CD31 and ASMA
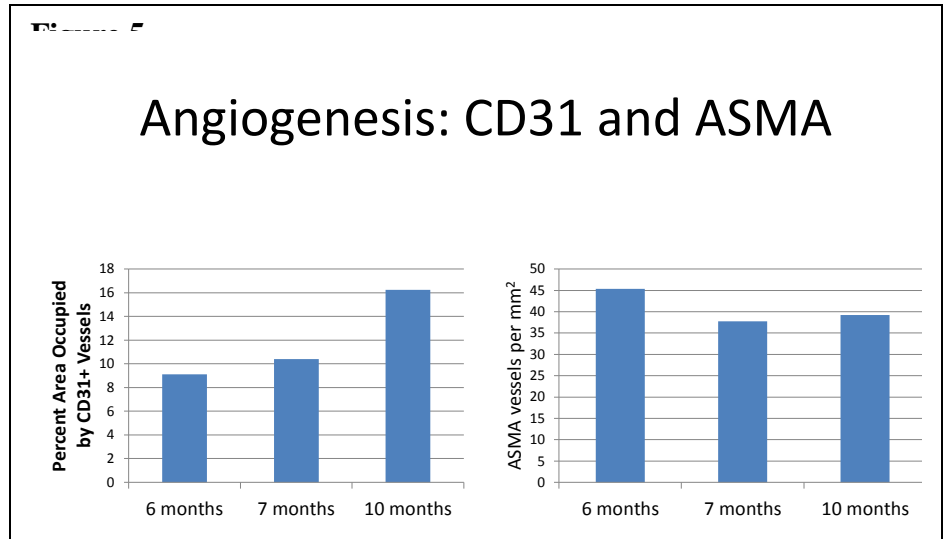
In conclusion, as DKO mice age cardiac fibrosis levels, dilation, and FAC get progressively worse making them a better model for DMD associated cardiomyopathy than the mdx mice, which do not develop severe cardiomyopathy until much later in life. Therefore, we have selected to use the DKO mouse model for the remaining of the experimental objectives which aim to develop biological approaches based on muscle derived stem cells to improve cardiac function after cardiomyopathy.
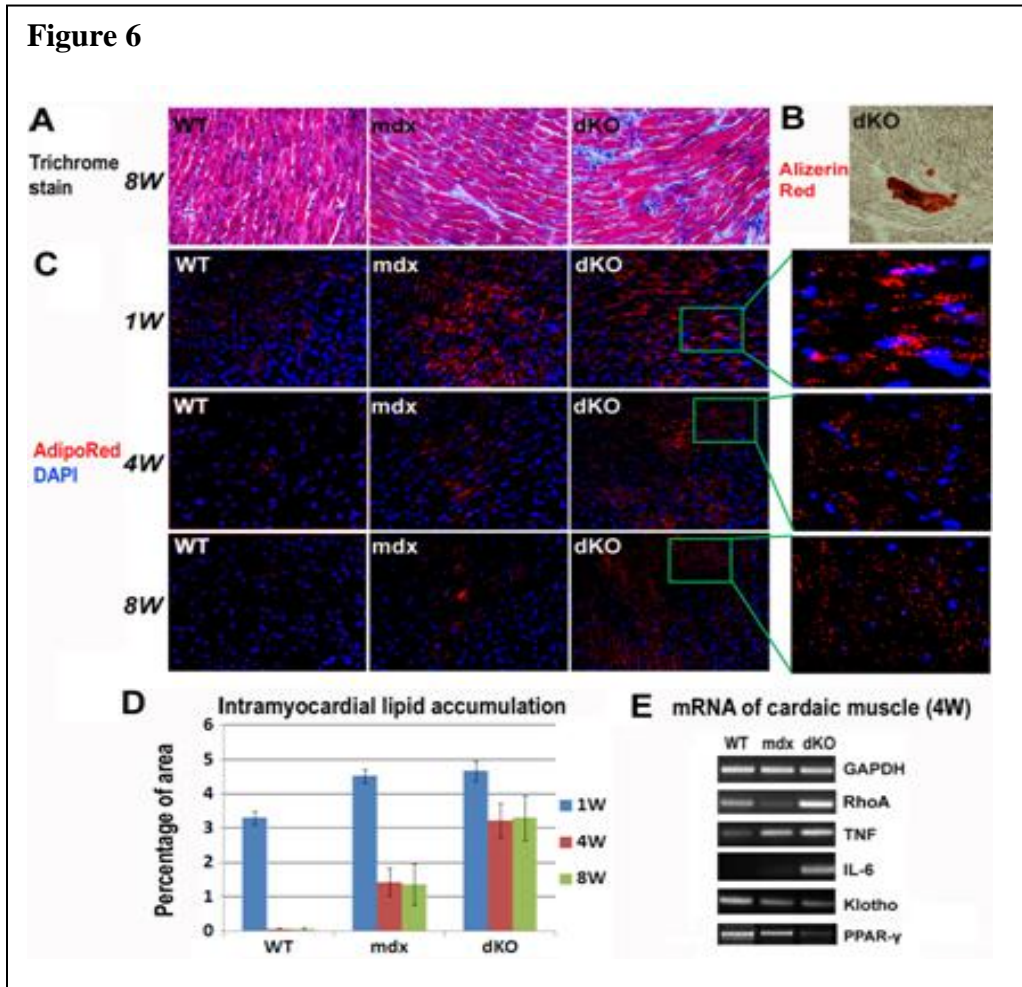
2) *Intramyocellular lipid accumulation, fibrosis and HO in cardiac muscle of dKO mice are more extensive then in mdx mice: The role of RhoA in the cardiac histopathology observed in dKO mice.*

Heterotopic ossification (HO) or ectopic fatty infiltration often occurs in muscle tissues in various disease states, and can contribute to impaired metabolism, muscle force production, and mobility function (10-11). HO is a process where bone tissue forms in soft tissues, which can be caused by trauma, surgery, neurologic injury and genetic abnormalities (11). Bone Morphogenetic Proteins (BMPs) are known to be responsible for the induction of HO in damaged skeletal muscle (12). Previous studies in our laboratory demonstrated that HO induced by BMP-4, demineralized bone matrix, and trauma in skeletal muscle mouse model could be repressed by overexpressing Noggin, a BMP antagonist (13). Fatty infiltration is the accumulation of fat cells outside the typical fat stores underneath skin, and has been reported to be associated with aging, inactivity, obesity, and diseases like diabetes (10, 14-15). Fatty infiltration into skeletal muscle (intramuscular adipose tissue, IMAT) is often associated with disorders in lipid metabolism (14-16); however, disorders in lipid metabolism in skeletal muscle can often cause another type of abnormal lipid deposition: intramyocellular lipid accumulation (17-19). More important for the current proposal, intramyocellular lipid accumulation also occurs in cardiac muscle (intramyocardial lipid accumulation) which can also be similarly caused by disorders in lipid metabolism or lipid overload, which leads to lipotoxicity and cardiac dysfunction, and can be a sign of myocardial degradation during the progression of cardiac dysfunction *(20-24)*. Intramyocellular lipid accumulation in cardiac muscle (intramyocardial lipid accumulation) has been observed in DMD patients, especially in the most damaged area of the heart (25-26). Here we suggest that intramyocellular lipid accumulation may occur in the cardiac muscles of DKO mice as well and could be correlated with the progress of phenotypes such as fibrosis formation.

RhoA is a small G-protein in the Rho family that regulates cell morphology and migration in response to extracellular signals, via reorganizing actin cytoskeleton (27-28). The RhoA-Rho kinase (ROCK) signaling pathway functions as a commitment switch for osteogenic and adipogenic differentiation of mesenchymal stem cells (MSCs) (5). Activation of RhoA-ROCK signaling in cultured MSCs *in vitro* induces their osteogenesis but

inhibits the potential of adipogenesis, while the application of Y-27632, a specific inhibitor of ROCK, reversed the process (5, 29-30). RhoA-ROCK inhibitor Y-27632 was found to induce adipogenic differentiation of myofiber-derived muscle cells *in vitro,* and resulted in fatty infiltration in skeletal muscle (31). Meanwhile, RhoA was shown to be activated by Wnt5a in inducing osteogenic differentiation and repressing adipogenic differentiation of human Adipose Stem Cells (ASCs) (32). Furthermore, the role of RhoA signaling in inflammatory reactions has been demonstrated, for example, TNF-α induces activation of RhoA signaling in smooth muscle cells (33), and RhoA was found to regulate Cox-2 activity in fibroblasts (34). In addition, an important role of RhoA in myogenic differentiation has also been demonstrated where the sustained activation of the RhoA pathway can block muscle differentiation by inhibiting myoblast fusion (7, 35-36).

Trichrome staining of cardiac muscles from WT, mdx and dKO mice (8-weeks old) was conducted to characterize extracellular matrix (ECM) collagen deposition in the muscles. Our findings showed that fibrosis formation was generally very severe in dKO mice, mild in mdx mice, and absent in WT mice (**Figure 6A**). Alizarin Red staining of the cardiac muscle also revealed the occurrence of HO in the cardiac muscle of dKO mice (**Figure 6B**), but not in WT and mdx mice (data not shown). Meanwhile, we did not observe obvious fatty infiltration in the cardiac muscle of any of the three mouse models (data not shown). Intramyocardial lipid accumulation was observed at 1 week of age in all 3 mouse models (**Figure 6C**); however, intramyocardial lipid accumulation in fetal WT mice is known to be common, because unlike the adult hearts, the fetal heart uses glucose and not fatty acids as sources of energy (37-38). Intramyocardial lipid accumulation was found to

Figure 6

decrease rapidly in WT mice from one week after birth, and became nearly non-detectable by 4 weeks of age (**Figure 6C**); however, both the mdx and dKO mouse models still exhibited extensive amounts of intramyocardial lipid (**Figure 6C, D**)*,* which was far more pronounced in the DKO mice than the mdx mice (**Figure 6C, D**). Compared to WT and mdx mice, the expression of RhoA and inflammatory signaling genes (TNF-α and IL-6) was found to be more up-regulated in the cardiac muscle of dKO mice, while the expression of Klotho gene was down-regulated (**Figure 6E**). We suggest that the activation of RhoA and inflammatory signaling may account for the higher levels of HO, intramyocardial lipid accumulation and fibrosis observed in the DKO cardiac muscles.

In vivo RhoA inactivation in DKO mice reduces intramyocellular lipid accumulation fibrosis, and HO in cardiac muscle.

We hypothesized that RhoA inactivation could reduce HO, intramyocellular lipid accumulation and fibrosis in the cardiac muscles of DKO mice. To verify this hypothesis, Y-27632 was injected intraperitoneally (IP) to achieve systematic inhibition of RhoA signaling in DKO mice (4-week old). After 3 weeks of continuous IP injection, the skeletal muscle phenotype of the DKO mice was found to be similarly improved as when we performed local injection of Y-27632 into skeletal muscle (data not shown). As anticipated the intramyocellular lipid accumulation, fibrosis and HO in cardiac muscle was also reduced (**Figure 7A-E**). Semi-quantitative PCR studies on the cardiac muscle tissues further revealed that, the expression of RhoA and inflammatory factors was down-regulated with Y-27632 administration and the expression of Klotho and PPARγ was up-regulated (**Figure 7F**).

Figure 7
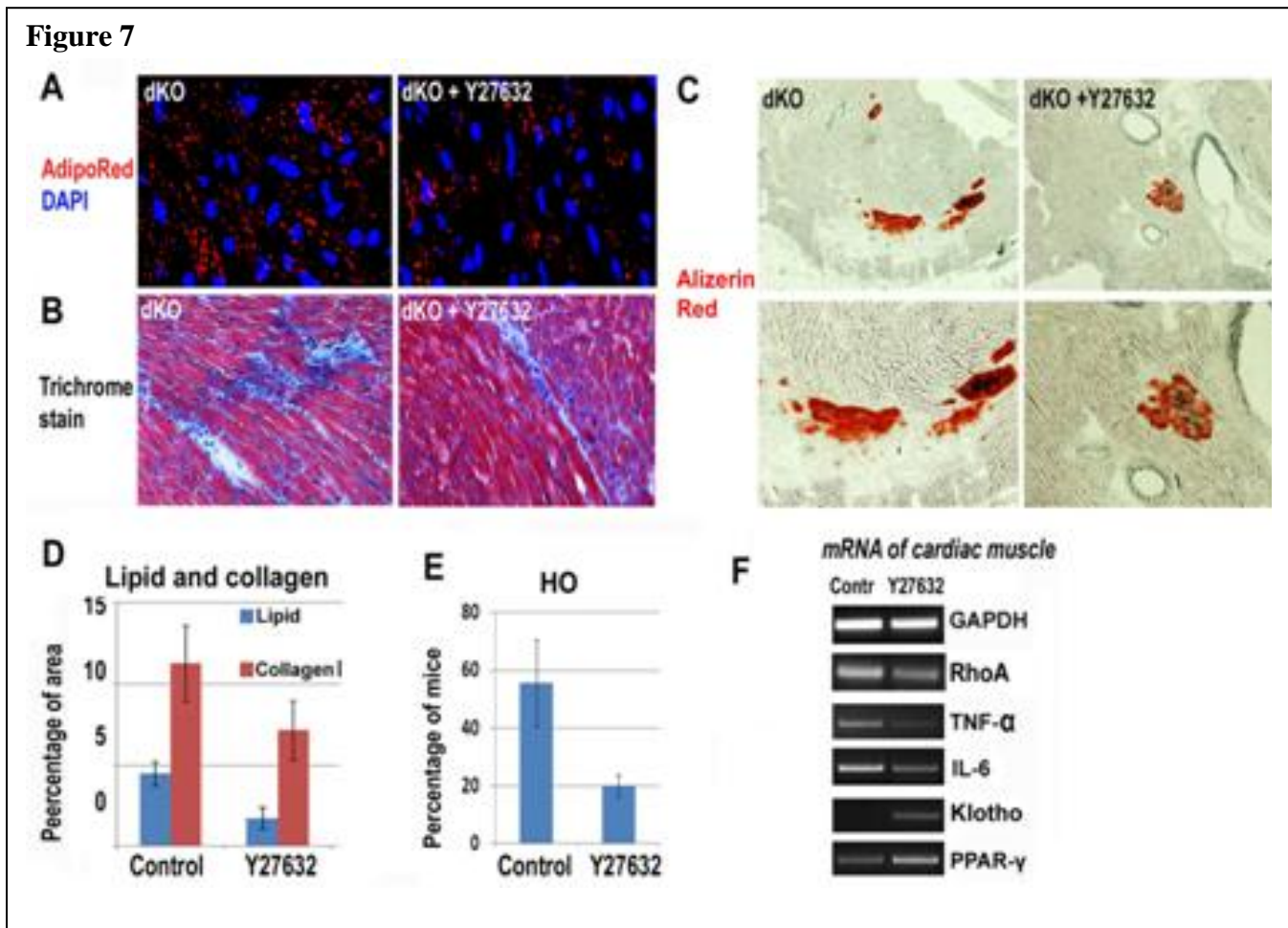
3) *The identification of human muscle progenitor cells for dystrophic heart repair and regeneration.*

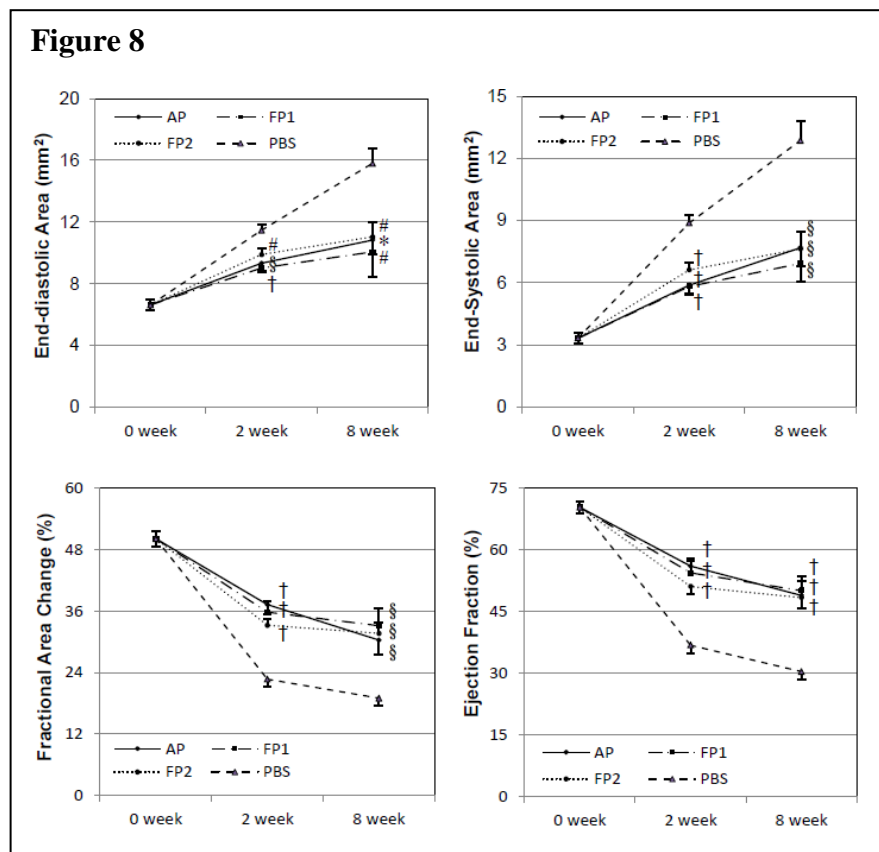## Human myo-endothelial cells repair injured cardiac tissue effectively

The potential of human myo-endothelial cells (MECs, CD34+/144+/56+/45-) to repair the injured heart was demonstrated in our recent study. When transplanted intramyocardially into acutely infarcted immunodeficient hearts of young adult mice, MECs more effectively restored cardiac function, reduced scar tissue formation, and

stimulated angiogenesis than purified conventional myoblasts and endothelial cells (39). This is presumably attributed to, at least in part, the augmented angiogenesis, resulted from more vascular endothelial growth factor (VEGF), a potent angiogenic factor, secreted by MECs under hypoxia. Similar to murine MDSCs, MECs regenerated significantly more fast-skeletal MHC-positive myofibers in the ischemic heart. A small fraction of engrafted MECs expressed cardiomyocyte markers, cardiac troponin-T and –I, indicating the likely cardiac differentiation and/or cell fusion in the injured heart. MECs also promoted proliferation and prevented apoptosis of endogenous cardiomyocytes. These results suggest that human MECs are an ideal donor cell population for cardiac repair.

Human pericytes restored the function of the injured heart through paracrine effect and cellular interaction

Human microvascular pericytes (CD146$^+$/34$^-$/45$^-$/56$^-$), with their inherent vascular functions and recently

Figure 8

documented multipotency, matched the scope of ideal cells for cardiac repair. (40). Transplantation of cultured human muscle pericytes into acutely infarcted hearts of immunodeficient mice significantly improved cardiac contractility and reduced heart dilatation, superior to CD56+ myogenic progenitor transplantation (**Figure 8**). Pericytes exhibited cardio-protective effects such as promotion of angiogenesis, decrease of chronic inflammation, and reduction of scar formation (41). Under hypoxia, pericytes suppressed murine fibroblast proliferation and macrophage proliferation *in vitro* through a paracrine mechanism. Pericytes demonstrated expression of a number of immunoregulatory molecules, including IL-6, LIF, COX-2 and HMOX-1, even under hypoxia. Pericytes not only supported microvascular structure formation in three-dimensional co-cultures but also significantly enhanced host angiogenesis *in vivo*. Under hypoxia, pericytes dramatically increased expression of VEGF-A, PDGF-β, TGF-β1.

In conclusion, intramyocardial transplantation of purified human muscle pericytes promotes functional and structural recovery, attributable to multiple mechanisms involving paracrine effects and cellular interactions.

Figure 9

Currently, to examine whether donor pericyte-derived VEGF is the primary molecular mediator required for the promotion of host angiogenesis, we used anti-human $VEGF_{165}$ shRNA to block VEGF secretion from donor pericytes. The angiogenic effect of transduced pericytes with VEGF blockage as well as their overall therapeutic benefits post-transplantation will be assessed. Human muscle pericytes were successfully transduced by lentiviral anti-VEGF-shRNA-eGFP vector. The transduction rate was roughly 70-80%. We observed no significant change to cell growth and phenotypes after transduction. To further purify transduced pericytes, we plan to use FACS to sort GFP-positive pericytes to homogeny. *In vitro* hypoxia assay showed that although anti-VEGF-shRNA transduction only reduced VEGF secretion from pericytes by 22.3% under normoxia, it effectively inhibited their VEGF secretion by 65.2% under hypoxia, as revealed by ELISA (**Figure 9**). To examine whether their vessel-forming capacity is affected by VEGF blockage, the Matrigel culture assay using pericytes has been performed and the data is currently being analyzed.

Figure 10

Figure 11

Figure 12

RAC   SAC   Control
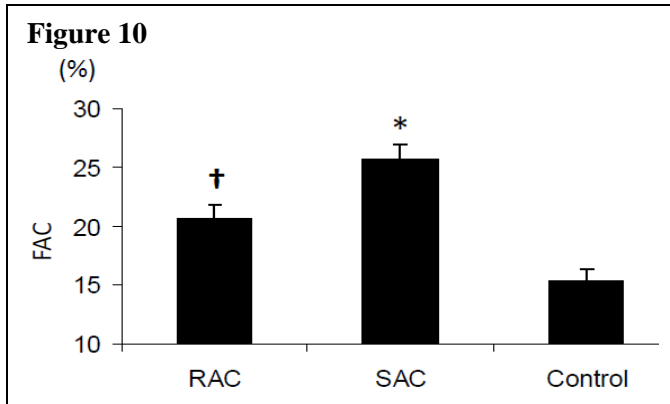
Pre-plated human muscle cells display a differential cardiac repair capacity.

Very recently, we applied the modified pre-plate technique to separate freshly dissociated human muscle cells into rapid- and slowly-adhering cell populations, equivalent to the murine early and late pre-plating cells. The slowly-adhering cells (SACs) displayed not only a greater myogenic potential but also better cell survival under oxidative and inflammatory stresses *in vitro* than rapidly-adhering cells (RACs), similar to murine MDSCs (Okada, Payne et al., Mol. Ther. 2012). We have investigated the therapeutic potential of human muscle pre-plating cells for the treatment of myocardial injury. The intramyocardial injection of SACs into the acutely infracted immunodeficient murine heart improved cardiac contractility more effectively than the injection of RACs (**Figure 10**; (42)). The functional recovery likely resulted from the decreased myocardial fibrosis (**Figure 11**), higher cell proliferation, reduction of cardiomyocyte apoptosis and increased revascularization (**Figure 12**) in SAC-injected hearts, similar to the therapeutic capacity of murine MDSCs.
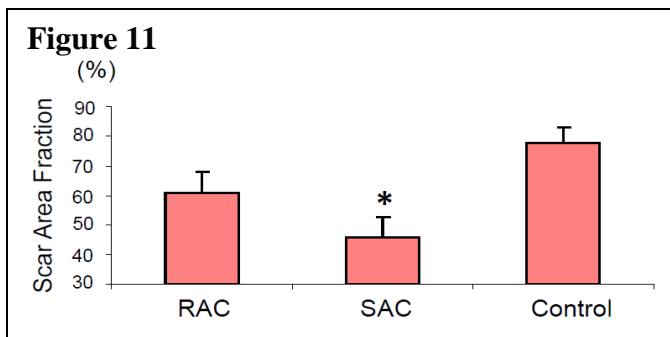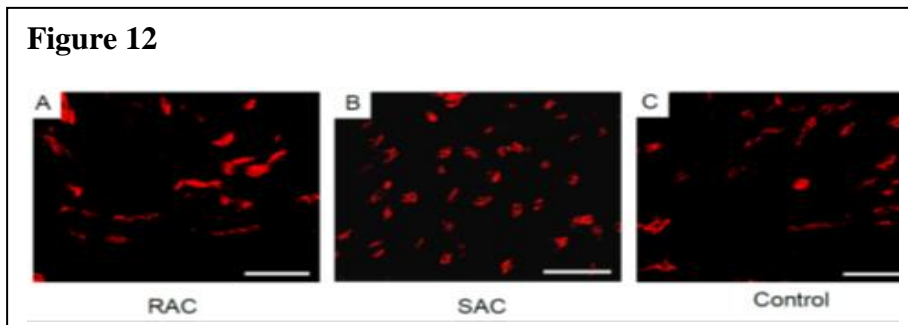
Technical Issues

As indicated in last year's report, we identified that our young adult mdx/scid mice do not exhibit prominent loss of cardiac function and dystrophic phenotypes in the cardiac tissue, so we aged these animals until they were nearly 2 years of age in order to obtain dystrophic symptoms in the heart similar to the DMD patients. However, the aging process significantly weakened the ability of the mdx/scid mice to withstand the invasive and traumatic open-chest surgery and intramyocardial injection of human cells. Therefore, in addition to the usage of the new dKO mouse model, we injected the human cells intra-peritoneally (IP) rather than intramyocardially in order to circumvent the invasive cardiac surgery. We labeled the human cells with a GFP reporter gene to track the migration of the transplanted cell. The results are reported above in the section entitled: Intraperitoneal injection of hMDSCs prevents progressive heart failure and promotes angiogenesis in the aging dystrophic hearts of mdx SCID mice, and the results were extremely encouraging, therefore we will continue utilizing this model as well as further exploring the dKO model. The limitation of utilizing the mdx model is the requirement to age the mice to 1.5-2 years of age, which is ongoing.

Future Direction

1) **We will continue to further investigate the dKO animal model and continue to explore RhoA's role in the development of DMD associated cardiomyopathy.**
2) **As indicated above we will continue to utilize the IP injection model described above using aged (1.5-2yr old) mdx/SCID mice. In the next series of experiments we will investigate the role that angiogenesis plays in the regeneration/repair capacity of human MDSCs transduced with VEGF or sFLT-1 and injected IP.**
3) **We will also continue to identify the potential protective factors that are shared by young unaffected mice when parabiotically paired with old dKO or old mdx/SCID animals that are presenting with cardiomyopathy.**

KEY RESEARCH ACCOMPLISHMENTS:

- **Identified and characterized a superior model of dystrophic related cardiomyopathy (the dKO mouse).**
- **Identified the relationship between the activation of RhoA and inflammatory signaling which appears to account for the higher levels of heterotopic ossification (HO), intramyocardial lipid accumulation and fibrosis observed in the dKO cardiac muscles.**
- **Demonstrated that in vivo RhoA inactivation with Y-27632 in dKO mice reduces intramyocellular lipid accumulation fibrosis, and HO in cardiac muscle.**
- **Demonstrated that purified human pericytes could restore the function of the injured heart through paracrine effects and cellular interaction**
- **Demonstrated that the intramyocardial injection of preplate isolated SACs into the acutely infracted immunodeficient murine heart improved cardiac contractility more effectively than the injection of RACs.**
- **Demonstrated that the intraperitoneal injection of human MDSCs could prevent progressive heart failure and promote angiogenesis in the dystrophic hearts of aged mdx SCID mice.**
- **Demonstrated that the parabiotic pairing of a young unaffected mouse with a dystrophic mouse could reduce cardiac fibrosis and intramyocardial lipid accumulation in the old dystrophic mice,**

which could lead to the identification of circulating factors from the young unaffected animals that could improve cardiac muscle weakness and cardiomyopathy in dystrophic mice without the need to replace dystrophin. This could lead to potential new therapies to treat DMD patients.

- **Demonstrated that RhoA signaling regulates calcification and fibrosis of cardiac muscle, and indicates RhoA may serve as a potential target for repressing injury-induced and congenital cardiac muscle calcification and fibrosis in human patients**

REPORTABLE OUTCOMES:

1. **RhoA signaling regulates heterotopic ossification and fatty infiltration in dystrophic skeletal muscle.** Xiaodong Mu, Arvydas Usas, Ying Tang, Aiping Lu, Jihee Sohn, Bing Wang, Kurt Weiss, and Johnny Huard. Orthopaedic Research Society; 2013 ORS Annual Meeting; January 26-29, 2013; San Antonio, TX. (**Appendix 1**)
2. **RhoA inactivation represses BMP-induced heterotopic ossification (HO) in skeletal muscle and potential for HO treatment.** Xiaodong Mu, Kurt Weiss, and Johnny Huard. Orthopaedic Research Society; 2013 ORS Annual Meeting; January 26-29, 2013; San Antonio, TX. (**Appendix 2**)
3. **Human Pericytes for Ischemic Heart Repair.** Chien-Wen Chen, Masaho Okada, Jonathan D. Proto, Xueqin Gao, Naosumi Sekiya, Sarah A. Beckman, Mirko Corselli, Mihaela Crisan, Arman Saparov, Kimimasa Tobita, Bruno Péault, Johnny Huard. Stem Cells, In Press. (**Appendix 3**)
4. **Human skeletal muscle cells with a slow adhesion rate after isolation and enhanced stress resistance improve functions if ischemic heart.** Okada M, Payne T, Drowley L, Jankowski R, Momoi N, Beckman S, Chen C, Keller B, Tobita K, **Huard J**. Mol Ther 2012 Jan; 20(1):138-45. PMID: 22068427 (**Appendix 4**)
5. **Myocardial Calcification and Fibrosis in Dystrophic Mice is Reduced by RhoA Inactivation.** Xiaodong Mu, Ying Tang, Koji Takayama, Bing Wang, Weiss Kurt, and Johnny Huard. Orthopaedic Research Society, 2014 Annual Meeting, March 15-18, New Orleans, LA. (**Appendix 5**)
6. **The Role of Antioxidation and Immunomodulation in Postnatal Multipotent Stem Cell-Mediated Cardiac Repair.** Saparov A, Chen C-W, Beckman SA, Wang Y, **Huard J**. International Journal of Molecular Sciences. 2013; 14(8):16258-16279. (**Appendix 6**)
7. **RhoA mediates defective stem cell function and heterotopic ossification in dystrophic muscle of mice,** Xiaodong M, Usas A, Tang Y, Lu A, Wang B, Weiss K, **Huard J.** FASEB Journal. 2013 May 23. PMID: 23704088. (**Appendix 7**)

CONCLUSIONS:

Our current results during this period (10-1-12 to 9-30-13) revealed that the IP injection of hMDSCs could impart a beneficial effect on the aging dystrophic hearts of mdx/ SCID mice, not only preventing progressive LV dilatation but also sustaining cardiac contractility. Moreover the data suggested that there was a promotion of angiogenesis and vasculogenesis in the myocardium following hMDSC intraperitoneal injection. Currently, we hypothesize that this is due to the production of angiogenic and/or vasculogenic signaling molecules by the injected hMDSCs that subsequently travel to the heart via systemic circulation. This contention is being confirmed by parabiosis experiments which are described below. We can therefore summarize that the intraperitoneal injection of hMDSCs prevents progressive heart failure and promotes angiogenesis in the aging the dystrophic hearts of mdx SCID mice. The results suggest from the parabiosis experiments suggest that the defect in the MPCs with in the dystrophic mice might be related to the dystrophic microenvironment or due to circulating factors, of which are currently unidentified.. These observations suggest that changes in the

dystrophic microenvironment could be a new approach to improve cardiac muscle weakness in DMD patients, despite a continued lack of dystrophin expression in dystrophic individuals. Finally, the involvement of RhoA signaling in regulating calcification and fibrosis of cardiac muscle, and indicates that RhoA may serve as a potential target for repressing injury-induced and congenital cardiac muscle calcification and fibrosis in humans due to the fact that we demonstrated that the RhoA signaling pathway may mediate the calcification and fibrosis processes in the cardiac muscles of dKO mice. RhoA seems to be co-activated with inflammatory signaling in severely dystrophic cardiac muscle, and the inactivation of RhoA signaling could repress this signaling. Therefore, our results indicate that the involvement of RhoA signaling in the therapeutic prevention of calcification and fibrosis in cardiac muscle should be further investigated as a potential target for treating DMD patients and other pathologic conditions of the heart.

REFERENCES:

1. El-Bialy A, Shenoda M, Saleh J, Tilkian A. Myocardial calcification as a rare cause of congestive heart failure: a case report. J Cardiovasc Pharmacol Ther. 2005;10(2):137-43.
2. Gowda RM, Boxt LM. Calcifications of the heart. Radiol Clin North Am. 2004;42(3):603-17, vi-vii.
3. Isaac C, Wright A, Usas A, Li H, Tang Y, Mu X, et al. Dystrophin and utrophin "double knockout" dystrophic mice exhibit a spectrum of degenerative musculoskeletal abnormalities. J Orthop Res. 2013;31(3):343-9.
4. Mu X, Usas A, Tang Y, Lu A, Wang B, Weiss K, et al. RhoA mediates defective stem cell function and heterotopic ossification in dystrophic muscle of mice. FASEB J. 2013;27(9):3619-31.
5. McBeath R, Pirone DM, Nelson CM, Bhadriraju K, Chen CS. Cell shape, cytoskeletal tension, and RhoA regulate stem cell lineage commitment. Dev Cell. 2004;6(4):483-95.
6. Zhou H, Li YJ, Wang M, Zhang LH, Guo BY, Zhao ZS, et al. Involvement of RhoA/ROCK in myocardial fibrosis in a rat model of type 2 diabetes. Acta Pharmacol Sin. 2011;32(8):999-1008.
7. Castellani L, Salvati E, Alema S, Falcone G. Fine regulation of RhoA and Rock is required for skeletal muscle differentiation. J Biol Chem. 2006;281(22):15249-57.
8. Deconinck N, Dan B. Pathophysiology of duchenne muscular dystrophy: current hypotheses. Pediatr Neurol. 2007;36(1):1-7.
9. Towbin JA, Bowles NE. The failing heart. Nature. 2002;415(6868):227-33.
10. Marcus RL, Addison O, Kidde JP, Dibble LE, Lastayo PC. Skeletal muscle fat infiltration: impact of age, inactivity, and exercise. J Nutr Health Aging. 2010;14(5):362-6.
11. Cipriano CA, Pill SG, Keenan MA. Heterotopic ossification following traumatic brain injury and spinal cord injury. J Am Acad Orthop Surg. 2009;17(11):689-97.
12. Shi S, de Gorter DJ, Hoogaars WM, t Hoen PA, Ten Dijke P. Overactive bone morphogenetic protein signaling in heterotopic ossification and Duchenne muscular dystrophy. Cell Mol Life Sci. 2012.
13. Hannallah D, Peng H, Young B, Usas A, Gearhart B, Huard J. Retroviral delivery of Noggin inhibits the formation of heterotopic ossification induced by BMP-4, demineralized bone matrix, and trauma in an animal model. J Bone Joint Surg Am. 2004;86-A(1):80-91.
14. Miljkovic-Gacic I, Wang X, Kammerer CM, Gordon CL, Bunker CH, Kuller LH, et al. Fat infiltration in muscle: new evidence for familial clustering and associations with diabetes. Obesity (Silver Spring). 2008;16(8):1854-60. PMCID: 2895815.
15. Zoico E, Rossi A, Di Francesco V, Sepe A, Olioso D, Pizzini F, et al. Adipose tissue infiltration in skeletal muscle of healthy elderly men: relationships with body composition, insulin resistance, and inflammation at the systemic and tissue level. J Gerontol A Biol Sci Med Sci. 2010;65(3):295-9.
16. Corcoran MP, Lamon-Fava S, Fielding RA. Skeletal muscle lipid deposition and insulin resistance: effect of dietary fatty acids and exercise. Am J Clin Nutr. 2007;85(3):662-77.
17. Savage DB, Petersen KF, Shulman GI. Disordered lipid metabolism and the pathogenesis of insulin resistance. Physiol Rev. 2007;87(2):507-20. PMCID: 2995548.

18.   Laforet P, Vianey-Saban C. Disorders of muscle lipid metabolism: diagnostic and therapeutic challenges. Neuromuscul Disord. 2010;20(11):693-700.

19.   Hulver MW, Dohm GL. The molecular mechanism linking muscle fat accumulation to insulin resistance. Proc Nutr Soc. 2004;63(2):375-80.

20.   Schulze PC. Myocardial lipid accumulation and lipotoxicity in heart failure. J Lipid Res. 2009;50(11):2137-8. PMCID: 2759818.

21.   Axelsen LN, Lademann JB, Petersen JS, Holstein-Rathlou NH, Ploug T, Prats C, et al. Cardiac and metabolic changes in long-term high fructose-fat fed rats with severe obesity and extensive intramyocardial lipid accumulation. Am J Physiol Regul Integr Comp Physiol. 2010;298(6):R1560-70.

22.   Ruberg FL. Myocardial lipid accumulation in the diabetic heart. Circulation. 2007;116(10):1110-2.

23.   Zhou YT, Grayburn P, Karim A, Shimabukuro M, Higa M, Baetens D, et al. Lipotoxic heart disease in obese rats: implications for human obesity. Proc Natl Acad Sci U S A. 2000;97(4):1784-9. PMCID: 26513.

24.   Sharma S, Adrogue JV, Golfman L, Uray I, Lemm J, Youker K, et al. Intramyocardial lipid accumulation in the failing human heart resembles the lipotoxic rat heart. FASEB J. 2004;18(14):1692-700.

25.   Saini-Chohan HK, Mitchell RW, Vaz FM, Zelinski T, Hatch GM. Delineating the role of alterations in lipid metabolism to the pathogenesis of inherited skeletal and cardiac muscle disorders: Thematic Review Series: Genetics of Human Lipid Diseases. J Lipid Res. 2012;53(1):4-27. PMCID: 3243479.

26.   Tahallah N, Brunelle A, De La Porte S, Laprevote O. Lipid mapping in human dystrophic muscle by cluster-time-of-flight secondary ion mass spectrometry imaging. J Lipid Res. 2008;49(2):438-54. PMCID: 2438276.

27.   Ridley AJ. Rho GTPases and cell migration. J Cell Sci. 2001;114(Pt 15):2713-22.

28.   Luo L. Rho GTPases in neuronal morphogenesis. Nat Rev Neurosci. 2000;1(3):173-80.

29.   Khatiwala CB, Kim PD, Peyton SR, Putnam AJ. ECM compliance regulates osteogenesis by influencing MAPK signaling downstream of RhoA and ROCK. J Bone Miner Res. 2009;24(5):886-98. PMCID: 2672206.

30.   Meyers VE, Zayzafoon M, Douglas JT, McDonald JM. RhoA and cytoskeletal disruption mediate reduced osteoblastogenesis and enhanced adipogenesis of human mesenchymal stem cells in modeled microgravity. J Bone Miner Res. 2005;20(10):1858-66. PMCID: 1351020.

31.   Hosoyama T, Ishiguro N, Yamanouchi K, Nishihara M. Degenerative muscle fiber accelerates adipogenesis of intramuscular cells via RhoA signaling pathway. Differentiation. 2009;77(4):350-9.

32.   Santos A, Bakker AD, de Blieck-Hogervorst JM, Klein-Nulend J. WNT5A induces osteogenic differentiation of human adipose stem cells via rho-associated kinase ROCK. Cytotherapy. 2010;12(7):924-32.

33.   Goto K, Chiba Y, Sakai H, Misawa M. Tumor necrosis factor-alpha (TNF-alpha) induces upregulation of RhoA via NF-kappaB activation in cultured human bronchial smooth muscle cells. J Pharmacol Sci. 2009;110(4):437-44.

34.   Slice LW, Bui L, Mak C, Walsh JH. Differential regulation of COX-2 transcription by Ras- and Rho-family of GTPases. Biochem Biophys Res Commun. 2000;276(2):406-10.

35.   Charrasse S, Comunale F, Grumbach Y, Poulat F, Blangy A, Gauthier-Rouviere C. RhoA GTPase regulates M-cadherin activity and myoblast fusion. Mol Biol Cell. 2006;17(2):749-59. PMCID: 1356585.

36.   Beqaj S, Jakkaraju S, Mattingly RR, Pan D, Schuger L. High RhoA activity maintains the undifferentiated mesenchymal cell phenotype, whereas RhoA down-regulation by laminin-2 induces smooth muscle myogenesis. J Cell Biol. 2002;156(5):893-903. PMCID: 2173321.

37.   Lindegaard ML, Nielsen LB. Maternal diabetes causes coordinated down-regulation of genes involved with lipid metabolism in the murine fetal heart. Metabolism. 2008;57(6):766-73.

38.   Lehman JJ, Kelly DP. Transcriptional activation of energy metabolic switches in the developing and hypertrophied heart. Clin Exp Pharmacol Physiol. 2002;29(4):339-45.

39.   Okada M, Payne TR, Zheng B, Oshima H, Momoi N, Tobita K, et al. Myogenic endothelial cells purified from human skeletal muscle improve cardiac function after transplantation into infarcted myocardium. Journal of the American College of Cardiology. 2008;52(23):1869-80. PMCID: 2719893.

40.   Crisan M, Yap S, Casteilla L, Chen CW, Corselli M, Park TS, et al. A perivascular origin for mesenchymal stem cells in multiple human organs. Cell stem cell. 2008;3(3):301-13.

41.   Chen CW, Okada M, Proto JD, Gao X, Sekiya N, Beckman SA, et al. Human pericytes for ischemic heart repair. Stem Cells. 2012.

42.   Okada M, Payne TR, Drowley L, Jankowski RJ, Momoi N, Beckman S, et al. Human skeletal muscle cells with a slow adhesion rate after isolation and an enhanced stress resistance improve function of ischemic hearts. Molecular therapy : the journal of the American Society of Gene Therapy. 2012;20(1):138-45. PMCID: 3255579.

Sub-project 2: Human hepatocytes for treatment of life-threatening liver injury

PI's: Ira Fox, MD and David Perlmutter, MD

INTRODUCTION: (New data is underlined in the text of the Introduction and body.)

These studies are focused on expanding human hepatocytes from control, marginal quality and cirrhotic livers for the treatment of life-threatening acute liver failure. Two technical objectives were proposed: 1) to characterize and expand hepatocytes from patients with cirrhosis and end-stage liver disease in immune deficient hosts whose livers permit extensive repopulation with donor cells, and 2) to determine the extent to which transplantation with human hepatocytes can reverse hepatic failure in a clinically relevant non-human primate model of this process. In order to accomplish these objectives, we continue to explore the range of liver diseases that allow expansion of human hepatocytes in FRG mice and have isolated the human hepatocytes for use in a non-human primate model of acute liver failure. We have also performed additional studies on hepatocytes isolated from the livers of rats with end-stage cirrhosis, identified a target molecule that controls liver-specific gene expression in these cells and demonstrated that re-expression of this gene, HNF4□, results in normalization of hepatocyte function in vitro and in vivo. We have also induced acute liver failure in monkeys and transplanted these animals with human hepatocytes. While we were unsuccessful in correcting liver failure in the first animal transplanted with human hepatocytes, we have made progress in optimizing the protocol for inducing acute liver failure. We used this optimized protocol in a second transplant experiment, however, the animal died from a technical complication before the efficacy of transplantation could be assessed. When personnel issues are resolved, experiments will continue. We have also demonstrated that we can recover an adequate number of human hepatocytes from repopulated FRG mice for transplantation in a primate model.

Body:

Technical Objective #1: To characterize and expand hepatocytes from patients with cirrhosis and end-stage liver disease in immune deficient hosts whose livers permit extensive repopulation with donor cells.

Hypothesis: Human hepatocytes derived from poor quality human cadaver donors can be resuscitated and expand in numbers that can be used for clinical application in the livers of immune deficient hosts where there is a selective repopulation advantage to transplanted donor hepatocytes.

1.1. Expanding human hepatocytes in FRG mice.

We have performed primary transplants using human hepatocytes from non-cirrhotic donors as a source of cells for Technical Objective #2 in FRG mice. Human hepatocytes from the explanted liver of two patients with ornithine transcarbamylase (OTC) deficiency were transplanted into immune-deficient mice with hereditary tyrosinemia (FAH-/-; FRG). The level of human serum albumin (HSA) in the peripheral blood of all

Human albumin in FRG mice transplanted with human hepatocytes from a 6-month old donor
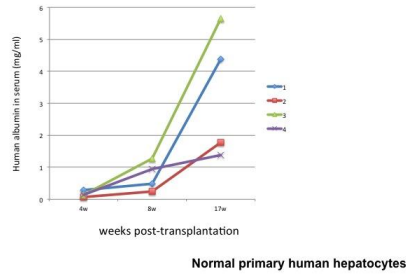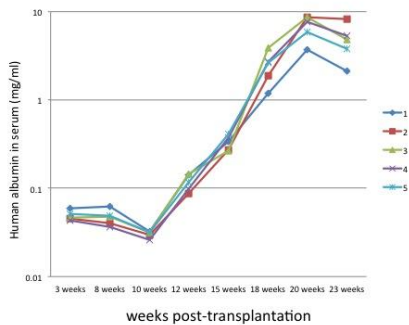

Normal primary human hepatocytes

Figure 1

animals was greater than 1.5mg/ml, indicating at least 20% of the liver was replaced with human hepatocytes. One recipient animal was sacrificed, and approximately 50% engraftment was confirmed by immunohistochemistry. We then isolated hepatocytes from the remaining repopulated FRG mice and secondary transplants were performed with the recovered cells in 5 naïve FRG mice. The HSA levels in the transplanted mice were detectable 4 weeks after transplant, with a mean HSA level of 6.87 ± 0.91 ug/ml. This level of re-population, at this time point, was as expected based on the literature.

Human albumin in FRG mice transplanted with human hepatocytes from a patient treated with one cycle of cancer chemotherapy

primary human hepatocytes from a patient treated with chemotherapy

Figure 2

Human albumin in FRGN mice transplanted with human hepatocytes from a patient treated with 6-cycles of cancer chemotherapy
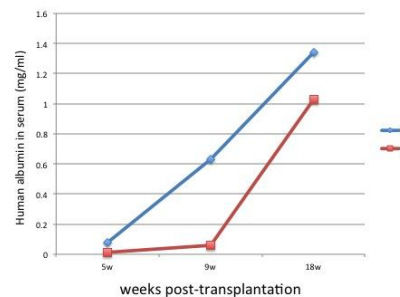
primary human hepatocytes from a patient treated with chemotherapy

Figure 3

The time course of repopulation following transplantation using control hepatocytes in FRG mice is demonstrated in **Figure 1**. In addition, we have transplanted FRG mice using human hepatocytes derived from liver resection specimens from patients with metastatic colon cancer that have received cancer chemotherapy. The HSA levels in the mice transplanted with hepatocytes from patients receiving one and 6 cycles of chemotherapy are shown in **Figures 2 and 3**. Full repopulation (based on HSA level of from 1-9

mg/ml) can be seen following transplantation with hepatocytes from patients receiving one cycle of chemotherapy. The repopulation is not as strong from the patient that received 6-cycles of chemotherapy, but greater than 20% repopulation is seen, based on HSA levels greater than 1 mg/ml. The rate of repopulation was not affected by exposure to chemotherapy. We have also successfully transplanted hepatocytes from three patients with cirrhosis. The diseases included alpha-1-antitrypsin deficiency, progressive familial intrahepatic cholestasis type 2, and Wilson's disease. As seen in **Figures 4-6**, engraftment and expansion of cells has been slower than that seen when hepatocytes from non-cirrhotic patients are transplanted, but there has been good expansion of cells. These experiments are ongoing. In the future, we would like to transplant cells from cirrhotic livers that do not have a genetic abnormality (such as from patients with Laennec's cirrhosis or from patients with steatohepatitis) to determine whether such cells may repopulate FRG mouse livers more completely.

Fig 4   **Fig 5**   **Fig 6**

We eventually intend to transplant and repopulate additional immune deficient mice to generate cells for the non-human primate acute liver failure studies outlined in Technical Objective #2.

1.2. Normalization of end-stage decompensated hepatocyte function in vitro and in vivo by re-expression of HNF4☐.

In a continuation of studies to determine the extent to which hepatocytes derived from livers with severe chronic injury could be resuscitated for use in clinical hepatocyte transplantation, we isolated hepatocytes from the livers of Lewis rats with compensated and end-stage decompensated cirrhosis. To assess the extent to which hepatocyte-specific characteristics are affected by cirrhosis and liver failure, mRNA from isolated hepatocytes derived from cirrhotic and control livers were compared for gene expression by microarray analysis. As noted previously, hierarchical cluster analysis demonstrated significant gene expression differences among groups depending on the extent of cirrhosis from which the hepatocytes were derived. As expected, there were progressive changes in the expression of genes representing signals promoting proliferation and regeneration, apoptosis, and cell-death, most likely mediated by inflammation and oxidative stress, and progressive loss of gene expression representing worsening of metabolic function. This work has now been published (**Liu, et al. The microenvironment in hepatocyte regeneration and function in rats with advanced cirrhosis. Hepatology 2012; 55(5): 1529-39**). Microarrays also showed marked decreases in

the expression of HNF4α, Foxa2, C/EBPα, and HNF1α, DNA binding proteins that are part of the network of hepatocyte-enriched transcription factors, sequentially established during development, that regulate the mature hepatocyte phenotype, controlling expression of proteins of coagulation, biliary metabolism, and lipid metabolism.

Since transcription factor deficiency could explain hepatocyte impairment, we investigated the therapeutic effects of forced re-expression. HNF4α was chosen for this therapy because it is the central regulator of the adult hepatocyte transcription factor network, has no other hepatocyte-expressed homolog, and showed the greatest reduction in the decompensated hepatocyte. We therefore performed a detailed analysis of the expression of HNF4α and its target genes in isolated hepatocytes and liver tissue. qRT-PCR analysis confirmed severe downregulation of HNF4α expression, and quantification of HNF4α in hepatocytes by western blot and by immunofluorescent staining of cytospin samples gave similar results. Thus, a significant decrease of HNF-4α in hepatocytes correlated with decompensation in cirrhosis.

To assess whether forced re-expression of HNF4α could affect the function of cirrhotic hepatocytes, we first used an *in vitro* culture system. Hepatocytes, isolated from animals with cirrhosis and decompensated liver function, were transduced with adeno-associated virus (AAV) vectors to express HNF4α and GFP or GFP alone. At 48 hours, qRT-PCR analysis showed HNF4α re-expression restored to nearly normal levels the network transcription factors C/EBPα, HNF1α, and PPARα, and the phenotypic target genes important for liver-specific activity. HNF4α expression also improved secretion of albumin into the culture supernatant— severely impaired in hepatocytes isolated from decompensated cirrhosis —and activity of Cytochrome P450 3A4, a major enzyme of xenobiotic metabolism. Animals with liver failure and cirrhosis were then transduced to re-express HNF4□ in their hepatocytes by intravenous infusion of $3x10^{11}$ AAV-HNF4α-GFP genomes. Animals sacrificed two weeks after infusion demonstrated high transduction efficiency uniformly distributed in most hepatocytes. Moreover, the impaired albumin expression of decompensated cirrhosis was dramatically improved and its expression increased until the time of sacrifice at 100 days following AAV treatment. Administration of the AAV-GFP control vector did not affect liver function. Finally, pathophysiologic testing showed striking and persistent improvement in liver function, ascites, activity, and neurologic function, and survival was prolonged to the end-point of the study at 100 days post AAV treatment. Functional analysis of cells isolated from treated animals showed significant improvement of albumin secretion and CYP3A4 activity. In addition, there was improvement in expression levels of HNF4α target genes and decreased expression of the hepatic progenitor cell markers AFP, CD44, and EpCAM. The healing effects of HNF4α re-expression did not depend on proliferation, since there was no increase apparent in Ki67 staining. HNF4α did not significantly augment TERT expression and telomere length in the cirrhotic hepatocytes remained critically short. Thus, HNF4α acted by phenotypically correcting diseased hepatoctyes, not by stimulating their replacement.

These studies show that down-regulation of HNF4α has a profound effect on the end-stage cirrhotic hepatocyte in vitro, since replenishment of this single factor immediately revitalizes function. Moreover, transduction of hepatocytes in cirrhotic animals with apparently irreversible decompensated function produced a profound and immediate improvement in hepatic function. Normalization of function took place in two weeks. It is likely

that cytokine/injury effects alter expression of the hepatocyte transcription factor network by extrinsic mechanisms, with the result that network factors establish a new steady-state equilibrium in the dysfunctional hepatocyte that can no longer compensate to restore normal gene expression. This possibility has important therapeutic implications, because it may require only transient therapy with HNF4α to restore the transcription factor network once the injury has been moderated. These studies suggest that in addition to regeneration mediated by expansion of mature hepatocytes or differentiation and expansion of induced progenitors, normalized function can be accomplished by transcriptional reprograming with reversal of de-differentiation but not senescence. The results also suggest HNF4α therapy could be effective in treating advanced liver cirrhosis with impaired hepatic function as a bridge to organ transplantation or possibly even as destination therapy. We will examine whether this therapy is effective in human hepatocytes from end-stage cirrhotic livers. If so, they may also be useful as a source of hepatocytes for cell therapy.

Technical Objective #2: To determine the extent to which transplantation with human hepatocytes can reverse hepatic failure in a clinically relevant non-human primate model of this process.

Hypothesis: Human hepatocytes derived from human cadaver donors or possibly from human stem cells can reverse hepatic failure.

2.1. Acute hepatic failure in a non-human primate model.
We have treated two additional non-human primates (NHP) with whole liver radiation therapy followed by total parenteral nutrition (TPN) in preparation for transplantation studies. The work has now been incorporated in a manuscript that has been submitted for publication (**Yannam GR, et al. Tolerable limits to whole liver irradiation in non-human primates. Int. Journal of Radiation Oncology, Biology, Physics. In Revision**).

Unfortunately, there has been a small setback in the ability to complete the transplant studies. The first NHP was irradiated with a dose of 40Gy to the whole liver. For logistical reasons, we delayed instituting TPN to induce acute liver failure. This has not been an issue in the past. In this case, however, it resulted in generating unanticipated non-lethal radiation induced liver disease (RILD) in the animal, which altered the architecture and vascular structure of the liver. We isolated human hepatocytes from several repopulated FRG mice to transplant into this animal, as outlined in the grant proposal. Because of the altered vascular structure we visualized severe shunting during the course of the hepatocyte transplant procedure by contrast imaging. Thus, no cells could be engrafted. The animal was electively euthanized and the liver histology confirmed the RILD and failure to engraft cells because of the altered vascular architecture. A dose of 35Gy to the whole liver was used on a second NHP. This dose was successful and the second animal was electively euthanized when we had determined that the RT dose was effective at ultimately inducing acute liver failure but did not lead to RILD.

Once the issue had been resolved we proceeded with an additional NHP transplant experiment for the treatment of acute liver failure. An animal was irradiated with a dose of 35Gy to the whole liver. The monkey was then transplanted through the inferior mesenteric vein with one billion hepatocytes. After the transplant, the 18G catheter was pulled and the mesenteric vein was ligated. The monkey recovered from the surgery, but his condition deteriorated afterwards in the first 24 hours. At autopsy, massive blood accumulation was found

in the abdomen of this animal. It appeared that the bleeding was from the inferior mesenteric vein, the site where cells were infused. Since this was a serious technical problem, a number of protocol issues were modified and team assignments were changed. Unfortunately, there was too much change in personnel after the procedure, and the senior technician in the lab with experience in NHP research left for a more senior position at Yerkes National Primate Center in Atlanta. When adequate personnel are available we will perform additional monkey transplant studies.

KEY RESEARCH ACCOMPLISHMENTS:

1. Engraftment and proliferation of human hepatocytes in immune-deficient FAH k/o transgenic (FRG) mice. Data supports our hypothesis that excellent quality human hepatocytes can be recovered from patients treated with chemotherapy and with end-stage cirrhosis.

2. Identification of a key transcription regulator of hepatocyte function in end-stage decompensated hepatocytes from cirrhotic livers.

3. Demonstration that re-expression of HNF4$\square$ in decompensated cirrhotic hepatocytes leads to normalization of function in vitro and in vivo. Ongoing studies, not shown, are examining whether this finding applies to human livers with hepatic failure.

4. Optimization of the non-human primate model of acute liver failure.

5. Isolation of an adequate supply of human hepatocytes from repopulated FRG mice for transplantation in NHP with acute liver failure.

REPORTABLE OUTCOMES:

1. Liu,L, Yannam GR, Nishikawa T, Yamamoto T, Basma H, Ito R, Nagaya M, Dutta-Moscato J, Stolz DB, Duan F, Kaestner KH,Vodovotz Y, Soto-Gutierrez A, Fox IJ.The microenvironment in hepatocyte regeneration and function in rats with advanced cirrhosis. Hepatology 2012;55(5):1529-39.

2. Zhou H, Dong X, Kabarriti R, Chen Y, Avsar Y, Wang X, Ding J, Liu L, Fox IJ, Roy-Chowdhury J, Roy-Chowdhury N, Guha C. Single liver lobe repopulation with wildtype hepatocytes using regional hepatic irradiation cures jaundice in Gunn rats. PLoS One 2012;7(10):e46775.

3. Nishikawa T, Bell A, Brooks JM, Setoyama K, Kaestner KH, Vodovotz Y, Locker J, Soto-Gutierrez A, Fox IJ. Resetting the transcription network using a single factor reverses liver failure in end-stage cirrhosis. Journal of Clinical Investigation (In revision).

4. Yannam R, Han B, Setoyama K, Yamamoto T, Ito R, Brooks JM, Guzman-Lepe J, Galambos C, Fong JV, Deutsch M, Quader MA, Yamanouchi K, Mehta K, Soto-Gutierrez A, Roy-Chowdhury J, Locker J, Abe M, Enke CA, Baranowska-Kortylewicz J, Solberg TB, Guha C, Fox IJ. Tolerable limits to whole liver irradiation in non-human primates. (Int. Journal of Radiation Oncology, Biology, Physics. In Revision).

5. Setoyama K, Fong JV, Han B, Ito R, Nagaya M, Ross M, Fukumitsu K, Gramignoli R, Rosensteel S, Strom SC, Stolz DB, Quader MA,Deutsch M, Baskin KM, Roy-Chowdhury J, Guha C, Soto-Gutierrez A, Fox IJ. 10-15% donor cell liver repopulation in non-human primates by low dose directed (right lobe) radiation therapy: a preclinical study. Hepatology 2011;54(S1):172A.

6. Yannam GR, Han B, Setoyama K, Yamamoto T, Ito R, Brooks JM, Guzman-Lepe J, Galambos C, Fong JV, Deutsch M, Quader MA, Yamanouchi K, Mehta K, Soto-Gutierrez A, Roy-Chowdhury J, Locker J, Abe M, Enke CA, Baranowska-Kortylewicz J, Solberg TD, Guha C, Fox IJ. Tolerable limits to whole liver irradiation in non-human primates. Hepatology 2012;56(S1):972A-973A.

7. NishikawaT, Bellance N, Damm A, Soto-Gutierrez A, Fox IJ, Nagrath D. Changes in Glycolysis are an Important Mechanism for Maintaining Cell Survival in Hepatic Failure in Advanced Cirrhosis. Hepatology 2012;56(S1):785A-786A.

8. Taichiro Nishikawa; Jenna M. Brooks; Yoram Vodovotz; Alejandro Soto-Gutierrez; Aaron W. Bell; Ira J. Fox 1284. Rescue of hepatic function in rats with advanced cirrhosis and end-stage liver failure following delivery of HNF4a. Hepatology 2012;56(S1):800A-801A.

9. Gramignoli R, Dorko K, Tahan V, Skvorak KJ, Ellis E, Jorns C, Ericzon BG, Fox IJ, Strom SC. Hypothermic storage of human hepatocytes for transplantation. Cell Transplant. 2013 Jun 13.

10. Gramignoli R, Tahan V, Dorko K, Skvorak KJ, Hansel MC, Zhao W, Venkataramanan R, Ellis EC, Jorns C, Ericzon BG, Rosenborg S, Kuiper R, Soltys KA, Mazariegos GV, **Fox IJ**, Wilson EM, Grompe M, Strom SC. New potential cell source for hepatocyte transplantation: discarded livers from metabolic disease liver transplants.Stem Cell Res. 2013 Jul;11(1):563-73.

11.   Invited Speaker, Research Seminar Series in Developmental and Regenerative Biology, University of Kansas Medical Center, "Use of hepatocytes and stem cells to study and treat liver disease", Kansas City, Kansas, November 9-10, 2011.

12.   Keynote Speaker, ISMRM Workshop on MRI-based cell tracking "Hepatocyte transplantation and the need to track engrafted cells", Miami Beach, Florida, January 29 – February 1, 2012.

13.   Invited Speaker, American Society of Gene & Cell Therapy 15th Annual Meeting, "Overcoming barriers to successful cell therapy to treat liver disease", Philadelphia, PA May 16-19, 2012

14.   Moderator, Mid-day Symposium: "Allotransplants, Cellular Transplants, Organ Repair, and Xenotransplants? A Debate about the Future of Organ Transplantation", American Transplant Congress, Boston, MA, June 2-6, 2012.

15. Invited Speaker, Liver Biology: Fundamental Mechanisms & Translational Application, FASEB Summer Research Conference, "Hepatocyte, stem cell transplantation, tissue engineering", Snowmass Village, Colorado, July 29 – August 3, 2012.

16. Invited Speaker, 8th Royan International Congress on Stem Cell Biology and Technology, "Overcoming barriers to the use of hepatocytes and stem cells in treating patients with liver diseases" and "Use of hepatocytes and stem cells in understanding and treating liver failure and cirrhosis", Tehran, Iran, September 5-7, 2012.

17. Invited Speaker, Masters of Surgery lecture series, Montefiore Medical Center, The University Hospital for Albert Einstein College of Medicine, "Bench to bedside: finding alternatives to organ transplantation for patients with life-threatening liver disease", New York, NY, November 4-5, 2012.

18. Faculty Member, American Association for the Study of Liver Diseases 2012 Postgraduate Course, "Tissue engineering and liver cell replacement – liver stem cells on the horizon", Boston, MA, November 10, 2012.

19. Invited Speaker, 23rd Conference of the Asian Pacific Association for the Study of the Liver (APASL 2013), "Future strategies for cellular transplantation", Singapore, June 6-10, 2013.

20. Invited Speaker, 19th Annual International Congress of ILTS, "Liver regeneration and hepatocyte repopulation", Sydney, Australia, June 14, 2013.

21. Invited Speaker, Cell Transplant Society, "Hepatocyte transplantation and regeneration in the treatment of liver disease", Milan, Italy, July 7-10, 2013.

22. Invited Speaker, AASLD/NASPGHAN Pediatric Symposium, The Liver Meeting 2013, "Pros and cons of hepatocyte transplantation for treatment of liver-based metabolic disease", Washington, DC, November 1, 2013.

CONCLUSIONS:

The outcomes of our studies are being accomplished.

RhoA signaling regulates heterotopic ossification and fatty infiltration in dystrophic skeletal muscle

Xiaodong Mu, Arvydas Usas, Ying Tang, Aiping Lu, Jihee Sohn, Bing Wang, Kurt Weiss, and Johnny Huard
Stem Cell Research Center, Department of Orthopaedic Surgery, University of Pittsburgh

Introduction: Frequent heterotopic ossification (HO) or fatty infiltration is observed in the dystrophic muscle of many animal models of human Duchenne muscular dystrophy (DMD); however, little is known about the correlated molecular mechanisms involved in the process. The RhoA-Rho kinase (ROCK) signaling pathway has been shown to function as a commitment switch of the osteogenic and adipogenic differentiation of mesenchymal stem cells (MSCs). Activation of RhoA-ROCK signaling in cultured MSCs *in vitro* induces their osteogenesis but inhibits the potential of adipogenesis, while the application of Y-27632, a specific inhibitor of ROCK, reversed the process. Inflammation has been shown to be one of main contributors to HO, while the role of RhoA signaling in inflammation reaction has been demonstrated. The objective of the current study is to investigate the potential role of RhoA signaling in regulating HO and fatty infiltration in dystrophic skeletal muscle.

Methods: 1.Mice models: Animal experiments were approved by IACUC of University of Pittsburgh. mdx mice (dystrophin-deficient) and dKO (Dystrophin/Utrophin double knockout) mice are both important mouse models of DMD; however, in contrast to the mild phenotype of mdx mice, dKO mice display a far more severe phenotype as is observed in human DMD patients, including a much shorter life span (~ 8 weeks compared to 2 years), more necrosis and fibrosis in the skeletal muscle, etc. 2. Tissue histological analysis: The gastrocnemius muscles (GM) of the mice were used for histological analysis. Alizarin red stain shows calcium deposition caused by HO or during osteogenic differentiation, Oil Red O stain shows fatty infiltration in muscle or fat cells, and Trichrome stain shows fibrosis. 3. Statistics: N >=6 for each group in animal study. Student's T-test was used to evaluate the significance.

Results: 1. Skeletal muscle of dKO mice features more HO but less fatty infiltration than mdx mice (Fig. 1). Both µ-CT scan of animals (**Fig. 1A**) and Alizarn Red stain (**Fig. 1B**) of the muscle tissues revealed greatly enriched HO in the dystrophic muscles of the dKO mice. While, Oil Red O stain (**Fig. 1C**) and Trichrome stain **(Fig. 1D)** of the muscle tissues revealed reduced fatty infiltration and a number of normal muscle fibers in the muscle of dKO mice.

2. RhoA signaling is more activated in both skeletal muscle and muscle-derived stem cells (MDSCs) from dKO mice. Both semi-quantitative PCR and immunohistochemistry study demonstrated that RhoA signaling is more activated in the muscles of dKO mice, as well as dKO MDSCs.

3. *In vitro* RhoA inactivation of cultured MDSCs from dKO mice decreases the osteogenesis potential and increases adipogenesis and myogenesis potential (Fig. 2). Semi-quantitative PCR study showed that Y27632 treatment *(*10 µM) of dKO-MDSCs down-regulated the expression of RhoA, BMP2 and 4, and inflammatory factors such as TNF-α and IL-6 (**Fig. 2A**). Osteogenesis potential was repressed while the adipogenesis and myogenesis potential of the dKO-MDSCs were increased by Y27632 (**Fig. 2B**).

4. RhoA inactivation in the skeletal muscle of dKO mice decreased HO and increased both fatty infiltration and muscle regeneration. GM muscles of 6 dKO mice were injected with Y27632 (5mM in 20µL of DMSO) (left limb) or control (20µL of DMSO) DMSO (right limb). Injections were conducted 3 times a week for 3 weeks. The skeletal muscles that received Y27632 injection demonstrated much slower development of HO and improved muscle regeneration, as well as reduced fibrosis formation.

Discussion: Our current results revealed that DMD mouse models featuring different severity of muscular dystrophy may have varied potentials for developing HO or fatty infiltration in the dystrophic muscle, and RhoA signaling might be a critical mediator of the determining these differential fates, including the progression towards HO, fatty infiltration, or normal muscle regeneration. RhoA inactivation is shown to have a great potential to repress HO and improve the phenotypes of dystrophic muscle. The status of RhoA activation in the skeletal muscle of human DMD patients and the potential effect of RhoA inactivation in human dystrophic muscle requires further investigation.

Significance: Our data reveals the involvement of RhoA signaling in regulating the process of heterotopic ossification, and indicates that RhoA may serve as a potential target for repressing injury-induced and congenital heterotopic ossification in humans.
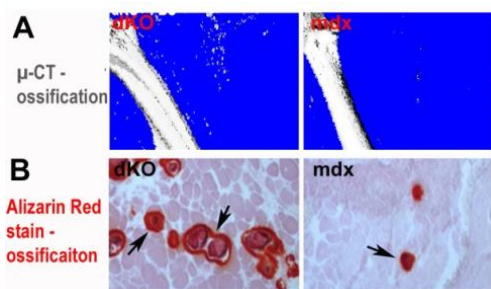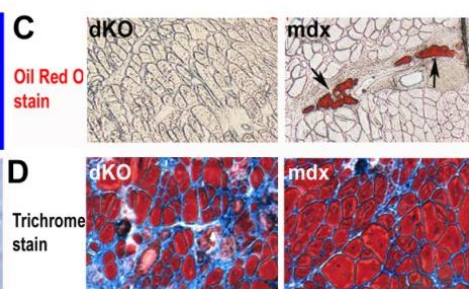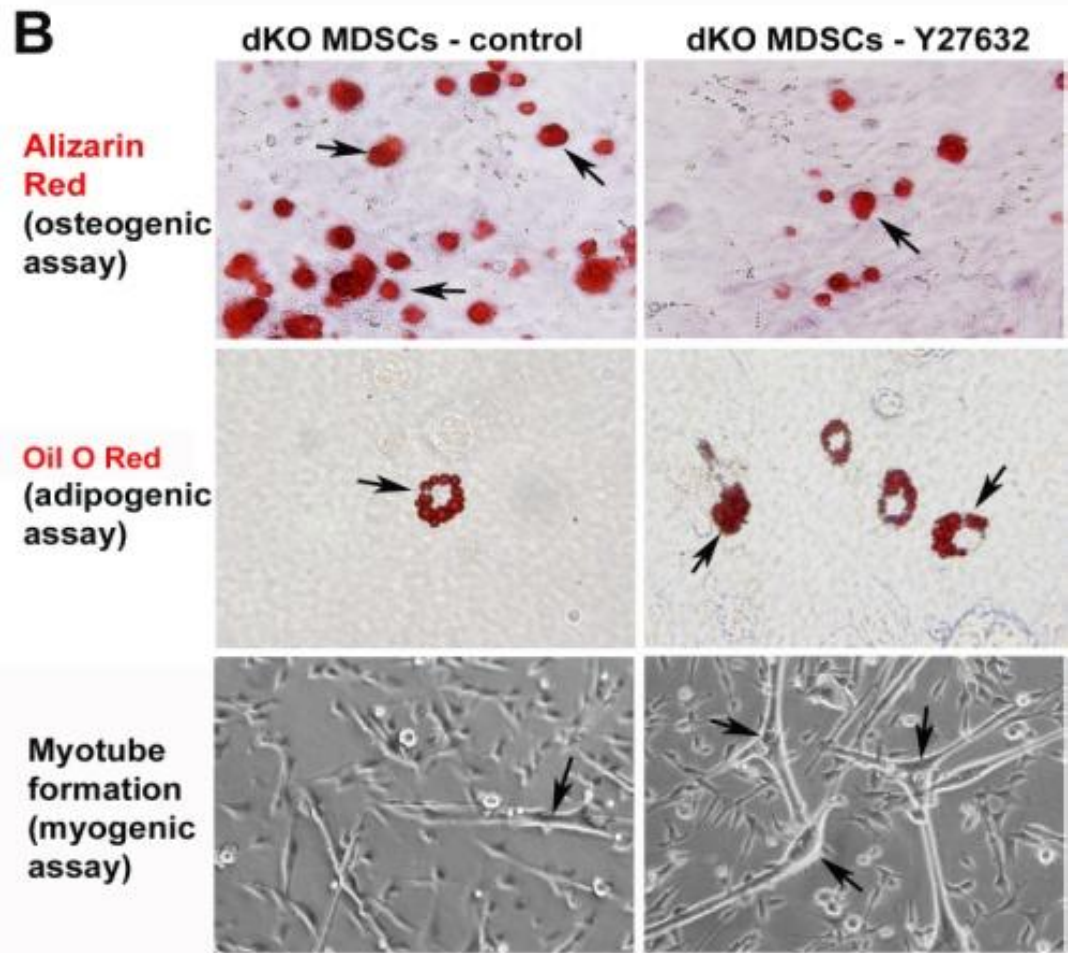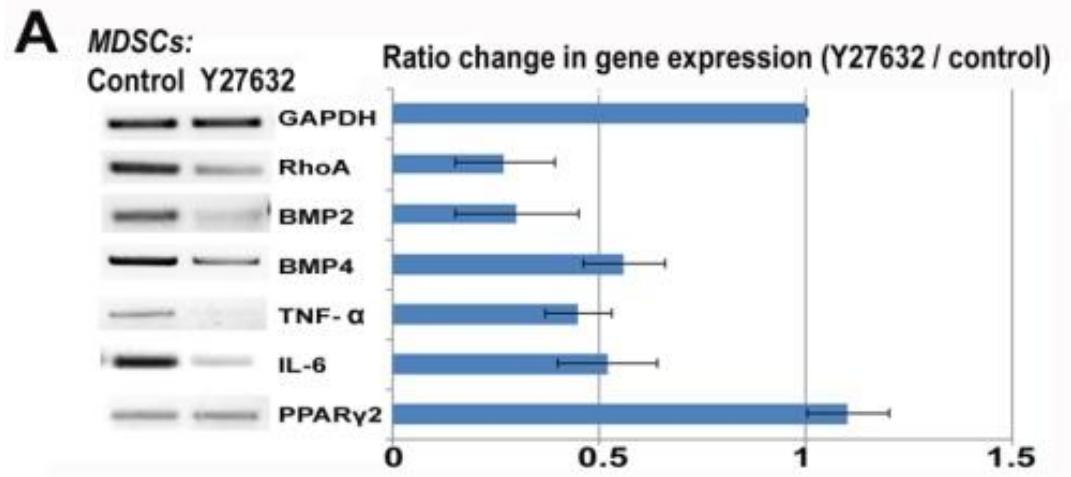
Fig 1   Fig 2

A — µ-CT - ossification: dKO, mdx
B — Alizarin Red stain - ossificaiton: dKO, mdx
C — Oil Red O stain: dKO, mdx
D — Trichrome stain: dKO, mdx

A

MDSCs: Control Y27632

Ratio change in gene expression (Y27632 / control)

GAPDH
RhoA
BMP2
BMP4
TNF- α
IL-6
PPARγ2

0   0.5   1   1.5

B

| | dKO MDSCs - control | dKO MDSCs - Y27632 |

Alizarin Red (osteogenic assay)

Oil O Red (adipogenic assay)

Myotube formation (myogenic assay)

RhoA inactivation represses BMP-induced heterotopic ossification (HO) in skeletal muscle and potential for HO treatment

Xiaodong Mu, Kurt Weiss, and Johnny Huard

Stem Cell Research Center, Department of Orthopaedic Surgery, University of Pittsburgh

Introduction: HO is a process where bone tissue forms in soft tissues which can be caused by trauma, neurologic injury *and* genetic abnormalities; however, little is known about the molecular regulatory mechanisms that cause HO. The RhoA-Rho kinase (ROCK) signaling pathway has been shown to function as a commitment switch of the osteogenesis and adipogenesis differentiation of mesenchymal stem cells (MSCs), and is involved in regulating myogenesis differentiation of muscle cells. Activation of RhoA-ROCK signaling in cultured MSCs *in vitro* induces their osteogenic differentiation but inhibits their potential for adipogenic differentiation, while the application of Y-27632, a specific inhibitor of ROCK, can reverse the process. An important role of RhoA in myogenic differentiation has also been demonstrated and the activation of the RhoA pathway can block muscle differentiation by inhibiting myoblast fusion. Inflammation has been shown to be one of main contributors to HO, while the role of RhoA signaling in inflammation has also been demonstrated. The objective of the current study was to discern whether the inactivation of RhoA signaling can improve muscle regeneration by repressing BMP-induced HO in injured skeletal muscle.

Methods: 1. Induction of HO and RhoA inactivation: The gastrocnemius muscles (GM) of C57BL/6J mice were injected with cardiotoxin. Two days later the muscles were co-injected with BMP2 and Y27632 (RhoA inhibitor) (left limb) or with BMP2 only. Four days later, the muscle tissues were harvested for histological analysis. 2. Tissue histological analysis and *in vitro* differentiation assay. Alizarin red stain was conducted to stain calcium deposition caused by HO, and immunostaining of dystrophin was conducted to show myofibers. Alkaline phosphatase *(*ALP*)* and Alizarin red stain was used for in vitro osteogenesis assay in osteogenic medium, and the progression of myotube formation in the myogenic medium was tracked by counting the number of myotubes. 3. Statistics: N >=6 for each group of animal study. Student's T-test was used to evaluate the significance.

Results: 1. *In vitro* inactivation of RhoA decreases osteogenic potential and increases the myogenic potential of muscle-derived stem cells (MDSCs) (Fig. 1). *In vitro* osteogenesis and myogenesis assays showed that, Y27632 treatment *(*10 µM) of MDSCs isolated from skeletal muscle greatly repressed their osteogenic differentiation **(Fig. 1A, B)** in osteogenic medium, but promoted their myogenic differentiation in myogenic medium **(Fig. 1C).**

2. *In vivo* inactivation of RhoA in the skeletal muscle of mice decreased BMP-induced HO and improved muscle regeneration (Fig. 2). The GM muscles of 6 C57BL/6J mice were injured by cardiotoxin 2 days before being injected with BMP2 +Y27632 (left limb) or BMP2 only (right limb). 4 days after Y27632 administration, skeletal muscles that received Y27632 injection demonstrated a much slower development of HO **(Fig. 2A)**, and improved muscle regeneration **(Fig. 2B)**.

Discussion: Our current results revealed that the RhoA signaling pathway may mediate BMP-induced HO in skeletal muscle. RhoA activity appears to be elevated by BMPs and mediates BMP-induced osteogenesis, and RhoA inactivation could therefore repress BMP-induced HO in injured skeletal muscle. RhoA activity was shown to be positive for osteogenesis of muscle stem cells and negative for myogenesis, therefore, inactivation of RhoA could serve to repress HO formation while promoting myofiber development in the injured muscle. The detailed mechanisms of RhoA signaling in regulating HO require further investigation.

Significance: Our data revealed that RhoA signaling is involved in regulating the process of heterotopic ossification and indicated that RhoA may serve as a potential target for repressing injury-induced and congenital heterotopic ossification in humans.
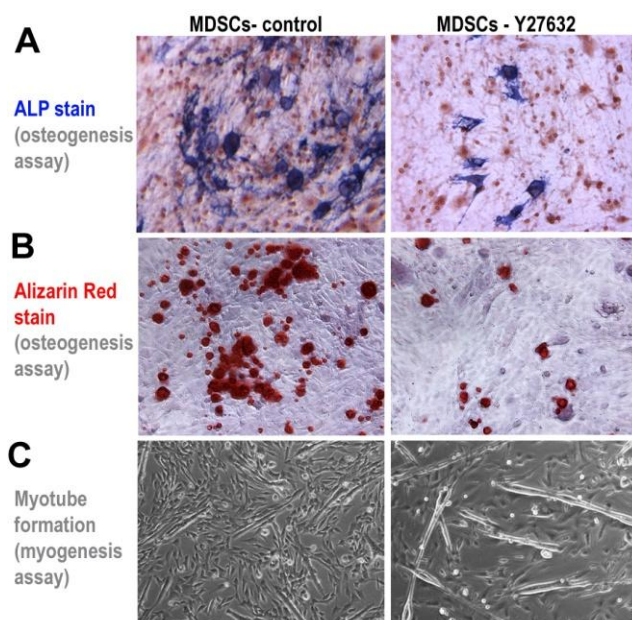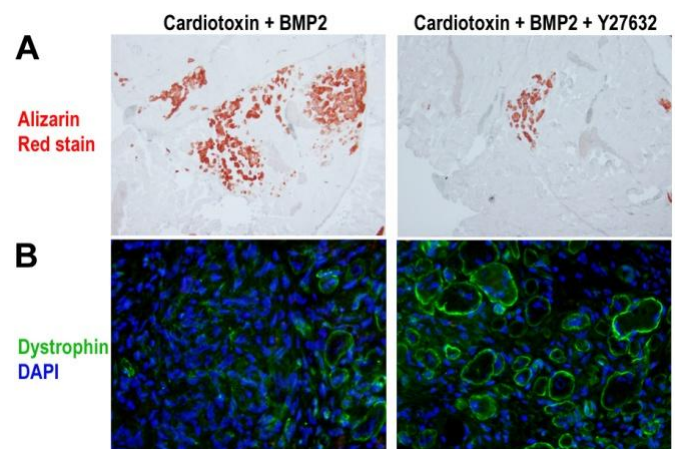
Fig 1   Fig 2

STEM CELLS Journal

Copy of e-mail Notification

STEM CELLS Co-Published by AlphaMed Press and Wiley-Blackwell

Dear Author,

YOUR PAGE PROOFS ARE AVAILABLE IN PDF FORMAT; please refer to this URL address
http://115.111.50.156/jw/retrieval.aspx?pwd=8ef55f617f63

Login: your e-mail address
Password: 8ef55f617f63

The site contains 1 file. You will need to have Adobe Acrobat Reader software to read these files. This is free
software and is available for user downloading at http://www.adobe.com/products/acrobat/readstep.html.

This file contains:

e-annotation Tools Instructions

Reprint Order Information

Publication Fee Form

A copy of your page proofs for your article

Please read the page proofs carefully and:

1) indicate changes or corrections using the e-annotation editing instructions at the front of the page proof packet;
2) answer all queries
3) proofread any tables and equations carefully;
4) check that any special characters have translated correctly.
5) complete Publication Fee Form and return with page proof corrections, if not previously returned.

Special Notes:

We strongly encourage you to return your corrections electronically to jrnlprod.STEM@cenveo.com. If you would
prefer to fax your corrections, please send them to 717 738 9478.

Please return your corrections within 48 hours to avoid a delay in the publication of your article. Thank you for your
cooperation.

Return to:

Production Editor, STEM

# USING e-ANNOTATION TOOLS FOR ELECTRONIC PROOF CORRECTION

Required software to e-Annotate PDFs: <u>Adobe Acrobat Professional</u> or <u>Adobe Reader</u> (version 8.0 or above). (Note that this document uses screenshots from <u>Adobe Reader X</u>)
The latest version of Acrobat Reader can be downloaded for free at: <u>http://get.adobe.com/reader/</u>

Once you have Acrobat Reader open on your computer, click on the Comment tab at the right of the toolbar:

📝	💾	🖨	✉	⬆	⬇	1 / 27	⊖	⊕	70.4% ▾		💾	⤢ ▾	Tools	Comment	Share
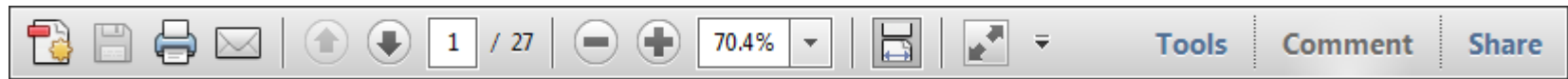
This will open up a panel down the right side of the document. The majority of tools you will use for annotating your proof will be in the Annotations section, pictured opposite. We've picked out some of these tools below:

▾ Annotations

💬 📝 📎 🔊 👤 ▾

T̂ T̂ T̄ T̲ T̂

---
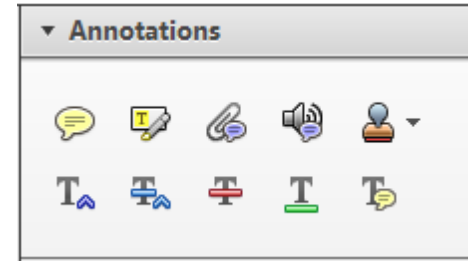
1. Replace (Ins) Tool – for replacing text.

Strikes a line through text and opens up a text box where replacement text can be entered.

How to use it

- Highlight a word or sentence.
- Click on the Replace (Ins) icon in the Annotations section.
- Type the replacement text into the blue box that appears.

ıdard framework for the analysis of m
icy. Nevertheless, it also led to exoge
ıle of strategi_____n fı
ıber of comp   o
: is that the st   of
ıain compo   be
level, are exc   nd
important works on entry by Onıro
.M henceforth)[1] we open the 'black

> **dthreshe**
> 08/06/2011 15:58:17
> , which led

---

2. Strikethrough (Del) Tool – for deleting text.

Strikes a red line through text that is to be deleted.

How to use it

- Highlight a word or sentence.
- Click on the Strikethrough (Del) icon in the Annotations section.

. there is no room for extra profits aı
k ups are zero and the number of
ket) values are not determined by
Blanchard ~~and Kiyotaki~~ (1987),
rfect competition in general equilil
ts of aggregate demand and supply
lassical framework assuming monoj
een an exogenous number of firms

---

3. Add note to text Tool – for highlighting a section to be changed to bold or italic.

Highlights text in yellow and opens up a text box where comments can be entered.

How to use it

- Highlight the relevant section of text.
- Click on the Add note to text icon in the Annotations section.
- Type instruction on what should be changed regarding the text into the yellow box that appears.

namic responses of mark ups
ent with the **VAR** evidence

sation_____ith
y Ma_____ell
ı and_____led
on n_____ber
to a_____on
stent also with the demand-

> **dthreshe**
> 08/06/2011 15:31:38

---

4. Add sticky note Tool – for making notes at specific points in the text.

Marks a point in the proof where a comment needs to be highlighted.

How to use it

- Click on the Add sticky note icon in the Annotations section.
- Click at the point in the proof where the comment should be inserted.
- Type the comment into the yellow box that appears.

land and supply shocks. Most of
a💬mi_____eti
numbe_____iff
dard fr_____sis
cy. Nev_____o
ıle of st_____wo
ıber of competitors and the imp
is that the structure of the secto

> **dthreshe**
> 08/06/2011 15:18:08

# USING e-ANNOTATION TOOLS FOR ELECTRONIC PROOF CORRECTION

5. Attach File Tool – for inserting large amounts of text or replacement figures.

Inserts an icon linking to the attached file in the appropriate pace in the text.

How to use it

- Click on the Attach File icon in the Annotations section.
- Click on the proof to where you'd like the attached file to be linked.
- Select the file to be attached from your computer or network.
- Select the colour and type of icon that will appear in the proof. Click OK.
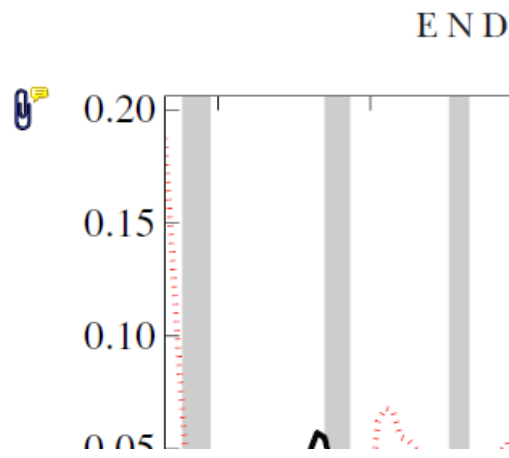
6. Add stamp Tool – for approving a proof if no corrections are required.

Inserts a selected stamp onto an appropriate place in the proof.

How to use it

- Click on the Add stamp icon in the Annotations section.
- Select the stamp you want to use. (The Approved stamp is usually available directly in the menu that appears).
- Click on the proof where you'd like the stamp to appear. (Where a proof is to be approved as it is, this would normally be on the first page).
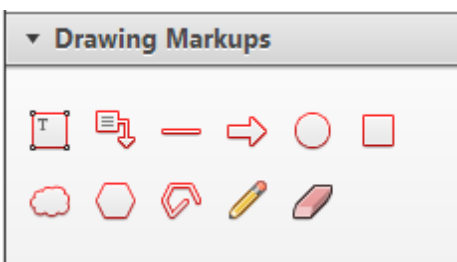
7. Drawing Markups Tools – for drawing shapes, lines and freeform annotations on proofs and commenting on these marks.

Allows shapes, lines and freeform annotations to be drawn on proofs and for comment to be made on these marks..

How to use it

- Click on one of the shapes in the Drawing Markups section.
- Click on the proof at the relevant point and draw the selected shape with the cursor.
- To add a comment to the drawn shape, move the cursor over the shape until an arrowhead appears.
- Double click on the shape and type any text in the red box that appears.
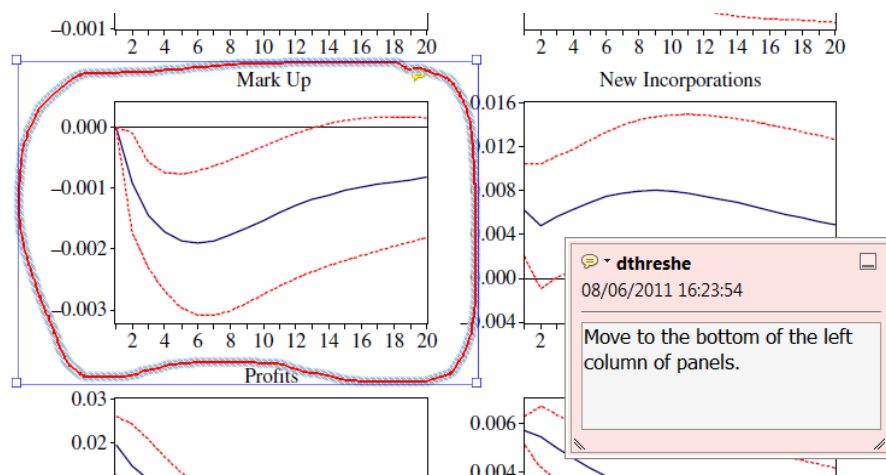
For further information on how to annotate proofs, click on the Help menu to reveal a list of further options:

WILEY-BLACKWELL
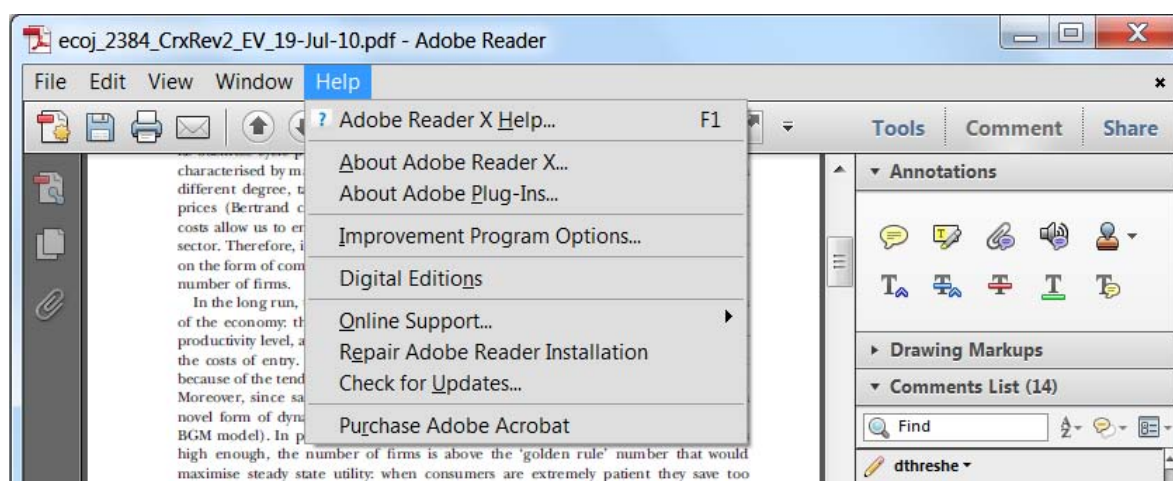
Additional reprint purchases

Should you wish to purchase additional copies of your article, please click on the link and follow the instructions provided:
https://caesar.sheridan.com/reprints/redir.php?pub=10089&acro=STEM

Corresponding authors are invited to inform their co-authors of the reprint options available.

Please note that regardless of the form in which they are acquired, reprints should not be resold, nor further disseminated in electronic form, nor deployed in part or in whole in any marketing, promotional or educational contexts without authorization from Wiley. Permissions requests should be directed to mail to: permissionsus@wiley.com

For information about 'Pay-Per-View and Article Select' click on the following link: wileyonlinelibrary.com/aboutus/ppv-articleselect.html

STEM CELLS®

WILEY-BLACKWELL
AlphaMed Press

PUBLICATION FEE FORM

Proffered manuscripts that are accepted for publication will be assessed a publication fee of $2,000, which includes all page charges and any applicable color charges. The author agrees to pay this fee to the Publisher within 30 days of receiving the Publisher's invoice. If an author is unable to support this publication fee, it is his or her responsibility to inform the Publisher at the time of manuscript submission. (Letters to the Editor and invited manuscripts are exempt from the publication fee.)

Please return this form with your corrected proofs to: Production Editor, e-mail: jrnlprod.STEM@cenveo.com

JOURNAL **Stem Cells** VOLUME _____ ISSUE _____

TITLE OF
MANUSCRIPT _____

NO. OF

MS. NO. _____ PAGES _____ AUTHOR(S) _____

Invited material is not subject to publication charges.

Flat Publication Fee $ 2000.00 US _____

International orders must be paid in currency and drawn on a U.S. bank

Please check one: ☐ Check enclosed ☐ Bill me ☐ Credit Card

If credit card order, charge to: ☐ American Express ☐ Visa ☐ MasterCard

Credit Card No _____ Signature _____ Exp. Date _____

BILL TO:

Name _____

Institution _____

Address _____
_____
_____

Phone: _____ Fax: _____

E-mail: _____

STEM CELLS®

REGENERATIVE MEDICINE

Human Pericytes for Ischemic Heart Repair

CHIEN-WEN CHEN,[a,b,c] MASAHO OKADA,[b,c] JONATHAN D. PROTO,[b,c,d] XUEQIN GAO,[b,c] NAOSUMI SEKIYA,[b,c,e] SARAH A. BECKMAN,[b,c,d] MIRKO CORSELLI,[f] MIHAELA CRISAN,[g] ARMAN SAPAROV,[h] KIMIMASA TOBITA,[i,j,k] BRUNO PÉAULT,[f,l] JOHNNY HUARD[b,c,k]

[a]Department of Bioengineering, [b]Department of Orthopedic Surgery, [c]Stem Cell Research Center, [d]Department of Pathology, [e]Department of Surgery, [i]Department of Pediatrics, [j]Department of Developmental Biology, [k]McGowan Institute for Regenerative Medicine, University of Pittsburgh, Pittsburgh, Pennsylvania, USA; [f]UCLA Orthopaedic Hospital, Department of Orthopaedic Surgery, and the Orthopaedic Hospital Research Center, University of California at Los Angeles, Los Angeles, California, USA; [g]Erasmus MC Stem Cell Institute, Department of Cell Biology, Rotterdam, The Netherlands; [h]Center for Energy Research, Nazarbayev University, Astana, Kazakhstan; [l]Centre for Cardiovascular Science and Centre for Regenerative Medicine, University of Edinburgh, Edinburgh, United Kingdom

AQ2

ABSTRACT

Human microvascular pericytes (CD146+/34−/45−/56−) contain multipotent precursors and repair/regenerate defective tissues, notably skeletal muscle. However, their ability to repair the ischemic heart remains unknown. We investigated the therapeutic potential of human pericytes, purified from skeletal muscle, for treating ischemic heart disease and mediating associated repair mechanisms in mice. Echocardiography revealed that pericyte transplantation attenuated left ventricular dilatation and significantly improved cardiac contractility, superior to CD56+ myogenic progenitor transplantation, in acutely infarcted mouse hearts. Pericyte treatment substantially reduced myocardial fibrosis and significantly diminished infiltration of host inflammatory cells at the infarct site. Hypoxic pericyte-conditioned medium suppressed murine fibroblast proliferation and inhibited macrophage proliferation in vitro. High expression by pericytes of immunoregulatory molecules, including interleukin-6, leukemia inhibitory factor, cyclooxygenase-2, and heme oxygenase-1, was sustained under hypoxia, except for monocyte chemotactic protein-1. Host angiogenesis was significantly increased. Pericytes supported microvascular structures in vivo and formed capillary-like networks with/without endothelial cells in three-dimensional cocultures. Under hypoxia, pericytes dramatically increased expression of vascular endothelial growth factor-A, platelet-derived growth factor-β, transforming growth factor-β1 and corresponding receptors while expression of basic fibroblast growth factor, hepatocyte growth factor, epidermal growth factor, and angiopoietin-1 was repressed. The capacity of pericytes to differentiate into and/or fuse with cardiac cells was revealed by green fluorescence protein labeling, although to a minor extent. In conclusion, intramyocardial transplantation of purified human pericytes promotes functional and structural recovery, attributable to multiple mechanisms involving paracrine effects and cellular interactions. Stem Cells 2012; 000:000–000

AQ3

Disclosure of potential conflicts of interest is found at the end of this article.

INTRODUCTION

Coronary heart disease (CHD) is the leading cause of death in the United States, affecting 16.3 million people and accounting for one of every three deaths in 2007 [1]. Prolonged pathological interference with the coronary blood supply, such as atherosclerosis and thromboemboli, results in ischemic cardiomyopathy and/or myocardial infarction (MI) [2]. MI often leads to heart failure (HF) due to the limited capacity of the human heart to repair/regenerate its damaged myocardium [2, 3]. As an alternative to heart transplantation, stem/progenitor cell therapy (SCT) is deemed promising for restoration of cardiac function and prevention of progressive HF [3, 4]. In particular, human bone marrow precursor cells, endothelial progenitor cells, skeletal myoblasts, and endogenous cardiac progenitor cells have been intensively investigated with uneven success in preclinical and clinical trials [3–6]. Given the vascular origin of CHD pathology, stem/progenitor cells capable of reconstituting host vascular networks, in addition to other merits, will be ideal cell sources for SCT.

AQ11

Microvascular pericytes (aka mural cells or Rouget cells) that tightly encircle capillaries and microvessels (arterioles and venules) and regulate microvascular physiology have recently been shown to contain precursor cells endowed with mesodermal differentiation potential [7]. Pericytes (CD146+/34−/45−/56−) purified by cell sorting from human skeletal muscle, adipose, placenta, pancreas, and other organs repair and regenerate damaged/defective tissues [8–12] and represent the CD146-positive developmental origin of the heterogeneous mesenchymal stem/stromal cells (MSCs) [12–16]. Owing to their wide distribution in the microvasculature, pericytes are regarded as a promising and attractive source of precursor cells for regenerative medicine [17–19]. We hypothesize SCT with purified pericytes to be a suitable approach for the treatment of ischemic heart disease (IHD) [20].

Besides cardiomyogenesis, cardioprotective mechanisms, including antifibrosis, anti-inflammation, and neovascularization, play critical roles in SCT-mediated cardiac repair following ischemic insults [21–23]. SCT reduces myocardial fibrosis and induces favorable tissue remodeling in the ischemic heart, which in turn increases myocardial compliance/strength and prevents the progressive, pathological decline toward HF [24, 25]. This antifibrotic feature was attributed in part to increased collagen degradation by matrix metalloproteinases (MMPs) and inhibition of fibroblast activation, possibly through a paracrine mechanism [26, 27]. Additionally, the immunosuppressive/anti-inflammatory capacity of MSCs through secretion of immunoregulatory molecules has recently attracted clinical attention in organ transplantation and immune regulation [28, 29]. Whether pericytes possess similar antifibrotic and immunoregulatory capacities within the ischemic microenvironment remains to be addressed.

To relieve the underlying cause of IHD, SCT-based approaches toward myocardial revascularization have been extensively pursued [30, 31]. Due to their native vascular localization and secretion of trophic factors that are associated with tissue repair and vascular growth/remodeling, pericytes may restore injured vascular networks more efficiently [18]. Proangiogenic signaling molecules released by stem/progenitor cells stimulate neovascularization in ischemic tissues [31]. Additionally, cell–cell interaction between vascular mural cells and endothelial cells was lately suggested to play essential roles in blood vessel remodeling and maturation [32, 33]. Whether pericytes mediate revascularization of the ischemic myocardium through any of these two mechanisms has yet to be tested.

AQ4   In this study, we investigated the therapeutic potential of purified human skeletal muscle pericytes in IHD, using an acute MI model in immunodeficient mice. Transplantation of pericytes not only reversed cardiac dilatation but also improved cardiac contractility. Major repair mechanisms were investigated, including reduction of fibrosis, inhibition of chronic inflammation, promotion of angiogenesis, and regeneration of the myocardium. We further describe putative mediators used by pericytes. Green fluorescence protein (GFP) labeling was used to track perivascular homing and lineage fate of transplanted pericytes. Our results demonstrate that the overall benefit of pericyte treatment is collectively attributed to multiple cardioprotective mechanisms that involve paracrine and direct cell–cell interactions.

MATERIALS AND METHODS

Human Tissue Biopsies and Cell Isolation

In total, three independent human skeletal muscle specimens (one adult and two fetal) were used for cell isolation. The procurement of adult muscle biopsies from the National Dis-

ease Research Interchange was approved by the Institutional Review Board (IRB) at the University of Pittsburgh. Muscle biopsies (male subject, 57 years old) were preserved in Dulbecco's modified Eagle's medium (DMEM) containing 1% antibiotics and transported to the laboratory on ice. Human fetal tissues (21 and 23 weeks of gestation) were obtained following voluntary pregnancy interruptions performed at Magee Womens Hospital, Pittsburgh, in compliance with IRB protocol 0506176. Informed consents for the use of fetal tissues were obtained from all patients. Cells were mechanically and enzymatically dissociated from muscle biopsies following the reported protocol [12]. Details are described in Supporting Information.

Fluorescence-Activated Cell Sorting and Flow Cytometry Analysis

Fluorescence-activated cell sorting (FACS) and flow cytometry were used to purify microvascular pericytes (CD146+/34−/45−/56−) and examine cell lineage marker expression, respectively, as we previously reported [12]. Details are documented in Supporting Information.

Cell Culture and Cell Labeling

Sorted pericytes were expanded in reported culture conditions [12]. Single donor-derived human umbilical cord vein endothelial cells (HUVECs, Lonza) were cultured in endothelial cell growth medium-2 (EGM-2, Lonza). Cultured pericytes   AQ5
were labeled with GFP following a published protocol [12], using a lentivirus-based CMV-driven eGFP-expression vector.   AQ6
For short-term experiments, cells were labeled with cell membrane dyes, PKH26 (red) and PKH67 (green) (both from Sigma-Aldrich, St. Louis, MO, http://www.sigmaaldrich.com), and used immediately without further expansion.   AQ7

Cell Transplantation in an Acute MI Model

The Institutional Animal Care and Use Committee at Children's Hospital of Pittsburgh and University of Pittsburgh approved the animal usage and surgical procedures (Protocol#37-04, 55-07, 0901681A-5). A total of 78 male NOD/SCID mice (Jackson Laboratory) were used. MI induction (by ligation of left anterior descending coronary artery) and intramyocardial cell injection (3×10^5 cells per heart) were performed by a blinded surgeon as previously reported [34]. Control mice received injections of 30 μl phosphate-buffered saline (PBS).

Evaluation of Cardiac Function by Echocardiography

Mice were anesthetized with isoflurane, and transthoracic echocardiography was performed by a blinded investigator repeatedly before and after surgery (at 2 and 8 weeks), using a high resolution ultrasound system (Vevo 770, Visual Sonics), as described previously [34]. Mice which died prior to 8 weeks postinjection were excluded. Echocardiographic measurements are listed in Supporting Information.

Histological and Immunohistochemical Analyses

At 1, 2, and 8 weeks after surgery, hearts were harvested and processed as previously described [34]. Cryosections at 6–8 μm thickness were used for histological and immunohistochemical analyses following published protocols [34]. Anti-GFP immunofluorescent staining was performed on 4% paraformaldehyde-fixed sections. Donor cell engraftment and perivascular homing were quantified on serial sections stained with anti-GFP antibody (Abcam, Cambridge, U.K., http://www.abcam.com) and dual-stained with anti-GFP/anti-mouse CD31 (BD Biosciences, San Diego, CA, http://www.bdbiosciences.com) antibodies,

respectively, using Image J. The engraftment ratio was defined as the extrapolated total number of engrafted GFP-positive cells to the initial 3×10^5 cells injected. Perivascular homing ratio was defined as the extrapolated number of GFP-positive cells juxtaposing CD31-positive mouse endothelial cells to the extrapolated total number of engrafted cells. Using Masson's trichrome staining (San Marcos), fibrotic area fraction and infarct wall thickness were estimated from six randomly selected sections at comparable infarct levels per heart as previously described [34]. Quantification of host angiogenesis and chronic inflammation was computed from 6–10 randomly selected images taken from the designated area in sections stained with anti-mouse CD31 and anti-mouse CD68 (Abcam) at the midinfarct level, respectively. Experimental details are documented in Supporting Information.

Hypoxia Assay and Enzyme-Linked Immunosorbent Assay

To simulate the lower oxygen tension at the tissue level, physiologically or pathologically, pericytes were cultured under 2.5% O_2 hypoxic conditions (with 5% CO_2 and 92.5% N_2)as formerly described [34]. Cells were washed twice before defined, serum-free DMEM medium was added upon the transition to low O_2 conditions. Culture supernatant and cell lysates were collected 24 hours later. Cells cultured under 21% O_2 (normoxia) served as controls. The secretion of vascular endothelial growth factor (VEGF), angiopoietin-1 (Ang-1), Ang-2, and transforming growth factor (TGF)-β1 in the culture supernatant was measured by respective enzyme-linked immunosorbent assay (ELISA) with human VEGF (Invitrogen, Carlsbad, CA, http://www.invitrogen.com), Ang-1, Ang-2, and TGF-β1 (all from R&D Systems, Minneapolis, MN, http://www.rndsystems.com) ELISA Kits.

Real-Time Quantitative Polymerase Chain Reaction and Semi-Quantitative Real Time Polymerase Chain Reaction

Real-time quantitative polymerase chain reaction (rt-qPCR) was performed as previously reported [9]. Total RNA ($n = 6$) was extracted for cDNA synthesis. The quantitative analyses were performed in the core facility at the University of Pittsburgh. All data are presented as expression level normalized to human cyclophilin (in arbitrary fluorescence units). For semi-quantitative RT-PCR (sqRT-PCR), total RNA ($n = 3$) was extracted using RNeasy plus-mini-kits (Qiagen, Hilden, Germany, http://www1.qiagen.com). From each sample, 500 ng of total RNA was reverse transcribed, followed by PCR. The intensity of the product bands was calculated using Quantify-One software and normalized to β-actin. The primer sequences are listed in Supporting Information Table T1 and T2.

In Vitro Vascular Network Formation

Cell culture/coculture experiments using two-dimensional (2D) and three-dimensional (3D) Matrigel systems were performed to observe the capillary-like network formation. For 2D culture, 5×10^4 pericytes or HUVECs were seeded onto Matrigel-coated well and incubated for 24 hours. For 3D culture, 25×10^4 pericytes or HUVECs were resuspended in EGM-2 medium and mixed with Matrigel in a 3:1 ratio. The Matrigel plug was subsequently incubated for 72 hours. Equal numbers of dye-labeled pericytes and HUVECs were well mixed in 2D or 3D coculture for 72 hours to observe pericyte–HUVEC interactions.

Measurement of Cell Proliferation

Murine RAW264.7 monocyte/macrophage cells (ATCC) or primary murine skeletal myoblasts, muscle fibroblasts, and cardiac fibroblasts were cultured with normoxic or hypoxic pericyte-culture conditioned medium, or with serum-free control medium, for 72 hours. Cell proliferation was measured by the absorbance at 490 nm after incubation with CellTiter Proliferation Assay Reagent (Promega, Madison, WI, http://www.promega.com) for 3 hours. Experiments were performed in quadruplicates and repeated three times independently.

Statistical Analysis

All measured data are presented as mean $\pm$ SE. Kaplan-Meier survival curve estimation with log-rank test was performed to compare the animal survival rate between treatment groups. Statistical differences were analyzed by Student's t test (two groups), one-way ANOVA (multiple groups), or two-way repeated ANOVA (repeated echocardiographic measurements) with 95% confidence interval. Statistical significance was set at $p < .05$. Student-Newman-Keuls multiple comparison test (or Bonferroni test if specified) was performed for ANOVA post hoc analysis. Statistical analyses were performed with SigmaStat 3.5 (Systat Software) and SPSS19 (IBM) statistics software.

RESULTS

Isolation and Transplantation of Human Pericytes

As reported in our previous studies [12], FACS was used to purify human microvascular pericytes (CD146$^+$/34$-$/45$-$/56$-$) to homogeneity from skeletal muscle biopsies of three donors (one adult and two fetal, designated as AP, FP1, and FP2, respectively), by their differential expression of cell lineage markers, including CD34 (endothelial/stem cells), CD45 (hematolymphoid cells), CD56 (myogenic cells), and CD146 (pericyte/endothelial cells) (Supporting Information Fig. S1). No phenotypical difference between adult and fetal pericytes was noted, consistent with our previous observations [12]. After in vitro expansion (25–35 cell doublings) and prior to transplantation, in all three pericyte populations, we have observed no alteration to their distinctive morphology as well as classic antigenic profile, including robust expression of CD146, alkaline phosphatase, and typical MSC markers: CD44, CD73, CD90, CD105 with the absence of CD34, CD45, and CD56 (Supporting Information Fig. S2A, S2B). Additionally, cell labeling (in subsequent experiments) did not alter pericyte phenotype (data not shown). Cells (3.0 $\times$ 10^5 cells per heart) resuspended in 30 μl PBS were injected into the acutely infarcted myocardium of immunodeficient mice. The control group received injections of 30 μl PBS following the induction of MI.

Human Pericyte Transplantation Improves Cardiac Function

The survival of animals receiving pericyte treatment or PBS injection was monitored over the course of 8 weeks (Kaplan-Meier survival curve, log-rank test $p = .529$, Fig. 1A). Cardiac function was assessed by echocardiography performed repeatedly before (healthy) and at 2 and 8 weeks after surgery (Supporting Information Fig. S3). Ischemic hearts injected with either of the three pericyte populations ($n = 8$ per donor) had significantly smaller left ventricular (LV) chamber size, as measured by LV end-diastolic area (LVEDA, Fig. 1B) and end-systolic area (LVESA, Fig. 1C), than the control group ($n = 8$)
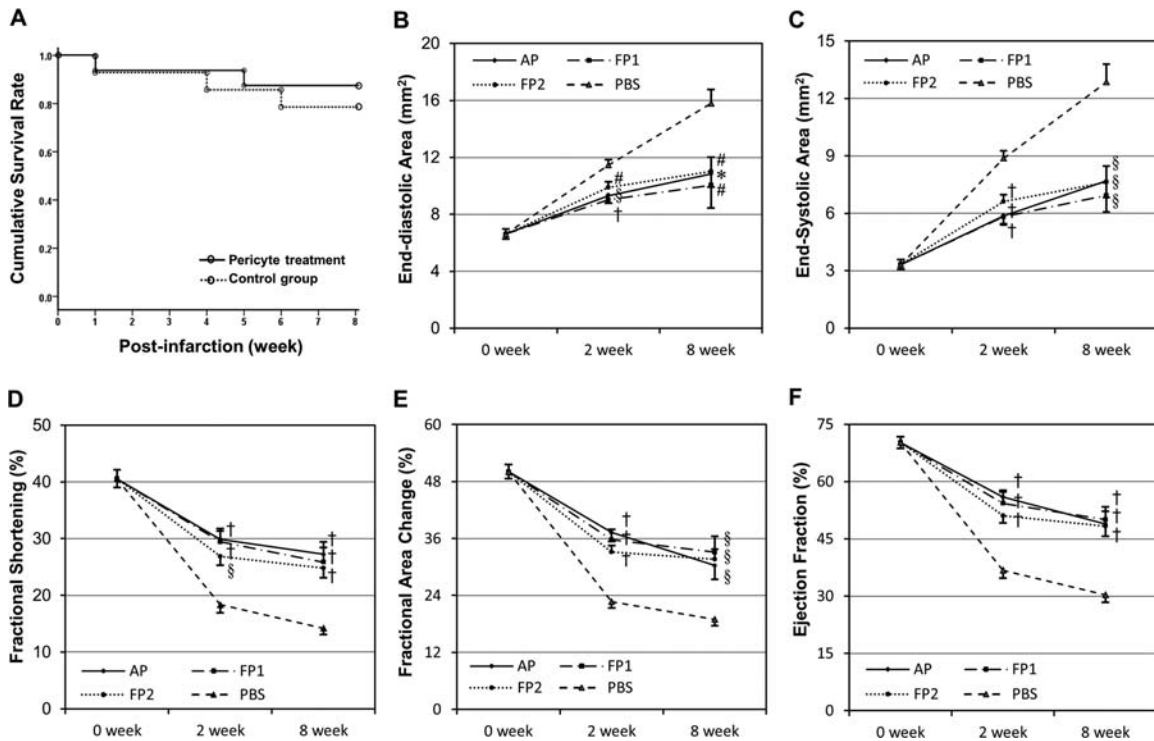
F1

Figure 1. Survival rate and cardiac functional assessment. (**A**): Cumulative survival rate of the animals over 8 weeks after surgery (Kaplan-Meier survival curve, log-rank test $p = .529$). Echocardiographic analyses revealed a significant reduction of left ventricular (LV) dilatation by transplantation of all three pericyte populations (AP, FP1, and FP2), as shown by the smaller LV area in end-diastole (**B**) and end-systole (**C**) of hearts at both time points. Injection of pericytes also resulted in substantial improvement in LV contractility, as indicated by greater fractional shortening (**D**), fractional area change (**E**), and ejection fraction (**F**), at both time points. (†, $p \leq .001$; §, $p \leq .005$; $^#$, $p \leq .01$; *, $p \leq .05$; vs. PBS control group at each time point). Abbreviation: PBS, phosphate-buffered saline.

(all $p < .05$), suggesting the reversal of progressive heart dilatation. Moreover, all pericyte-transplantation groups displayed significantly better LV contraction, evaluated by LV fraction shortening (LVFS, Fig. 1D), LV fractional area change (LVFAC, Fig. 1E), and LV ejection fraction (LVEF, Fig. 1F), than the control group (all $p < .05$). Collectively, when compared to vehicle treatment, pericyte treatment not only resulted in considerably smaller LV chamber dimension ($p < .001$, two-way repeated ANOVA) but also notably improved LV contractility ($p < .001$, two-way repeated ANOVA) for up to 2 months. Dimensional and functional echocardiographic parameters are documented in Supporting Information Table T3. In a separate experiment, we compared cardiac function of acutely infarcted hearts injected with either APs or CD56+ myogenic progenitors, sorted from a single adult muscle biopsy. The echocardiographic results at 2 weeks postinfarction showed that pericyte-treated hearts ($n = 6$) have significantly better LV function than CD56+ progenitor-treated ones ($n = 6$) in five parameters examined, including LVEDA ($p = .004$), LVESA ($p = .002$), LVFS ($p = .003$), LVFAC ($p = .003$), and LVEF ($p \leq .001$) (Supporting Information Fig. S4).

Transplantation of Pericytes Reduces Cardiac Fibrosis

To understand the influence of pericyte treatment on cardiac fibrosis, we evaluated scar tissue formation using Masson's trichrome histological staining. At 2 weeks postinfarction, pericyte-treated hearts displayed less collagen deposition F2 (stained in blue/purple) at the ischemic area (Fig. 2A). Estimation of the total fibrotic tissue ratio unveiled a 45.3% reduction of cardiac fibrosis in the pericyte-injected myocardium ($n = 5$, 22.03% ± 1.81%) when comparing to saline-

injected controls ($n = 5$, 40.28% ± 2.15%) (Fig. 2B, $p \leq .001$), suggesting the antifibrotic efficacy of pericytes. Measurement of LV wall thickness at the center of the infarct indicated no significant difference ($p > .05$) between the pericyte group (0.255 ± 0.026 mm) and the PBS group (0.202 ± 0.040 mm), suggesting that pericytes had limited beneficial effects to reduce transmural infarct thinning following MI (Fig. 2C).

Paracrine Antifibrotic Effects of Pericytes Under Hypoxia

Oxygen tension within tissues, physiologically or pathologically, is considerably lower than the ambient oxygen concentration in vitro. To elucidate the mechanism involved in pericyte-mediated reduction of fibrosis, we mimicked, at least in part, the hostile hypoxic microenvironment that donor cells encounter within the ischemic myocardium by culturing pericytes under 2.5% oxygen for 24 hours in defined, serum-free medium. Pericytes cultured under 21% oxygen (normoxia) served as controls. We then performed a cell proliferation assay using primary murine skeletal muscle and cardiac fibroblasts as well as skeletal myoblasts cultured with pericyte-conditioned medium (P-CM). Cardiac fibroblast proliferation was significantly reduced when cultured in hypoxic P-CM, compared to normoxic P-CM ($p = .019$) (Fig. 2D). Muscle fibroblast proliferation exhibited the same inhibitory pattern ($p < .001$, hypoxic vs. normoxic P-CM) with normoxic P-CM showing a pro-proliferative effect over control serum-free medium ($p < .05$) (Fig. 2D). Neither of the two P-CMs had significant influence over skeletal myoblast proliferation ($p = .76$). One-way ANOVA with Bonferroni multiple comparisons was performed for statistical analysis. This suggests a
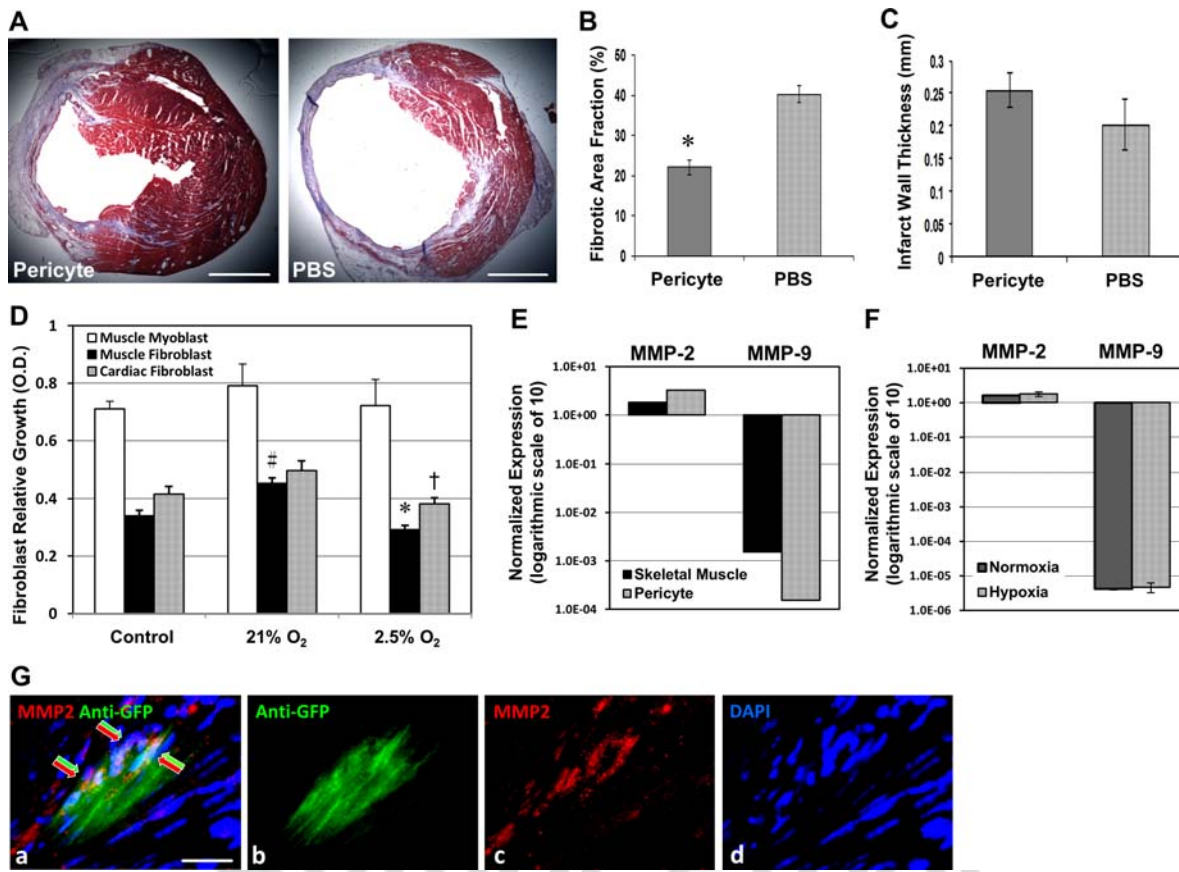
Figure 2. Attenuation of myocardial fibrosis by pericyte treatment. **(A):** Masson's trichrome-stained transverse sections of hearts injected with pericytes or PBS (collagen in blue/purple, cardiac muscle in red; scale bar = 1 mm). **(B):** The fibrotic area fraction was dramatically decreased in pericyte-injected hearts ($p \leq .001$). **(C):** Pericyte group had no significant increase in the infarct wall thickness. **(D):** When culturing with hypoxic pericyte-conditioned medium (P-CM), the proliferation of murine cardiac fibroblasts was significantly reduced (†, $p = .019$, vs. normoxic P-CM) while muscle fibroblast proliferation exhibited the same pattern (*, $p < .001$). Normoxic P-CM had a pro-proliferative effect over control medium in muscle fibroblasts but not in cardiac fibroblasts ($^{\#}$, $p < .05$). Skeletal myoblast proliferation was not significantly affected by either of the P-CMs. **(E):** Expression of MMP-2 in cultured pericytes was higher than that in skeletal muscle lysates. Conversely, MMP-9 expression in pericytes was nearly 10 times less (logarithmic scale of 10 in arbitrary fluorescence units). **(F):** Expression of both MMP-2 and -9 in pericytes did not change significantly under hypoxia ($p > .05$, logarithmic scale of 10 in arbitrary fluorescence units). **(G):** Immunohistochemistry revealed MMP-2 expression (red arrows) by some of the GFP-labeled donor pericytes (green arrows) within the infarct area at 2 weeks postinfarction (a) merge (b) anti-GFP in green (c) MMP-2 in red (d) DAPI nuclei staining in blue (scale bar = 20 μm). Abbreviations: DAPI, •••; GFP, green fluorescent protein; MMP, matrix metalloproteinase; PBS, phosphate-buffered saline.

paracrine antifibrotic effect by pericytes in hypoxia. We further proposed a fibrolytic role of pericyte-derived MMPs and examined gene expression of MMP-2 and MMP-9 by real-time qPCR. Cultured pericytes expressed more MMP-2 but nearly 10 times less MMP-9 than total skeletal muscle lysates (tissue origin control) (Fig. 2E). We then explored MMP expression in hypoxia-cultured pericytes and demonstrated that MMP-2 expression in pericytes was well sustained under 2.5% oxygen, compared to normoxic culture (Fig. 2F, $p > .05$), while MMP-9 expression remained extremely low without significant change (Fig. 2F, $p > .05$). Immunohistochemical study revealed that some of the transplanted pericytes within the infarct region expressed MMP-2 (Fig. 2G, a–d).

Transplantation of Pericytes Inhibits Chronic Inflammation

Histological analysis of pericyte- and PBS-injected hearts after hematoxylin and eosin staining indicated an increased focal infiltration of inflammatory cells (cluster of cells with dark blue-stained nuclei) within the infarct region in the latter

(Fig. 3A). To more precisely evaluate the immunomodulatory effect of pericyte transplantation, we detected host CD68-positive monocytes/macrophages by immunohistochemistry. Pericyte-injected hearts exhibited diminished infiltration of host phagocytic cells within the infarct region at 2 weeks postinfarction (Fig. 3B). Districts of the myocardium unaffected by the ischemic insult (posterior and septal walls) contained few CD68-positive cells in either group, similar to healthy hearts (Fig. 3C). Quantitatively, injection of pericytes ($n = 5$) resulted in a 34% reduction in infiltration of CD68-positive cells at 2 weeks postinfarction when compared to PBS controls ($n = 5$) (Fig. 3D, $p < .001$).

Paracrine Immunomodulation by Pericytes

To understand the underlying mechanism of pericyte-induced inhibition of phagocytic cell infiltration, we analyzed the proliferation of murine macrophages cultured with P-CM. Murine macrophage proliferation was significantly inhibited when culturing with both normoxic ($p = .018$) and hypoxic ($p < .001$) P-CM, compared to control medium (Fig. 3E). Furthermore,
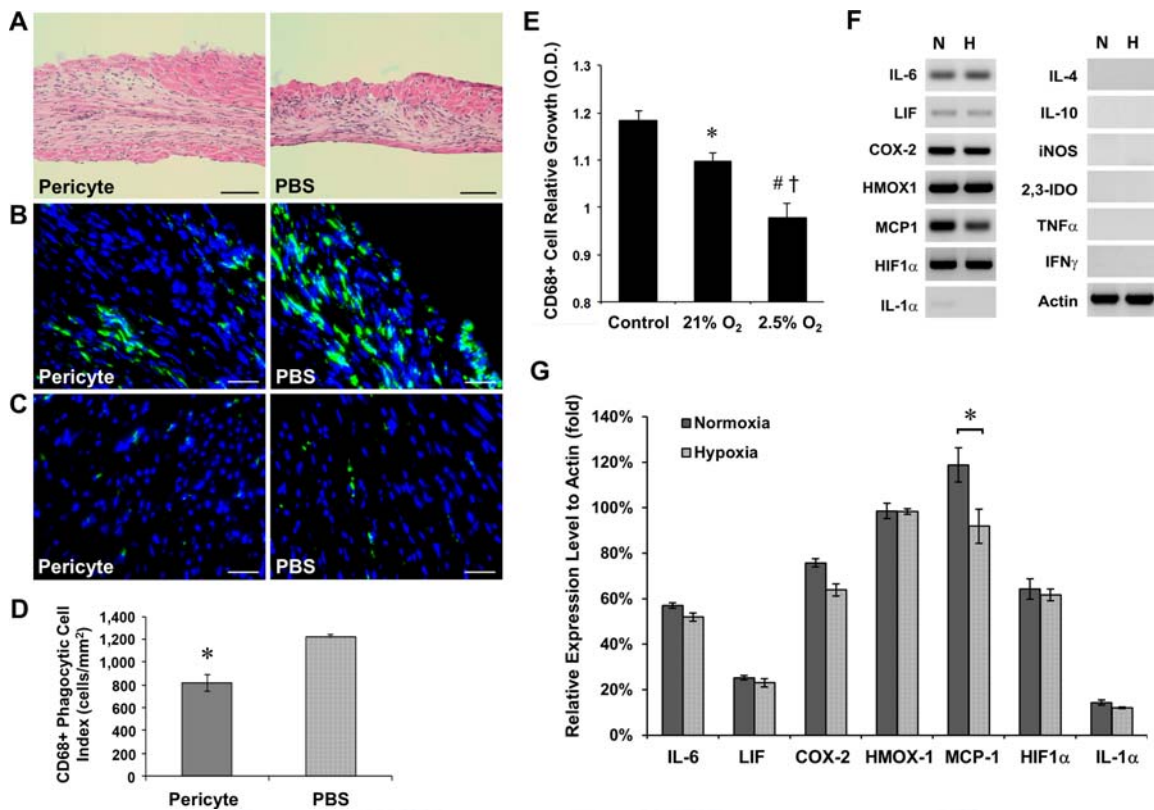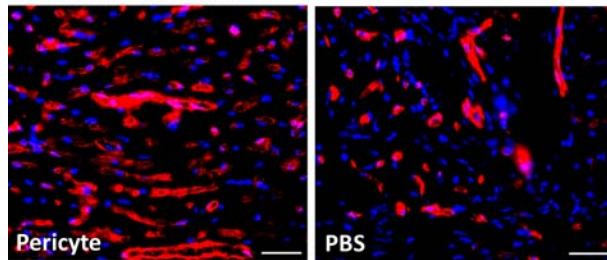
F3

Figure 3. Reduction of host phagocytic cell infiltration by pericyte transplantation. **(A):** Hematoxylin and eosin staining revealed a greater focal infiltration of leukocytes (dark blue-stained nuclei) within the infarct region in PBS-injected controls at 2 weeks postinfarction (scale bar = 100 μm). **(B):** Anti-mouse CD68 immunostaining showed that the infarct region of pericyte-injected hearts contains less host phagocytic cells (scale bar = 50 μm). **(C):** Host CD68-positive cells were locally attracted to the infarct region but not to the unaffected myocardium (posterior ventricular wall) in both groups (scale bars = 50 μm). **(D):** Host monocytes/macrophage infiltration at the infarct site was significantly reduced ($p <$ .001). **(E):** The proliferation of murine macrophages was significantly inhibited when culturing with pericyte-conditioned media (*, $p =$ .018; #, $p <$ .001, vs. control medium), an effect more prominent with hypoxic pericyte-conditioned medium (†, $p =$ .002, hypoxia vs. normoxia). **(F):** Cultured pericytes exhibited sustained, high expression of genes regulating the inflammatory responses, even under 2.5% O_2. Little expression of IL-1α and no expression of IL-4, IL-10, iNOS, 2,3-IDO, TNF-α, and IFNγ were detected. **(G):** No statistically significant difference in expression of genes of immunoregulatory molecules between normoxic- and hypoxic-cultured pericytes except MCP-1, which notably decreased in hypoxic cultures (semiquantitative real time polymerase chain reaction analysis, $p =$ .027). Abbreviations: COX-2, cyclooxygenase-2; HMOX-1, heme oxygenase-1; HIF-1α, hypoxia-inducible factor-1α; H, hypoxia)IL-6, interleukin-6; iNOS, inducible nitric oxide synthase; 2,3-IDO, indoleamine 2,3-dioxygenase; IFNγ, interferon-γ; LIF, leukemia inhibitory factor; MCP-1, monocyte chemotactic protein-1; N, normoxia; PBS, phosphate-buffered saline.

hypoxic P-CM exhibited a more prominent immunomodulatory effect than the normoxic counterpart (Fig. 3E, $p =$ .002). We then investigated by sqRT-PCR the differential expression of genes encoding immunoregulatory molecules that are potentially accountable for this paracrine immunomodulation by pericytes. Under either normoxia or hypoxia, pericytes indeed expressed a considerable array of anti-inflammatory cytokines: interleukin-6 (IL-6), leukemia inhibitory factor (LIF), cyclooxygenase-2 (COX-2/prostaglandin endoperoxide synthase-2), and heme oxygenase-1 (HMOX-1) (Fig. 3F). Similarly, monocyte chemotactic protein-1 (MCP-1) and hypoxia-inducible factor-1α (HIF-1α) were highly expressed by pericytes (Fig. 3F). Conversely, we detected very low to no expression of proinflammatory cytokines including IL-1α, tumor necrosis factor-α (TNF-α), and interferon-γ (IFNγ) (Fig. 3F). No expression of IL-4, IL-10, inducible nitric oxide synthase (iNOS), and indoleamine 2,3-dioxygenase (2,3-IDO) was observed (Fig. 3F). Quantitatively, there was no significant alteration of expression under hypoxia of immunoregulatory genes investigated, except MCP-1, whose expression was notably decreased in hypoxia-cultured pericytes (Fig. 3G, all $p >$ .05; MCP-1, $p =$ .027).

Transplanted Pericytes Promote Host Angiogenesis

We examined whether intramyocardial transplantation of pericytes restores the host vascular network postinfarction. Capillaries in the peri-infarct areas (Fig. 4A) and within the infarct region (Fig. 4B) were revealed by anti-mouse CD31 (platelet endothelial cell adhesion molecule-1) immunofluorescent staining and subsequently quantified. Capillary structure density in the peri-infarct areas of pericyte-injected hearts ($n =$ 5) was increased by 45.4% when compared to PBS-injected controls ($n =$ 5) (Fig. 4C, $p =$ .01). Higher microvascular density was also observed within the infarct region, with 34.8% more capillaries in the pericyte-treated hearts (Fig. 4C, $p =$ .002). Detection of the proliferating host endothelial cells (ECs) by Ki-67, a cell proliferation marker, and CD31 showed that pericyte-injected hearts ($n =$ 3) had significantly more proliferating ECs than PBS-injected controls ($n =$ 3) in both the infarct region ($p =$ .034) and peri-infarct areas ($p =$ .025) (Supporting Information Fig. S5A-S5C). These findings suggest that transplanted pericytes promote host angiogenesis not only in the peri-infarct areas, where blood vessels were generally better preserved after the ischemic injury, but also within the blood vessel-deprived infarct region.

F4

STEM CELLS

ID: **nareshrao** | Black Lining: **[ON]** | Time: **13:36** | Path: **N:/3b2/STEM/Vol00000/120293/APPFile/JW-STEM120293**
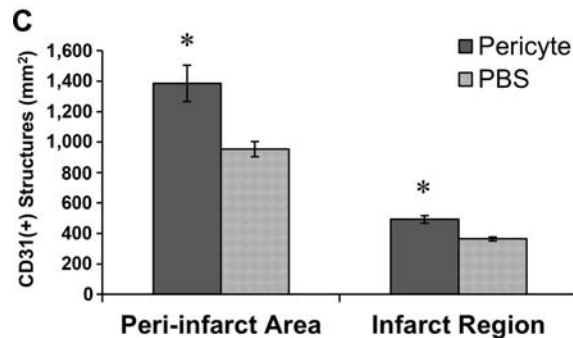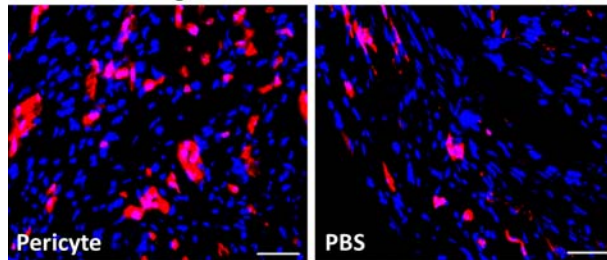
Chen, Okada, Proto et al. 7

Figure 4. Promotion of host angiogenesis by pericyte treatment. Representative images of anti-mouse CD31 immunostaining **(A)** in the peri-infarct area and **(B)** within the infarct region of hearts injected with pericytes or PBS (scale bar = 50 μm). **(C):** Pericyte-treated hearts displayed significantly higher capillary densities in the peri-infarct area ($p < .05$) and within the infarct region ($p < .001$). Abbreviation: PBS, phosphate-buffered saline.

Pericytes Support Microvascular Structures

To demonstrate that pericytes benefit host vascular networks through their support of microvascular structures, we developed 2D and 3D Matrigel cultures/cocultures using pericytes and HUVECs. HUVECs seeded onto Matrigel-coated wells formed typical capillary-like networks after 24 hours (Fig. 5A). Pericytes, however, formed similar structures within 6–12 hours of seeding (Fig. 5B). To illustrate the reciprocal influence between pericytes and endothelial cells (ECs), dye-labeled pericytes (PKH67, green) and HUVECs (PKH26, red) were mixed and cocultured in 2D Matrigel, which resulted in the formation within 6–12 hours of capillary-like structures that included both cell types (Fig. 5C). Pericytes (green) were observed to collocate with HUVECs (red) in the co-formed three-dimensional structures after incubation for 24 hours (Fig. 5C, inset). Additionally, HUVECs (red) appeared to morphologically align with pericytes (green) (Fig. 5D). To further unveil the vascular supportive role of pericytes, an in vitro 3D Matrigel system designed to simulate native capillary formation was used. HUVECs evenly distributed within the 3D Matrigel plug were unable to form organized structures after 72 hours (Fig. 5E). To the contrary, pericytes started to form capillary-like networks 24 hours after gel casting, with

structural remodeling over time (Fig. 5F). The dynamic interaction between pericytes and ECs was best depicted by encapsulating dye-labeled pericytes (green) and HUVECs (red) in a 3D Matrigel plug. Together these two types of cells formed capillary-like structures after incubation for 72 hours (Fig. 5G) with pericytes surrounding HUVECs (Fig. 5H). These data suggest that pericytes retained vascular cell features and formed structures supportive of microvascular networks even after purification and long-term culture, while pericyte–EC association may play a role in the pericyte-facilitated angiogenic process.

Differential Expression of Proangiogenic Factors and Associated Receptors by Pericytes Under Hypoxia

The paracrine angiogenic potential of pericytes in the ischemic heart was investigated using the simulated hypoxic environment in vitro. Expression of genes encoding proangiogenic factors and corresponding receptors was assessed by real-time qPCR. VEGF-A, platelet-derived growth factor-β (PDGF-β), and transforming growth factor (TGF)-β1 were notably upregulated by 307% ($p \leq .001$), 437% ($p = .067$), and 178% ($p = .037$), respectively, in pericytes cultured under hypoxic conditions (Fig. 6A). Expression of other proangiogenic factors, including basic fibroblast growth factor (bFGF), hepatocyte growth factor (HGF), and epidermal growth factor (EGF), was downregulated to 44% ($p < .05$), 23% ($p \leq .001$), and 60% ($p > .05$) of their expression levels in normoxia (Fig. 6A). On the other hand, VEGF receptor-1 (VEGFR-1/Flt-1) and -2 (VEGFR-2/KDR/Flk-1) were substantially upregulated by 458% ($p = .004$) and 572% ($p \leq .001$), respectively, under 2.5% oxygen (Fig. 6B). PDGF receptor-β (PDGF-Rβ) expression was not significantly changed (161%, $p > .05$) (Fig. 6B). VEGF secretion by pericytes, measured by ELISA, significantly increased over threefold ($p \leq .001$) under hypoxic culture conditions while Ang-1 secretion reduced by 35% ($p > .05$) (Fig. 6C). Very little secretion of Ang-2 by pericytes was detected under both conditions ($p > .05$) (Fig. 6C). Additionally, TGF-β1 secretion increased by 30.1% under hypoxia ($p = .028$) (Fig. 6C), consistent with its upregulated gene expression. The expression of human VEGF$_{165}$ by engrafted pericytes within the infarct region was confirmed by immunohistochemistry (Fig. 6D, a–c).

Transplanted Pericytes Home to Perivascular Locations

It is not known whether purified pericytes home back to perivascular areas in vivo. To reveal their engraftment and homing pattern, cultured pericytes were transduced with a GFP reporter gene at near 95% efficiency (Fig. 7A) and injected (3.0 × 10^5 cells) into acutely infarcted hearts. GFP-labeled pericytes engrafted throughout the ventricular myocardium (Fig. 7B), particularly in the peri-infarct area (Supporting Information Fig. S6). Many donor pericytes retained expression of NG2, a pericyte marker (Supporting Information Fig. S7). Confocal microscopy showed that a fraction of pericytes were identified in perivascular positions, adjacent to host CD31-positive endothelial cells (Fig. 7C). Indeed, pericytes were aligned with (Fig. 7C, main) or surrounding (Fig. 7C, inset) CD31-positive microvessels, suggestive of perivascular homing. The number of engrafted GFP-positive pericytes was approximately 9.1% ± 1.3% of total injected cells at the first week and declined over time to 3.4% ± 0.5% at 8 weeks post-infarction ($n = 3$ per time point) (Fig. 7D, dash-dot line). The perivascular homing rate instead increased from 28.6% to 40.1% over the course of 8 weeks, implicating the

F5

F6

F7

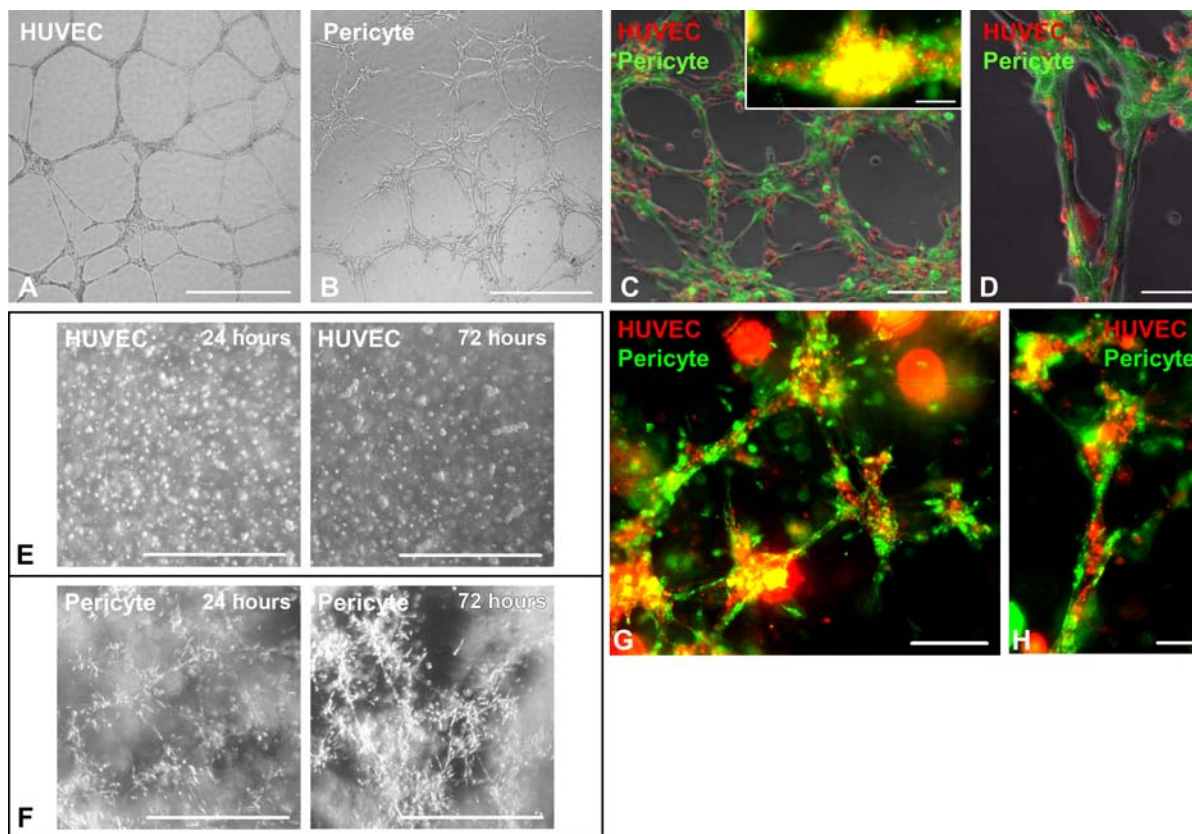C O L O R

C
O
L
O
R

Figure 5. Pericytes support microvascular structures. **(A):** While HUVECs seeded onto Matrigel-coated wells formed typical capillary-like networks after 24 hours, **(B)** pericytes formed similar structures within 6–12 hours (scale bar = 1 mm). **(C):** When cocultured on Matrigel, dye-labeled pericytes (green) and HUVECs (red) coformed capillary-like networks within 6–12 hours, (C, inset) with collocations of pericytes and HUVECs in three-dimensional structures formed 24 hours after seeding (scale bars: main = 200 μm; inset = 100 μm). **(D):** HUVECs (red) appear to line and spread out on top of the pericyte-formed structures (green) (scale bar = 100 μm). **(E):** To simulate native capillary formation, HUVECs were evenly encapsulated into 3D Matrigel plug for 72 hours but unable to form any organized structure (scale bars = 1 mm). **(F):** Pericytes instead formed capillary-like networks in Matrigel plug with structural organization and maturation over time (scale bar = 1 mm). **(G):** When dye-labeled pericytes (green) and HUVECs (red) were cocasted into the 3D-gel plug, the two types of cells formed microvessel-like networks within 72 hours, **(H)** with pericytes surrounding HUVECs (scale bars: (G) = 200 μm; (H) = 50 μm). Abbreviation: HUVEC, human umbilical cord vein endothelial cell.

merit of niche-homing for long-term donor cell survival (Fig. 7D, solid line). To demonstrate cellular interactions between donor pericytes and host ECs, we performed immunohistochemical studies for ephrin type-B receptor 2 (EphB2) and connexin43, a gap junction protein. Confocal images revealed that some GFP-positive pericytes juxtaposing host ECs expressed human-specific EphB2 (Fig. 7E) or formed gap junctions with ECs (Fig. 7F). These results suggest that cellular interactions between host ECs and donor pericytes homed to perivascular locations.

Cell Lineage Fate of Transplanted Pericytes

GFP-labeled pericytes were used to track cell lineages developed from donor pericytes and investigate the capacity of human muscle pericytes to reconstitute major cardiac cell types after injury. Immunohistochemistry was performed to simultaneously detect GFP and cell lineage markers: the cardiomyocyte marker, cardiac troponin-I (cTn-I); the smooth muscle cell marker, smooth muscle myosin heavy chain (SM-MHC); the endothelial cell (EC) marker, CD31. Confocal microscopy revealed that in the peri-infarct area, a minor fraction of transplanted pericytes coexpress GFP and cTn-I (Supporting Information Fig. S8A–S8C, main), a few of which appear single-nucleated (Supporting Information Fig. S8A–S8C, inset).

Some GFP-positive cardiomyocytes were identified within the remaining myocardium (Supporting Information Fig. S8D–S8F) with organized sarcomeric patterns (Supporting Information Fig. S8G–S8I). A very small number of donor pericytes coexpressed GFP and human-specific CD31 (<1%) (Supporting Information Fig. S8J-S8L). Similarly, coexpression of GFP and human-specific SM-MHC was detected in very few transplanted cells (<0.5%) (Supporting Information Fig. S8M–S8O). Negative control images were stained only with matching fluorescence-conjugated secondary antibodies (Supporting Information Fig. S8P–S8R).

DISCUSSION

Pericytes constitute a major structural component of small blood vessels, regulating vascular development, integrity, and physiology. The recent identification of microvascular pericytes as one of the native sources of MSC ancestors raised the possibility that these cells participate in the repair of injured/ageing organs [11–16, 35]. The therapeutic potential of microvascular pericytes was indicated by structural and functional regeneration of skeletal muscle involving direct pericyte differentiation into regenerative units as well as
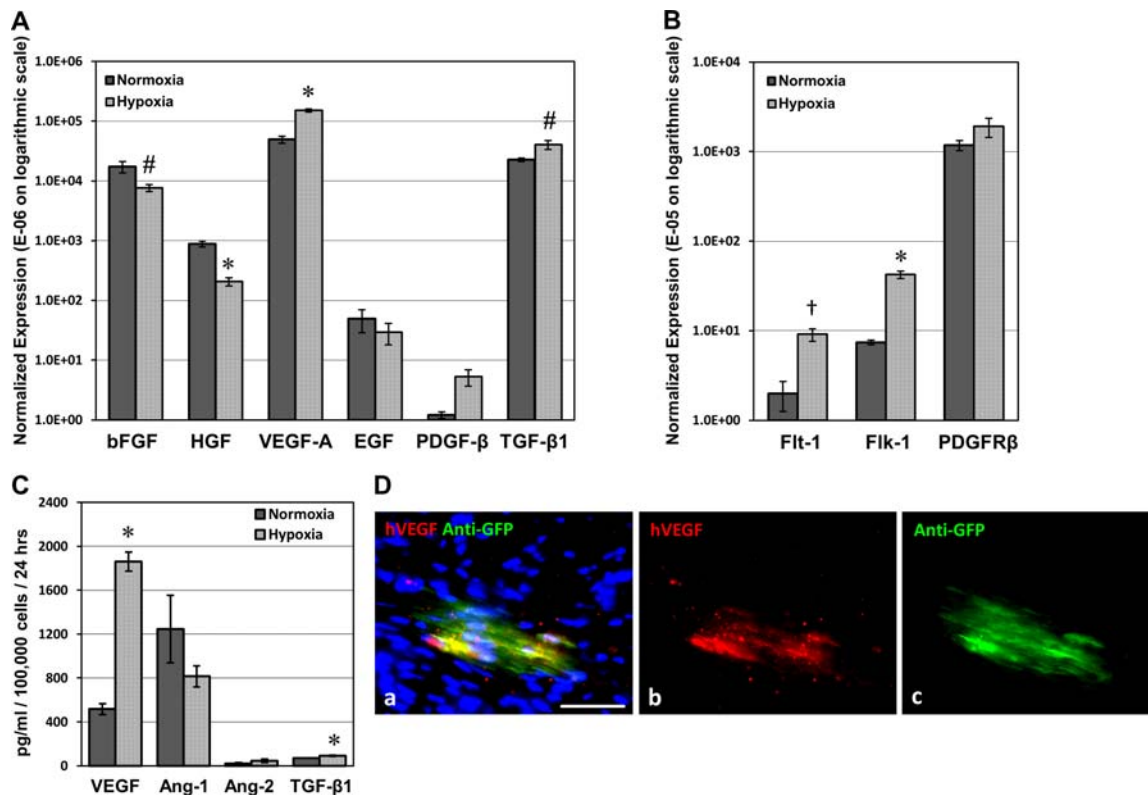
STEM CELLS

Figure 6. Expression of proangiogenic factors and associated receptors under hypoxia. **(A):** Pericytes dramatically upregulated VEGF-A, PDGF-β, TGF-β1 gene expression under hypoxic conditions (2.5% O_2) while expression of other proangiogenic factors, including bFGF, HGF, and EGF were distinctively repressed. **(B):** Simultaneously, VEGFR-1 (Flt-1) and -2 (Flk-1) were substantially upregulated, and PDGF-Rβ expression was moderately increased. All expression levels are normalized to human cyclophilin and presented in arbitrary fluorescence units on an expanded logarithmic scale (#, $p < .05$, *, $p \leq .001$; †, $p < .01$, hypoxia vs. normoxia). **(C):** Significantly increased secretion of VEGF ($p \leq .001$) and TGF-β1 ($p = .028$) by pericytes under hypoxic culture conditions was detected by ELISA while secretion of Ang-1 was reduced by 35% ($p > .05$). Very little secretion of Ang-2 was detected under both conditions ($p > .05$). **(D):** Immunohistochemistry revealed human VEGF$_{165}$ expression by GFP-labeled donor pericytes within the infarct area at 2 weeks postinfarction (a) merge (b) hVEGF$_{165}$ in red (c) anti-GFP in green (scale bar = 50 μm). Abbreviations: Ang-1, angiopoietin-1; bFGF, basic fibroblast growth factor; EGF, epidermal growth factor; GFP, green fluorescent protein; HGF, hepatocyte growth factor; PDGF, platelet-derived growth factor; PDGFR, PDGF receptor; TGF, transforming growth factor; VEGF, vascular endothelial growth factor.

applications in lung repair and vascular tissue engineering [8, 11, 12, 35, 36]. Pericytes can also repair tissue via secretion of trophic factors, implying broad usage in clinical settings [8, 18]. Recent studies indicated a possible developmental hierarchy among different stem/progenitor cell populations residing in the blood vessel walls [15, 37]. Katare et al. [38] reported that transplantation of adventitial progenitor cells repairs infarcted hearts through angiogenesis involving micro-RNA-132. Herein we demonstrate that transplantation of human FACS-purified microvascular pericytes contributes to the functional and structural repair of the ischemic heart, albeit unequally, through both paracrine effects and cellular interactions. A major goal of SCT, the prevention of progressive LV dilatation and consequent HF, was largely achieved by pericyte treatment, implicating the attenuation of deleterious remodeling. We also observed significant improvement of cardiac contractility in an acute infarction milieu, with up to 70% of healthy contractile function consistently maintained for at least 2 months. No significant difference was observed between adult and fetal pericytes in terms of heart repair. The therapeutic benefits observed could be explained, at least in part, by antifibrotic, anti-inflammatory, angiogenic, and to a lesser extent, cardiomyogenic properties of pericytes.

The antifibrotic action of mesodermal stem/progenitor cells in the injured heart has been reported [25–27]. MSC-

conditioned medium diminished viability, proliferation, collagen synthesis, and α-SMA expression in cardiac fibroblasts but stimulated MMP2/9 activities, indicating a paracrine antifibrotic property of MSCs [26, 27]. Our results demonstrated a near 50% reduction of myocardial fibrosis following pericyte injection. Along with the attenuation of progressive LV dilatation, pericyte treatment appears to result in propitious remodeling, leading to improved myocardial compliance and strengthening of the ischemic cardiac tissue.

We speculated that decreased fibrosis/scar formation is, at least partially, associated with a reduced number of fibrotic cells resulting from the administration of pericytes. Interestingly, pericyte-treated hearts contained significantly less cells within the infarct area than PBS-injected controls ($p < .05$, Supporting Information Fig. S9A) with no statistical difference in Ki-67(+) proliferating cell density ($p = .808$, Supporting Information Fig. S9B). Additionally, TUNEL staining revealed no significant difference between pericyte- and PBS-injected hearts in the number of apoptotic cells within the infarct region ($p = .296$, Supporting Information Fig. S10A, S10B). Due to the highly fibrotic nature of MI, we were unable to quantitate fibrotic cells in vivo. Nevertheless, murine fibroblast proliferation was notably inhibited when cultured in hypoxic P-CM in vitro, indicating the paracrine fibrosuppressive effect of pericytes under hypoxia. MMPs were suggested to play
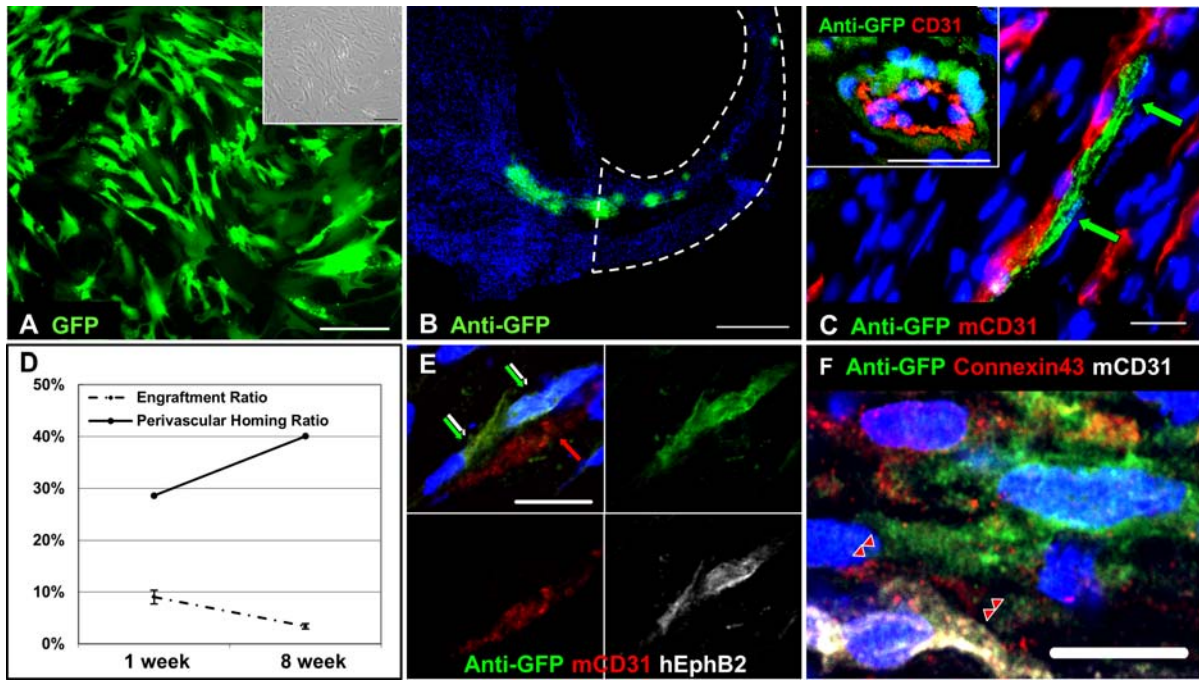
Figure 7. Transplanted pericytes home to perivascular locations. **(A):** Pericytes were transduced with GFP reporter at nearly 95% efficiency. Fluorescence (A, main) and bright-field (A, inset) images were taken from the same low-power field (scale bar = 200 μm). **(B):** Engraftment of GFP-labeled pericytes within host myocardium was revealed by anti-GFP immunostaining at 1 week postinjection (scale bar = 500 μm, infarct site encircled by dotted lines). **(C):** Pericytes were lining with (C, main) or surrounding (C, inset) host CD31-positive microvasculature (scale bar = 20 μm). **(D):** The engraftment efficiency of pericytes at 1 week (9.1% ± 1.3%) and 8 weeks (3.4% ± 0.5%) postinfarction was depicted (dash-dot line). The perivascular homing ratio instead increased from 28.6% to 40.1% and was delineated separately (solid line). Some GFP-positive pericytes juxtaposing host ECs **(E)** expressed human-specific EphB2 (green/white arrows) or **(F)** formed connexin43-positive gap junctions with endothelial cells (red arrow heads) (scale bar = 10 μm). Abbreviation: GFP, green fluorescent protein.

important roles in postinjury scar remodeling, angiogenesis, and vascular cell proliferation/migration [27, 39]. In particular, a preponderant role of MMP-2 in preventing collagen accumulation by cardiac fibroblasts was proposed [27]. Consequently, we postulated the existence of a fibrolytic activity from donor pericytes, involving MMPs, which contributes to the attenuation of cardiac fibrosis. Indeed, high expression of MMP-2, but not MMP-9, by pericytes, even under hypoxic conditions, was observed. The expression of MMP-2 was confirmed in some, but not all, transplanted pericytes, implying a minor role of pericyte-mediated fibrolysis. Overall, our data suggest that the gross amelioration of fibrosis presumably involves decreased collagen deposition, reduced proliferation of fibroblasts, and altered remodeling of the extracellular matrix (ECM). Yet whether there exists one or more determining mechanism(s) remains to be investigated.

The immunosuppressive potential of MSCs, demonstrated by inhibiting T-lymphocyte proliferation in culture and counteracting graft-versus-host reaction in recipients of allogeneic blood stem cells, is currently exploited in clinical trials [28, 29]. In the cardiac milieu, MSC transplantation in a rat model of acute myocarditis mitigated the increase in CD68+ phagocytic cells [40]. In this study, pericyte treatment significantly diminished host monocyte/macrophage infiltration in the infarcted myocardium, suggesting an anti-inflammatory potential which contributed to the reduction of fibrosis, amelioration of adverse remodeling, and improvement of cardiac function. Nevertheless, whether pericytes inhibit the acute-phase inflammation occurring soon after the incidence of MI is unknown. Inhibition of murine macrophage proliferation in culture by P-CM suggests a paracrine mechanism of their immunomodulatory capacity.

The immunosuppressive and anti-inflammatory capacities of MSCs are primarily attributed to soluble factors/molecules, as IL-6, LIF, and HMOX-1 were shown to exercise beneficial immunosuppressive effects [28, 29]. The attenuation of intense inflammation and mitigation of multiorgan damage by MSCs during sepsis are dependent on monocyte/macrophage-derived cytokines and regulated via PGE$_2$ signaling [41]. The immunoregulatory and cardioprotective functions of these molecules appear to be similar in the cardiac milieu [22, 42]. Our data demonstrate that pericytes express high levels of IL-6, LIF, COX-2, HMOX-1, and HIF-1α, which are sustained under hypoxic conditions. MCP-1 expression, however, notably decreased under hypoxia, corresponding with the reduced CD68+ cell infiltration in vivo. Little to no expression of proinflammatory cytokines including IL-1α, TNF-α, and IFNγ was detected. Virtually no expression of IL-4, IL-10, iNOS, and 2,3-IDO was observed in pericytes, suggestive of an immunoregulatory cytokine secretome that is unique to human microvascular pericytes [29, 43]. Intriguingly, TGF-β1, also an anti-inflammatory yet fibrogenic cytokine, was strongly expressed by pericytes [22, 44]. Our data suggested increased TGF-β1 expression/secretion by pericytes under hypoxic conditions (Fig. 6A, 6C). Given the multiple functions each proposed growth factor/cytokine possesses, it is likely that a dynamic, interactive, and intricately orchestrated balance of trophic factors between donor and host cells holds the key to a successful ischemic tissue remodeling and regeneration.

A linear correlation between secretion of proangiogenic factors, angiogenesis, and cardiac restoration was illustrated by blocking the bioactivity of VEGF secreted from transplanted murine muscle-derived stem cells in a mouse MI model, which not only abolished their stimulation of neovascularization but in

STEM CELLS

ID: **nareshrao** | Black Lining: **[ON]** | Time: **13:37** | Path: **N:/3b2/STEM/Vol00000/120293/APPFile/JW-STEM120293**

turn negatively influenced LV contractility and infarct size [45]. Okada et al. [34] further delineated the superior angiogenic properties of human myoendothelial progenitor cells and increased secretion of VEGF in response to hypoxia. Given the indigenous vascular association of pericytes, we hypothesized that pericytes are able to repair the damaged host vasculature. Indeed, upon pericyte treatment, we observed a significantly larger host microvascular network not only in the peri-infarct collateral circulation but also within the infarct region. Cultured pericytes secrete growth factors/cytokines/chemokines related to vascular physiology and remodeling [18]; among which, only VEGF-A, PDGF-β, and TGF-β1 were substantially upregulated under hypoxia, suggesting their role in pericyte-enhanced angiogenesis [39, 46].

Angiogenesis may follow cell–cell contact between donor pericytes and host ECs, in addition to stimulation by angiogenic factors. Recent studies reported that MSCs and vascular mural/adventitial cells support ECs in small blood vessel formation and maturation in culture and in vivo [33, 47]. We did observe the perivascular homing of donor pericytes in the ischemic heart. Some donor pericytes juxtaposing host ECs expressed interactive molecules including EphB2 and connexin43, suggestive of cellular interactions [48, 49]. Planar Matrigel culture confirmed the vascular cell characteristics of pericytes and their capability to enhance the angiogenic behavior of ECs. We further demonstrated microvessel formation and vascular support by pericytes in 3D cultures, indicating that associations between pericytes and ECs may contribute to revascularization. Nevertheless, the vibrant angiogenic response of pericytes observed in vitro may be reduced in vivo because of the harsh microenvironment caused by post-MI, ischemia, and inflammation. Altogether, these results demonstrate that the angiogenic properties of pericytes may result from indirect paracrine effects and, albeit minor, direct cellular interactions.

Compared to other types of stem/progenitor cells, pericytes appear to engraft well in the infarcted heart initially, presumably attributable to several factors [50]. We did not observe apparent cell death of pericytes cultured under 2.5% O_2 for up to 48 hours, implying their resistance to hypoxia (data not shown). The increased proliferation and migration of pericytes in response to low oxygen concentration and ECM degradation products have important implications for ischemic injury repair [10]. The perivascular niche-homing capacity may further benefit the long-term survival of pericytes. Nonetheless, it remains unclear whether pericytes actively migrated to perivascular locations or served as a revascularizing center inducing/recruiting angiogenic proliferation/migration of host ECs. Future studies are needed to reveal the kinetics of pericyte-EC interaction and migration in vivo.

The potential of human muscle pericytes to reconstitute major cell types in the injured myocardium, although to a small extent, was hereby demonstrated. Cell fate tracking suggests that a minor fraction of donor pericytes differentiated into and/or fused with cardiomyocytes. Given the small number of GFP-cTnI dual-positive cells present, it is unlikely that these cells contributed significantly to functional recovery [21]. Pericytes, all of which were α-SMA-positive during culture expansion, lost α-SMA expression once homing to host microvasculature (data not shown), consistent with our finding that a subset of native microvascular pericytes do not express α-SMA in situ. [12]

CONCLUSION   AQ8

In summary, FACS-purified human microvascular pericytes contribute to anatomic and functional cardiac improvement postinfarction through multiple cardioprotective mechanisms: reverse of ventricular remodeling, reduction of cardiac fibrosis, diminution of chronic inflammation, and promotion of host angiogenesis. Vessel-homing and small-scale regenerative events by pericytes partially reconstitute lost cardiac cells and contribute to the structural recovery. These cardioprotective and cardioregenerative activities of a novel stem cell population that can be purified to homogeneity and expanded in vitro await further research and exploitation in ischemic cardiovascular diseases.

DISCLOSURE OF CONFLICTS OF INTEREST

J.H. received remuneration from Cook MyoSite, Inc. for consulting services and for royalties received from technology licensing during the period that the above research was performed. All other authors have no conflict of interest to disclose.

REFERENCES

1   American Heart Association. Heart disease and stroke statistics–2011 update: A report from the American Heart Association. Circulation 2011;123:e18–209.
2   Kumar V, Fausto N, Abbas A. Robbins & Cotran Pathologic Basis of Disease. 7th ed. Philadelphia, PA: Saunders, 2004.
3   Hansson EM, Lindsay ME, Chien KR. Regeneration next: Toward heart stem cell therapeutics. Cell Stem Cell 2009;5:364–377.
4   Segers VFM, Lee RT. Stem-cell therapy for cardiac disease. Nature 2008;451:937–942.
5   Janssens S. Stem cells in the treatment of heart disease. Ann Rev Med 2010;61:287–300.
6   Menasche P. Cardiac cell therapy: Lessons from clinical trials. J Mol Cell Cardiol 2011;50:258–265.
7   Armulik A, Abramsson A, Betsholtz C. Endothelial/pericyte interactions. Circ Res 2005;97:512–523.
8   Montemurro T, Andriolo G, Montelatici E et al. Differentiation and migration properties of human foetal umbilical cord perivascular cells: Potential for lung repair. J Cell Mol Med 2011;15:796–808.
9   Park TS, Gavina M, Chen C-W et al. Placental perivascular cells for human muscle regeneration. Stem Cells Dev 2011;20:451–463.
10 Tottey S, Corselli M, Jeffries EM et al. Extracellular matrix degradation products and low-oxygen conditions enhance the regenerative

potential of perivascular stem cells. Tissue Eng Part A 2011;17:37–44.

11 Dellavalle A, Sampaolesi M, Tonlorenzi R et al. Pericytes of human skeletal muscle are myogenic precursors distinct from satellite cells. Nat Cell Biol 2007;9:255–267.

12 Crisan M, Yap S, Casteilla L et al. A perivascular origin for mesenchymal stem cells in multiple human organs. Cell Stem Cell 2008;3:301–313.

13 Sacchetti B, Funari A, Michienzi S et al. Self-renewing osteoprogenitors in bone marrow sinusoids can organize a hematopoietic microenvironment. Cell 2007;131:324–336.

14 Feng J, Mantesso A, De Bari C et al. Dual origin of mesenchymal stem cells contributing to organ growth and repair. Proc Natl Acad Sci USA 2011;108:6503–6508.

15 Corselli M, Chen C-W, Sun B et al. The tunica adventitia of human arteries and veins as a source of mesenchymal stem cells. Stem Cells Dev 2011;21:1299–1308.

16 Tormin A, Li O, Brune JC et al. CD146 expression on primary nonhematopoietic bone marrow stem cells is correlated with in situ localization. Blood 2011;117:5067–5077.

17 Corselli M, Chen CW, Crisan M et al. Perivascular ancestors of adult multipotent stem cells. Arterioscler Thromb Vasc Biol 2010;30:1104–1109.

18 Chen CW, Montelatici E, Crisan M et al. Perivascular multi-lineage progenitor cells in human organs: Regenerative units, cytokine sources or both?Cytokine Growth Factor Rev 2009;20:429–434.

19 James A, Zara J, Zhang X et al. Perivascular stem cells: A prospectively purified mesenchymal stem cell population for bone tissue engineering. Stem Cells, in press.

20 Chen CW, Okada M, Tobita K et al. Purified human muscle-derived pericytes support formation of vascular structures and promote angiogenesis after myocardial infarction. Circulation 2009;120:S1053.

21 Gnecchi M, Zhang Z, Ni A et al. Paracrine mechanisms in adult stem cell signaling and therapy. Circ Res 2008;103:1204–1219.

22 Frangogiannis NG. The immune system and cardiac repair. Pharmacol Res 2008;58:88–111.

23 Caplan AI, Dennis JE. Mesenchymal stem cells as trophic mediators. J Cell Biochem 2006;98:1076–1084.

24 Berry MF, Engler AJ, Woo YJ et al. Mesenchymal stem cell injection after myocardial infarction improves myocardial compliance. Am J Physiol Heart Circ Physiol 2006;290:H2196–H2203.

25 Pittenger MF, Martin BJ. Mesenchymal stem cells and their potential as cardiac therapeutics. Circ Res 2004;95:9–20.

26 Ohnishi S, Sumiyoshi H, Kitamura S et al. Mesenchymal stem cells attenuate cardiac fibroblast proliferation and collagen synthesis through paracrine actions. FEBS Lett 2007;581:3961–3966.

27 Mias C, Lairez O, Trouche E et al. Mesenchymal stem cells promote matrix metalloproteinase secretion by cardiac fibroblasts and reduce cardiac ventricular fibrosis after myocardial infarction. Stem Cells 2009;27:2734–2743.

28 Ghannam S, Bouffi C, Djouad F et al. Immunosuppression by mesenchymal stem cells: Mechanisms and clinical applications. Stem Cell Res Ther 2010;1:2.

29 Shi Y, Hu G, Su J et al. Mesenchymal stem cells: A new strategy for immunosuppression and tissue repair. Cell Res 2010;20:510–518.

30 Renault MA, Losordo DW. Therapeutic myocardial angiogenesis. Microvasc Res 2007;74:159–171.

31 Sieveking DP, Ng MKC. Cell therapies for therapeutic angiogenesis: Back to the bench. Vasc Med 2009;14:153–166.

32 Saunders WB, Bohnsack BL, Faske JB et al. Coregulation of vascular tube stabilization by endothelial cell TIMP-2 and pericyte TIMP-3. J Cell Biol 2006;175:179–191.

33 Au P, Tam J, Fukumura D, Jain RK. Bone marrow-derived mesenchymal stem cells facilitate engineering of long-lasting functional vasculature. Blood 2008;111:4551–4558.

34 Okada M, Payne TR, Zheng B et al. Myogenic endothelial cells purified from human skeletal muscle improve cardiac function after transplantation into infarcted myocardium. J Am Coll Cardiol 2008;52:1869–1880.

35 Dellavalle A, Maroli G, Covarello D et al. Pericytes resident in postnatal skeletal muscle differentiate into muscle fibres and generate satellite cells. Nat Commun 2011;2:499.

36 He W, Nieponice A, Soletti L et al. Pericyte-based human tissue engineered vascular grafts. Biomaterials 2010;31:8235–8244.

37 Zimmerlin L, Donnenberg VS, Pfeifer ME et al. Stromal vascular progenitors in adult human adipose tissue. Cytometry A 2010;77:22–30.

38 Katare R, Riu F, Mitchell K et al. Transplantation of human pericyte progenitor cells improves the repair of infarcted heart through activation of an angiogenic program involving Micro-RNA-132/novelty and significance. Circ Res 2011;109:894–906.

39 Enciso JM, Hirschi KK. Understanding abnormalities in vascular specification and remodeling. Pediatrics 2005;116:228–230.

40 Ohnishi S, Yanagawa B, Tanaka K et al. Transplantation of mesenchymal stem cells attenuates myocardial injury and dysfunction in a rat model of acute myocarditis. J Mol Cell Cardiol 2007;42:88–97.

41 Nemeth K, Leelahavanichkul A, Yuen PS et al. Bone marrow stromal cells attenuate sepsis via prostaglandin E(2)-dependent reprogramming of host macrophages to increase their interleukin-10 production. Nat Med 2009;15:42–49.

42 Liu X, Pachori AS, Ward CA et al. Heme oxygenase-1 (HO-1) inhibits postmyocardial infarct remodeling and restores ventricular function. Faseb J 2006;20:207–216.

43 Ren G, Su J, Zhang L et al. Species variation in the mechanisms of mesenchymal stem cell-mediated immunosuppression. Stem Cells 2009;27:1954–1962.

44 Abarbanell AM, Coffey AC, Fehrenbacher JW et al. Proinflammatory cytokine effects on mesenchymal stem cell therapy for the ischemic heart. Ann Thorac Surg Sep 2009;88:1036–1043.

45 Payne TR, Oshima H, Okada M et al. A relationship between vascular endothelial growth factor, angiogenesis, and cardiac repair after muscle stem cell transplantation into ischemic hearts. J Am Coll Cardiol 2007;50:1677–1684.

46 Ohnishi S, Yasuda T, Kitamura S et al. Effect of hypoxia on gene expression of bone marrow-derived mesenchymal stem cells and mononuclear cells. Stem Cells 2007;25:1166–1177.

47 Campagnolo P, Cesselli D, Al Haj Zen A et al. Human adult vena saphena contains perivascular progenitor cells endowed with clonogenic and proangiogenic potential. Circulation 2010;121:1735–1745.

48 Salvucci O, de la Luz Sierra M, Martina JA et al. EphB2 and EphB4 receptors forward signaling promotes SDF-1-induced endothelial cell chemotaxis and branching remodeling. Blood 2006;108:2914–2922.

49 Hirschi KK, Burt JM, Hirschi KD et al. Gap junction communication mediates transforming growth factor-β activation and endothelial-induced mural cell differentiation. Circ Res 2003;93:429–437.

50 Wu KH, Mo XM, Han ZC et al. Stem cell engraftment and survival in the ischemic heart. Ann Thoracic Surg 2011;92:1917–1925.

AQ9

🖥 See www.StemCells.com for supporting information available online.

STEM CELLS

AQ1: Please provide running title for your manuscript.

AQ2: Please confirm whether the affiliations are OK as typeset.

AQ3: Per journal style, most nonstandard abbreviations must be used at least two times in the abstract to be retained; IL, LIF, COX, HMOX, Ang, MCP, VEGF, PDGF, TGF, bFGF, HGF, EGF, GFP were used once and have thus been deleted.

AQ4: Per journal style, most nonstandard abbreviations must be used at least two times in the text to be retained; AMI, ALP, PTGS, PECAM, SMC were used once and have thus been deleted.

AQ5: Please provide locations for the manufacturer names mentioned in the experimental section.

AQ6: Please spell out CMV, NOD/SCID, ATCC, SMA, and TUNEL in the text at the first occurrence.

AQ7: Please note that manufacturer data have been edited/updated. Please check.

AQ8: Please confirm whether the insertion of Conclusion section head is OK.

AQ9: Please update reference 19 (if possible).

AQ10: Please spell out DAPI in Fig. 2.

AQ11: Please confirm whether the author contributions section is OK as typeset.

original article

Human Skeletal Muscle Cells With a Slow Adhesion Rate After Isolation and an Enhanced Stress Resistance Improve Function of Ischemic Hearts

Masaho Okada[1,2], Thomas R Payne[1–4], Lauren Drowley[1,2], Ron J Jankowski[4], Nobuo Momoi[5], Sarah Beckman[1], William CW Chen[1], Bradley B Keller[5], Kimimasa Tobita[5] and Johnny Huard[1–3,6]

[Q1] [1]*Stem Cell Research Center, Children's Hospital of Pittsburgh, Pittsburgh, Pennsylvania, USA;* [2]*Department of Orthopaedic Surgery, University of Pittsburgh, Pittsburgh, Pennsylvania, USA;* [3]*Department of Bioengineering, University of Pittsburgh, Pittsburgh, Pennsylvania, USA;* [4]*Cook Myosite, Pittsburgh, Pennsylvania, USA;* [5]*Department of Pediatrics, Children's Hospital of Pittsburgh, Pittsburgh, Pennsylvania, USA;* [6]*Department of Molecular Genetics and Biochemistry, University of Pittsburgh, Pittsburgh, Pennsylvania, USA*

Identification of cells that are endowed with maximum potency could be critical for the clinical success of cell-based therapies. We investigated whether cells with an enhanced efficacy for cardiac cell therapy could be enriched from adult human skeletal muscle on the basis of their adhesion properties to tissue culture flasks following tissue dissociation. Cells that adhered slowly displayed greater myogenic purity and more readily differentiated into myotubes *in vitro* than rapidly adhering cells (RACs). The slowly adhering cell (SAC) population also survived better than the RAC population in kinetic *in vitro* assays that simulate conditions of oxidative and inflammatory stress. When evaluated for the treatment of a myocardial infarction (MI), intramyocardial injection of the SACs more effectively improved echocardiographic indexes of left ventricular (LV) remodeling and contractility than the transplantation of the RACs. Immunohistological analysis revealed that hearts injected with SACs displayed a reduction in myocardial fibrosis and an increase in infarct vascularization, donor cell proliferation, and endogenous cardiomyocyte survival and proliferation in comparison with the RAC-treated hearts. In conclusion, these results suggest that adult human skeletal muscle-derived cells are inherently heterogeneous with regard to their efficacy for enhancing cardiac function after cardiac implantation, with SACs outperforming RACs.

INTRODUCTION

[Q2] Skeletal muscle is an attractive source of progenitor cells for autologous cell therapy due to its abundance and accessibility. Progenitor cells in skeletal muscle, generally referred to as myoblasts (or satellite cells), are numerous and heterogeneous in nature.[1] The potential use of myoblasts for treating muscle disorders has been hindered, at least in part, by high rates of cell death after transplantation.[2–4] Recently, there has been interest in the identification and purification of populations of skeletal muscle-derived cells with the greater potential for cell-based therapies.[1,2,4–16]

We and others have used the preplate isolation technique to fractionate skeletal muscle progenitor cells from rodent skeletal muscle on the basis of selective adhesion characteristics to tissue culture flasks.[17] Isolating cells with this method yields cell populations that are classified by a rapid or slow adherence to the culture flask. Skeletal myoblasts derived from the rapidly adhering cell (RAC) fraction of rodent skeletal muscle were poor at muscle regeneration when transplanted into both skeletal and cardiac muscles.[14–16] In contrast, murine skeletal muscle-derived stem cells (MDSC) derived from the slowly adhering cell (SAC) fraction demonstrated a significant improvement in skeletal muscle regeneration in comparison with the rapidly adhering myoblast population.[14,15] In addition, after intramyocardial injection into a murine model of an acute myocardial infarction (MI), hearts transplanted with MDSCs demonstrated a greater improvement in cardiac function in comparison with hearts transplanted with myoblasts.[16] The mechanisms underlying the functional difference between MDSC and myoblasts were attributed to the ability of the MDSCs to survive and engraft significantly better than the myoblasts.[16] The survival of MDSCs may have led to improvements in the attenuation of adverse remodeling and capillary density throughout the infarcted tissue. These effects were presumably mediated through long-term secretion of factors by the engrafted MDSCs, since differentiation into *de novo* cardiomyocytes was an extremely rare occurrence.[16] Although these promising results were observed with rodent skeletal muscle, it remained to be determined whether RAC and SAC isolated from human skeletal muscle would produce similar outcomes after cell transplantation into the heart.

Here, we isolated and characterized RAC and SAC from human skeletal muscle. The efficacy of both populations was evaluated in an MI model using immunodeficient mice. Our results indicate that the slowly adhering fraction of human skeletal muscle-derived cells more effectively improved cardiac function when compared with the rapidly adhering fraction. The SAC also demonstrated greater survival under conditions of oxidative and inflammatory conditions of stress *in vitro* when compared with the RAC.

Correspondence: Johnny Huard, 450 Technology Drive, 2 Bridgeside Point, Suite 206, Pittsburgh, Pennsylvania 15219, USA. E-mail: jhuard@pitt.edu

RESULTS

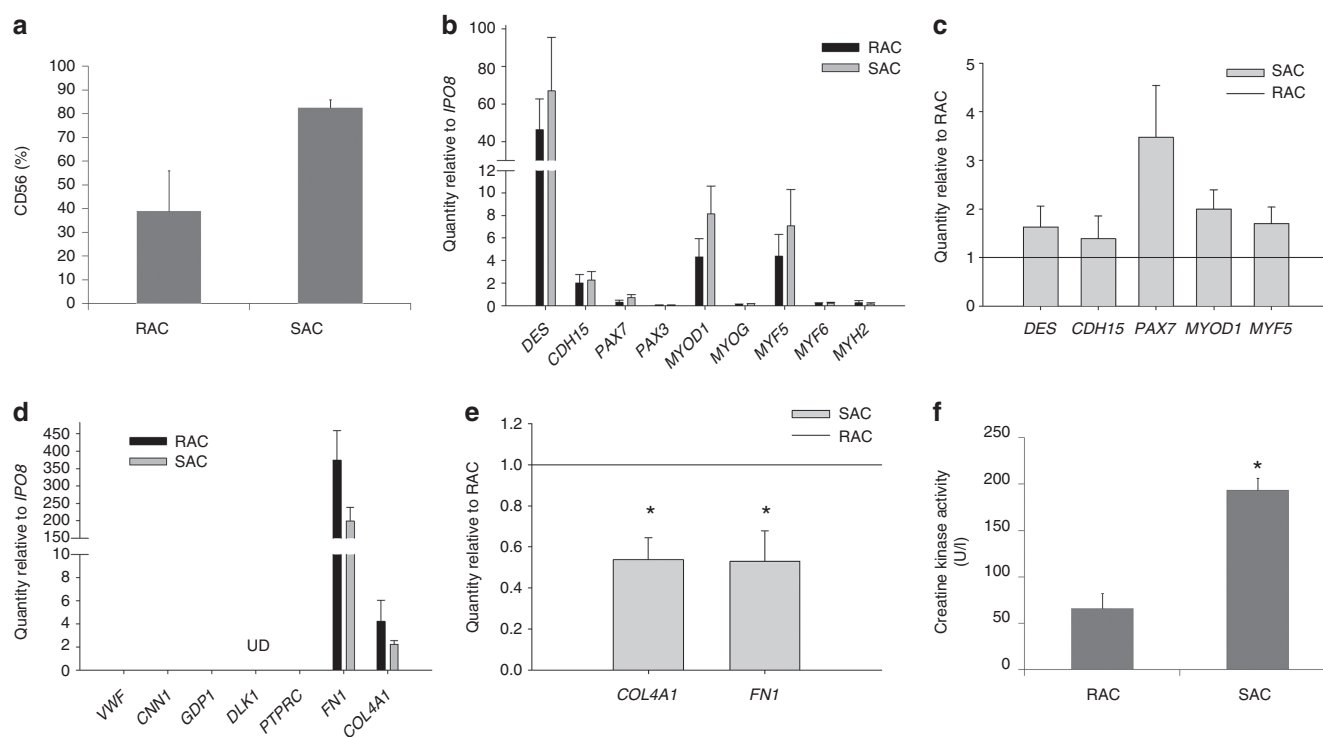### Myogenic purity of RAC and SAC populations

Each cell population was analyzed for myogenic purity as determined by CD56 flow cytometry analysis. SAC populations contained a higher percentage of CD56-expressing cells when compared with the RAC populations (**Figure 1a**, SAC 83 ± 3% CD56-positive, RAC 39 ± 17%, $n = 3$ populations per group, $P = 0.07$).

Myogenic gene expression profiles

Evaluation of myogenic lineage genes in both the RAC and SAC populations demonstrated substantial expression of the myogenic cell markers desmin (*DES*) and m-cadherin (*CDH15*) as well as the myogenic determination gene *MYOD1* and the myogenic regulatory factor *MYF5* relative to the endogenous control gene *IPO8* (**Figure 1b**, average values of $n = 3$ donors). A modest expression of the *PAX7* transcription factor, which regulates the myogenic differentiation of satellite cells, was also detected (**Figure 1b**). Very low expression of the early satellite cell marker *PAX3* and the myogenic regulatory factors myogenin (*MYOG*) and *MYF6*, which are both involved in the specification of skeletal myoblasts into terminally differentiated myotubes, were observed (**Figure 1b**). As expected, a very low level of the skeletal muscle myosin heavy chain 2 (*MYH2*) gene, which is specifically expressed by terminally-differentiated skeletal myotubes, was detected in both populations, confirming that the RAC and SAC populations did not undergo terminal differentiation during

expansion under normal culture conditions (**Figure 1b**). Of the myogenic genes expressed by both cell populations, the SAC populations demonstrated increased expression of the following myogenic lineage genes relative to the RAC populations: *DES* (SAC: 1.6 ± 0.4 relative to RAC, $n = 3$ donors, $P = 0.218$), *CDH15* (1.4 ± 0.5, $P = 0.454$), *PAX7* (3.5 ± 1.1, $P = 0.082$), *MYOD1* (2.0 ± 0.4, $P = 0.066$), and *MYF5* genes (1.7 ± 0.3, $P = 0.108$) (**Figure 1c**). These findings correlate with the higher levels of myogenic purity observed in the SAC populations in comparison with the RAC populations (**Figure 1a**).

The presence of other cell types in the RAC and SAC populations that could have been co-isolated from human skeletal muscle was evaluated based on the expression levels of lineage-specific genes. We observed undetectable or minimal expression of the endothelial cell-specific gene von Willebrand factor (*VWF*), the smooth muscle cell lineage gene calponin 1 (*CNN1*), the adipocyte-expressed gene glycerol-3-phosphate dehydrogenase 1 (*GPD1*), the preadipocyte gene delta-like homolog (*DLK1*, alias *PREF*,[1] and the pan-hematopoietic gene protein tyrosine phosphatase receptor type C (*PTPRC*, alias *CD45*) (**Figure 1d**). The SAC populations also displayed lower expression relative to the RAC populations of the extracellular matrix genes fibronectin (*FN1*, 0.53 ± 0.15, $P < 0.05$) and collagen type IV (*COL4A1*, 0.54 ± 0.11 quantity relative to RAC, $P < 0.05$), which are highly expressed by fibroblasts.[18] Taken together, these results suggest that the nonmyogenic cells (CD56⁻) within the RAC and SAC populations were fibroblasts, as expected.

[Q3] **Figure 1 Characterization of the RAC and SAC after culture expansion.** (**a**) Each cell population was analyzed for myogenic purity by CD56 flow cytometry. (**b**) Myogenic gene expression profiles were measured in the RAC and SAC populations. Gene expression values are relative to the endogenous control gene *IPO8*. (**c**) SAC populations demonstrated increased expression of all expressed myogenic genes relative to the RAC populations. (**d**) Detection of other cell types within the RAC and SAC populations: *VWF* for endothelial cells, *CNN1* for smooth muscle cells, *GPD1* for adipocytes, *DLK1* for preadipocytes (UD, undetectable), *PTPRC* for blood cells, and *FN1* and *COL4A1* for fibroblasts. (**e**) SAC populations displayed decreased expression of *FN1* and *COL4A1* relative to the RAC populations (*$P < 0.05$). (**f**) SAC populations more rapidly differentiated into multi-nucleated myotubes than the RAC populations as signified by increased creatine kinase activity (*$P < 0.05$). RAC, rapidly adhering cell; SAC, slowly adhering cell.

Myogenic differentiation

The myogenic differentiation potential of RAC and SAC was measured *in vitro* by creatine kinase activity, an enzyme expressed in differentiated myogenic cells. When subjected to culture conditions that support terminal differentiation, the SAC populations displayed higher creatine kinase activity values when compared with the RAC populations, indicating that SAC more rapidly differentiated into skeletal myotubes than [Q4] RAC (**Figure 1f**, SAC 194 ± 13 U/L, RAC 66 ± 16, *n* = 3 populations per group, *P* < 0.05).

Expression of paracrine factors

Under normal culture conditions, RAC and SAC highly expressed vascular endothelial growth factor A (*VEGFA*) and transforming growth factor-β1 (*TGFβ1*) genes. At lower levels, RAC and SAC populations also expressed fibroblast growth factor 2 (*FGF2*), platelet-derived growth factor-β (*PDGFβ*), angiopoietin 1 (*ANGPT1*), and hepatocyte growth factor (*HGF*) genes (**Supplementary Figure S1**). The RAC and SAC displayed minimal expression of insulin-like growth factor 1 (*IGF1*) and growth factors associated with neural development including nerve growth factor (*NGF*), brain-derived neurotrophic factor (*BDNF*), glial cell-derived neurotrophic factor (*GDNF*), and neuregulin 1 (*NRG1*) (**Supplementary Figure S1**). Overall, both cell populations displayed a similar gene expression profile of these paracrine factors.

Cell proliferation and survival under stress *in vitro*

The proliferation of RAC and SAC in culture was measured by a live cell imaging system every 12 hours for a period of 60 hours (**Figure 2a**). The SAC displayed a higher growth rate than the RAC (**Figure 2a**, 60 hours time point values: SAC 3.6 ± 0.4 cells normalized to initial cell number, RAC 2.4 ± 0.3, *n* = 3 populations per group; *P* < 0.05).

The cells' ability to survive conditions of oxidative and inflammatory stresses was evaluated *in vitro* with a cellular viability assay that was monitored in real-time with the live cell imaging system (**Figure 2b,c**). Under culture conditions of hydrogen peroxide-induced oxidative stress, a greater percentage of viable SAC were observed at all time points when compared with the RAC (**Figure 2b**, 72 hours time point values: SAC 48.1 ± 4.4% viability, RAC 27.7 ± 3.1%, *n* = 3 populations per group, *P* < 0.05). When exposed to inflammatory stress conditions with tumor necrosis factor-α, almost 40% of the RAC died whereas more than 85% of the SAC remained viable (**Figure 2c**, 72 hours time point values: SAC 86.1 ± 3.7% viability, RAC 61.2 ± 6.4%, *n* = 2 populations per group, *P* < 0.05). These results suggest that the SAC are more resistant to cellular death than the RAC when subjected to oxidative [Q5] and inflammatory stresses, which are both likely conditions that cells will experience when injected directly into an acute MI.[19]

Intramyocardial injection and echocardiographic evaluation of cardiac function

The effect of human skeletal muscle-derived RAC and SAC for cardiac cell transplantation was assessed in an immunodeficient mouse model of an acute MI. We injected infarcted mice with cell populations isolated from three male donors (*n* = 27 mice for RAC, *n* = 22 for SAC, and *n* = 21 for control injections). The RAC
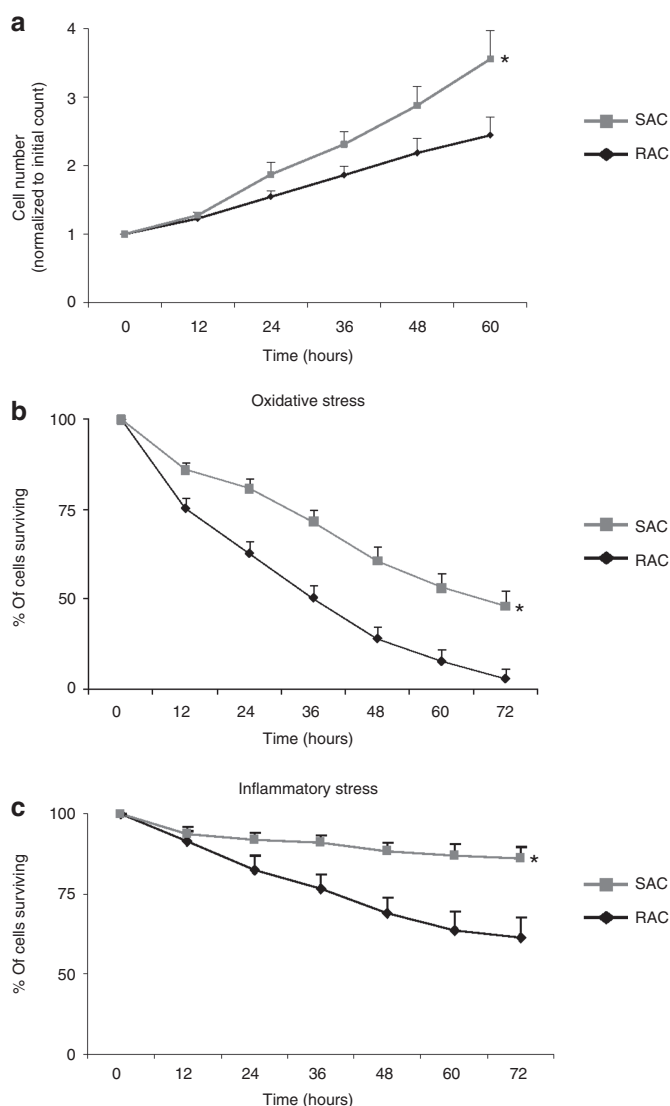

Figure 2 Cell proliferation and survival under oxidative and inflammatory stress. (**a**) Cell proliferation was measured in the RAC and SAC cultures (*P < 0.05). (**b**,**c**) SAC demonstrated greater survival under conditions of (**b**) oxidative and (**c**) inflammatory stress than the RAC (*P < 0.05). RAC, rapidly adhering cell; SAC, slowly adhering cell.

and SAC prepared for injection and frozen in cryopreservation medium displayed comparable viability and recovery post-thaw at the time of injection (post-thaw viability: RAC 89.4 ± 3.1%, SAC 89.6 ± 1.2%, *P* = 0.963; post-thaw recovery: RAC 68.4 ± 1.6%, SAC 74.9 ± 3.7%, *P* = 0.189).

Two weeks after infarction, cellular transplantation induced a modest decrease in left ventricular (LV) diastolic dimensions, as measured by end diastolic area, when compared with control vehicle injection (**Figure 3a**, SAC 11.9 ± 0.5 mm², RAC 12.6 ± 0.6, control 14.0 ± 0.7). Both cell groups had significantly smaller LV systolic dimensions when compared with the control group, as assessed by end systolic area (SAC 8.8 ± 0.4 mm², RAC 10.1 ± 0.6, control 11.9 ± 0.6; *P* < 0.05, RAC and SAC versus control). A greater improvement in LV contractility, as determined by fractional area change values, was observed in the cell-treated hearts when compared with the control vehicle-treated hearts 2 weeks after MI
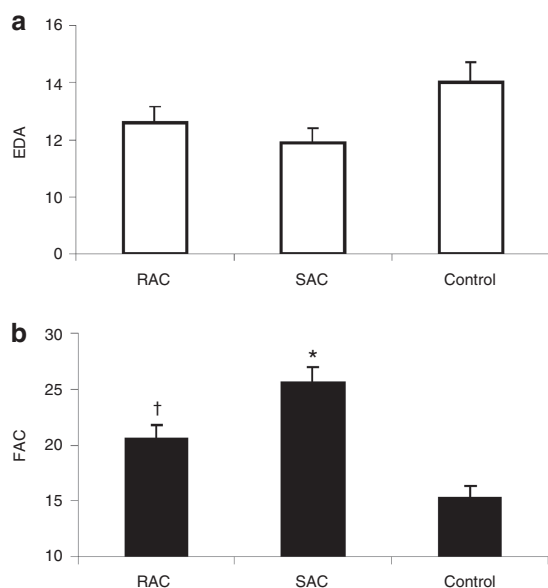
Figure 3 Functional assessments. (**a**) Left ventricular end diastolic area (DA) was slightly reduced in hearts injected with the RAC and SAC populations when compared with control hearts injected with saline. (**b**) Hearts injected with SAC displayed stronger left ventricular contractility, as measured by percent fractional area change (FAC), when compared with hearts injected with RAC (*$P < 0.05$, SAC versus RAC and control; †$P < 0.05$, RAC versus control). RAC, rapidly adhering cell; SAC, slowly adhering cell.

Figure 4 Infarct histology. (**a**–**c**) Representative images were taken from transverse sections of the Masson's trichrome–stained hearts. Muscle tissue is stained red, and collagenous tissue is stained blue. Bars equal 500 μm. (**d**) SAC-injected hearts demonstrated the greatest reduction of scar tissue when compared with the control (*$P < 0.05$, SAC versus control). SAC, slowly adhering cell.

(**Figure 3b**, SAC 25.6 ± 1.4%, RAC 20.6 ± 1.2%, control 15.3 ± 1.1%; $P < 0.05$, RAC and SAC versus control). The hearts injected with the SAC demonstrated significant improvement of LV performance when compared with the RAC (**Figure 3b**; $P < 0.05$, SAC versus RAC). When cardiac echocardiography data was separated by donor age, the SAC showed greater efficacy versus the RAC primarily in the older donors (57 and 70 year males) (**Supplementary Table S1**). In contrast, the SAC and RAC derived from the young donor (13-year-old male) demonstrated comparable outcomes, indicating that the selection of SAC may be the most critical from older donors (**Supplementary Table S1**). Overall, these results indicate that the SAC more effectively attenuated adverse remodeling and improved cardiac function when compared with the RAC, particularly when these cell populations were isolated from older donors.

Cardiac scar tissue

The extent of scar tissue formation within the LV was evaluated using Masson's trichrome stain (**Figure 4a–c**). Two weeks following a MI, a reduction in scar tissue was observed in both RAC- and SAC-injected hearts compared with control vehicle-injected hearts (**Figure 4d**, SAC 45.8 ± 6.6% scar, RAC 60.9 ± 7.1%, control 77.5 ± 5.3%). However, only the SAC significantly attenuated scar tissue formation following an acute MI when compared with the controls (**Figure 4d**, $P < 0.05$, SAC versus control).

Transplanted cell engraftment and proliferation

Donor myocytes were observed within the infarct zone by colocalization of Masson's trichrome stain (arrows, **Figure 5a**) and fast skeletal MYH immunostaining (arrows, **Figure 5b**). These e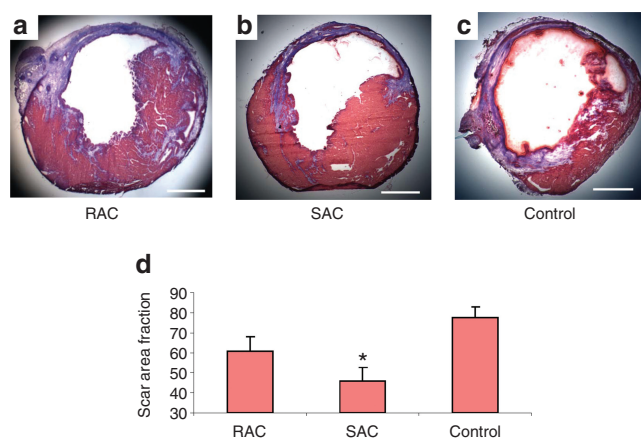ngraftments were frequently surrounded by scar tissue along the ischemic border zone (arrowheads, **Figure 5a,b**). The area of MYH+ tissue within the myocardium of the LV was comparable between hearts injected with the RAC and SAC (SAC 3.5 ± 1.2% MYH+ tissue in the myocardium, RAC 3.8 ± 0.8%, $P = 0.864$, SAC versus RAC). The presence of nuclei expressing proliferating cell nuclear antigen (PCNA) using a human-specific PCNA antibody further confirmed donor cell engraftment and indicated donor cell proliferation *in vivo* (**Figure 5c**). We observed proliferative, PCNA-positive donor cells more frequently in the SAC-injected hearts than in the RAC-injected hearts (**Figure 5d**, SAC 2.0 ± 0.3 PCNA+/MYH+ cells, RAC 0.4 ± 0.3; $P < 0.05$, SAC versus RAC). These findings confirm the engraftment of the injected human cells within the murine myocardium, and suggest that the SAC proliferate at higher levels than the RAC *in vivo*.

Angiogenesis

Capillary density within the infarct tissue was assessed by CD31 immunostaining (**Figure 6a–c**). More capillaries were observed within the infarct area of hearts treated with the SAC when compared with hearts injected with the RAC and the control vehicle (**Figure 6d**, SAC 723 ± 63 capillaries/mm^2, RAC 560 ± 21, control 548 ± 31; $P < 0.05$, SAC versus RAC and control). These findings indicate that transplanted SAC may induce a more potent angiogenic effect within the infarcted hearts when compared with transplanted RAC and the control.

Endogenous cardiomyocyte apoptosis and proliferation

Endogenous cardiomyocyte apoptosis and proliferation was evaluated at 3 days after MI. Multi-label staining for terminal dUPT nick end-labeling (TUNEL) and cardiac Troponin I (cTnI) was performed to determine the effect of cell implantation on endogenous cardiomyocyte apoptosis in the peri-infarct regions (**Figure 7a**). Hearts injected with SAC contained less apoptotic cardiomyocytes within the peri-infarct regions when compared with hearts transplanted with RAC and the control vehicle (**Figure 7b**, SAC 203 ± 29
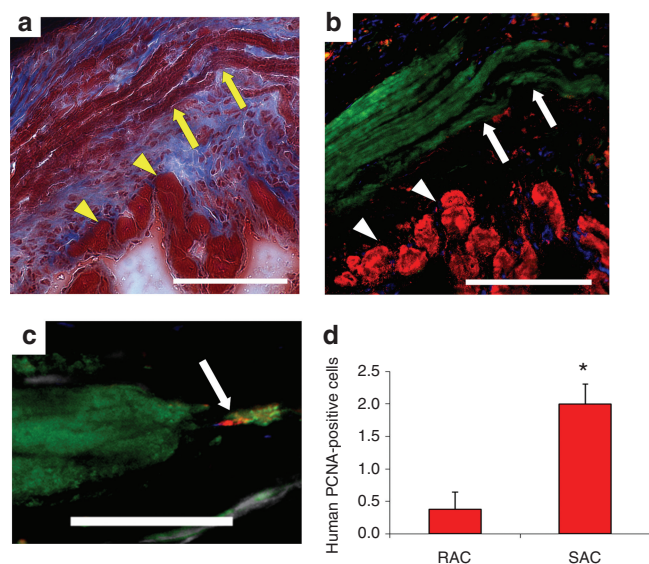
Figure 5 Engraftment and proliferation of injected cells *in vivo*. (**a**) The arrows designate the engraftment area of the SAC, and the arrowheads indicate host cardiac tissue in Masson's trichrome–stained hearts. Bar = 125 μm. Image **a** colocalizes with image **b**. (**b**) Fast skeletal myosin heavy chain (MYH)-positive myofibers (green stain, arrows) designate the SAC engraftment region. Cardiac troponin I-positive cardiomyocytes (red, arrowheads) identifies peri-infarct zone. Bar equals 125 μm. (**c,d**) Mitotic human PCNA-positive cells (red stain) that colocalized with the MYH-positive engraftment region (green stain) were more frequently observed in the SAC-injected hearts when compared with the RAC-injected hearts (*$P < 0.05$, SAC versus RAC). Cardiac troponin I-positive cardiomyocytes are stained grey, and nuclei are stained blue. PCNA, proliferating cell nuclear antigen; RAC, rapidly adhering cell; SAC, slowly adhering cell.
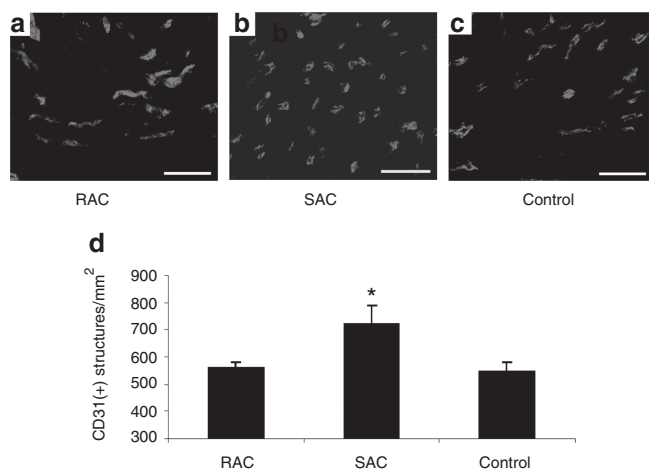

Figure 6 Angiogenesis. (**a–c**) Representative images are shown of CD31 immunostaining. Bars equal 50 μm. (**d**) The infarcts of hearts transplanted with SAC displayed higher capillary densities when compared with hearts injected with RAC and control vehicle (*$P < 0.05$, SAC versus RAC and control). RAC, rapidly adhering cell; SAC, slowly adhering cell.

TUNEL⁺/cTnI⁺ cells in four high power fields, RAC 321 ± 68, control 404 ± 81; $P < 0.05$, SAC versus control).

The number of proliferating cardiomyocytes present within the infarct border zone was measured by Ki-67 and cTnI dual label immunostaining (**Figure 7c**). Hearts injected with SAC contained more proliferating cardiomyocytes within the infarct border zone
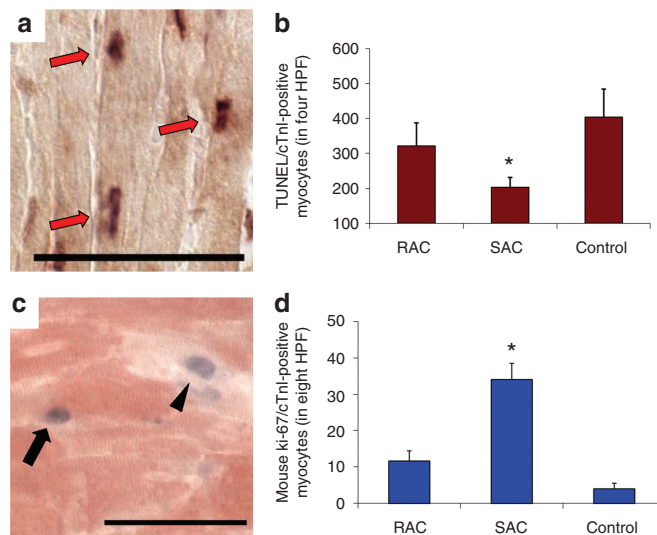

Figure 7 Endogenous cardiomyocyte apoptosis and proliferation. (**a**) Identification of apoptotic endogenous cardiomyocytes (arrows) by concomitant staining for cardiac troponin I (cTnI, light brown cytoplasmic stain) and TUNEL assay (arrows, dark nuclear stain). (**b**) The number of apoptotic cardiomyocytes was measured in four high power fields (HPF, *$P < 0.05$, SAC versus control). (**c**) Proliferating cardiomyocytes (arrow) within the peri-infarct region were identified by colocalization of both Ki-67 (blue nuclear stain) and cTnI (red) within the peri-infarct region. Some of the proliferating cells stained by Ki-67 did not colocalize with cTnI (arrowhead). Bars equal 50 μm. (**d**) The number of proliferating Ki-67-positive endogenous cardiomyocytes was measured in the peri-infarct region of the hearts (*$P < 0.05$, SAC versus RAC and control). RAC, rapidly adhering cell; SAC, slowly adhering cell, TUNEL, terminal dUPT nick end-labeling.

than hearts injected with either the RAC or the control (**Figure 7d**, SAC 34 ± 5 Ki-67⁺/cTnI⁺ cardiomyocytes in 8 high power fields, RAC 12 ± 3, control 4 ± 2; $P < 0.05$, SAC versus RAC and control). Taken together, these results suggest that the transplantation of SAC induced a beneficial effect on endogenous cardiomyocyte proliferation and apoptosis within the peri-infarct region.

DISCUSSION

The main finding in this study is that the SAC fraction is more effective at improving cardiac function than the RAC fraction derived from human skeletal muscle, which is a result that is consistent with our studies investigating progenitor cells from murine skeletal muscle for cardiac repair.[16] These results support the notion that human skeletal muscle-derived progenitor cells are heterogeneous not just in terms of cellular composition but of potency for cardiac cell transplantation.

Isolation of human skeletal muscle-derived cells on the basis of adhesion rates to tissue culture flasks using the preplate technique produced RAC and SAC populations that exhibit distinct characteristics and behavior. Our results *in vitro* demonstrate that myogenic progenitor cells with the highest myogenic purity and the strongest propensity for myogenic differentiation are purified in the SAC fraction rather than the RAC fraction. Interestingly, these findings in human skeletal muscle are consistent with the use of the preplate technique to isolate progenitor cells from murine skeletal muscle.[14] In the mouse, we observed that cells that adhered slowly also displayed greater myogenic purity based on *DES*

Remove Italics

expression when compared with cells that adhered rapidly.[14] In addition, the murine SAC population displayed a greater ability to regenerate skeletal muscle than the RAC population.[14] The mechanism underlying differential adhesion rates to tissue culture flasks is unknown at this point; however, these differences may result from a variety of factors including the expression of specific adhesion molecules and cellular density.[17] We are initiating research to determine whether other human skeletal muscle-derived cell populations, including CD34+CD90− cells,[5] myogenic endothelial cells[12,13] and pericytes,[10,11] are being collected preferentially in the slowly adhering fraction. Due to the limited number of cells (<100) contained within the slowly adhering fraction before expansion, and the known change in expression of many surface markers with time *in vitro*, flow cytometry characterization with a series of cell surface markers on the same populations used in this study for injection was not achievable.

The mechanism underlying the advantage of the SAC over RAC population for functional restoration after a MI may be multi-faceted.[7,16,20–25] A proposed aspect for the observed functional difference might be the varying ability of the transplanted cells to prevent adverse remodeling. SAC-treated hearts displayed a considerable reduction in end-systolic geometry when compared with RAC-injected hearts, suggesting that SAC induced a more effective attenuation of adverse remodeling. In clinical trials, skeletal myoblasts have shown a positive remodeling effect in the first randomized, placebo-controlled study of skeletal myoblast transplantation for cardiac repair (MAGIC trial).[26] The observed differences in end-systolic dimensions between the SAC and RAC could be attributed to the greater reduction in scar tissue in SAC-treated hearts when compared with hearts treated with RAC.

The reduced size of the infarct scar may be due to the preservation of at-risk cardiomyocytes, stimulation of endogenous cardiomyocyte proliferation, vascularization of the infarct scar, and/or the secretion of paracrine factors that regulate fibrosis. Three days after MI, we observed a significant increase in the number of proliferating cardiomyocytes and decrease in the number of apoptotic cardiomyocytes within the peri-infarct zone of hearts injected with SAC when compared with hearts injected with RAC and the control vehicle. We did not determine how the injected cells stimulated proliferation and protection of at-risk myocardium; however, at such an early time point after MI (3 days), a reasonable hypothesis is that this effect is due to the release of paracrine factors by the injected cells that stimulate cell survival and proliferation. Furthermore, various reports have shown that implanted cells promote infarct angiogenesis and have established a correlation between neovascularization and functional recovery of the heart after MI.[13,16,27,28] Here, we also observed a greater induction of angiogenesis within the infarct in SAC-treated hearts than in RAC-treated hearts, which may also support the attenuation of adverse infarct remodeling.[26,29]

The cells' ability to influence the host cells within the microenvironment through the release of paracrine molecules may represent a major determinant in the healing capacity of transplanted cells.[30,31] Here, we showed that both RAC and SAC express similar levels of various angiogenic and neurogenic genes under normal culture conditions. Many of the angiogenic factors expressed by the RAC and SAC, especially *VEGFA*, *HGF*, *TGFB1*, and *FGF2*,

have been shown to be expressed by human skeletal myoblasts, bone marrow mononuclear cells, adipose stromal cells, and bone marrow stromal cells.[32–37] In addition to stimulating angiogenesis, factors secreted by transplanted cells may activate signaling cascades that regulate fibrosis and the survival and proliferation of recipient cells in and around the infarct zone. Human skeletal muscle-derived cells likely express a wide variety of paracrine factors that far surpass the small battery of genes evaluated by others and us.[32,33] It is not unexpected that both the RAC and SAC populations express similar levels of the tested paracrine factors under normal culture conditions, since the level of cellular secretion of these factors may be primarily dependent on the cells' response to the environmental cues of the myocardial microenvironment and disease state (e.g., ischemia).[13,16,27,28]

Furthermore, the magnitude of the paracrine effect may be contingent on cell survival post-transplantation. The ability of transplanted cells to survive and proliferate, particularly when implanted directly into the harsh *milieu* of a myocardial infarct, may be critical for the cells to exert a lasting and significant biological effect, including the extended release of paracrine factors.[19] In our research with muscle progenitor cells isolated from human and murine skeletal muscle, we have consistently observed that transplanted SAC regenerate larger and more durable engraftments of skeletal myocytes than transplanted RAC.[14–16] We hypothesize that the preplate technique inherently selects for stress-resistant cells in the slowly adhering fraction, since these cells are able to tolerate suspension-induced stresses and anoikis during isolation.[38,39] Therefore, the SAC may represent a cell population endowed with an elevated resistance to stress. We have recently shown that muscle stem cells derived from the SAC fraction of murine skeletal muscle have an ability to survive under stress due to elevated levels of antioxidant expression.[40,41] Future research will evaluate whether human SAC also display similar antioxidant characteristics.

A limitation of this study is of the fact that the skeletal muscle-derived cells were injected immediately after a MI, which is not entirely relevant to an actual clinical scenario for autologous transplantation. In reality, the cells would require at least several weeks in order to cultivate a sufficient number of cells before treatment. Although we could not replicate the exact clinical conditions with this animal model, these findings may still provide meaningful information regarding the heterogeneity of human skeletal muscle-derived cells for cardiac cell transplantation.

In conclusion, the isolation of adult human skeletal muscle-derived cells on the basis of adhesion rates to tissue culture flasks enriches for cell fractions that support distinct levels of functional improvement when transplanted into ischemic myocardium. Selection of the best progenitor cell population from human skeletal muscle may aid in the translation of cell-based products for clinical applications of tissue repair.

MATERIALS AND METHODS

Animals. The Institutional Animal Care and Use Committee at the Children's Hospital of Pittsburgh approved the animal and surgical procedures performed in this study (Protocol 37/04). A total of 70 male nonobese diabetic/severe combined immunodeficient mice (NOD/SCID, strain NOD. CB17-*Prkdc^scid*/SzJ, The Jackson Laboratory, Bar Harbor, ME) between

13 and 22 weeks of age were used for this study. Creation of the acute MI model in adult mice and injection of thawed cells (3×10^5 cells in 30 µl) or control medium (30 µl) was performed in a blinded fashion, as previously described.[16] Echocardiography was also conducted in a blinded fashion to assess heart function, as previously described.[13,16] Additional information can be found in the **Supplementary Materials and Methods**.

Cells. RAC and SAC populations were isolated from human rectus abdominus skeletal muscle biopsies (50–250 mg) using the preplate technique.[17] Tissues were procured from 13, 57, and 70-year-old male donors (13M, 57M, and 70M, respectively). Isolation, culture expansion, and preparation of cells for injection are further detailed in **Supplementary Materials and Methods**. Cell populations from each donor were cryopreserved for injection at the following culture passages: 13M–RAC passage 4 and SAC passage 5–7, 57M–RAC passage 6 and SAC passage 5, 70M–RAC passage 8 and SAC passage 7. Post-thaw recovery and viability were evaluated from aliquots of the frozen cell suspensions that were prepared and cryopreserved for injection using the Viacount viability stain (Millipore, Hayward, CA) and Guava PCA flow cytometry system (Millipore).

Gene expression profile. RNA was purified from 1×10^5 cells for gene expression analysis immediately following the thaw of the cryopreserved stocks of cultured cells. The number of passages of the RAC and SAC were closely matched for the populations derived from the 13M (passage 7 for RAC and passage 6 for SAC), 57M (passage 6 for both populations), and 70M donor tissues (passage 3 for both populations).

Total RNA was isolated using the RNeasy Mini kit (Qiagen, Valencia, CA) and was reverse transcribed to cDNA (Applied Biosystems, Foster City, CA). Gene expression was measured using real-time quantitative PCR (see **Supplementary Materials and Methods** for detailed methods). All target genes were normalized to the reference housekeeping gene *IPO8* (Applied Biosystems, Hs00183533_m1). Relative quantity of gene expression was calculated as total amount of RNA based on the comparative ΔC_T (*i.e.*, relative expression level to endogenous control gene *IPO8*) and $\Delta\Delta C_T$ methods (i.e., relative expression level to the RAC population for each donor).

[Q6]

Myogenic assays. Myogenic purity analysis was performed on cellular suspensions using a PE-conjugated CD56 antibody (1:50; BD Pharmingen, San Diego, CA). The Guava PCA flow cytometry system measured the percentage of cells expressing CD56. Cell populations from each donor were evaluated at the following culture passages: 13M–RAC passage 4 and SAC passage 5–7, 57M–RAC passage 6 and SAC passage 5, 70M–RAC passage 8 and SAC passage 7.

To determine the myogenic differentiation potential of each population, cells were seeded onto a culture plate with low-serum differentiation medium and allowed to differentiate. Cell populations from each donor were evaluated at the following culture passages: 13M–RAC passage 4–5 and SAC passage 6–7, 57M–RAC passage 6 and SAC passage 5, 70M–RAC passage 4 and SAC passage 4. Terminal differentiation into multi-nucleated myotubes was measured with an assay that measured creatine kinase (CK) activity levels of differentiated cultures using the CK Liqui-UV Test Kit (Stanbio Laboratory, Boerne, TX) according to the manufacturer's instructions.[42]

[Q7]

Cell proliferation and survival assays. Cell proliferation under normal culture conditions and cell viability under stress conditions were evaluated with kinetic assays.[12,40,41] Cells were cultured for 60 hours in a live cell imaging system (Automated Cell, Pittsburgh, PA), which contains an incubation chamber for controlling temperature, humidity and CO_2 gas levels. The number of cells was measured in images acquired at 12-hour intervals.

Cell viability under stress conditions was analyzed as previously described.[12,40,41] Briefly, cells were cultured in a live cell imaging system for 72 hours in medium supplemented with propidium iodide (1:500, Sigma, St Louis, MO) to stain dead cells and either hydrogen peroxide (300 µmol/l;

[Q8]

Sigma) or tumor necrosis factor-α (10 ng/ml; Sigma) to induce cell death by oxidative and inflammatory stresses, respectively. Brightfield and fluorescent images were captured repeatedly at 10-minute intervals in the live cell imaging system for the entire 72-hour period. The percentage of viable cells (*i.e.*, propidium iodide exclusion) was measured from images acquired at 12-hour intervals using imaging software.

Histology and immunohistochemistry. Mice were sacrificed at 3 days, 2 weeks or 6 weeks after cell transplantation. We harvested the hearts, froze the tissue in 2-methylbutane precooled in liquid nitrogen, and serially sectioned the hearts from the apex to the base, as previously described.[13] Sections were then stained for fast skeletal MYH (1:200–1:400; Sigma) expression, as previously described.[20] The engraftment area ratio was defined as the area of MYH-positive tissue divided by the total area of the LV myocardium, which was identified by co-staining for cTnI (1:20,000; Scripps, San Diego, CA). To detect proliferating cells within the engraftment, tissue was stained with human anti-human PCNA antibody (1:400; US Biological, Swampscott, MA).[13] In sections stained with Masson's trichrome (IMEB, San Marcos, CA), scar area fraction was defined as the ratio of scar area to the cardiac LV muscle area and was averaged from five sections per heart, as previously described.[13] To measure capillary density, we stained heart muscle sections with an anti-mouse CD31 (platelet/endothelial cell adhesion molecule-1) antibody (BD Pharmingen).[16] The TUNEL assay was performed using the ApopTag Plus Peroxidase In Situ Apoptosis Detection Kit (Chemicon, Temecula, CA) according to manufacturer's instructions.[13] We carried out the Ki-67 (1:50; Dako, Glostrup, Denmark) and cTnI dual label immunostaining, as previously described, using the SG substrate kit (blue stain, Vector Laboratories, Burlingame, CA) and the AEC (3-amino-9-ethylcarbazole) substrate kit (red stain, Vector Laboratories), respectively.[13] Additional immunostaining methods are provided in the **Supplementary Materials and Methods**.

[Q9]

[Q10]

[Q11]

[Q12]

Statistical analysis. All measured data are presented as the mean ± SE of the mean. A *t*-test or a one-way analysis of variance was performed when comparing two groups or more than two groups, respectively. Analysis of variance *post hoc* analysis was conducted with the Tukey multiple comparison test. Statistical significance was defined by a value of $P < 0.05$. All calculations were performed using SigmaStat (Systat Software, San Jose, CA).

SUPPLEMENTARY MATERIAL
Figure S1. Cytokine gene expression profile.
Table S1. Echocardiographic data separated by donor cell populations.
Materials and Methods.

REFERENCES
1. Péault, B, Rudnicki, M, Torrente, Y, Cossu, G, Tremblay, JP, Partridge, T *et al.* (2007). Stem and progenitor cells in skeletal muscle development, maintenance, and therapy. *Mol Ther* **15**: 867–877.
2. Menasché, P (2004). Cellular transplantation: hurdles remaining before widespread clinical use. *Curr Opin Cardiol* **19**: 154–161.
3. Huard, J, Acsadi, G, Jani, A, Massie, B and Karpati, G (1994). Gene transfer into skeletal muscles by isogenic myoblasts. *Hum Gene Ther* **5**: 949–958.

4. Beauchamp, JR, Morgan, JE, Pagel, CN and Partridge, TA (1999). Dynamics of myoblast transplantation reveal a discrete minority of precursors with stem cell-like properties as the myogenic source. *J Cell Biol* **144**: 1113–1122.

5. Proksch, S, Bel, A, Puymirat, E, Pidial, L, Bellamy, V, Peyrard, S *et al.* (2009). Does the human skeletal muscle harbor the murine equivalents of cardiac precursor cells? *Mol Ther* **17**: 733–741.

6. Negroni, E, Riederer, I, Chaouch, S, Belicchi, M, Razini, P, Di Santo, J *et al.* (2009). *In vivo* myogenic potential of human CD133+ muscle-derived stem cells: a quantitative study. *Mol Ther* **17**: 1771–1778.

7. Sarig, R, Baruchi, Z, Fuchs, O, Nudel, U and Yaffe, D (2006). Regeneration and transdifferentiation potential of muscle-derived stem cells propagated as myospheres. *Stem Cells* **24**: 1769–1778.

8. Morosetti, R, Mirabella, M, Gliubizzi, C, Broccolini, A, Sancricca, C, Pescatori, M *et al.* (2007). Isolation and characterization of mesoangioblasts from facioscapulohumeral muscular dystrophy muscle biopsies. *Stem Cells* **25**: 3173–3182.

9. Motohashi, N, Uezumi, A, Yada, E, Fukada, S, Fukushima, K, Imaizumi, K *et al.* (2008). Muscle CD31(-) CD45(-) side population cells promote muscle regeneration by stimulating proliferation and migration of myoblasts. *Am J Pathol* **173**: 781–791.

10. Dellavalle, A, Sampaolesi, M, Tonlorenzi, R, Tagliafico, E, Sacchetti, B, Perani, L *et al.* (2007). Pericytes of human skeletal muscle are myogenic precursors distinct from satellite cells. *Nat Cell Biol* **9**: 255–267.

11. Crisan, M, Yap, S, Casteilla, L, Chen, CW, Corselli, M, Park, TS *et al.* (2008). A perivascular origin for mesenchymal stem cells in multiple human organs. *Cell Stem Cell* **3**: 301–313.

12. Zheng, B, Cao, B, Crisan, M, Sun, B, Li, G, Logar, A *et al.* (2007). Prospective identification of myogenic endothelial cells in human skeletal muscle. *Nat Biotechnol* **25**: 1025–1034.

13. Okada, M, Payne, TR, Zheng, B, Oshima, H, Momoi, N, Tobita, K *et al.* (2008). Myogenic endothelial cells purified from human skeletal muscle improve cardiac function after transplantation into infarcted myocardium. *J Am Coll Cardiol* **52**: 1869–1880.

14. Qu, Z, Balkir, L, van Deutekom, JC, Robbins, PD, Pruchnic, R and Huard, J (1998). Development of approaches to improve cell survival in myoblast transfer therapy. *J Cell Biol* **142**: 1257–1267.

15. Qu-Petersen, Z, Deasy, B, Jankowski, R, Ikezawa, M, Cummins, J, Pruchnic, R *et al.* (2002). Identification of a novel population of muscle stem cells in mice: potential for muscle regeneration. *J Cell Biol* **157**: 851–864.

16. Oshima, H, Payne, TR, Urish, KL, Sakai, T, Ling, Y, Gharaibeh, B *et al.* (2005). Differential myocardial infarct repair with muscle stem cells compared to myoblasts. *Mol Ther* **12**: 1130–1141.

17. Gharaibeh, B, Lu, A, Tebbets, J, Zheng, B, Feduska, J, Crisan, M *et al.* (2008). Isolation of a slowly adhering cell fraction containing stem cells from murine skeletal muscle by the preplate technique. *Nat Protoc* **3**: 1501–1509.

18. Pilling, D, Fan, T, Huang, D, Kaul, B and Gomer, RH (2009). Identification of markers that distinguish monocyte-derived fibrocytes from monocytes, macrophages, and fibroblasts. *PLoS ONE* **4**: e7475.

19. Suzuki, K, Murtuza, B, Beauchamp, JR, Smolenski, RT, Varela-Carver, A, Fukushima, S *et al.* (2004). Dynamics and mediators of acute graft attrition after myoblast transplantation to the heart. *FASEB J* **18**: 1153–1155.

20. Payne, TR, Oshima, H, Sakai, T, Ling, Y, Gharaibeh, B, Cummins, J *et al.* (2005). Regeneration of dystrophin-expressing myocytes in the mdx heart by skeletal muscle stem cells. *Gene Ther* **12**: 1264–1274.

21. Reinecke, H, Poppa, V and Murry, CE (2002). Skeletal muscle stem cells do not transdifferentiate into cardiomyocytes after cardiac grafting. *J Mol Cell Cardiol* **34**: 241–249.

22. Reinecke, H, Minami, E, Poppa, V and Murry, CE (2004). Evidence for fusion between cardiac and skeletal muscle cells. *Circ Res* **94**: e56–e60.

23. Reinecke, H, MacDonald, GH, Hauschka, SD and Murry, CE (2000). Electromechanical coupling between skeletal and cardiac muscle. Implications for infarct repair. *J Cell Biol* **149**: 731–740.

24. Leobon, B, Garcin, I, Menasche, P, Vilquin, JT, Audinat, E and Charpak, S (2003). Myoblasts transplanted into rat infarcted myocardium are functionally isolated from their host. *Proc Natl Acad Sci USA* **100**: 7808–7811.

25. Rubart, M, Soonpaa, MH, Nakajima, H and Field, LJ (2004). Spontaneous and evoked intracellular calcium transients in donor-derived myocytes following intracardiac myoblast transplantation. *J Clin Invest* **114**: 775–783.

26. Menasché, P, Alfieri, O, Janssens, S, McKenna, W, Reichenspurner, H, Trinquart, L *et al.* (2008). The Myoblast Autologous Grafting in Ischemic Cardiomyopathy (MAGIC) trial: first randomized placebo-controlled study of myoblast transplantation. *Circulation* **117**: 1189–1200.

27. Kocher, AA, Schuster, MD, Szabolcs, MJ, Takuma, S, Burkhoff, D, Wang, J *et al.* (2001). Neovascularization of ischemic myocardium by human bone-marrow-derived angioblasts prevents cardiomyocyte apoptosis, reduces remodeling and improves cardiac function. *Nat Med* **7**: 430–436.

28. Payne, TR, Oshima, H, Okada, M, Momoi, N, Tobita, K, Keller, BB *et al.* (2007). A relationship between vascular endothelial growth factor, angiogenesis, and cardiac repair after muscle stem cell transplantation into ischemic hearts. *J Am Coll Cardiol* **50**: 1677–1684.

29. White, HD, Norris, RM, Brown, MA, Brandt, PW, Whitlock, RM and Wild, CJ (1987). Left ventricular end-systolic volume as the major determinant of survival after recovery from myocardial infarction. *Circulation* **76**: 44–51.

30. Gnecchi, M, Zhang, Z, Ni, A and Dzau, VJ (2008). Paracrine mechanisms in adult stem cell signaling and therapy. *Circ Res* **103**: 1204–1219.

31. Cheng, AS and Yau, TM (2008). Paracrine effects of cell transplantation: strategies to augment the efficacy of cell therapies. *Semin Thorac Cardiovasc Surg* **20**: 94–101.

32. Perez-Ilzarbe, M, Agbulut, O, Pelacho, B, Ciorba, C, San Jose-Eneriz, E, Desnos, M *et al.* (2008). Characterization of the paracrine effects of human skeletal myoblasts transplanted in infarcted myocardium. *Eur J Heart Fail* **10**: 1065–1072.

33. Ebelt, H, Jungblut, M, Zhang, Y, Kubin, T, Kostin, S, Technau, A *et al.* (2007). Cellular cardiomyoplasty: improvement of left ventricular function correlates with the release of cardioactive cytokines. *Stem Cells* **25**: 236–244.

34. Kinnaird, T, Stabile, E, Burnett, MS, Shou, M, Lee, CW, Barr, S *et al.* (2004). Local delivery of marrow-derived stromal cells augments collateral perfusion through paracrine mechanisms. *Circulation* **109**: 1543–1549.

35. Kinnaird, T, Stabile, E, Burnett, MS, Lee, CW, Barr, S, Fuchs, S *et al.* (2004). Marrow-derived stromal cells express genes encoding a broad spectrum of arteriogenic cytokines and promote *in vitro* and *in vivo* arteriogenesis through paracrine mechanisms. *Circ Res* **94**: 678–685.

36. Tse, HF, Siu, CW, Zhu, SG, Songyan, L, Zhang, QY, Lai, WH *et al.* (2007). Paracrine effects of direct intramyocardial implantation of bone marrow derived cells to enhance neovascularization in chronic ischaemic myocardium. *Eur J Heart Fail* **9**: 747–753.

37. Rehman, J, Traktuev, D, Li, J, Merfeld-Clauss, S, Temm-Grove, CJ, Bovenkerk, JE *et al.* (2004). Secretion of angiogenic and antiapoptotic factors by human adipose stromal cells. *Circulation* **109**: 1292–1298.

38. Feng, J, Yang, S, Xu, L, Tian, H, Sun, L and Tang, X (2007). Role of caspase-3 inhibitor in induced anoikis of mesenchymal stem cells in vitro. *J Huazhong Univ Sci Technol Med Sci* **27**: 183–185.

39. Luebke-Wheeler, JL, Nedredal, G, Yee, L, Amiot, BP and Nyberg, SL (2009). E-cadherin protects primary hepatocyte spheroids from cell death by a caspase-independent mechanism. *Cell Transplant* **18**: 1281–1287.

40. Urish, KL, Vella, JB, Okada, M, Deasy, BM, Tobita, K, Keller, BB *et al.* (2009). Antioxidant levels represent a major determinant in the regenerative capacity of muscle stem cells. *Mol Biol Cell* **20**: 509–520.

41. Drowley, L, Okada, M, Beckman, S, Vella, J, Keller, B, Tobita, K *et al.* (2010). Cellular antioxidant levels influence muscle stem cell therapy. *Mol Ther* **18**: 1865–1873.

42. Kumar, A, Mohan, S, Newton, J, Rehage, M, Tran, K, Baylink, DJ *et al.* (2005). Pregnancy-associated plasma protein-A regulates myoblast proliferation and differentiation through an insulin-like growth factor-dependent mechanism. *J Biol Chem* **280**: 37782–37789.

Myocardial Calcification and Fibrosis in Dystrophic Mice is Reduced by RhoA Inactivation
Xiaodong Mu, Ying Tang, Koji Takayama, Bing Wang, Weiss Kurt, and Johnny Huard
Stem Cell Research Center, Department of Orthopaedic Surgery, University of Pittsburgh

Introduction:
Myocardial calcification refers to the excessive deposition of calcium in the cardiac muscle and is usually observed in the aging population as-well-as long-term survivors of substantial myocardial infarctions (1-2). Myocardial calcification could either be the result of chronic degeneration or reflect ongoing pathologic processes (2); however, the cellular and molecular mechanisms leading to myocardial calcification remains largely unknown. We have recently reported the observation of extensive skeletal muscle calcification/heterotopic ossification in the dystrophin/utrophin double knockout (dKO) mouse model of Duchenne muscular dystrophy (3), which could be mediated by the over-activation of the RhoA signaling in muscle stem cells (MSCs) (4). RhoA is a small GTPase protein that regulates cell morphology and migration in response to extracellular signaling and stresses. RhoA activation in MSCs induces their osteogenesis potential, inhibits their adipogenic potential, mediates BMP-induced signaling, and promotes osteoblastic cell survival (5). The involvement of RhoA in mediating inflammatory processes and myocardial fibrosis has previously been described (6). In addition, previous studies have indicated that the sustained activation of the RhoA pathway can block the differentiation of muscle cells by inhibiting myoblast fusion (7). Cardiac involvement is the leading cause of early death in DMD patients, and the current study was performed to elucidate the role of RhoA in mediating fibrosis and calcification in the cardiac muscle of dystrophic mice.

Methods:
1. Animals: Wild-type (WT, C57BL/10J) mice were purchased from Jackson Laboratory. The mdx and dKO (mdx; utrn$^{-/-}$) mice are maintained in our in house colony. Compared to mdx mice which feature a normal life span (~2 years), dKO mice undergo early death (~8 weeks) and have a more severe phenotype that more closely resembles the DMD pathology. All procedures were approved by the Institutional Animal Care and Use Committee (IACUC) at the University of Pittsburgh. **2. RhoA inactivation with Y-27632:** dKO mice from 3 weeks of age received either an intraperitoneal (IP) injection of Y-27632 [5mM in Phosphate Buffered Saline (PBS), 10mg/kg per mouse], which is a systematic inhibitor of RhoA signaling or PBS only (control). IP injections were conducted 3 times a week for 4 weeks. **3. Histology:** Mice were sacrificed and 10μm cryostat sections were prepared from the cardiac muscles of the mice. Alizarin red stain was conducted to stain calcium deposition in the cardiac muscle. **4. Statistics**: N >=6 for each group. Student's T-test was used to evaluate for significance.

Results:
1. Cardiac muscle of dKO mice featured increased fibrosis and calcification when compared to mdx and WT mice.
Trichrome staining of the cardiac muscles from 8-week old WT, mdx, and dKO mice was conducted to characterize ECM collagen deposition, which revealed that fibrosis formation was generally severe in the dKO mice, mild in the mdx mice, and absent in WT mice (**Figure 1A**). Alizarin red staining of the cardiac muscle revealed that calcification occurred in the dKO mice (**Figure 1B**), but not in the WT or mdx mice.

2. Up-regulation of RhoA in the cardiac muscle of the dKO mice.
Semi-quantitative PCR showed that, compared to the WT and mdx mice, the expression of RhoA and the inflammation signaling genes, TNF-α and IL-6, was up-regulated in the dKO cardiac muscle, while the expression of the anti-inflammation gene Klotho was down-regulated (**Figure 1C**). We suggest that the activation of RhoA and inflammatory mediators are involved in the cardiac fibrosis and calcification seen in dKO mice.
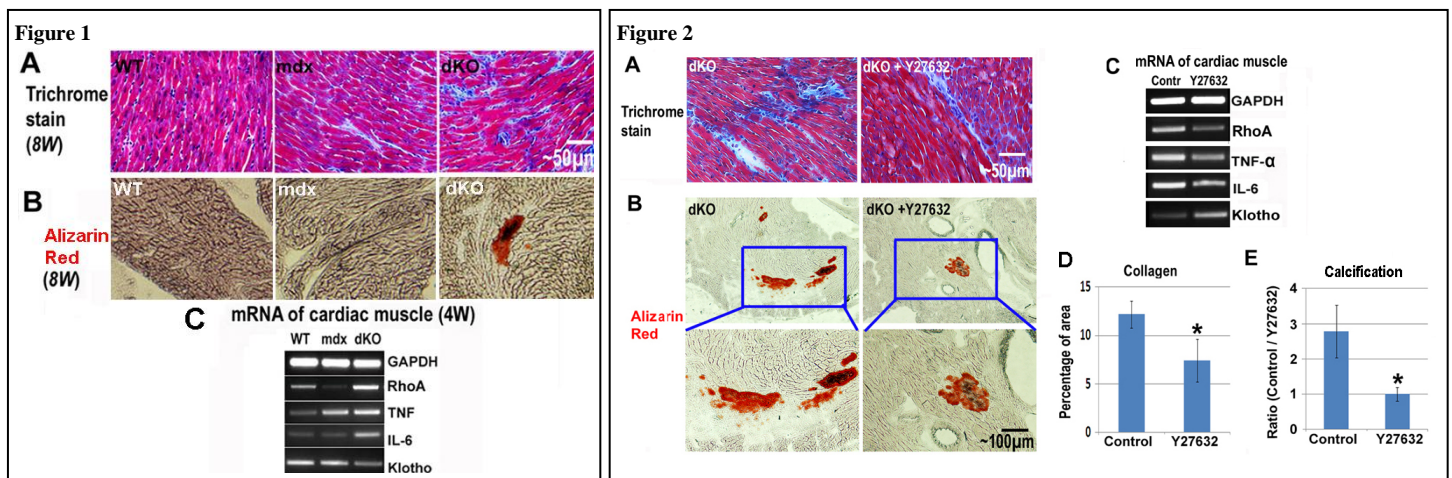
3. Systemic RhoA inactivation via intraperitoneal injection (IP) of Y-27632 reduced fibrosis and HO in dKO cardiac muscle.

We hypothesized that RhoA inactivation could reduce fibrosis and calcification in the cardiac muscles of the dKO mice. To confirm this hypothesis, Y-27632 was injected intraperitoneally (IP) to achieve the systemic inhibition of RhoA signaling in 3-week old dKO mice. As expected, after 4 weeks of continuous injection. Semi-quantitative PCR revealed that the expression of RhoA, TNF-α and IL-6 was down-regulated with Y-27632 administration, while the expression of Klotho was up-regulated (**Figure 2E**). Fibrosis and calcification in the cardiac muscles of dKO mice was decreased compared to non-treated mice (**Figure 2A-D**).

Discussion:

Both calcification and fibrosis in cardiac muscle is typically the result of a pathologic process. Our current results revealed that the RhoA signaling pathway may mediate the calcification and fibrosis processes in the cardiac muscles of dKO mice. RhoA seems to be co-activated with inflammatory signaling in severely dystrophic cardiac muscle, and the inactivation of RhoA signaling could repress this signaling. Therefore, our results indicate that the involvement of RhoA signaling in the therapeutic prevention of calcification and fibrosis in cardiac muscle should be further investigated as a potential target for treating DMD patients and other pathologic conditions of the heart.

Significance: Our data reveals the involvement of RhoA signaling in regulating calcification and fibrosis of cardiac muscle, and indicates RhoA may serve as a potential target for repressing injury-induced and congenital cardiac muscle calcification and fibrosis in humans.

References:

1.   El-Bialy A, Shenoda M, Saleh J, Tilkian A. Myocardial calcification as a rare cause of congestive heart failure: a case report. J Cardiovasc Pharmacol Ther. 2005;10(2):137-43.

2.   Gowda RM, Boxt LM. Calcifications of the heart. Radiol Clin North Am. 2004;42(3):603-17, vi-vii.

3.   Isaac C, Wright A, Usas A, Li H, Tang Y, Mu X, et al. Dystrophin and utrophin "double knockout" dystrophic mice exhibit a spectrum of degenerative musculoskeletal abnormalities. J Orthop Res. 2013;31(3):343-9.

4.   Mu X, Usas A, Tang Y, Lu A, Wang B, Weiss K, et al. RhoA mediates defective stem cell function and heterotopic ossification in dystrophic muscle of mice. FASEB J. 2013;27(9):3619-31.

5.   McBeath R, Pirone DM, Nelson CM, Bhadriraju K, Chen CS. Cell shape, cytoskeletal tension, and RhoA regulate stem cell lineage commitment. Dev Cell. 2004;6(4):483-95.

6.   Zhou H, Li YJ, Wang M, Zhang LH, Guo BY, Zhao ZS, et al. Involvement of RhoA/ROCK in myocardial fibrosis in a rat model of type 2 diabetes. Acta Pharmacol Sin. 2011;32(8):999-1008.

7.   Castellani L, Salvati E, Alema S, Falcone G. Fine regulation of RhoA and Rock is required for skeletal muscle differentiation. J Biol Chem. 2006;281(22):15249-57.

Type of the Paper (Review)

The Role of Antioxidation and Immunomodulation in Post-natal Multipotent Stem Cell-Mediated Cardiac Repair

Arman Saparov [1,2,]*, **Chien-Wen Chen** [2,3,4], **Sarah A. Beckman** [2,4,5], **Yadong Wang** [3,6] **and Johnny Huard** [2,4,6]*

[1] Nazarbayev University Research and Innovation System, Nazarbayev University, Astana, Kazakhstan; E-Mail: asaparov@nu.edu.kz

[2] Department of Orthopedic Surgery, University of Pittsburgh, Pittsburgh, USA; E-Mails: chc88@pitt.edu (C.W.C); jhuard@pitt.edu (J.H.)

[3] Department of Bioengineering, University of Pittsburgh, Pittsburgh, USA; E-Mail: yaw20@pitt.edu (Y.W.)

[4] Stem Cell Research Center, University of Pittsburgh, Pittsburgh, USA

[5] Department of Molecular Cardiovascular Biology, Cincinnati Children's Hospital Medical Center, Cincinnati, USA; E-Mail: beckman.sarah@gmail.com

[6] McGowan Institute for Regenerative Medicine, University of Pittsburgh, Pittsburgh, USA

* Authors to whom correspondence should be addressed; E-Mail: asaparov@nu.edu.kz; Tel.: +7-717-270-6140; Fax: +7-717-270-6054 (A.S.) or E-Mail: jhuard@pitt.edu; Tel.: +1-412- 648-2798; Fax: +1-412- 648-4066 (J.H.).

Abstract: Oxidative stress and inflammation play major roles in the pathogenesis of coronary heart disease including myocardial infarction (MI). The pathological progression following MI is very complex and involves a number of cell populations including cells localized within the heart as well as cells recruited from the circulation and other tissues that participate in inflammatory and reparative processes. These cells, with their secretory factors, have pleiotropic effects that depend on the stage of inflammation and regeneration. Excessive inflammation leads to enlargement of the infarction site, pathological remodeling and eventually, heart dysfunction. Stem cell therapy represents a unique and innovative approach to ameliorate oxidative stress and inflammation caused by ischemic heart disease. Consequently it is crucial to understand the crosstalk between stem cells and other cells involved in post-MI cardiac tissue repair, especially immune cells, in order to harness the beneficial effects of the immune response following MI and further improve

stem cell-mediated cardiac regeneration. This paper reviews the recent findings on the role of antioxidation and immunomodulation in post-natal multipotent stem cell-mediated cardiac repair following ischemic heart disease, particularly acute MI and focuses specifically on mesenchymal, muscle and blood-vessel-derived stem cells due to their antioxidant and immunomodulatory properties.

Keywords: stem cells; myocardial infarction; oxidative stress; inflammation; immune system; cardiac repair

1. Introduction

Cardiovascular disease is the leading cause of mortality in the world with over 17 million deaths in 2008 alone [1], which is estimated to increase to over 23 million by 2030 and to remain the leading cause of deaths [2]. Coronary heart disease causes the majority of deaths in cardiovascular disease with myocardial infarction (MI) often leading to the development of heart failure. MI is caused by occlusion of a coronary artery, which leads to a deficiency of oxygen and nutrients at the site of infarction and the subsequent death of cardiomyocytes. The exposure of danger-associated molecular patterns (DAMPs) from dead cardiomyocytes triggers the migration of neutrophils, monocytes, dendritic cells, lymphocytes and other cells with subsequent initiation of inflammation, oxidative stress, tissue regeneration and cardiac remodeling; however, the mechanisms behind these processes are still not fully understood [3-6].

Stem cell therapy is considered a promising approach in treating coronary heart disease including MI due to the ability of stem cells and/or their secretory factors to influence host cell migration, cellular functions, cardiomyocyte survival, tissue regeneration and healing [7-9]. The use of stem cells and/or their secretory factors may lead to effective therapeutic approaches for reducing the infarct size, generating more functional heart tissue, eliminating heart failure and improving the life of patients who have suffered from MI. The current review highlights the role of oxidative stress and the immune system in pathogenesis of acute MI and focuses specifically on mesodermal stem cells, including mesenchymal, muscle and blood-vessel-derived stem cells, due to their antioxidant and immunomodulatory properties.

2. Oxidative Stress and Inflammation Following Myocardial Infarction

Oxidative stress and inflammation play major roles in tissue damage, clearance of cell debris, myocardial fibrosis, and remodeling of heart tissue following MI, although the details of the initiation, development and control of these processes have not been fully deciphered. In this section, we briefly review the sequence of events related to oxidative stress and inflammation mediated by the cells of the immune system to better understand possible therapeutic targets using stem cells or their factors described in the following sections.

MI causes necrosis and apoptosis of cardiomyocytes and exposure of DAMPs, which are molecules produced by stressed/damaged cells or extracellular matrix fragments, and initiate the innate immune

response and inflammation [10]. The DAMPs that are involved in MI are mainly high motility group box 1 (HMGB1), heat shock proteins (HSPs), fibronectin and hyaluronan fragments (Figure 1). HMGB1, a chromatin binding protein located in the nucleus, which can be secreted from the stressed cells and form a heterodimer with IL-1β [11], stimulates the production of pro-inflammatory cytokines such as TNF-α, IL-1 and IL-6 by macrophages after binding to Toll-like receptor (TLR) 4 [12,13]. In addition, HMGB1 enhances cell migration by forming a heterocomplex with chemokine CXCL12, which is mediated by CXCR4, the receptor for CXCL12 [14]. HSP60, which is a stress protein released from cardiac myocytes after hypoxic shock, can induce the expression of pro-inflammatory cytokines TNF-α and IL-1β, activate caspase 3 and 8, as well as cause DNA fragmentation and apoptosis of cardiac myocytes by binding to TLR4 [15,16]. Both fibronectin and hyaluronan fragments, which are both constituents of the extracellular matrix, can activate the innate immune system by binding to TLR2 and TLR4 [17,18].

Figure 1. Schematic depiction of representative events following MI. MI causes the exposure of DAMPs, initiation of oxidative stress and inflammation, and can lead to the resolution of inflammation, reduction of oxidative stress, formation of scar tissue and left ventricular remodeling. Nevertheless, the pathological processes following MI are very complex with overlaps of depicted events and participation of additional cell types/secretory factors that are not included in this figure.
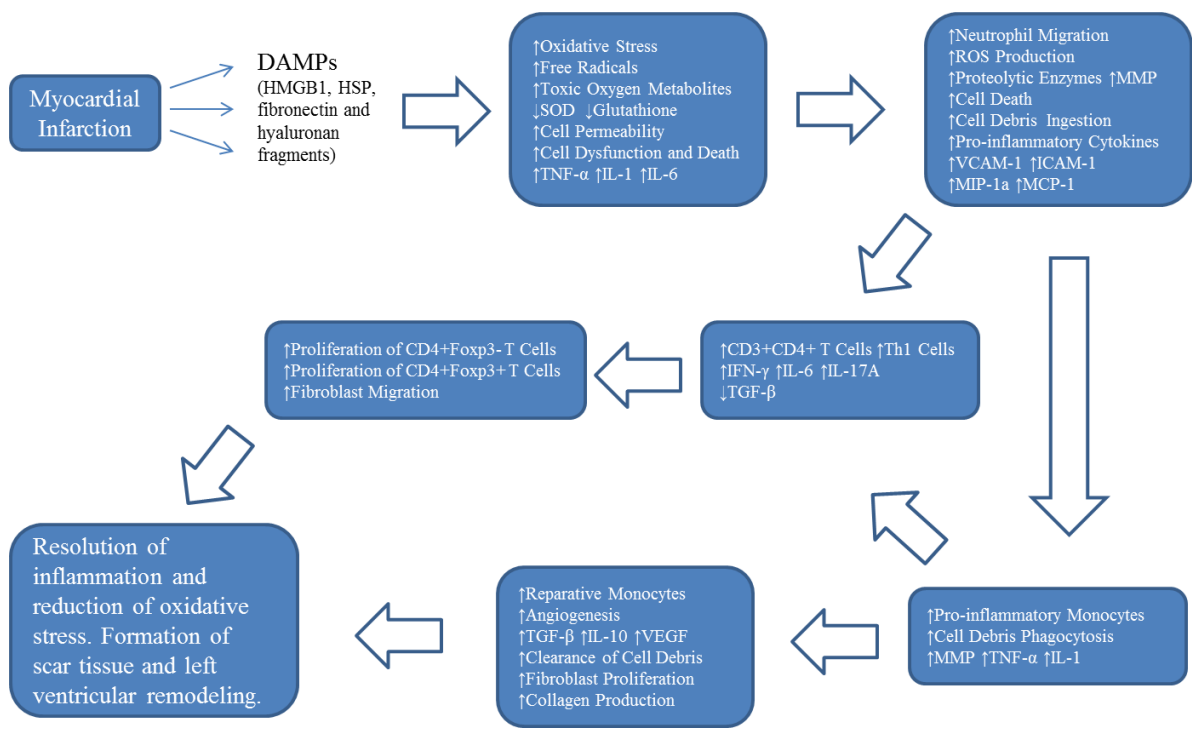
DAMPs are recognized by TLR on the surface of cardiac myocytes, endothelial cells and cells of the immune system. TLR in humans were discovered by Madzhidov and colleagues [19] and are pattern recognition receptors and a part of the innate immune system. TLR4 plays a key role in the response of the innate immune system following MI. Indeed, the TLR4 knockout animals demonstrated diminished inflammation, a reduction in the number of apoptotic cells and CD3+ T cells

in the infarcted area, attenuated left ventricular remodeling and improved animal survival [20,21]. Similarly, the TLR2 knockout mice showed better survival, reduced fibrosis and downregulation of TGF-β expression in the heart tissue [22]. TLR binding results in the recruitment of myeloid differentiation primary response 88 (MyD88), and eventually, the translocation of NF-κB into the nucleus and activation of chemokine and pro-inflammatory cytokine gene expression [23,24]. Furthermore, components of the apoptotic cardiac myocytes and DAMPs can activate the complement system that plays an active role in the pathogenesis of MI [25,26]. Cardiac myocytes express the receptor to C5a, which is up-regulated following MI, and antibodies against C5a decrease infarct size, reduce vascular permeability and adherence of neutrophils to endothelial cells in experimental models of MI [27,28].

Oxidative stress, which results from the excessive production of reactive oxygen species (ROS) and the inability of the antioxidant system to neutralize them, plays a pivotal role in damaging and remodeling cardiac tissue. ROS are oxygen-containing compounds such as superoxide anion, hydroxyl radical and hydrogen peroxide, mainly produced in the heart by neutrophils, cardiac myocytes and endothelial cells. Myocardial ischemia leads to increased ROS activity through two mechanisms: 1) a decrease in the defensive activity including reduced mitochondrial superoxide dismutase function and diminished reserve of reduced glutathione, and 2) an increase in the offensive action including elevated production of free radicals and toxic oxygen metabolites, especially following the post-ischemic reperfusion [29]. ROS cause cell apoptosis by breaking down DNA and stimulating pro-apoptotic signaling pathways. In addition, ROS induce the production of pro-inflammatory cytokines and matrix metalloproteases (MMP) that further aggravate inflammation and pathological remodeling. The regulation of gene expression by ROS is mediated by NF-κB, AP-1 and peroxisome proliferator-activated receptor. Oxidative stress causes endothelial cell dysfunction, up-regulation of adhesion molecules, secretion of pro-inflammatory cytokines, and increase of endothelial cell permeability and migration of neutrophils [30,31].

Neutrophils are the first cells of the immune system that migrate to the site of injury in the heart and produce ROS and proteolytic enzymes (Figure 1). The migration of neutrophils is mediated by up-regulated P-selectin (CD62P) and E-selectin (CD62E) on the surface of endothelial cells [32] and up-regulated L-selectin (CD62L) on the surface of neutrophils [33] as well as an enhanced ability of intercellular cell adhesion molecule-1 (ICAM-1) on the surface of endothelial cells to bind neutrophils [34]. Double knockout mice for P-selectin and ICAM-1 demonstrated a significantly reduced migration of neutrophils without affecting the infarct size [35]. C5, a factor of activated complement, and IL-8 play important roles in neutrophil chemotaxis [36]. The recruited neutrophils ingest dead cell debris, produce MMP to degrade the extracellular matrix, release ROS, and secrete proteolytic enzymes and pro-inflammatory cytokines that further aggravate inflammation. Neutrophils can bind cardiac myocytes via ICAM-1 and directly damage them by producing ROS and proteolytic enzymes [37]. In addition, neutrophils contribute to the initiation of monocyte migration by up-regulating adhesion molecules and by producing chemotactic factors. Neutrophils secrete granules that up-regulate the expression of vascular cell adhesion molecule-1 (VCAM-1) and ICAM-1 on the surface of endothelial cells, stimulate production of IL-8 and macrophage inhibitory protein-1a (MIP-1a) by monocytes and macrophages, and monocyte chemotactic protein-1 (MCP-1) by endothelial cells [38].

Nahrendorf and colleagues demonstrated the biphasic migration of monocytes to the heart tissue in a mouse model of MI [39]. The first population of monocytes that possess pro-inflammatory properties migrate to the site of inflammation via a MCP-1 dependent pathway during the first four days after infarction, phagocytose cell debris, produce MMP which degrade the extracellular matrix and express pro-inflammatory cytokines TNF-α and IL-1β (Figure 1). The second population of monocytes with reparative properties stimulates angiogenesis, expresses TGF-β, IL-10 as well as vascular endothelial growth factor (VEGF), and can be found at the site of inflammation starting by day four after MI with the recruitment mediated by fractalkine. The turnover of monocytes in the infarcted heart is about twenty hours with the death of the majority of cells at the site of inflammation and only a minority of undifferentiated monocytes remaining which can be found mainly in the blood and liver, with smaller numbers present in the spleen and lymph nodes. The spleen serves as a main source of newly differentiated monocytes, and IL-1β plays an essential role in monocytopoesis [40]. Differentiated macrophages phagocytose dead cells and cell debris and clear apoptotic neutrophils and cardiac myocytes. Apoptotic neutrophils produce factors that inhibit neutrophil recruitment and contribute to the production of TGF-β and IL-10 by macrophages [41]. On the other hand, macrophages produce cytokines that stimulate fibroblast proliferation, angiogenesis and the production of collagen. The differentiated macrophages can be divided into two major subsets: 1) classically activated M1, which are stimulated by IFN-γ, and 2) alternatively activated M2, which are induced by IL-4 and IL-13 [42,43]. In addition to neutrophils and monocytes/macrophages, dendritic cells (DC) also play an important role in the pathogenesis of MI. Anzai and colleagues reported that DC migrate to the site of injury reaching their peak concentration at one week following MI and the deletion of DC adversely affected left ventricular remodeling and cardiac function. Furthermore, the deletion of DC caused the elevation in the expression of pro-inflammatory cytokines and a reduction in the level of anti-inflammatory cytokines as well as a shift towards the accumulation of pro-inflammatory monocytes/macrophages in the infarcted myocardium [44].

T lymphocytes are instrumental in the regulation of the immune response and the response following myocardial infarction is no exception. There are two major subtypes of T cells: CD4+ and CD8+ lymphocytes. CD4+ T cells can be divided into several populations based on their functional activity and cytokine profile: Th1 cells produce IFN-γ and are responsible for the defense against intracellular pathogens, Th2 cells secrete IL-4, IL-5 and IL-13 and play a pivotal role in the clearance of extracellular parasites, Th17 cells are characterized by IL-17 production and participate in inflammation and autoimmunity, and regulatory T cells secrete TGF-β and IL-10 to regulate the immune response [45-47]. In contrast, CD8+ T lymphocytes are cytotoxic cells mainly responsible for killing infected and tumor cells [48]. Maisel and colleagues demonstrated that the adoptive transfer of *ex vivo* activated splenocytes, isolated from animals with MI, into healthy syngeneic animals' caused myocardial injury with predominantly lymphocyte and plasma cell infiltration. The injury was cardiac specific with a good correlation between the infarct size in the donor animals and the size of injury in the recipient animals [49]. Interestingly, MI generates cytotoxic T cells that can kill syngeneic cardiomyocytes in a MHC dependent manner [50].

The induction of MI in the experimental animals showed that the levels of IL-17A and IL-6, which can be produced by Th17 cells, were elevated in the infarcted zone compared to the non-infarcted zone [51] and the implication of γδT cells in the local production of IL-17A [52]. The importance of γδT

cells, IL-17A and IL-23 genes in the pathogenesis of MI was demonstrated by using knockout mice when the deletion of any of above mentioned parameters improved animal survival and cardiac function with the reduction of the infarct size [52]. Furthermore, Hofmann and colleagues reported that MI induces the increase in the number of CD3+CD4+ T cells in the myocardium with up-regulation of IFN-γ expression, one of the main pro-inflammatory cytokines produced by Th1 cells, and stimulates proliferation of both conventional CD4+Foxp3- T cells and regulatory CD4+Foxp3+ T cells in the heart-draining lymph nodes. The generation of the adaptive immune response and regulatory T cells plays an important role in the resolution of inflammation since MI in CD4 knockout mice demonstrated an increase in the number of granulocytes and monocytes/macrophages with pro-inflammatory properties in the infarct zone and collagen formation impairment compared to the wild type mice with MI [53]. In addition, it has been shown that the impairment in the recruitment of CD4+Foxp3+ regulatory T cells to the site of tissue injury, which is mediated via CCR5/MIP, causes an increase in the expression of pro-inflammatory cytokines TNF-α, IL-1β and IL-6, and elevates the expression as well as activity of MMP which results in an adverse effect on heart tissue remodeling [54]. The clinical data demonstrated that there is a shift towards the Th1 immune response in patients with acute MI [55], with increased levels of Th1 cells in the blood and IFN-γ in the plasma as well as decreased levels of CD4+CD25+Foxp3+ regulatory T cells in the blood and TGF-β in the plasma [56]. Moreover, the cells of the immune system contribute to scar tissue formation by producing MMP and paracrine factors and by stimulating the migration of fibroblasts [57]. These findings demonstrate that in addition to the innate immune system, the adaptive immune system also plays a major role in tissue damage, clearance of cell debris, and left ventricular remodeling following MI (Figure 1).

Thus, initiation, development and resolution of inflammation in the heart following MI represent a very complex and dynamic process. Consequently, it is crucial to define the balance between detrimental and beneficial effects resulting from the innate and adaptive immune responses in injured myocardium, presumably through paracrine cross-talk and/or cellular interactions between immune cells and various cell populations including cardiac myocytes, endothelial cells, cardiac fibroblasts, and resident/circulating stem cells.

3. Cellular Antioxidant Level Represents a Major Determinant in the Cardiac Regenerative Capacity of Stem Cells

The microenvironment after ischemic injury in the cardiac milieu is deleterious to local cells due to oxidative and inflammatory stress, excessive fibrosis, and inadequate angiogenesis [58]. This harsh microenvironment has been suggested as a principal reason for a universally low survival rate of implanted stem cells [59]. Cell survival is an integral and key component of cell-mediated tissue recovery, which can be the result of a reduction in the death of native cells, an increased persistence of donor cells, or a combination of the two [60].

Numerous attempts to repair the infarcted heart using exogenous stem cells have been made; however, very few of the transplanted donor cells actually survive or engraft long-term, a formidable obstacle that needs to be addressed [61]. Alternatively, muscle derived stem cells (MDSCs), a CD34+/Sca-1+ stem cell population that has been extensively investigated for tissue repair and regeneration, restored the heart function and tissue structures (increased angiogenesis, reduced

ventricular remodeling, and cardiomyocyte differentiation) after ischemic injury more effectively than conventional CD56+ myoblasts [62,63]. This is attributed to, at least in part, the greater number of MDSCs that survived after 12 weeks post-transplantation as well as the robust paracrine function of the MDSCs secreting a number of angiogenic/trophic factors [62]. Nevertheless, it is not clear how the MDSCs survived the unfavorable environment following the ischemic cardiac insult more efficiently than the CD56+ myoblasts.

In an attempt to elucidate the mechanism(s) behind MDSC-mediated heart repair, various cellular functionalities were examined, including apoptosis under oxidative and inflammatory stress. It was found that under conditions of oxidative stress, there were less apoptotic MDSCs than CD56+ myoblasts [62]. This indicates that MDSCs are more resistant to oxidative stress-induced apoptosis than myoblasts. Inflammatory stress-induced cell death was also examined following TNF-α stimulation. The results showed significantly more cell death in the myoblast population compared to the MDSC population, highlighting the unique survival advantage of MDSCs over myoblasts under stressful conditions [64]. Additional analyses revealed that MDSCs exhibit increased levels of the antioxidant glutathione (GSH) and super-oxide dismutase (SOD) as well as decreased levels of ROS after exposure to H_2O_2 [64].

To further assess the role of antioxidant capacity after cell transplantation, MDSCs were treated with diethyl maleate (DEM), a thiol-depleting agent that decreases GSH levels. The DEM treatment resulted in a decreased ratio of MDSC engraftment in skeletal muscles, to a similar level seen in myoblast transplantation, indicating that both *in vitro* and *in vivo*, antioxidant levels are critical to the survival and transplantation efficiency of MDSCs [64]. On the other hand, to investigate whether the protection by antioxidant can be augmented, antioxidant levels were increased by treating the MDSCs with the glutathione precursor N-acetylcysteine (NAC). It was shown that NAC treatment of MDSCs increased their survival under oxidative and inflammatory stress *in vitro* compared to untreated MDSCs while, conversely, treatment with DEM decreased their survival [65].

Furthermore, MDSCs pre-treated with NAC 24 hours prior to the intramyocardial transplantation into the ischemic heart notably increased cardiac contractility, compared to untreated MDSCs. There were also improvements in angiogenesis and a reduction of fibrosis. These results indicate that cell survival is indeed an important aspect of cellular therapy for cardiac repair. Methods increasing survival of transplanted cells, as well as native tissue/cells, may substantially aid in the repair process. When the cells are pre-treated with an antioxidant, their capacity to neutralize oxidative species will thus increase, which explains their augmented survival. Other studies have also indicated that cell survival is a key to cardiac cell therapy. Though mesenchymal stem cells have been shown to promote functional and histological improvements after myocardial infarction, when the cells were transduced with the survival factor Akt, this improvement was significantly increased [66]. On another note, VEGF, a potent angiogenic factor, has also been shown to exert a protective effect on the surrounding cardiomyocytes [67]. Consequently, the cell survival and paracrine function of MDSCs appear to be two independent yet inter-related areas where further improvements can be made to further improve cardiac cell therapy.

Similarly, when preconditioned with Carvedilol, which is a nonselective β-blocker with independent antioxidant properties for scavenging superoxide anions and hydroxyl radicals, treated MSCs exhibited significant protection against H_2O_2-induced oxidative stress and cell death, compared

with untreated cells [68]. Furthermore, transplantation of MSCs with adjuvant treatment of Carvedilol following MI resulted in significant improvement in cardiac function, decreased fibrosis, and reduced cellular apoptosis when compared with the MSC-only group. Additionally, the paracrine mechanism by which MSCs protect cardiomyocyte following ischemia/reperfusion (I/R) injury was further demonstrated by Desantiago et al. using an *in vitro* model of I/R [69]. Reperfusion of mouse cardiomyocytes with MSC-conditioned tyrode (MSC-ConT) led to a decreased number of attenuated cardiomyocyte shortening that resulted from depolarization of mitochondrial membrane potential and subsequent increase of diastolic Ca2+ as well as prolonged cardiomyocyte survival. The antioxidant capacity of MSC-ConT can be tied, at least partly, to the presence of extracellular superoxide dismutase (SOD3) in the solution, reducing reperfusion-induced ROS production.

4. Mesenchymal Stem Cells as Immunomodulators in Cardiac Repair

Mesenchymal stem cells (MSCs), which were initially identified in the bone marrow but can be found and isolated from umbilical cord, placenta, adipose, muscle and other tissues, have attracted the attention of scientists and clinicians as a good source for stem cell-mediated therapy for the following three main reasons. First, MSCs can differentiate into a number of different cell types including cardiac myocytes, endothelial cells, osteoblasts, chondrocytes and adipocytes [70-74]. Second, MSCs are immunoprivileged because of high expression of immunomodulatory MHC-Ib and low or no expression of immunogenic MHC-Ia, MHC-II and co-stimulatory molecules [75,76]. In addition, MSCs possess strong immunosuppressive properties that are mediated via a cell contact-dependent mechanism and production of soluble factors such as prostaglandin E2, nitric oxide, hepatocyte growth factor, TGF-β1, IL-10, indoleamine 2,3-dioxygenase and heme oxygenase-1 [77-81]. However, MSCs become immunogenic after differentiation because of the down-regulation of MHC-Ib and up-regulation of MHC-Ia and MHC-II [76]. Third, MSCs have the ability to migrate to the site of injury and repair the tissue [82,83]. This section of the review is dedicated to the immunomodulatory properties of MSCs in cardiac repair, particularly following acute MI, although their mechanisms of action are complex and still not fully understood. The immunomodulatory effect of MSCs is mainly mediated by paracrine factors because only a minority of injected stem cells is present in the heart tissue [84].

Human MSCs prolong the survival of neutrophils that is mediated by IL-6 with subsequent stimulation of STAT-3 [85,86] and inhibit ROS production, particularly hydrogen peroxide, by stimulated neutrophils that is mediated by IL-6 without affecting their phagocytic and chemotactic activities [86]. A direct myocardial injection of cells that contain human mesenchymal and hematopoietic progenitor cells significantly reduced the number of neutrophils at an earlier time point compared to the control group in a rat experimental model of MI [87]. Moreover, the reduction in the number of recruited neutrophils is probably mediated by a decrease in the levels of pro-inflammatory cytokines such as IFN-γ, TNF-α and IL-1 in the group of animals injected with MSCs.

The systemic administration of human MSCs in the experimental model of acute MI causes a reduction in the total number of monocytes/macrophages in the cardiac tissue. However, the number of CD206+ and F4/80+ cells increased in the group of animals that received MSCs. The increase in the number of alternatively activated/anti-inflammatory macrophages may be mediated by an increase of

IL-10 expression and a decrease in the expression of IL-1β and IL-6 at the site of cardiac injury [88]. The *in vitro* data are consistent with the data obtained on experimental animals and demonstrated that human MSCs decrease the number of classically activated mouse bone marrow derived Ly6C+ macrophages and increase the number of alternatively activated CD206+ macrophages, the latter effect is mediated by IL-10 [88]. In addition, the *in vitro* analyses using MSCs and macrophages from the same species confirmed the data obtained on experimental animals. Indeed, mouse MSCs increased the production of IL-10 and IL12p40 while the production of IFN-γ, TNF-α, IL-6 and IL12p70 by activated peritoneal macrophages decreased. The modulatory effect of MSCs was dependent on cell-cell contact and soluble factors, which was partially mediated by prostaglandin E2. Furthermore, mouse MSCs polarized macrophages towards the alternatively activated phenotype with increased phagocytic activity of apoptotic cells and caused the impairment of antigen-presenting capacity [89].

Similar results were reported by other groups using human MSCs and human macrophages. The incubation of human MSCs with human macrophages polarized macrophages toward the alternatively activated/anti-inflammatory phenotype with up-regulation of CD206, CD163 and CD16 as well as the increased secretion of IL-4, IL-10, IL-13 and VEGF, while the levels of IFN-γ, TNF-α, IL-1α, IL-12, IL-17 and IL-23 were decreased [90]. The polarization effect of MSCs on macrophages in these experiments was mediated by IL-6. Kim and colleagues demonstrated that the polarization of monocyte-derived macrophages towards the CD206+ phenotype under the influence of MSCs is mediated by both direct cell-cell contacts and soluble factors [91]. The incubation of human MSCs with stimulated macrophages further increased the intra-cellular levels of IL-10 and IL-6 compared to the control group. In addition, IFN-γ and TNF-α stimulated human MSCs induced the polarization of CD14+ monocytes towards the CD206+ phenotype with significant IL-10 up-regulation, and blocking indoleamine 2,3-dioxygenase partially reduced IL-10 production [92] .

There are a number of published papers on the influence of MSCs on adaptive immunity, particularly on T cells, following MI. Indeed, the number of CD3+ and CD4+ T cells decreased at 24 and 72 hours after direct myocardial injection in animals that received a population of cells containing mesenchymal and hematopoietic progenitor cells [87]. Similar results were obtained by Burchfield and colleagues who reported that intra-myocardial injection of mouse bone marrow derived mononuclear cells (BM-MNCs) into the mice with MI significantly reduced CD3+ T cell recruitment, which is mediated by IL-10 produced by BM-MNCs [93]. The *in vitro* analysis showed that IFN-γ and TNF-α treated human MSCs suppress the proliferation of nonspecifically stimulated human CD3+ T cells that is directly mediated by indoleamine 2,3-dioxygenase, which catalyzes tryptophan degradation, an important amino acid required for T cell proliferation, and indirectly via the generation of alternatively activated macrophages, which produce IL-10 [92]. In addition to the immunosuppressive ability of MSCs on the T cell population, MSCs contribute to the generation of regulatory T cells. Human MSCs stimulate the generation of CD4+CD25+Foxp3+ regulatory T cells in allogeneic culture of purified human CD4+ T cells, which is mediated through a contact-dependent mechanism and the production of soluble factors such as PGE2 and TGF-β, although the presence of soluble factors alone is not sufficient for the generation of regulatory T cells [94]. Similarly, human MSCs contribute to regulatory T cell generation, which is mediated via the Notch1 signaling pathway [95], and maintain their suppressive activity in a mixed lymphocyte reaction [96]. In the experimental model of acute MI, the adoptive transfer of CD4+CD25+ regulatory T cells improved left ventricular contraction and cardiac

function, which may be mediated by the local reduction of IFN-γ levels [97], and by the decrease in the recruitment of neutrophils, macrophages and lymphocytes as well as by the down-regulation of TNF-α and IL-1β expression and elevation of IL-10 at the site of injury [98]. Moreover, CD4+CD25+ regulatory T cells suppress cytotoxic T lymphocyte-mediated lysis of cardiac myocytes and inhibit apoptosis of cardiomyocytes via a contact-dependent mechanism and IL-10 production [98].

In addition to various growth factors and cytokines produced by MSCs, exosomes recently attracted the attention of researchers. Exosomes are small extracellular vesicles that are secreted by a number of cell types and contain RNAs and proteins, which can affect various biological functions. It has been demonstrated that exosomes derived from MSCs reduce infarct size, decrease oxidative stress and cell death in an experimental model of myocardial infarction/reperfusion injury [99,100]. Taken together, the reviewed data indicate that MSCs, through cell-cell contact mechanisms and/or production of soluble factors, create an environment that suppresses ROS production by neutrophils, polarizes monocytes/macrophages towards an alternatively activated/anti-inflammatory phenotype, inhibits proliferation and generation of effector T cells as well as contributes to the increase in the number of regulatory T cells, and as a result, prevents adverse left ventricular remodeling, promotes angiogenesis and improves cardiac function.

5. Human Blood Vessel-Derived Stem Cells for Cardiac Repair and Regeneration

Blood vessels throughout the human body are typically composed of three structural layers: intima, media, and adventitia [101]. At the microvascular level, the structure of the vascular wall is reduced to only endothelial cells (ECs) and surrounding perivascular stromal/mural cells, i.e. pericytes [102]. It has been suggested that PCs as well as other vascular cell population(s) represent an origin of adult multipotent stem/progenitor cells [103-106]. Recently, our group and other laboratories have successfully identified several subpopulations of multi-lineage precursor cells within the human vasculature, including myogenic endothelial cells (MECs), pericytes (PCs), and adventitial cells (ACs) [106-108]. Collectively we named these three precursor subpopulations, "human blood-vessel-derived stem cells (hBVSCs)". These subsets of hBVSCs can be purified from blood vessels using fluorescence-activated cell sorting (FACS), based on their unique profiles of cell surface markers, and share striking similarities to typical mesenchymal stem/stromal cells in culture [105]. Specifically within the human skeletal muscle, MECs and PCs can be identified and isolated from the microvasculature [105-107]. Purified MECs and PCs have been shown to repair/regenerate injured and/or genetically defective tissues more efficiently than vascular ECs and/or conventional CD56+ myoblasts [106,107]. In this section, we summarize the recent progress in the translational applications of MECs and PCs in cardiovascular regenerative medicine.

MECs, a putative developmental intermediate between ECs and myogenic cells (MCs), have been proposed as the human counterpart of murine MDSCs due to their similar anatomical localization and scarcity *in situ* as well as versatile regenerative functionality [109]. MECs not only express MC markers such as CD56 and Pax7, but also express EC markers including CD34, CD144 (VE-cadherin), von Willebrand factor (vWF), and Ulex europaeus agglutinin-1 (UEA-1) [107,110]. Though present at a very low frequency *in situ*, MECs (CD34+/CD56+/CD144+/CD45-) can be purified by FACS to homogeneity. MECs can be expanded efficiently in long-term culture, at the clonal level, and exhibit

myogenic, adipogenic, osteogenic, and chondrogenic developmental potentials *in vitro* and *in vivo* [107,109,110]. MECs have also been shown to participate in angiogenesis/vasculogenesis *in vitro* and *in vivo* [109]. The regenerative capacity of MECs in the cardiac milieu has been demonstrated by Okada and colleagues in an ischemic injury model [63]. When transplanted intramyocardially into the ischemic hearts of immunodeficient mice, MECs restored cardiac contractile function more effectively than conventional CD56+ MCs and ECs as is observed with murine MDSCs [62]. Histological analyses showed a significant reduction in cardiac fibrosis and cellular apoptosis as well as augmented angiogenesis and cell proliferation in MEC-injected hearts. These beneficial effects have been largely attributed to the paracrine function of MECs, especially the elevated secretion of VEGF under hypoxia. Nevertheless, transplanted MECs generated robust engraftments and a small number of donor cell-derived cardiomyocytes within the ischemic myocardium, indicating the role of cell survival and differentiation in MEC-mediated cardiac repair [63].

PCs are microvascular mural cells commonly known for their vascular regulatory and supportive functions [111-113], and PC-EC interactions modulate EC proliferation and vascular remodeling [114-116]. Nevertheless, the lack of homogeneous PCs in the past hindered further investigations to explore their regenerative potential. Using similar immunohistochemical and flow cytometry strategies, our group identified and purified PCs from multiple human tissues based on the expression of CD146 (Mel-CAM), NG2 (chondroitin sulphate), platelet-derived growth factor receptor-beta (PDGFRβ), alkaline phosphatase (ALP), with the absence of myogenic (CD56), hematopoietic (CD45), and endothelial (CD31, CD34, and CD144) cell surface markers [106]. Interestingly, only PCs surrounding microvessels (arterioles and venules), but not those around most capillaries, expressed alpha-smooth muscle actin (a-SMA). PCs, natively and in culture, displayed typical MSC differentiation capacities and expressed classic MSC markers: CD44, CD73, CD90 and CD105, indicating their developmental role as precursors of MSCs [106]. The potential applications of FACS-purified PCs (CD146+/CD34-/CD45-/CD56-) in cardiovascular diseases have recently been investigated [117,118]. When transplanted into ischemic hearts of immunodeficient mice, PCs derived from human skeletal muscle were shown to notably improve cardiac contractility and attenuate left ventricular dilatation, superior to CD56+ MCs, for up to 8 weeks [117]. Histological analyses revealed considerable structural recovery in PC-treated hearts, including increased host angiogenesis and substantial reduction of chronic inflammation and myocardial fibrosis at the infarct site. The beneficial effects of PC treatment were attributed to the robust paracrine function of PCs and, to a lesser extent, their direct cellular involvement including perivascular homing, direct interactions with host cells, and differentiation into cardiac cell types [117]. Moreover, PCs were seeded onto small-diameter, bi-layered elastomeric scaffolds to investigate their vascular reparative capacity [118]. After implantation for 8 weeks in Lewis rats, PC-seeded aortic interposition grafts showed a significantly higher rate of vessel patency than unseeded controls and exhibited favorable tissue remodeling including the presence of multiple layers of smooth muscle cells, elastin deposition, and endothelialization in the lumen, suggesting the potential of PCs in vascular tissue engineering.

Apart from MECs and PCs, another distinct subset of hBVSCs, i.e. ACs, which resides in the adventitia of human vasculature, has recently been described as a putative pericyte progenitor population [108,119,120]. Campagnolo and colleagues and Katare and colleagues respectively reported that ACs (CD34+/31-) derived from adventitial vasa vasorum of human saphenous vein exert

significant therapeutic efficacy in murine ischemic limbs and infarcted hearts, owing primarily to their robust angiogenic/vasculogenic and angiocrine capacities [119,120]. On the other hand, applying the same pre-plating technique used for murine MDSC isolation, our group recently reported the isolation of human slowly adhering cells (hSACs) and explored their therapeutic effect in the ischemic mouse heart [121]. hSACs not only exhibited significantly greater survival under oxidative and inflammatory stress than their rapidly adhering counterparts, but also notably promoted functional and structural recovery of ischemic hearts [121]. Altogether these data indicate robust therapeutic capacities of hBVSC subsets and mMDSC counterparts in cardiovascular regenerative medicine.

6. The Role of Human Pericytes in Antioxidation and Immunomodulation

PCs, also known as mural or Rouget cells, are located around endothelial cells in the blood microvessels, incompletely surrounding them, and play a major role in promoting the survival, adhesion and mechanical stabilization of endothelial cells. Moreover, PCs are essential in tissue repair and fibrosis, the development and maintenance of the blood brain barrier, diabetic retinopathy and cancer development [102,122]. In this section, we will review the role of human PCs in antioxidation and immunomodulation.

Using purified MECs and PCs from the same donor, we are currently investigating the antioxidative capacities of these two hBVSC subpopulations under simulated oxidative stress conditions induced by hydrogen peroxide (H_2O_2). Our preliminary results showed that PCs proliferated at a higher rate than MECs when stimulated with H_2O_2 (100 and 250μM) while more MECs survived in a higher concentration of H_2O_2 (400μM) than the PCs, implicating differential cellular antioxidation in MECs and PCs (Chen and Saparov, unpublished results) [64]. Regarding the published data on the role of PCs in immunomodulations, Stark and colleagues reported [123] that TNF-α and LPS stimulated human placental PCs up-regulated the expression of TLR2, TLR4, TNF receptor and NLRP3 (NLR family, pyrin domain containing 3). The stimulation of PCs by DAMPs as well as TNF-α and LPS also elevated the expression of ICAM-1 on the surface of PCs that is used to bind neutrophils and monocytes via β2-integrins. The analysis of cytokine and chemokine mRNA expression by human placental PCs showed that they constitutively expressed IL-6, macrophage migration inhibitory factor (MIF) and the following chemokines: CXCL1, CXCL8 and CCL2. The stimulation of PCs by DAMPs as well as with TNF-α and LPS up-regulated the expression of all cytokines and chemokines, although the levels of up-regulation depended on the stimulus. Moreover, the human placental PCs constitutively express NF-κB and IL-1β, and stimulation with TNF-α increased their expression. The analysis of protein production demonstrated that un-stimulated PCs produced detectable levels of MIF, CXCL1, CXCL8 and CCL2. Both TNF-α and LPS increased MIF production as early as 6 hours after stimulation by LPS. However, lysate of necrotic cells increased MIF production 1 hour after stimulation, which is indicative of MIF pre-existence within the PCs. Furthermore, the secretion of chemokines was also elevated after stimulation. The combination of secreted MIF and ICAM-1 expressed on the surface of PCs are crucial for their interaction with neutrophils and monocytes via integrins expressed on the surface of these cells. The analysis of factors, which are secreted by human placental PCs and are necessary for the *in vitro* migration of neutrophils and monocytes, revealed that MIF and CXCL8 are required for neutrophil migration, while MIF in combination with CCL2 are

implicated in monocyte migration. In addition, TNF-α stimulated PCs activated both neutrophils and monocytes to up-regulate mRNA expression of TLR, MMP and integrins as well as increased the surface expression of CD69 on monocytes, CD11b on neutrophils and extended neutrophil survival [123,124]. These experiments indicate that PCs express pattern recognition receptors to DAMPs and pathogen-associated molecular patterns (PAMPs) and their activation causes the secretion of cytokines and chemokines, some of which are capable of activating neutrophils and monocytes, and influencing their migration which demonstrates the important role of PCs in innate immunity.

Maier and Pober demonstrated [125] that human placental PCs express MHC class I, ICAM-1, PD-L1, PD-L2 without MHC class II and co-stimulatory molecules (CD80 and CD86) expression. The stimulation with IFN-γ in addition to further increase in the expression of MHC-I, ICAM-1, PD-L1 and PD-L2 also up-regulated the expression of MHC-II. Similar results were reported by Verbeek and colleagues using human brain PCs, that in addition to MHC-I and ICAM-1, un-stimulated human brain PCs also express VCAM-1, and stimulation with TNF-α further up-regulated the expression of all three markers. The authors also demonstrated that VLA-4/VCAM-1 is important for T cell interaction with human brain PCs [126]. The experiments with co-culturing placental PCs with allogeneic CD4+ T cells showed that IFN-γ pre-stimulated PCs activated CD4+ T cells to up-regulate the activation markers, CD25 and CD69, to produce very low but detectable levels of IFN-γ and IL-2 without entering into the cell cycle, compared to the un-stimulated PCs. As a result, it caused CD4+ T cells to enter into an anergic state with up-regulation of genes associated with human T cell anergy. However, IFN-γ pre-stimulated PCs are capable of inducing allogeneic CD4+ T cell proliferation if these cells are pre-activated with autologous to PCs cells, which indicate that PCs can activate the effector/memory cells. In addition, both IFN-γ stimulated and un-stimulated placental PCs suppress the CD4+ T cell response to allogeneic cells in a transwell system that is partially inhibited by TGF-β and IL-10 [125,127]. Tu and colleagues also reported that human retinal PCs inhibit the proliferation of activated CD4+ T cells [128]. Our preliminary data showed that un-stimulated human PCs, which were isolated from human skeletal muscle based on the expression of the reported phenotype CD146+/CD34-/CD45-/CD56-, secrete MCP-1 (Chen and Saparov, unpublished results). Both oxidative stress and inflammatory stimulus with LPS further increased MCP-1 production by human PCs while secretion of TGF-β by un-stimulated PCs slightly increased after exposure to oxidative stress *in vitro*, implicating the role of microenvironmental stimulation on the immunomodulatory function of PCs (Chen and Saparov, unpublished results). Overall, the published data demonstrate that human PCs can influence both innate and adaptive immune responses via a cell-cell contact mechanism and by producing soluble factors such as IL-1, IL-6, MIF as well as several chemokines, and can be a good source for stem cell-mediated therapy.

7. Conclusions

The lack of oxygen and nutrients following MI triggers a complex and dynamic process that involves the resident cells at the site of infarction as well as the recruited cells from the circulation and other organs, generating inflammation and oxidative stress and further causing cardiac tissue damage, repair and heart remodeling. Both innate and adaptive immune systems play pivotal roles in this process by producing pro-inflammatory cytokines, reactive oxygen species, proteolytic enzymes as

well as chemokines. In addition to damaging cardiac tissue, the cells of the immune system actively clean the site of infarction, resolve inflammation, promote angiogenesis and participate in heart regeneration. Stem cell therapy diminishes the detrimental effect caused by the immune system and contributes to resolving inflammation as well as improving cardiac function. Understanding the crosstalk between cellular parties involved in this process will facilitate the enhancement of therapeutic approaches in improving cardiac regeneration, potentially eliminating heart failure and reducing mortality following MI.

Acknowledgments

Conflict of Interest

J.H. received remuneration from Cook MyoSite, Inc. for consulting services and for royalties received from technology licensing. All other authors have no conflict of interest to disclose.

References and Notes

[1] Alwan, A. *Global Status Report on Noncommunicable Diseases 2010.*; World Health Organization, 2011.

[2] Mathers, C.D.; Loncar, D. Projections of Global Mortality and Burden of Disease from 2002 to 2030. PLoS medicine **2006**, *3*, e442.

[3] Arslan, F.; de Kleijn, D.P.; Pasterkamp, G. Innate Immune Signaling in Cardiac Ischemia. Nature Reviews Cardiology **2011**, *8*, 292-300.

[4] Coggins, M.; Rosenzweig, A. The Fire within: Cardiac Inflammatory Signaling in Health and Disease. Circ. Res. **2012**, *110*, 116-125.

[5] Frangogiannis, N.G. Regulation of the Inflammatory Response in Cardiac Repair. Circ. Res. **2012**, *110*, 159-173.

[6] Swirski, F.K.; Nahrendorf, M. Leukocyte Behavior in Atherosclerosis, Myocardial Infarction, and Heart Failure. Science **2013**, *339*, 161-166.

[7] Ptaszek, L.M.; Mansour, M.; Ruskin, J.N.; Chien, K.R. Towards Regenerative Therapy for Cardiac Disease. The Lancet **2012**, *379*, 933-942.

[8] Choudry, F.A.; Mathur, A. Stem Cell Therapy in Cardiology. Regenerative medicine **2011**, *6*, 17-23.

[9] Anversa, P.; Kajstura, J.; Rota, M.; Leri, A. Regenerating New Heart with Stem Cells. J. Clin. Invest. **2013**, *123*, 62-70.

[10] Matzinger, P. The Danger Model: A Renewed Sense of Self. Science Signaling **2002**, *296*, 301.

[11] Sha, Y.; Zmijewski, J.; Xu, Z.; Abraham, E. HMGB1 Develops Enhanced Proinflammatory Activity by Binding to Cytokines. The Journal of Immunology **2008**, *180*, 2531-2537.

[12] Yang, H.; Hreggvidsdottir, H.S.; Palmblad, K.; Wang, H.; Ochani, M.; Li, J.; Lu, B.; Chavan, S.; Rosas-Ballina, M.; Al-Abed, Y. A Critical Cysteine is Required for HMGB1 Binding to Toll-Like Receptor 4 and Activation of Macrophage Cytokine Release. Proceedings of the National Academy of Sciences **2010**, *107*, 11942-11947.

[13] Tsung, A.; Sahai, R.; Tanaka, H.; Nakao, A.; Fink, M.P.; Lotze, M.T.; Yang, H.; Li, J.; Tracey, K.J.; Geller, D.A. The Nuclear Factor HMGB1 Mediates Hepatic Injury After Murine Liver Ischemia-Reperfusion. J. Exp. Med. **2005**, *201*, 1135-1143.

[14] Schiraldi, M.; Raucci, A.; Muñoz, L.M.; Livoti, E.; Celona, B.; Venereau, E.; Apuzzo, T.; De Marchis, F.; Pedotti, M.; Bachi, A. HMGB1 Promotes Recruitment of Inflammatory Cells to Damaged Tissues by Forming a Complex with CXCL12 and Signaling Via CXCR4. J. Exp. Med. **2012**, *209*, 551-563.

[15] Kim, S.; Stice, J.P.; Chen, L.; Jung, J.S.; Gupta, S.; Wang, Y.; Baumgarten, G.; Trial, J.; Knowlton, A.A. Extracellular Heat Shock Protein 60, Cardiac Myocytes, and Apoptosis. Circ. Res. **2009**, *105*, 1186-1195.

[16] Li, Y.; Si, R.; Feng, Y.; Chen, H.H.; Zou, L.; Wang, E.; Zhang, M.; Warren, H.S.; Sosnovik, D.E.; Chao, W. Myocardial Ischemia Activates an Injurious Innate Immune Signaling Via Cardiac Heat Shock Protein 60 and Toll-Like Receptor 4. J. Biol. Chem. **2011**, *286*, 31308-31319.

[17] Taylor, K.R.; Yamasaki, K.; Radek, K.A.; Nardo, A.D.; Goodarzi, H.; Golenbock, D.; Beutler, B.; Gallo, R.L. Recognition of Hyaluronan Released in Sterile Injury Involves a Unique Receptor Complex Dependent on Toll-Like Receptor 4, CD44, and MD-2. Science Signaling **2007**, *282*, 18265.

[18] Arslan, F.; Smeets, M.B.; Vis, P.W.R.; Karper, J.C.; Quax, P.H.; Bongartz, L.G.; Peters, J.H.; Hoefer, I.E.; Doevendans, P.A.; Pasterkamp, G. Lack of Fibronectin-EDA Promotes Survival and Prevents Adverse Remodeling and Heart Function Deterioration After Myocardial InfarctionNovelty and Significance. Circ. Res. **2011**, *108*, 582-592.

[19] Medzhitov, R.; Preston-Hurlburt, P.; Janeway, C.A. A Human Homologue of the Drosophila Toll Protein Signals Activation of Adaptive Immunity. Nature **1997**, *388*, 394-397.

[20] Oyama, J.; Blais Jr, C.; Liu, X.; Pu, M.; Kobzik, L.; Kelly, R.A.; Bourcier, T. Reduced Myocardial Ischemia-Reperfusion Injury in Toll-Like Receptor 4-Deficient Mice. Circulation **2004**, *109*, 784-789.

[21] Riad, A.; Jäger, S.; Sobirey, M.; Escher, F.; Yaulema-Riss, A.; Westermann, D.; Karatas, A.; Heimesaat, M.M.; Bereswill, S.; Dragun, D. Toll-Like Receptor-4 Modulates Survival by Induction of Left Ventricular Remodeling After Myocardial Infarction in Mice. The Journal of Immunology **2008**, *180*, 6954-6961.

[22] Shishido, T.; Nozaki, N.; Yamaguchi, S.; Shibata, Y.; Nitobe, J.; Miyamoto, T.; Takahashi, H.; Arimoto, T.; Maeda, K.; Yamakawa, M. Toll-Like Receptor-2 Modulates Ventricular Remodeling After Myocardial Infarction. Circulation **2003**, *108*, 2905-2910.

[23] Akira, S.; Takeda, K. Toll-Like Receptor Signalling. Nature Reviews Immunology **2004**, *4*, 499-511.

[24] Chen, C.; Kono, H.; Golenbock, D.; Reed, G.; Akira, S.; Rock, K.L. Identification of a Key Pathway Required for the Sterile Inflammatory Response Triggered by Dying Cells. Nat. Med. **2007**, *13*, 851-856.

[25] Diepenhorst, G.M.; van Gulik, T.M.; Hack, C.E. Complement-Mediated Ischemia-Reperfusion Injury: Lessons Learned from Animal and Clinical Studies. Ann. Surg. **2009**, *249*, 889-899.

[26] Banz, Y.; Rieben, R. Role of Complement and Perspectives for Intervention in Ischemia-Reperfusion Damage. Ann. Med. **2012**, *44*, 205-217.

[27] Zhang, H.; Qin, G.; Liang, G.; Li, J.; Barrington, R.A.; Liu, D. C5aR-Mediated Myocardial ischemia/reperfusion Injury. Biochem. Biophys. Res. Commun. **2007**, *357*, 446-452.

[28] van der Pals, J.; Koul, S.; Andersson, P.; Götberg, M.; Ubachs, J.; Kanski, M.; Arheden, H.; Olivecrona, G.; Larsson, B.; Erlinge, D. Treatment with the C5a Receptor Antagonist ADC-1004 Reduces Myocardial Infarction in a Porcine Ischemia-Reperfusion Model. BMC cardiovascular disorders **2010**, *10*, 45.

[29] Ferrari, R.; Guardigli, G.; Mele, D.; Percoco, G.; Ceconi, C.; Curello, S. Oxidative Stress during Myocardial Ischaemia and Heart Failure. Curr. Pharm. Des. **2004**, *10*, 1699-1711.

[30] Elahi, M.M.; Kong, Y.X.; Matata, B.M. Oxidative Stress as a Mediator of Cardiovascular Disease. Oxidative Medicine and Cellular Longevity **2009**, *2*, 259-269.

[31] Tsutsui, H.; Kinugawa, S.; Matsushima, S. Oxidative Stress and Heart Failure. American Journal of Physiology-Heart and Circulatory Physiology **2011**, *301*, H2181-H2190.

[32] Palazzo, A.J.; Jones, S.P.; Anderson, D.C.; Granger, D.N.; Lefer, D.J. Coronary Endothelial P-Selectin in Pathogenesis of Myocardial Ischemia-Reperfusion Injury. American Journal of Physiology-Heart and Circulatory Physiology **1998**, *275*, H1865-H1872.

[33] Ivetic, A. Signals Regulating L-Selectin-Dependent Leucocyte Adhesion and Transmigration. Int. J. Biochem. Cell Biol. **2013**, *45*, 550-555.

[34] Sellak, H.; Franzini, E.; Hakim, J.; Pasquier, C. Reactive Oxygen Species Rapidly Increase Endothelial ICAM-1 Ability to Bind Neutrophils without Detectable Upregulation. Blood **1994**, *83*, 2669-2677.

[35] Briaud, S.A.; Ding, Z.; Michael, L.H.; Entman, M.L.; Daniel, S.; Ballantyne, C.M. Leukocyte Trafficking and Myocardial Reperfusion Injury in ICAM-1/P-Selectin-Knockout Mice. American Journal of Physiology-Heart and Circulatory Physiology **2001**, *280*, H60-H67.

[36] Williams, M.R.; Azcutia, V.; Newton, G.; Alcaide, P.; Luscinskas, F.W. Emerging Mechanisms of Neutrophil Recruitment Across Endothelium. Trends Immunol. **2011**, *32*, 461-469.

[37] Entman, M.L.; Youker, K.; Shoji, T.; Kukielka, G.; Shappell, S.B.; Taylor, A.A.; Smith, C. Neutrophil Induced Oxidative Injury of Cardiac Myocytes. A Compartmented System Requiring CD11b/CD18-ICAM-1 Adherence. J. Clin. Invest. **1992**, *90*, 1335.

[38] Soehnlein, O.; Weber, C.; Lindbom, L. Neutrophil Granule Proteins Tune Monocytic Cell Function. Trends Immunol. **2009**, *30*, 538-546.

[39] Nahrendorf, M.; Swirski, F.K.; Aikawa, E.; Stangenberg, L.; Wurdinger, T.; Figueiredo, J.; Libby, P.; Weissleder, R.; Pittet, M.J. The Healing Myocardium Sequentially Mobilizes Two Monocyte Subsets with Divergent and Complementary Functions. J. Exp. Med. **2007**, *204*, 3037-3047.

[40] Leuschner, F.; Rauch, P.J.; Ueno, T.; Gorbatov, R.; Marinelli, B.; Lee, W.W.; Dutta, P.; Wei, Y.; Robbins, C.; Iwamoto, Y. Rapid Monocyte Kinetics in Acute Myocardial Infarction are Sustained by Extramedullary Monocytopoiesis. J. Exp. Med. **2012**, *209*, 123-137.

[41] Gregory, C.D.; Devitt, A. The Macrophage and the Apoptotic Cell: An Innate Immune Interaction Viewed Simplistically? Immunology **2004**, *113*, 1-14.

[42] Martinez, F.O.; Helming, L.; Gordon, S. Alternative Activation of Macrophages: An Immunologic Functional Perspective. Annu. Rev. Immunol. **2009**, *27*, 451-483.

[43] Geissmann, F.; Manz, M.G.; Jung, S.; Sieweke, M.H.; Merad, M.; Ley, K. Development of Monocytes, Macrophages, and Dendritic Cells. Science **2010**, *327*, 656-661.

[44] Anzai, A.; Anzai, T.; Nagai, S.; Maekawa, Y.; Naito, K.; Kaneko, H.; Sugano, Y.; Takahashi, T.; Abe, H.; Mochizuki, S. Regulatory Role of Dendritic Cells in Postinfarction Healing and Left Ventricular RemodelingClinical Perspective. Circulation **2012**, *125*, 1234-1245.

[45] Zhu, J.; Paul, W.E. Peripheral CD4 T-cell Differentiation Regulated by Networks of Cytokines and Transcription Factors. Immunol. Rev. **2010**, *238*, 247-262.

[46] Locksley, R.M. Nine Lives: Plasticity among T Helper Cell Subsets. J. Exp. Med. **2009**, *206*, 1643-1646.

[47] Zhou, L.; Chong, M.; Littman, D.R. Plasticity of CD4 T Cell Lineage Differentiation. Immunity **2009**, *30*, 646-655.

[48] Zhang, N.; Bevan, M.J. CD8< Sup> </sup> T Cells: Foot Soldiers of the Immune System. Immunity **2011**, *35*, 161-168.

[49] Maisel, A.; Cesario, D.; Baird, S.; Rehman, J.; Haghighi, P.; Carter, S. Experimental Autoimmune Myocarditis Produced by Adoptive Transfer of Splenocytes After Myocardial Infarction. Circ. Res. **1998**, *82*, 458-463.

[50] Varda-Bloom, N.; Leor, J.; Ohad, D.G.; Hasin, Y.; Amar, M.; Fixler, R.; Battler, A.; Eldar, M.; Hasin, D. Cytotoxic T Lymphocytes are Activated Following Myocardial Infarction and can Recognize and Kill Healthy Myocytes< i> in Vitro</i>. J. Mol. Cell. Cardiol. **2000**, *32*, 2141-2149.

[51] Ávalos, A.M.; Apablaza, F.A.; Quiroz, M.; Toledo, V.; Peña, J.P.; Michea, L.; Irarrazabal, C.E.; Carrión, F.A.; Figueroa, F.E. IL-17A Levels Increase in the Infarcted Region of the Left Ventricle in a Rat Model of Myocardial Infarction. Biol. Res. **2012**, *45*, 193-200.

[52] Yan, X.; Shichita, T.; Katsumata, Y.; Matsuhashi, T.; Ito, H.; Ito, K.; Anzai, A.; Endo, J.; Tamura, Y.; Kimura, K. Deleterious Effect of the IL-23/IL-17A Axis and γδT Cells on Left Ventricular Remodeling After Myocardial Infarction. Journal of the American Heart Association **2012**, *1*.

[53] Hofmann, U.; Beyersdorf, N.; Weirather, J.; Podolskaya, A.; Bauersachs, J.; Ertl, G.; Kerkau, T.; Frantz, S. Activation of CD4 T Lymphocytes Improves Wound Healing and Survival After Experimental Myocardial Infarction in MiceClinical Perspective. Circulation **2012**, *125*, 1652-1663.

[54] Dobaczewski, M.; Xia, Y.; Bujak, M.; Gonzalez-Quesada, C.; Frangogiannis, N.G. CCR5 Signaling Suppresses Inflammation and Reduces Adverse Remodeling of the Infarcted Heart, Mediating Recruitment of Regulatory T Cells. The American journal of pathology **2010**, *176*, 2177-2187.

[55] Cheng, X.; Liao, Y.; Ge, H.; Li, B.; Zhang, J.; Yuan, J.; Wang, M.; Liu, Y.; Guo, Z.; Chen, J. TH1/TH2 Functional Imbalance After Acute Myocardial Infarction: Coronary Arterial Inflammation Or Myocardial Inflammation. J. Clin. Immunol. **2005**, *25*, 246-253.

[56] Zhao, Z.; Wu, Y.; Cheng, M.; Ji, Y.; Yang, X.; Liu, P.; Jia, S.; Yuan, Z. Activation of Th17/Th1 and Th1, but Not Th17, is Associated with the Acute Cardiac Event in Patients with Acute Coronary Syndrome. Atherosclerosis **2011**, *217*, 518-524.

[57] van den Borne, Susanne WM; Diez, J.; Blankesteijn, W.M.; Verjans, J.; Hofstra, L.; Narula, J. Myocardial Remodeling After Infarction: The Role of Myofibroblasts. Nature Reviews Cardiology **2009**, *7*, 30-37.

[58] Hausenloy, D.J.; Yellon, D.M. Myocardial Ischemia-Reperfusion Injury: A Neglected Therapeutic Target. J. Clin. Invest. **2013**, *123*, 92-100.

[59] Segers, V.F.; Lee, R.T. Stem-Cell Therapy for Cardiac Disease. Nature **2008**, *451*, 937-942.

[60] Haider, H.K.; Ashraf, M. Preconditioning and Stem Cell Survival. Journal of cardiovascular translational research **2010**, *3*, 89-102.

[61] Deutsch, M.; Sturzu, A.; Wu, S.M. At a Crossroad Cell Therapy for Cardiac Repair. Circ. Res. **2013**, *112*, 884-890.

[62] Oshima, H.; Payne, T.R.; Urish, K.L.; Sakai, T.; Ling, Y.; Gharaibeh, B.; Tobita, K.; Keller, B.B.; Cummins, J.H.; Huard, J. Differential Myocardial Infarct Repair with Muscle Stem Cells Compared to Myoblasts. Molecular Therapy **2005**, *12*, 1130-1141.

[63] Okada, M.; Payne, T.R.; Zheng, B.; Oshima, H.; Momoi, N.; Tobita, K.; Keller, B.B.; Phillippi, J.A.; Péault, B.; Huard, J. Myogenic Endothelial Cells Purified from Human Skeletal Muscle Improve Cardiac Function After Transplantation into Infarcted Myocardium. J. Am. Coll. Cardiol. **2008**, *52*, 1869-1880.

[64] Urish, K.L.; Vella, J.B.; Okada, M.; Deasy, B.M.; Tobita, K.; Keller, B.B.; Cao, B.; Piganelli, J.D.; Huard, J. Antioxidant Levels Represent a Major Determinant in the Regenerative Capacity of Muscle Stem Cells. Mol. Biol. Cell **2009**, *20*, 509-520.

[65] Drowley, L.; Okada, M.; Beckman, S.; Vella, J.; Keller, B.; Tobita, K.; Huard, J. Cellular Antioxidant Levels Influence Muscle Stem Cell Therapy. Molecular Therapy **2010**, *18*, 1865-1873.

[66] Mangi, A.A.; Noiseux, N.; Kong, D.; He, H.; Rezvani, M.; Ingwall, J.S.; Dzau, V.J. Mesenchymal Stem Cells Modified with Akt Prevent Remodeling and Restore Performance of Infarcted Hearts. Nat. Med. **2003**, *9*, 1195-1201.

[67] Jiang, S.; Haider, H.K.; Idris, N.M.; Salim, A.; Ashraf, M. Supportive Interaction between Cell Survival Signaling and Angiocompetent Factors Enhances Donor Cell Survival and Promotes Angiomyogenesis for Cardiac Repair. Circ. Res. **2006**, *99*, 776-784.

[68] Hassan, F.; Meduru, S.; Taguchi, K.; Kuppusamy, M.L.; Mostafa, M.; Kuppusamy, P.; Khan, M. Carvedilol Enhances Mesenchymal Stem Cell Therapy for Myocardial Infarction Via Inhibition of Caspase-3 Expression. J. Pharmacol. Exp. Ther. **2012**, *343*, 62-71.

[69] DeSantiago, J.; Bare, D.J.; Banach, K. Ischemia-Reperfusion Injury Protection by Mesenchymal Stem Cell Derived Antioxidant Capacity. Stem cells and development **2013**.

[70] Pittenger, M.F.; Mackay, A.M.; Beck, S.C.; Jaiswal, R.K.; Douglas, R.; Mosca, J.D.; Moorman, M.A.; Simonetti, D.W.; Craig, S.; Marshak, D.R. Multilineage Potential of Adult Human Mesenchymal Stem Cells. Science **1999**, *284*, 143-147.

[71] Toma, C.; Pittenger, M.F.; Cahill, K.S.; Byrne, B.J.; Kessler, P.D. Human Mesenchymal Stem Cells Differentiate to a Cardiomyocyte Phenotype in the Adult Murine Heart. Circulation **2002**, *105*, 93-98.

[72] Jiang, Y.; Jahagirdar, B.N.; Reinhardt, R.L.; Schwartz, R.E.; Keene, C.D.; Ortiz-Gonzalez, X.R.; Reyes, M.; Lenvik, T.; Lund, T.; Blackstad, M. Pluripotency of Mesenchymal Stem Cells Derived from Adult Marrow. Nature **2002**, *418*, 41-49.

[73] Amado, L.C.; Saliaris, A.P.; Schuleri, K.H.; John, M.S.; Xie, J.; Cattaneo, S.; Durand, D.J.; Fitton, T.; Kuang, J.Q.; Stewart, G. Cardiac Repair with Intramyocardial Injection of Allogeneic Mesenchymal Stem Cells After Myocardial Infarction. Proc. Natl. Acad. Sci. U. S. A. **2005**, *102*, 11474-11479.

[74] Miyahara, Y.; Nagaya, N.; Kataoka, M.; Yanagawa, B.; Tanaka, K.; Hao, H.; Ishino, K.; Ishida, H.; Shimizu, T.; Kangawa, K. Monolayered Mesenchymal Stem Cells Repair Scarred Myocardium After Myocardial Infarction. Nat. Med. **2006**, *12*, 459-465.

[75] Gebler, A.; Zabel, O.; Seliger, B. The Immunomodulatory Capacity of Mesenchymal Stem Cells. Trends Mol. Med. **2012**, *18*, 128-134.

[76] Huang, X.; Sun, Z.; Miyagi, Y.; Kinkaid, H.M.; Zhang, L.; Weisel, R.D.; Li, R. Differentiation of Allogeneic Mesenchymal Stem Cells Induces Immunogenicity and Limits their Long-Term Benefits for Myocardial RepairClinical Perspective. Circulation **2010**, *122*, 2419-2429.

[77] Duffy, M.M.; Pindjakova, J.; Hanley, S.A.; McCarthy, C.; Weidhofer, G.A.; Sweeney, E.M.; English, K.; Shaw, G.; Murphy, J.M.; Barry, F.P. Mesenchymal Stem Cell Inhibition of T-helper 17 cell-differentiation is Triggered by cell–cell Contact and Mediated by Prostaglandin E2 Via the EP4 Receptor. Eur. J. Immunol. **2011**, *41*, 2840-2851.

[78] Shi, Y.; Hu, G.; Su, J.; Li, W.; Chen, Q.; Shou, P.; Xu, C.; Chen, X.; Huang, Y.; Zhu, Z. Mesenchymal Stem Cells: A New Strategy for Immunosuppression and Tissue Repair. Cell Res. **2010**, *20*, 510-518.

[79] DelaRosa, O.; Lombardo, E.; Beraza, A.; Mancheño-Corvo, P.; Ramirez, C.; Menta, R.; Rico, L.; Camarillo, E.; García, L.; Abad, J.L. Requirement of IFN-γ–Mediated Indoleamine 2, 3-Dioxygenase Expression in the Modulation of Lymphocyte Proliferation by Human Adipose–Derived Stem Cells. Tissue Engineering Part A **2009**, *15*, 2795-2806.

[80] Chabannes, D.; Hill, M.; Merieau, E.; Rossignol, J.; Brion, R.; Soulillou, J.P.; Anegon, I.; Cuturi, M.C. A Role for Heme Oxygenase-1 in the Immunosuppressive Effect of Adult Rat and Human Mesenchymal Stem Cells. Blood **2007**, *110*, 3691-3694.

[81] Uccelli, A.; Moretta, L.; Pistoia, V. Mesenchymal Stem Cells in Health and Disease. Nature Reviews Immunology **2008**, *8*, 726-736.

[82] Bernardo, M.E.; Fibbe, W.E. Safety and Efficacy of Mesenchymal Stromal Cell Therapy in Autoimmune Disorders. Ann. N. Y. Acad. Sci. **2012**, *1266*, 107-117.

[83] Williams, A.R.; Hare, J.M. Mesenchymal Stem Cells Biology, Pathophysiology, Translational Findings, and Therapeutic Implications for Cardiac Disease. Circ. Res. **2011**, *109*, 923-940.

[84] Segers, V.F.; Lee, R.T. Stem-Cell Therapy for Cardiac Disease. Nature **2008**, *451*, 937-942.

[85] Cassatella, M.A.; Mosna, F.; Micheletti, A.; Lisi, V.; Tamassia, N.; Cont, C.; Calzetti, F.; Pelletier, M.; Pizzolo, G.; Krampera, M. Toll-Like Receptor-3-Activated Human Mesenchymal Stromal Cells significantly Prolong the Survival and Function of Neutrophils. Stem Cells **2011**, *29*, 1001-1011.

[86] Raffaghello, L.; Bianchi, G.; Bertolotto, M.; Montecucco, F.; Dallegri, F.; Ottonello, L.; Pistoia, V. Human Mesenchymal Stem Cells Inhibit Neutrophil Apoptosis: A Model for Neutrophil Preservation in the Bone Marrow Niche. Stem Cells **2008**, *26*, 151-162.

[87] Henning, R.J.; Shariff, M.; Eadula, U.; Alvarado, F.; Vasko, M.; Sanberg, P.R.; Sanberg, C.D.; Delostia, V. Human Cord Blood Mononuclear Cells Decrease Cytokines and Inflammatory Cells in Acute Myocardial Infarction. Stem cells and development **2008**, *17*, 1207-1220.

[88] Dayan, V.; Yannarelli, G.; Billia, F.; Filomeno, P.; Wang, X.; Davies, J.E.; Keating, A. Mesenchymal Stromal Cells Mediate a Switch to Alternatively Activated monocytes/macrophages After Acute Myocardial Infarction. Basic Res. Cardiol. **2011**, *106*, 1299-1310.

[89] Maggini, J.; Mirkin, G.; Bognanni, I.; Holmberg, J.; Piazzón, I.M.; Nepomnaschy, I.; Costa, H.; Cañones, C.; Raiden, S.; Vermeulen, M. Mouse Bone Marrow-Derived Mesenchymal Stromal Cells Turn Activated Macrophages into a Regulatory-Like Profile. PLoS One **2010**, *5*, e9252.

[90] Adutler-Lieber, S.; Ben-Mordechai, T.; Naftali-Shani, N.; Asher, E.; Loberman, D.; Raanani, E.; Leor, J. Human Macrophage Regulation Via Interaction with Cardiac Adipose Tissue-Derived Mesenchymal Stromal Cells. J. Cardiovasc. Pharmacol. Ther. **2013**, *18*, 78-86.

[91] Kim, J.; Hematti, P. Mesenchymal Stem cell–educated Macrophages: A Novel Type of Alternatively Activated Macrophages. Exp. Hematol. **2009**, *37*, 1445-1453.

[92] François, M.; Romieu-Mourez, R.; Li, M.; Galipeau, J. Human MSC Suppression Correlates with Cytokine Induction of Indoleamine 2, 3-Dioxygenase and Bystander M2 Macrophage Differentiation. Molecular Therapy **2011**, *20*, 187-195.

[93] Burchfield, J.S.; Iwasaki, M.; Koyanagi, M.; Urbich, C.; Rosenthal, N.; Zeiher, A.M.; Dimmeler, S. Interleukin-10 from Transplanted Bone Marrow Mononuclear Cells Contributes to Cardiac Protection After Myocardial Infarction. Circ. Res. **2008**, *103*, 203-211.

[94] English, K.; Ryan, J.; Tobin, L.; Murphy, M.; Barry, F.; Mahon, B. Cell Contact, Prostaglandin E2 and Transforming Growth Factor Beta 1 Play non-redundant Roles in Human Mesenchymal Stem Cell Induction of CD4 CD25Highforkhead Box P3 Regulatory T Cells. Clinical & Experimental Immunology **2009**, *156*, 149-160.

[95] Del Papa, B.; Sportoletti, P.; Cecchini, D.; Rosati, E.; Balucani, C.; Baldoni, S.; Fettucciari, K.; Marconi, P.; Martelli, M.F.; Falzetti, F. Notch1 Modulates Mesenchymal Stem Cells Mediated Regulatory T-cell Induction. Eur. J. Immunol. **2013**, *43*, 182-187.

[96] Di Ianni, M.; Del Papa, B.; De Ioanni, M.; Moretti, L.; Bonifacio, E.; Cecchini, D.; Sportoletti, P.; Falzetti, F.; Tabilio, A. Mesenchymal Cells Recruit and Regulate T Regulatory Cells. Exp. Hematol. **2008**, *36*, 309-318.

[97] Matsumoto, K.; Ogawa, M.; Suzuki, J.; Hirata, Y.; Nagai, R.; Isobe, M. Regulatory T Lymphocytes Attenuate Myocardial Infarction-Induced Ventricular Remodeling in Mice. International heart journal **2011**, *52*, 382-387.

[98] Tang, T.; Yuan, J.; Zhu, Z.; Zhang, W.; Xiao, H.; Xia, N.; Yan, X.; Nie, S.; Liu, J.; Zhou, S. Regulatory T Cells Ameliorate Cardiac Remodeling After Myocardial Infarction. Basic Res. Cardiol. **2012**, *107*, 1-17.

[99] Lai, R.C.; Arslan, F.; Lee, M.M.; Sze, N.S.K.; Choo, A.; Chen, T.S.; Salto-Tellez, M.; Timmers, L.; Lee, C.N.; El Oakley, R.M. Exosome Secreted by MSC Reduces Myocardial ischemia/reperfusion Injury. Stem cell research **2010**, *4*, 214-222.

[100] Arslan, F.; Lai, R.C.; Smeets, M.B.; Akeroyd, L.; Choo, A.; Aguor, E.N.; Timmers, L.; van Rijen, H.V.; Doevendans, P.A.; Pasterkamp, G. Mesenchymal Stem Cell-Derived Exosomes Increase ATP Levels, Decrease Oxidative Stress and Activate PI3K/Akt Pathway to Enhance Myocardial Viability and Prevent Adverse Remodeling After Myocardial ischemia/reperfusion Injury. Stem cell research **2013**, *10*, 301-312.

[101] Kumar, V.; Abbas, A.K.; Fausto, N.; Aster, J.C. *Robbins & Cotran Pathologic Basis of Disease*.; Saunders, 2009.

[102] Armulik, A.; Genové, G.; Betsholtz, C. Pericytes: Developmental, Physiological, and Pathological Perspectives, Problems, and Promises. Developmental cell **2011**, *21*, 193-215.

[103] Caplan, A.I. All MSCs are Pericytes? Cell Stem Cell **2008**, *3*, 229-230.

[104] Chen, C.; Montelatici, E.; Crisan, M.; Corselli, M.; Huard, J.; Lazzari, L.; Péault, B. Perivascular Multi-Lineage Progenitor Cells in Human Organs: Regenerative Units, Cytokine Sources Or both? Cytokine Growth Factor Rev. **2009**, *20*, 429-434.

[105] Chen, C.; Corselli, M.; Péault, B.; Huard, J. Human Blood-Vessel-Derived Stem Cells for Tissue Repair and Regeneration. BioMed Research International **2012**, *2012*.

[106] Crisan, M.; Yap, S.; Casteilla, L.; Chen, C.; Corselli, M.; Park, T.S.; Andriolo, G.; Sun, B.; Zheng, B.; Zhang, L. A Perivascular Origin for Mesenchymal Stem Cells in Multiple Human Organs. Cell stem cell **2008**, *3*, 301-313.

[107] Zheng, B.; Cao, B.; Crisan, M.; Sun, B.; Li, G.; Logar, A.; Yap, S.; Pollett, J.B.; Drowley, L.; Cassino, T. Prospective Identification of Myogenic Endothelial Cells in Human Skeletal Muscle. Nat. Biotechnol. **2007**, *25*, 1025-1034.

[108] Corselli, M.; Chen, C.; Sun, B.; Yap, S.; Rubin, J.P.; Péault, B. The Tunica Adventitia of Human Arteries and Veins as a Source of Mesenchymal Stem Cells. Stem cells and development **2012**, *21*, 1299-1308.

[109] Zheng, B.; Li, G.; Chen, W.C.; Deasy, B.M.; Pollett, J.B.; Sun, B.; Drowley, L.; Gharaibeh, B.; Usas, A.; Péault, B. Human Myogenic Endothelial Cells Exhibit Chondrogenic and Osteogenic Potentials at the Clonal Level. Journal of Orthopaedic Research **2013**, *31*, 1089-1095.

[110] Zheng, B.; Chen, C.; Li, G.; Thompson, S.D.; Poddar, M.; Peault, B.; Huard, J. Isolation of Myogenic Stem Cells from Cultures of Cryopreserved Human Skeletal Muscle. Cell Transplant. **2012**, *21*, 1087-1093.

[111] Rucker, H.K.; Wynder, H.J.; Thomas, W.E. Cellular Mechanisms of CNS Pericytes. Brain Res. Bull. **2000**, *51*, 363-369.

[112] Hellström, M.; Gerhardt, H.; Kalén, M.; Li, X.; Eriksson, U.; Wolburg, H.; Betsholtz, C. Lack of Pericytes Leads to Endothelial Hyperplasia and Abnormal Vascular Morphogenesis. J. Cell Biol. **2001**, *153*, 543-554.

[113] von Tell, D.; Armulik, A.; Betsholtz, C. Pericytes and Vascular Stability. Exp. Cell Res. **2006**, *312*, 623-629.

[114] Armulik, A.; Abramsson, A.; Betsholtz, C. Endothelial/pericyte Interactions. Circ. Res. **2005**, *97*, 512-523.

[115] Gaengel, K.; Genové, G.; Armulik, A.; Betsholtz, C. Endothelial-Mural Cell Signaling in Vascular Development and Angiogenesis. Arterioscler. Thromb. Vasc. Biol. **2009**, *29*, 630-638.

[116] Dulmovits, B.M.; Herman, I.M. Microvascular Remodeling and Wound Healing: A Role for Pericytes. Int. J. Biochem. Cell Biol. **2012**.

[117] Chen, C.; Okada, M.; Proto, J.D.; Gao, X.; Sekiya, N.; Beckman, S.A.; Corselli, M.; Crisan, M.; Saparov, A.; Tobita, K. Human Pericytes for Ischemic Heart Repair. Stem Cells **2013**, *31*, 305-316.

[118] He, W.; Nieponice, A.; Soletti, L.; Hong, Y.; Gharaibeh, B.; Crisan, M.; Usas, A.; Peault, B.; Huard, J.; Wagner, W.R. Pericyte-Based Human Tissue Engineered Vascular Grafts. Biomaterials **2010**, *31*, 8235-8244.

[119] Campagnolo, P.; Cesselli, D.; Zen, A.A.H.; Beltrami, A.P.; Kränkel, N.; Katare, R.; Angelini, G.; Emanueli, C.; Madeddu, P. Human Adult Vena Saphena Contains Perivascular Progenitor Cells Endowed with Clonogenic and Proangiogenic Potential. Circulation **2010**, *121*, 1735-1745.

[120] Katare, R.; Riu, F.; Mitchell, K.; Gubernator, M.; Campagnolo, P.; Cui, Y.; Fortunato, O.; Avolio, E.; Cesselli, D.; Beltrami, A.P. Transplantation of Human Pericyte Progenitor Cells Improves the Repair of Infarcted Heart through Activation of an Angiogenic Program Involving Micro-RNA-132Novelty and Significance. Circ. Res. **2011**, *109*, 894-906.

[121] Okada, M.; Payne, T.R.; Drowley, L.; Jankowski, R.J.; Momoi, N.; Beckman, S.; Chen, W.C.; Keller, B.B.; Tobita, K.; Huard, J. Human Skeletal Muscle Cells with a Slow Adhesion Rate After Isolation and an Enhanced Stress Resistance Improve Function of Ischemic Hearts. Molecular Therapy **2012**, *20*, 138-145.

[122] Quaegebeur, A.; Lange, C.; Carmeliet, P. The Neurovascular Link in Health and Disease: Molecular Mechanisms and Therapeutic Implications. Neuron **2011**, *71*, 406-424.

[123] Stark, K.; Eckart, A.; Haidari, S.; Tirniceriu, A.; Lorenz, M.; von Brühl, M.; Gärtner, F.; Khandoga, A.G.; Legate, K.R.; Pless, R. Capillary and Arteriolar Pericytes Attract Innate Leukocytes Exiting through Venules and'Instruct'them with Pattern-Recognition and Motility Programs. Nat. Immunol. **2012**, *14*, 41-51.

[124] Alon, R.; Nourshargh, S. Learning in Motion: Pericytes Instruct Migrating Innate Leukocytes. Nat. Immunol. **2012**, *14*, 14-15.

[125] Maier, C.L.; Pober, J.S. Human Placental Pericytes Poorly Stimulate and Actively Regulate Allogeneic CD4 T Cell Responses. Arterioscler. Thromb. Vasc. Biol. **2011**, *31*, 183-189.

[126] Verbeek, M.M.; Westphal, J.R.; Ruiter, D.J.; De Waal, R. T Lymphocyte Adhesion to Human Brain Pericytes is Mediated Via very Late Antigen-4/vascular Cell Adhesion Molecule-1 Interactions. The Journal of Immunology **1995**, *154*, 5876-5884.

[127] Pober, J.S.; Tellides, G. Participation of Blood Vessel Cells in Human Adaptive Immune Responses. Trends Immunol. **2012**, *33*, 49-57.

[128] Tu, Z.; Li, Y.; Smith, D.S.; Sheibani, N.; Huang, S.; Kern, T.; Lin, F. Retinal Pericytes Inhibit Activated T Cell Proliferation. Invest. Ophthalmol. Vis. Sci. **2011**, *52*, 9005-9010.

The FASEB Journal

Your article (# 13-233460) from The FASEB Journal is available for downloading.

_____

The FASEB Journal is published by the Federation of American Societies for Experimental Biology (FASEB)

Dear author,

Please click on this URL address

http://rapidproof.cadmus.com/RapidProof/retrieval/index.jsp then
Login: your e-mail address

Password: 77x99vEHZweU

(You may copy and paste this case-sensitive password.)

The site contains one file. You will need to have Adobe Acrobat® Reader software (Version 4.0 or higher) to read it. This free software is available for user downloading at http://www.adobe.com/products/acrobat/readstep.html.

If you have any problems with downloading your article from the Rapid Proof site, please contact rpmhelp@cadmus.com. Please include your article number (9373) with all correspondence.

This file contains instructions for correcting the PDF proof electronically and a copy of the page proof for your article. The proof contains 13 pages.

Please read over your article carefully. Please be sure to respond to any queries that appear on the last page of the proof. Proofread the following elements of your article especially carefully:

- Non-English characters and symbols
- Tables
- Equations and mathematical symbols
- Figures (including figure and caption placement):
 * If you need to provide the editorial office with a revised figure, please indicate this with a comment on the incorrect figure and write 'NEW FIGURE FILE REQUIRED' in the comment and include the new figure as an attachment to your email.
 * Color figures have the word 'COLOR' in the margins. Grayscale (black and white) figures have no tag. If you wish to change a color figure to grayscale, include a comment instructing the figure to print in grayscale.
 * Publication charges will be calculated based on your changes to this proof. Please note that figures are published the same way in the online and print versions of the journal. Authors may not publish figures in color online while publishing the same figures in grayscale in print or vice-versa.

Please use the comments and notes features in Adobe Acrobat (instructions provided in the PDF file to be downloaded) and return the annotated PDF to fjproduction@faseb.org within 24 hours. If you are unable to use Adobe Acrobat and your changes are minimal, you may summarize them in an email (sent to the same fjproduction email address), clearly indicating the location of each change. If you are unable to use Adobe Acrobat and have changes too extensive to summarize in an e-mail, please scan your marked-up proof and send it to fjproduction@faseb.org. If you are unable to provide your proof corrections in any of the above manners, please fax your corrections to: 1-717-738-9479.

Fax PUBLICATION FORMS to: 1-240-407-4430
Publication forms sent by any other means or faxed to any other number may result in substantial publication delays.

NOTE: Proofs or publication forms retained by the author for an excessive length of time may not be published online in a timely way and may need to be scheduled for a later print issue.

If you have any problems or questions, please contact me. Always include your article number in all correspondence.

Sincerely,
Mary Kiorpes Hayden
FASEB Office of Publications
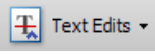9650 Rockville Pike
Bethesda, MD 20814-3998
phone: 301-634-7151
fax: 1-240-407-4430
mhayden@faseb.org

Adding Comments and Notes to Your PDF

To facilitate electronic transmittal of corrections, we encourage authors to utilize the comments and notes features in Adobe Acrobat. The PDF provided has been "comment-enabled," which allows you to utilize the comments and notes features, even if using only the free Adobe Acrobat reader (see note below regarding acceptable versions). Adobe Acrobat's Help menu provides additional details on the tool. When you open your PDF, the comments/notes/edit tools are clearly shown on the tool bar (though icons may differ slightly among versions from what is shown below).

For purposes of correcting the PDF proof of your journal article, the important features to know are the following:
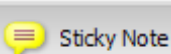
- Use the **Text Edits tool** () to insert, replace, or delete text.

    o To **insert text**, place your cursor at a point in text and select "Insert Text at Cursor" from the text edits menu. Type your additional text in the pop-up box.
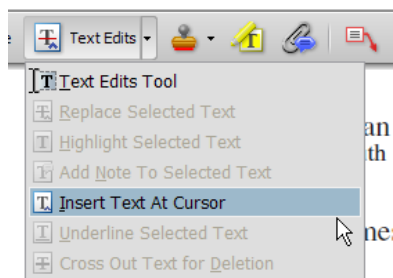
    o To **replace text** (do this instead of deleting and then re-inserting), highlight the text to be changed, select "Replace Selected Text" from the text edits menu, and type the new text in the pop-up box.
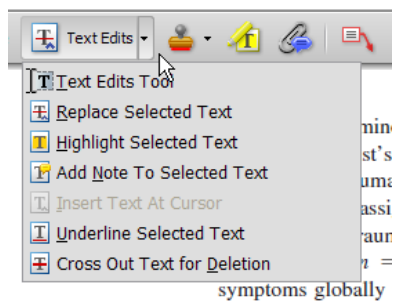
    o To **delete text**, highlight the text to be deleted and select "Cross Out Text for Deletion" from the text edits menu (see graphic above).

- Use the **Sticky Note tool** () to describe changes that need to be made (e.g., changes in bold, italics, or capitalization use; altering or replacing a figure) or to answer a question or approve a change that was posed by the editor. To use this feature, click on the sticky note tool and then click on a point in the PDF where you would like to make a comment, then type your comment in the pop-up box.

- Use the **Callout tool** () to point directly to changes that need to be made. Try to put the callout box in an area of white space so that you do not obscure the text, as in the example below.

Table 5

Experiment 4: Comparative Optimism as a Function of Self-Presentation and Event Valence

	Event					
	Positive		Negative		Total	
Self-presentation	M	SD	M	SD	M	SD
Public/student	3.46	0.13	3.60	0.10	3.53	0.12
Public/expert	2.66	0.12	2.78	0.13	2.73	0.13
Control	2.39	0.11	2.46	0.09	2.43	0.11
Total	2.84	0.47	2.95	0.50		

The first column's entries should be flush left (except for "Total", which should be indented one em-space), as in Tables 1 and 2 previously.

- Use the **Highlight tool** () to indicate font problems, bad breaks, and other textual inconsistencies. Describe the inconsistencies with the callout tool (shown) or a sticky note. One callout (or sticky note) can describe many changes.

$$du/dt = -\lambda v^\alpha = -\lambda u$$
$$du/u = -\lambda dt$$
$$u_t = ue^{-\lambda t}.$$

Close up minus sign to lambda (3 times, highlighted)

An alternate method is to select the appropriate text with your cursor, select **"Add Note to Selected Text"** from the text edits menu, and then type your note in the pop-up box (the selected text is highlighted automatically).

As with hand-annotated proof corrections, the important points are to communicate changes clearly and thoroughly; to answer all queries and questions; and to provide complete information for us to make the necessary changes to your article so it is ready for publication.

To utilize the comments/notes features on this PDF you will need Adobe Reader version 7 or higher. This program is freely available and can be downloaded from http://get.adobe.com/reader/

AUTHOR INSTRUCTIONS

Copyright Transfer and Publication Costs Approval Form

All authors are required to sign the following copyright transfer and cost agreement form prior to publication. **If you have not yet submitted this form to the editorial office, please fax it to 240-407-4430 as soon as possible.** Multiple forms may be submitted for the same article. Instructions for calculating publication charges are also attached for your convenience. Please read that sheet carefully. Do not fax your estimate sheet to the editorial office.

Mandatory Copyright Transfer and Publication Costs Approval Form

Manuscript No.: _____

Title: _____

Author Names (Please Print All Names): _____

Signatures Below Certify Compliance With the Following Statements:

Copyright Transfer. In consideration of the acceptance of the above work for publication, I do herby assign and transfer to the Federation of American Societies for Experimental Biology (FASEB) all rights, titles, and interest in and to the copyright in *The FASEB Journal*. This includes preliminary display/posting of the abstract of the accepted article in electronic form before publication. The journal grants the author permission to provide a copy of the accepted manuscript to NIH upon acceptance for Journal publication, with public release in PubMed Central twelve months after final print publication by *The FASEB Journal*.

This form must be signed by all authors. If any changes in authorship (order, deletions, or additions) occur after the manuscript is submitted, agreement by all authors for such changes must be on file with FASEB. An author's name may only be removed at his/her own request and with written consent from all of the other authors, as well as final approval by the Editor-in-Chief. Material prepared by employees of the US Government in the course of their official duties cannot be copyrighted; work prepared by employees of the British or British Commonwealth government in the course of their official duties is subject to Crown Copyright and cannot be transferred to FASEB. Nevertheless, authors must sign the form to indicate acceptance of all terms other than copyright transfer.

○ Please check if this article was written as part of the official duties of an employee of the US government.
○ Please check if this article was written as part of the official duties of an employee of the British or British Commonwealth government.

Authorship Responsibilities. I attest that:
1. the manuscript is not currently under consideration, in press, or published elsewhere, and the research reported will not be submitted for publication elsewhere until a final decision has been made as to its acceptability by *The FASEB Journal* (posting of submitted material on a web site or by any other electronic means may be considered prior publication—note this in your cover letter);
2. the manuscript is truthful, original work without fabrication, fraud, or plagiarism;
3. I have made an important scientific contribution to the study and am thoroughly familiar with the primary data and;
4. I have read the complete manuscript and take responsibility for the content and completeness of the manuscript and understand that I share responsibility if the paper, or part of the paper, is found to be faulty or fraudulent.

Conflict of Interest Disclosure. All funding sources supporting the work and all institutional or corporate affiliations of mine are acknowledged. Except as disclosed on a separate attachment, I certify that I have no commercial associations (e.g., consultancies, stock ownership, equity interests, patent-licensing arrangements, etc.) that might pose a conflict of interest in connection with the submitted article, and that I accept full responsibility for the conduct of the trial, had full access to all the data, and controlled the decision to publish.

Author Fees. I agree to pay the following publication charges. Page charges are $80 per printed page for the first 8 pages; $160 per page for the 9th page and beyond. Color figures are $350 each. Articles containing eight or more figures and/or tables will be charged an additional $150 per figure and table. Supplemental units (maximum of 4) uploaded to the journal website are $160 for each unit. All figures are in U.S. dollars.

Author Signatures. For more than 10 authors, use an extra sheet. Multiple forms are acceptable.

1. Print Name: _____ Signature: _____ Date: _____
2. Print Name: _____ Signature: _____ Date: _____
3. Print Name: _____ Signature: _____ Date: _____
4. Print Name: _____ Signature: _____ Date: _____
5. Print Name: _____ Signature: _____ Date: _____
6. Print Name: _____ Signature: _____ Date: _____
7. Print Name: _____ Signature: _____ Date: _____
8. Print Name: _____ Signature: _____ Date: _____
9. Print Name: _____ Signature: _____ Date: _____
10. Print Name: _____ Signature: _____ Date: _____

Signed forms should be faxed to 240-407-4430 or scanned and emailed to Chanel George at cgeorge@faseb.org.

AUTHOR INSTRUCTIONS
Calculating Publication Costs

The FASEB Journal now uses an online bill pay system for publication and reprint order fees. The corresponding author will receive a separate e-mail containing a link to a web page where charges can be paid by credit card. The e-mail link also will provide information about invoices, check payment, and wire transfers.

Publication charges are calculated based on the final version of the article and not this proof.
Color figures have the word "COLOR" in the margins. Grayscale (black and white) figures have no tag. If you wish to change a color figure to grayscale, cross out the word "color" and write in "grayscale." Please note that figures are published the same way in the online and print versions of the journal. Authors may not publish figures in color online while publishing the same figures in print or vice-versa.

For your convenience and records, the following table should help you estimate publication charges. Please account for any changes you have made to your proofs. **Please <u>do not</u> fax this sheet to the editorial office. Your charges will be calculated automatically based on the final article.**

	Quantity		Unit Price		Total
Per page cost, first 8 pages		×	$80 per page	=	
					+
Per page cost, 9th page and beyond		×	$160 per page	=	
					+
Color figures		×	$350 per figure	=	
					+
Any combination of figures and/or tables over 7		×	$150 per figure or table	=	
					+
Individual supplemental files		×	$160 per unit, maximum of four units	=	

Total Publication Charges:

This sheet is for estimation purposes only. Final costs are calculated using the final printed version of the article. All prices are in U.S. dollars. Open access fees are calculated separately. Reprints can be purchased when paying publication charges online.

The FASEB Journal • Research Communication

RhoA mediates defective stem cell function and heterotopic ossification in dystrophic muscle of mice

Xiaodong Mu, Arvydas Usas, Ying Tang, Aiping Lu, Bing Wang, Kurt Weiss, and Johnny Huard[1]

Stem Cell Research Center, Department of Orthopaedic Surgery, University of Pittsburgh, Pittsburgh, Pennsylvania, USA

ABSTRACT Heterotopic ossification (HO) and fatty infiltration (FI) often occur in diseased skeletal muscle and have been previously described in various animal models of Duchenne muscular dystrophy (DMD); however, the pathological mechanisms remain largely unknown. Dystrophin-deficient *mdx* mice and dystrophin/utrophin double-knockout (dKO) mice are mouse models of DMD; however, *mdx* mice display a strong muscle regeneration capacity, while dKO mice exhibit a much more severe phenotype, which is similar to patients with DMD. Our results revealed that more extensive HO, but not FI, occurred in the skeletal muscle of dKO mice versus *mdx* mice, and RhoA activation specifically occurred at the sites of HO. Moreover, the expression of RhoA, BMPs, and inflammatory factors were significantly up-regulated in muscle stem cells isolated from dKO mice; while inactivation of RhoA in the cells with RhoA/ROCK inhibitor Y27632 led to reduced osteogenic potential and improved myogenic potential. Finally, inactivation of RhoA signaling in the dKO mice with Y-27632 improved muscle regeneration and reduced the expression of BMPs, inflammation, HO, and intramyocellular lipid accumulation in both skeletal and cardiac muscle. Our results revealed that RhoA represents a major molecular switch in the regulation of HO and muscle regeneration in dystrophic skeletal muscle of mice.—Mu, X., Usas, A., Tang, Y., Lu, A., Wang, B., Weiss, K., Huard, J. RhoA mediates defective stem cell function and heterotopic ossification in dystrophic muscle of mice. *FASEB J.* 27, 000–000 (2013). www.fasebj.org

Key Words: *ROCK · mdx · utrophin$^{-/-}$ · intramyocellular lipid accumulation*

HETEROTOPIC OSSIFICATION (HO) and/or fatty infiltration (FI) are two distinct histological processes that often occur in diseased muscle tissues. HO refers to the formation of bone in the soft tissues of the body and can occur as a result of trauma, surgery, neurological injury, or genetic abnormalities (1). FI has been reported to be associated with aging, inactivity, obesity, and various diseases, such as diabetes, and results in the accumulation of fat cells outside the typical fat stores (2–3). FI located within skeletal muscle is often the result of disordered lipid metabolism (3); however, abnormal lipid metabolism can also cause another type of abnormal lipid deposition in skeletal muscle, known as intramyocellular lipid accumulation (IMCL; refs. 4–5). Notably, IMCL in cardiac muscle, (intramyocardial lipid accumulation) can be caused by lipid overload, which has the potential to lead to lipotoxicity and progressive cardiac dysfunction (6–9). However, the pathological mechanisms regulating these distinct processes in diseased muscles remain largely unknown.

Duchenne muscular dystrophy (DMD) features progressive muscle degeneration and has no cure yet. Obesity occurs in >50% of patients wtih DMD after 14 yr of age, and a reduction in myocardial fatty acid metabolism has been observed in ~50% of patients wtih DMD (10, 11). FI is commonly observed in the skeletal muscles of patients wtih DMD, and it is one of the main factors responsible for patients' decline in muscular strength (12). Lipid mapping analysis of the hearts and skeletal muscles of patients wtih DMD revealed IMCL within the most damaged areas of the dystrophic muscles (11, 13); however, there are very few studies on the mechanisms and prevention of IMCL in patients wtih DMD. Although less documented in human patients wtih DMD, the presence of HO has been reported in the skeletal muscles of various animal models of human DMD, including *mdx* mice and golden retriever muscular dystrophy (GRMD) dogs (14–16). *In vitro* studies with muscle stem cells showed that bone morphogenetic protein (BMPs) or adipogenic media can promote the differentiation of muscle

---

[1] Correspondence: Stem Cell Research Center, Department of Orthopaedic Surgery, University of Pittsburgh, Bridgeside Point 2, Ste. 206, 450 Technology Dr., Pittsburgh, PA 15219, USA. E-mail: jhuard@pitt.edu

1

stem cells into osteogenic and adipogenic cells, respectively (17), suggesting that muscle stem cells may represent a cell source of HO and/or FI in skeletal muscle.

The experiments described in this article were conducted using two animal models of human DMD, dystrophin-deficient (*mdx*) mice and dystrophin/utrophin double-knockout (dKO) mice(14, 18–20). Compared with *mdx* mice, which actually feature potent muscle regeneration capacity, the phenotype of dKO mice is more severe and more closely resembles the phenotype seen in patients wtih DMD (19–20). For example, dKO mice feature a much shorter life span (~8 wk compared with ~2 yr), more necrosis and fibrosis in their skeletal muscles, scoliosis/kyphosis of the spine, and severe cardiac involvement and eventual cardiac failure (14, 19, 20). The occurrence of FI and HO in the skeletal muscles of *mdx* mice has been previously described (15), and more extensive HO in dKO mice has also been recently reported by our group (21). IMCL, on the other hand, has not been studied in either *mdx* or dKO mice or in any other DMD animal models. It is also clear that the knowledge about the molecular regulation of HO, fatty infiltration, and IMCL in dystrophic muscle remains limited.

Inflammation is directly involved in the dystrophic process and represents an important therapeutic target to treat DMD. For example, corticosteroids are capable of repressing systematic inflammation and are the only known effective drugs that can provide relief of the symptoms of DMD (22). Inflammation has been identified as a main contributor of HO (23); hence, the administrations of various anti-inflammatory medications have been used to prevent HO (24–25). For example, Cox-2 inhibitors were found to be effective at preventing HO after total hip arthroplasty (THA) and following spinal cord injury (26–27). Although inflammation and FI often occur simultaneously in diseased or injured skeletal muscles, inflammation has not been directly linked to FI (28–29). On the other hand, it has been well established, in studies of diabetes and obesity, that there is a close association between the occurrence of IMCL and chronic systematic inflammation during the progression of cardiac disease (30, 31). Similarly, lipid peroxidation has been shown to activate nuclear factor-κB (NF-κB), and consequently, has contributed to the histopathological cascade observed in *mdx* muscles (32). Finally, inflammatory cytokines have been shown to inhibit myogenic differentiation through the activation of NF-κB (33–34), and the activation of NF-κB signaling in skeletal muscle has been correlated with muscular dystrophies and inflammatory myopathies (34, 35).

In the current study, we examined the role that RhoA signaling pathway plays in regulating HO, FI, and IMCL in these models of DMD (dKO and *mdx* mice), due to the fact that RhoA signaling has been shown to play an important role in regulating osteogenesis, adipogenesis, myogenesis, and inflammation. RhoA is a small G protein in the Rho family that regulates cell morphology and migration by reorganizing the actin cytoskeleton in response to extracellular signaling (36). The RhoA signaling pathway is involved in the commitment of mesenchymal stem cells (MSCs) toward their osteogenic or adipogenic differentiation (37). RhoA signaling activation in MSCs *in vitro* induces osteogenesis potential and inhibits adipogenic potential of the cells; however, the application of Y-27632, a specific inhibitor of RhoA/Rho kinase (ROCK), reverses this process (37–39). RhoA also mediates BMP-induced signaling in MSCs and promotes osteoblastic cell survival (40, 41). Moreover, the inhibition of RhoA with Y-27632 was found to induce the adipogenic differentiation of muscle-derived cells *in vitro*, and resulted in the manifestation of FI in skeletal muscle (42). RhoA is also activated by Wnt5a, which results in the induction of osteogenic differentiation of human adipose stem cells (ASCs) and the repression of adipogenic differentiation (43). RhoA's role in the inflammatory process has been previously described, where TNF-α induces the activation of RhoA signaling in smooth muscle cells (44), RhoA regulates Cox-2 activity in fibroblasts (45), and RhoA induces the expression of inflammatory cytokines in adipocytes (46). Moreover, involvement of RhoA in mediating myocardial and pulmonary fibrosis has been described (47–48). In addition, previous studies have indicated that the sustained activation of the RhoA pathway can block the differentiation of muscle cells by inhibiting myoblast fusion (49–51).

Because of RhoA's potential involvement in the regulation of osteogenesis, adipogenesis, and myogenesis of stem cells and inflammation, we hypothesized that RhoA may act as a critical regulator of these processes in dystrophic muscle. In the current study, we investigated the status of HO, FI, IMCL, and muscle regeneration in the skeletal muscle of *mdx* and dKO mice, as well as the potential role that RhoA signaling plays in regulating these processes.

MATERIALS AND METHODS

Animals

Wild-type (C57BL/10J) mice were obtained from the Jackson Laboratory (Bar Harbor, ME, USA). The *mdx* and dKO (*mdx; utrn$^{-/-}$*) mice were derived from our in-house colony. Mice were housed in groups of 4 on a 12:12-h light-dark cycle at 20–23°C. At least 6 mice were used in each experimental sample group. All procedures were approved by the Institutional Animal Care and Use Committee (IACUC) at the University of Pittsburgh.

Stem cell isolation from skeletal muscle

Muscle-derived stem cells (MDSCs) were isolated from the skeletal muscle of dKO and *mdx* mice (4 wk old) *via* a modified preplate technique (52). Mice were sacrificed in a carbon dioxide chamber, as described in the IACUC protocol. Cells were cultured in proliferation medium [DMEM supplemented with 20% fetal bovine serum (FBS), 1% peni-

cillin-streptomycin antibiotics, and 0.5% chicken embryo extract (CEE)].

Micro-computed tomography (micro-CT)

To observe HO in the soft tissues of *mdx* and dKO mice, 8-wk-old mice were anesthetized with 3% isoflurane in O_2 gas (1.5 L/min), and the lower extremities, including the pelvis, were scanned using the Viva CT 40 (Scanco, Wangen-Brüttisellen, Switzerland) with the following settings: energy, 70 kVp; intensity, 114 µA; integration time, 200 ms; isotropic voxel size, 35 µm; threshold, 163.

In vitro RhoA inactivation with Y-27632 and multipotent differentiation assays

dKO MDSCs cultured *in vitro* were treated with the RhoA/Rock inhibitor Y-27632 (10 µM; EMD Millipore, Billerica, MA, USA) in proliferation medium for 2 d, before being plated in 12-well flasks and set up for osteogenesis, adipogenesis, or myogenesis assays. The osteogenesis assay was conducted with osteogenic medium (DMEM supplemented with 110 µg/ml sodium pyruvate, 584 µg/ml L-glutamine, 10% FBS, 1% penicillin/streptomycin, 10^{-7} µM dexamethasone, 50 µg/ml ascorbic-acid-2-phosphate, and 10^{-2} µM β-glycerophosphate), supplemented with BMP2 (50 ng/ml for 7 d). Calcium deposition was assessed with alizarin red stain. Adipogenesis assay was conducted with adipogenic induction medium (Lonza, Basel, Switzerland) for 10 d and tested for lipid droplets with Oil red O stain (Sigma, St. Louis, MO, USA). The myogenesis assay was conducted by switching the proliferation medium into myogenic differentiation medium (DMEM containing 2% horse serum). Myotube formation was tracked during the following 4 d. 10 µM of Y-27632 was continuously present in the differentiation medium.

mRNA analysis with reverse transcriptase-PCR

Total RNA was obtained from MDSCs or the skeletal muscles of mice using a RNeasy Mini Kit (Qiagen, Valencia, CA, USA), according to the manufacturer's instructions. Reverse transcription was performed using the iScript cDNA synthesis kit (Bio-Rad, Hercules, CA, USA). PCR reactions were performed using an iCycler Thermal Cycler (Bio-Rad). The cycling parameters used for all primers were as follows: 95°C for 10 min; PCR, 40 cycles of 30 s at 95°C for denaturation, 1 min at 54°C for annealing, and 30 s at 72°C for extension. Products were separated by size, and they were visualized on 1.5% agarose gels stained with ethidium bromide. All data were normalized to the expression of GAPDH. Genes and primers used in the study included GAPDH: TCCATGA-CAACTTTGGCATTG (sense) and TCACGCCACAGCTT-TCCA (antisense); RhoA: GTAGAGTTGGCTTTATGGGA-CAC (sense), and TGGAGTCCATTTTTCTGGGATG (antisense); BMP2: TCTTCCGGGAACAGATACAGG (sense), and TGGTGTCCAATAGTCTGGTCA (antisense); BMP4: ATTC-CTGGTAACCGAATGCTG (sense), and CCGGTCTCAGG-TATCAAACTAGC (antisense); TNF-α: GATTATGGCTCAGGG-TCCAA (sense), and CTCCCTTTGCAGAACTCAGG (antisense); IL6: GGAAATCGTGGAAATGAG (sense), and GCT-TAGGCATAACGCACT (antisense); Klotho: CCCAAACCATC-TATGAAAC (sense), and CTACCGTATTCTATGCCTTC (antisense); and peroxisome proliferator-activated receptor γ (PPARγ): CCACCAACTTCGGAATCAGCT (sense) and TTT-GTGGATCCGGCAGTTAAGA (antisense).

In vivo RhoA inactivation with Y-27632

Intramuscular injections into the gastrocnemius muscles (GMs) of dKO mice were conducted with Y-27632 (5 mM in 30 µl of PBS solution; left limb) or control (30 µl of PBS; right limb), starting from 4 wk of age. Intramuscular injections were conducted 3×/wk for 4 wk. Differential HO formation in the skeletal muscle with or without Y-27632 treatment was assessed by micro-CT scan or alizarin red stain. Systematic inhibition of RhoA signaling was conducted by intraperitoneal injection of Y-27632 (5 mM in PBS, 10 mg/kg/mouse) or control (PBS only) into dKO mice from 3 wk of age. Intraperitoneal injections into dKO mice were conducted 3×/wk for 4 wk.

Histology

Cryostat sections (10 µm) were prepared using standard techniques from GMs of mice. HO in muscle tissue was assessed by alizarin red stain: tissue sections of skeletal muscle were fixed with 4% formalin (10 min) and rinsed with ddH₂O; slides were then incubated with alizarin red working solution for 10 min before being washed with ddH₂O. FI was detected by Oil red O stain: fixed tissue sections were rinsed with ddH₂O and 60% isopropanol; slides were then incubated with Oil red O working solution for 15 min before being rinsed with 60% isopropanol and ddH₂O. The IMCL was detected by AdipoRed assay reagent (Lonza): fixed tissue sections were rinsed with PBS and incubated with AdipoRed assay reagent for 15 min before being washed with PBS. For immunofluorescent staining of tissue sections, the sections were blocked with horse serum (10%) for 1 h, and the primary antibodies RhoA (Santa Cruz Biotechnology, Santa Cruz, CA, USA), CD68 (Abcam, Cambridge, MA, USA), or MyoD (Santa Cruz Biotechnology) were applied at 1:100–1:200. Negative controls were performed concurrently with all immunohistochemical staining. Necrosis with damaged myofibers in muscle was assayed by incubating with biotinylated anti-mouse IgG (1:300; Vector Laboratory, Burlingame, CA, USA) for 1 h at room temperature, which was followed by a 15-min incubation with streptavidin Cy3 conjugate (1:500; Sigma-Aldrich). All incubations were performed at room temperature. All slides were analyzed using fluorescent microscopy (Leica Microsystemic, Buffalo Grove, IL, USA) and photographed at ×4–40 view.

Measurement of results and statistical analysis

The measurement of results from images was performed using commercially available software (Northern Eclipse 6.0; Empix Imaging, Mississauga, ON, Canada) and ImageJ 1.32j (U.S. National Institutes of Health, Bethesda, MD, USA). Data from ≥3 samples from each subject were pooled for statistical analysis. Results are given as means ± SD. Statistical significance of any difference was calculated using Student's *t* test. Values of $P <$ 0.05 were considered statistically significant.

RESULTS

Extensive intramuscular HO and IMCL occurred in the skeletal muscle of dKO mice

Micro-CT scan and alizarin red staining revealed extensive HO in the hind-limb muscles (*i.e.*, GMs) of dKO mice at 8 wk of age (**Fig. 1*A*, *B***), while in age-matched *mdx* mice, only mild HO was observed (Fig. 1*A*, *B*). Oil **F1**
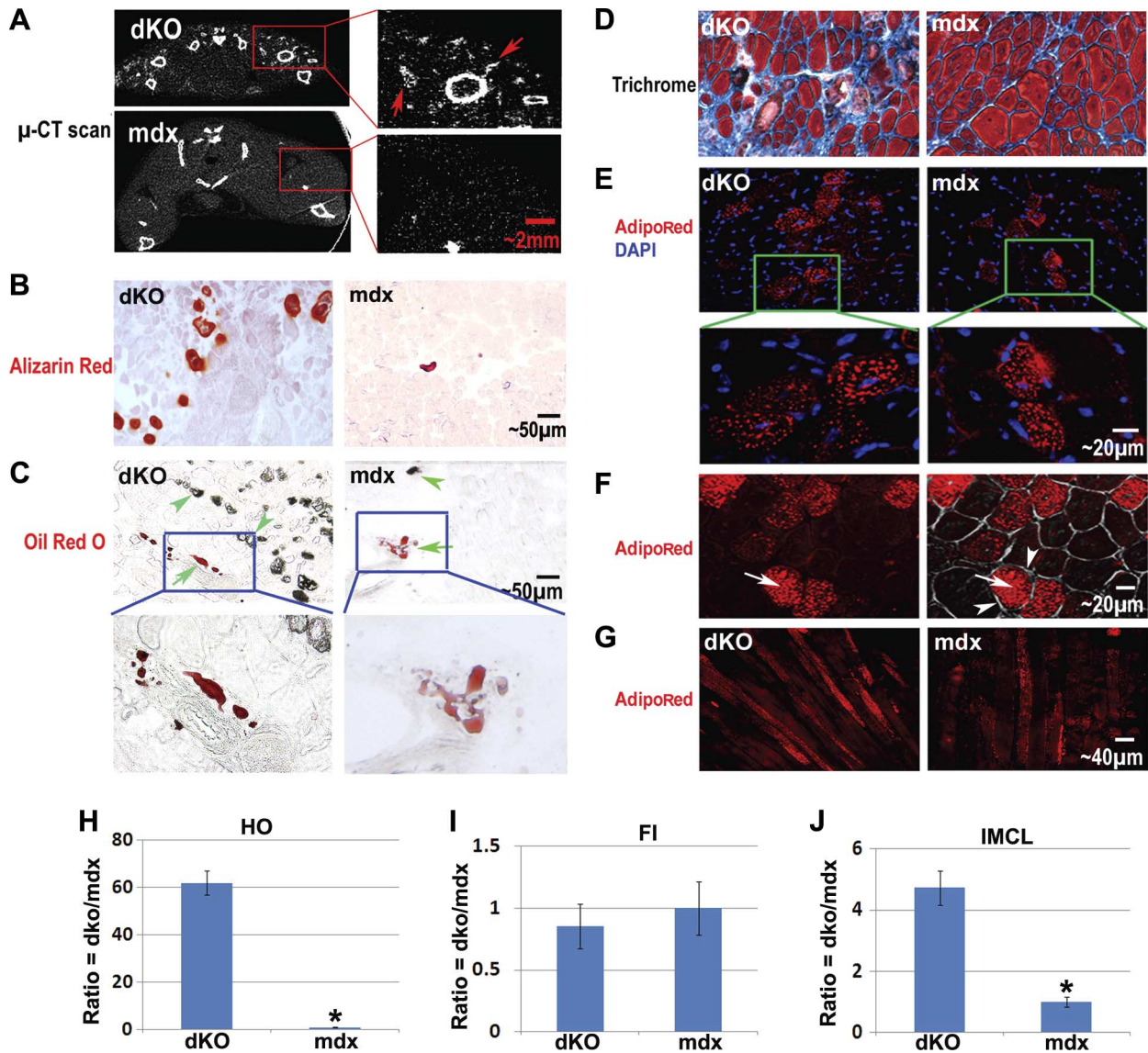
Figure 1. Differential formation of HO, FI, fibrosis, and IMCL in the skeletal muscle of dKO mice and *mdx* mice. *A*) Micro-CT scan revealed extensive HO formation (arrows) in the hind-limb skeletal muscles of dKO mice (8 wk of age), especially in the thigh and GM. Much less HO was observed in *mdx* mice (8 wk of age). *B*) Alizarin red stain of muscle tissue sections also showed more extensive HO formation in the GMs of the dKO mice. *C*) Oil red O stain revealed comparable amounts of intramuscular FI in dKO and *mdx* mice (but a much lower ratio of fat/HO), and the distinct localization of fat and HO (HO is visible with brightfield light). Arrows denote FI; arrowheads denote HO. *D*) Trichrome stain showed more fibrotic tissue (blue) and less normal myofibers in the skeletal muscle of dKO mice. *E*) AdipoRed stain indicated that IMCL occurred in the skeletal muscle of both *mdx* and dKO mice but was more extensive in the dKO mice. *F*) Representative images showing the localization of lipids (arrows) inside the membrane (arrowheads) of myofibers. Left panel: fluorescent image showing AdipoRed signal. Right panel: overlay of fluorescent and brightfield images. *G*) AdipoRed stain of longitudinal sections of GMs, verifying that the identity of the cells with positive signals were myofibers and not fat cells. *H*) Statistics of HO in GMs of dKO mice compared to *mdx* mice. *I*) Statistics of FI in GMs of dKO mice compared to *mdx* mice. *J*) Statistics of IMCL in GMs of dKO mice compared to *mdx* mice. *P < 0.05.

red O stain revealed mild intramuscular FI in the GMs of both 8-wk-old *mdx* and dKO mice (Fig. 1*C*). Notably, the FI/HO ratio was much lower in the dKO mice, and the sites of intramuscular HO and FI did not colocalize (Fig. 1*C* and Supplemental Fig. S1*A*). The fact that HO and FI never colocalized in the muscle suggests that these two processes are mutually exclusive and could implicate different cell types and/or niches involved in the two processes. In addition, trichrome staining of the skeletal muscle tissue further revealed more fibrosis

in the skeletal muscle of dKO mice when compared with skeletal muscle of the *mdx* mice (Fig. 1*D*). These observations suggest that the microenvironment differs between dKO and *mdx* skeletal muscle, and the micro-milieu in the dKO skeletal muscle is more conductive to osteogenesis or fibrogenesis processes. Much like our observation in the dKO mice, other important animal models of human DMD, including the GRMD dog and the canine X-linked muscular dystrophy (CXMD) dog, feature extensive HO and mild FI in their skeletal

muscle, especially before the age of 4–6 mo (16, 53–54).

Interestingly, contrary to the mild FI observed in the skeletal muscles of dKO mice, extensive IMCL was observed; while in the skeletal muscle of *mdx* mice, less extensive amounts of IMCL were noted (Fig. 1*E–G*). This severe lipid accumulation in the mature muscle cells (myofibers) of dKO muscle is indicative of disordered lipid metabolism in their skeletal muscle (55).

In addition, intramuscular HO and FI development was compared between the dKO and *mdx* mice at different ages (dKO mice at 4 or 8 wk and *mdx* mice at 4 wk or 24 mo). Eight weeks and 24 mo represent ~100% of the life span of the dKO and *mdx* mice, respectively. Results showed that HO increased with age in the dKO mice within their very short life span, but it remained mild in the *mdx* mice across their entire life span (**Fig. 2***A*, **C**, **D**). Meanwhile, FI increased with age in both the *mdx* and dKO mice and became quite exces-

F2

sive in aged *mdx* mice but not in the 8-wk-old dKO mice (Fig. 2*B–D*). Notably, in both the 4- and 8-wk-old dKO mice, the presence of FI was much less extensive than HO (Fig. 2*C*), while in *mdx* mice, FI became more extensive than HO with aging (Fig. 2*D*).

HO localizes at the sites of necrosis and fibrosis in the skeletal muscle of dKO mice

Alizarin red or hematoxylin and eosin staining was performed on serial sections of the skeletal muscle of 8-wk-old dKO mice, and HO generally localized at the sites enriched with damaged myofibers, but not in areas where normal myofibers existed (Fig. 2*E*). Also, Trichrome stain and IgG stain further indicated that localization of HO is generally surrounded by fibrotic tissues (Supplemental Fig. S1*B*) or necrotic tissues (Supplemental Fig. S1*C*). Therefore, it appears that
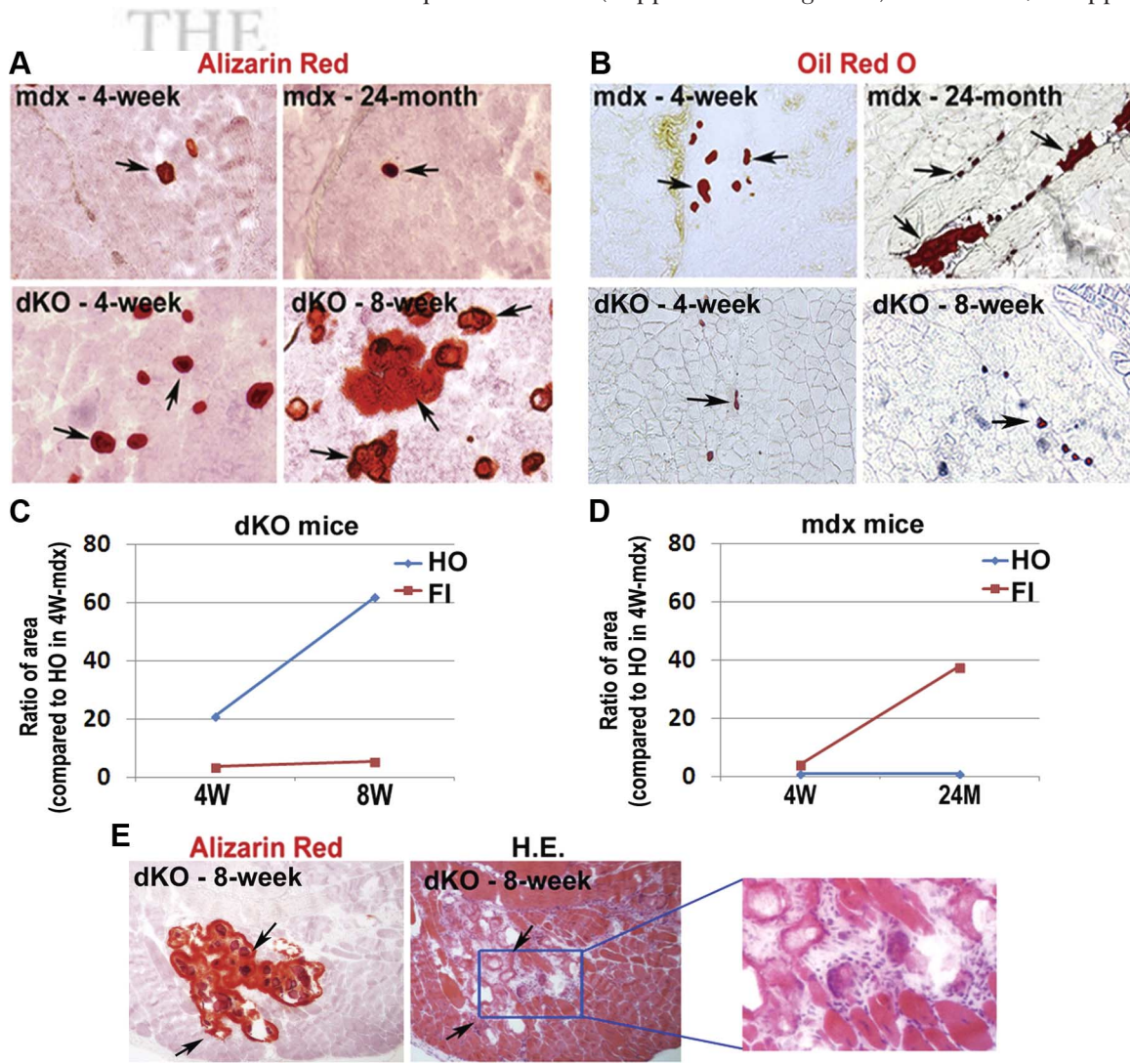
Figure 2. Development of HO and FI in the skeletal muscle of "younger" and "older" dKO mice (4 and 8 wk) and *mdx* mice (4 wk and 24 mo). *A*) HO (arrows) increased significantly with age in dKO mice but not in *mdx* mice. *B*) FI (arrows) increased with age in both *mdx* mice and dKO mice, but to a lesser extent in the dKO mice. *C*) Statistics on the change of HO and FI with aging in dKO mice. *D*) Statistics on the change of HO and FI with aging in *mdx* mice. *E*) Serial sections of the skeletal muscle of 8-wk-old dKO mice were stained with either alizarin red or hematoxylin and eosin (H.E.); it shows that HO was generally localized at the sites enriched with damaged myofibers and fibrosis (arrows) but not at the sites possessing normal myofibers.

AQ: 2

HO formation in the skeletal muscle of dKO mice is concurrent with necrosis and fibrosis.

RhoA signaling was activated in the skeletal muscle of dKO mice and RhoA+ cells specifically localized at the sites of necrosis and HO

Semiquantitative RT-PCR analyses revealed that the expression of the inflammatory factor TNF-α, and osteogenesis-related genes *BMP2, BMP4*, and *RhoA* were all up-regulated in the dKO skeletal muscle, when compared to the age-matched *mdx* skeletal muscle (**Fig. 3***A*). BMPs are known to induce HO in damaged skeletal muscle, and elevated BMP signaling has been observed in satellite cells of patients wtih DMD (56). We also found that the expression of Klotho, an antiinflammatory and antiaging factor (57), was down-regulated in the dKO skeletal muscle when compared to the *mdx* skeletal muscle (Fig. 3*A*). Because inflammation has been implicated as an important contributor to HO (1, 27, 58), it is possible that highly activated inflammation signaling in the dKO skeletal muscle is involved with the extensive HO observed in this animal model. A similar differential expression of these genes was found in MDSCs isolated from dKO and *mdx* mice.

Furthermore, immunofluorescent staining for the RhoA protein revealed an increased number of RhoA+ cells in the skeletal muscle of dKO mice when compared to *mdx* mice (Fig. 3*B, C*), further confirming elevated RhoA signaling in the dKO skeletal muscle. Notably, it was noted that RhoA+ cells were usually localized at the sites of excessive necrosis and HO (Fig. 3*B* and Supplemental Fig. S2), but not in area of FI, indicating potential involvement of RhoA+ cells in the progression of HO.

In addition, through colocalization analyses, it was demonstrated that RhoA+ cells do not colocalize with CD68+ inflammatory cells (Fig. 3*D*) and MyoD+ myogenic cells (Fig. 3*E*), indicating that the RhoA+ cells did not represent inflammatory or myogenic cells.

RhoA inactivation of dKO MDSCs decreased their osteogenic potential, while it increased their adipogenic and myogenic potentials

Similar to what was observed with skeletal muscle tissues, immunofluorescent staining of MDSCs isolated from dKO and *mdx* mice for MyoD and RhoA also demonstrated a greater number of RhoA+ cells in the MDSCs isolated from the dKO mice than the *mdx* mice (**Fig. 4***A*). Therefore, we hypothesized that the inactiva-
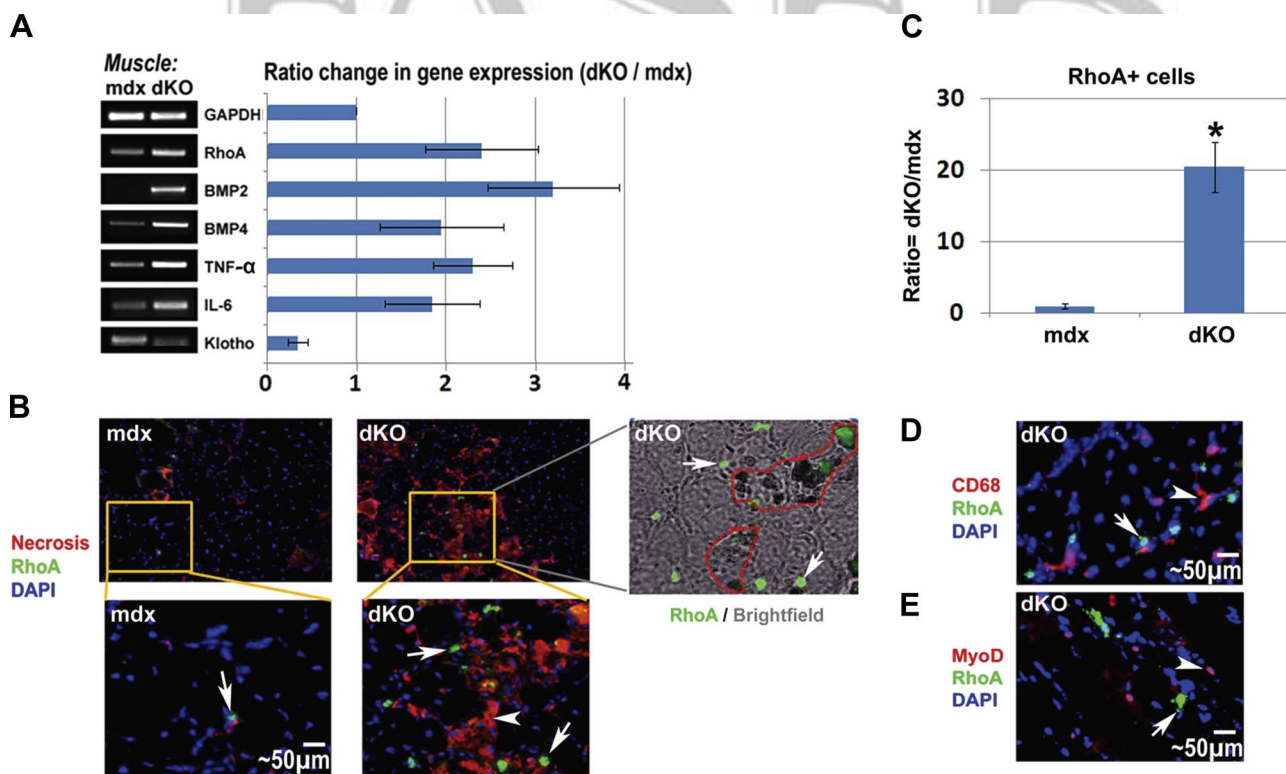
Figure 3. RhoA+ cells in the skeletal muscle of dKO and *mdx* mice. *A*) RT-PCR of mRNA isolated from the skeletal muscle of dKO and *mdx* mice (8 wk of age) showed that the expression of RhoA, BMP2/4, TNF-α, IL-6 was up-regulated in dKO mice, and the expression of the anti-inflammation factor Klotho was down-regulated. *B*) Immunofluorescent staining of RhoA demonstrated a greater number of RhoA+ cells (arrows) in the skeletal muscle of dKO mice. Necrotic areas (arrowheads) were localized by staining with fluorescent anti-mouse IgG, and RhoA+ cells were found to localize at or around the necrotic areas; overlay of images of brightfield and immunofluorescent staining of RhoA further revealed that the same areas enriched with RhoA+ cells (arrows) are the area of HO (circled) too. *C*) Statistics of RhoA+ cells in *mdx* and dKO skeletal muscle. *D*) Representative image of immunofluorescent staining of CD68 and RhoA in the dKO muscle demonstrated that CD68+ cells (arrowheads) and RhoA+ cells (arrows) were two different cell populations. *E*) Representative image of immunofluorescent staining of MyoD and RhoA in the dKO muscle demonstrated that MyoD+ cells (arrowheads) and RhoA+ cells (arrows) were two different cell populations. *P < 0.05.
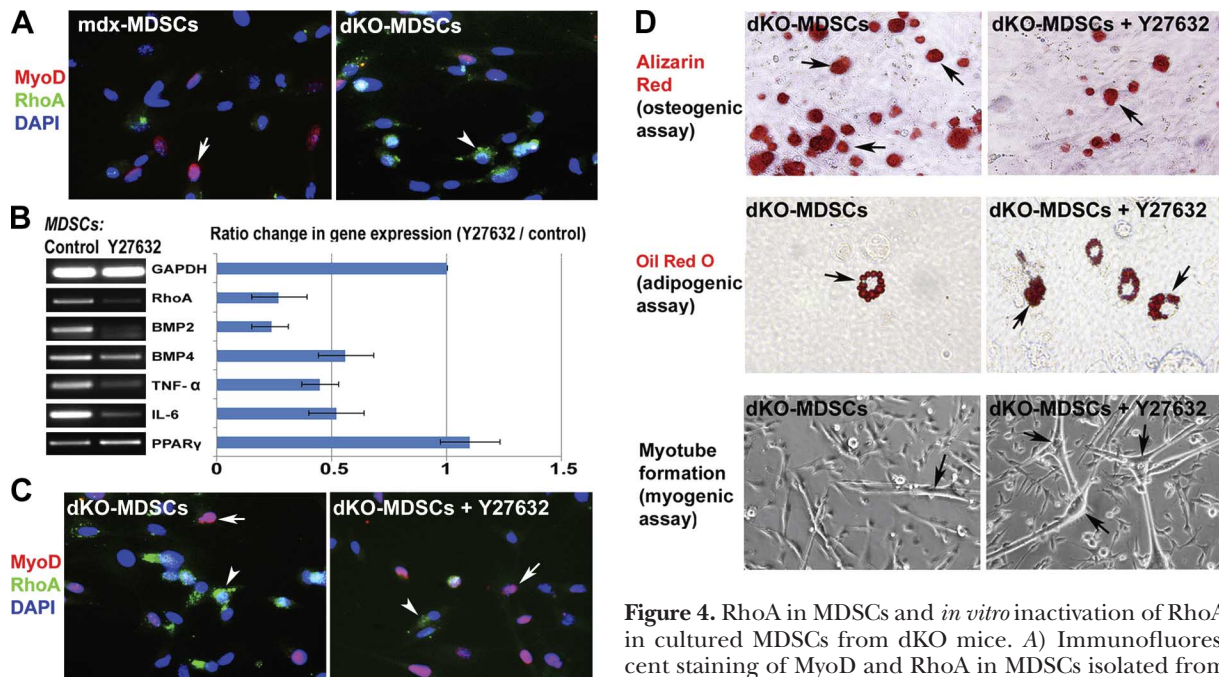
COLOR

Figure 4. RhoA in MDSCs and *in vitro* inactivation of RhoA in cultured MDSCs from dKO mice. *A*) Immunofluorescent staining of MyoD and RhoA in MDSCs isolated from *mdx* and dKO mice demonstrated that RhoA⁺ cells (arrowhead) and MyoD⁺ cells (arrow) were two distinct cell populations, and there were more RhoA⁺ cells in the MDSCs isolated from dKO mice than *mdx* mice. *B*) Pretreatment of dKO-MDSCs with the RhoA/Rock inhibitor Y-27632 in proliferation medium for 2 d down-regulated the expression of RhoA, BMP2/4, TNF-α, and IL-6, and up-regulated the expression of PPARγ. *C*) Y-27632 treatment decreased the number of RhoA⁺ cells (arrowheads) and increased the number of MyoD⁺ cells (arrows). *D*) *In vitro* osteogenesis, adipogenesis, and myogenesis assays indicated that, Y-27632 pretreated dKO-MDSCs demonstrated decreased osteogenic potential (less cells with positive alizarin red signal) in osteogenic medium and increased adipogenesis potential (more cells with positive Oil red O signal) in adipogenic medium, as well as increased myogenic potential (more myotube formation) in the myogenic medium.

tion of RhoA signaling in the MDSCs may change the osteogenic, adipogenic, and myogenic potentials of the cells because RhoA is a proosteogenic and antiadipogenic/myogenic signaling pathway. To test the hypothesis, dKO MDSCs were cultured in proliferation medium and pretreated with the RhoA/Rock inhibitor, Y-27632, for 2 d before undergoing osteogenic, adipogenic, and myogenic assays. Y-27632 pretreatment of dKO MDSCs significantly down-regulated the expression of the inflammation-related genes (TNF-α and IL-6), BMPs, and RhoA (Fig. 4*B*). Also, Y-27632 pretreatment up-regulated the expression of the key adipogenic factor, PPARγ, which is known to have anti-inflammatory activities (59). Immunostaining of RhoA and MyoD showed that RhoA⁺ cells and MyoD⁺ cells were 2 distinct cell populations, and the number of RhoA⁺ cells was decreased, while the number of MyoD⁺ cells was increased with Y-27632 treatment (Fig. 4*C*), indicating decreased osteogenic but increased myogenic potentials of the treated cell population. Osteogenesis and adipogenesis assays revealed a decreased osteogenic potential and increased adipogenic potential of the MDSCs treated with Y-27632 (Fig. 4*D*). Meanwhile, the dKO MDSCs treated with Y-27632 showed an increase in their myogenic potential (Fig. 4*D*).

RhoA inactivation in dKO skeletal muscle decreased HO and IMCL, while it increased muscle regeneration

The RhoA/Rock inhibitor Y-27632 was injected intramuscularly into the GM muscles of 4-wk-old dKO mice

to determine the effect of RhoA inactivation on the development of HO, FI, IMCL, and muscle regeneration. Four weeks after the administration of Y-27632, we observed slower development of HO in the dKO skeletal muscle, as determined by micro-CT scanning and histological staining (**Fig. 5*A*, *B***). At the same time, skeletal muscle regeneration was enhanced in the treated dKO skeletal muscle (Fig. 5*C*) despite slightly increased FI (Fig. 5*D*). Notably, the increase of FI in the dKO muscle with Y-27632 administration was mild compared to the increase of muscle regeneration, and the overall phenotype of the dystrophic muscle was greatly improved (Fig. 5). Finally, IMCL was decreased (Fig. 5*E*), indicating improved fatty acid metabolism in the skeletal muscle with RhoA inactivation. Immunofluorescent staining of RhoA revealed that the number of RhoA⁺ cells decreased with the administration of Y-27632 (Fig. 5*F*), which may correlate with the reduced number of osteogenic cells in the skeletal muscle. Furthermore, the number of CD68⁺ inflammatory cells (mainly macrophages; ref. 60) was also reduced after the administration of Y-27632 (Fig. 5*G*). In addition, semiquantitative RT-PCR showed that the expression of RhoA, BMPs, and inflammation-related genes were down-regulated in skeletal muscle treated with Y-27632, while the expression of PPARγ was up-regulated (Fig. 5*H*). PPARγ activation may have improved fatty acid metabolism and reduced the accumulation of lipid within the muscle cells (61–62). The overall pheno-

F5
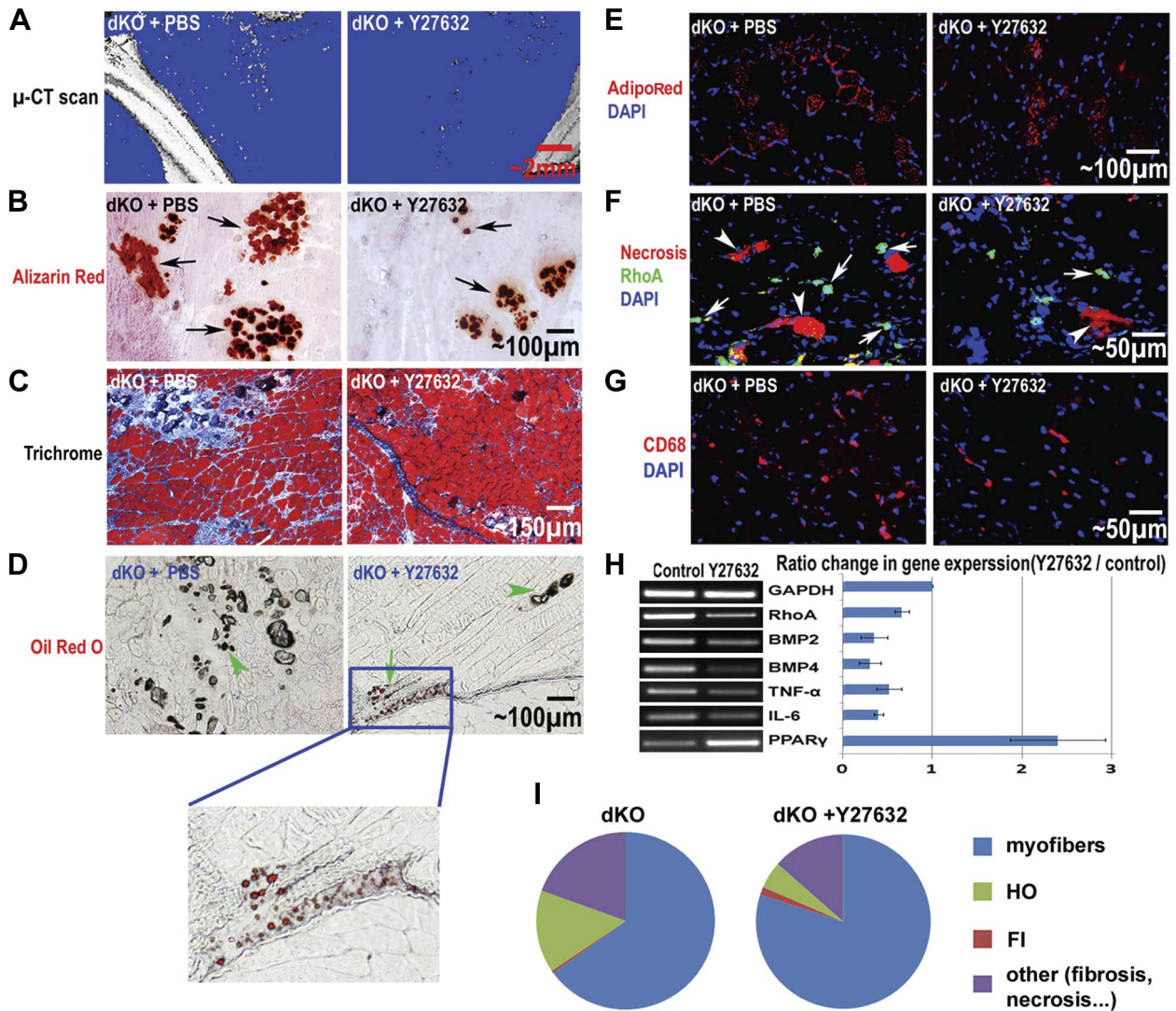
Figure 5. *In vivo* inactivation of RhoA in the skeletal muscle of dKO mice. *A*) Micro-CT scan of the hind-limb skeletal muscles, including the GM, 4 wk after beginning the administration of the RhoA/Rock inhibitor Y-27632 in dKO mice (from 4 to 8 wk of age) showed a reduction in HO. *B*) Alizarin red stain of muscle tissues also revealed greatly reduced HO (arrows) in the GM muscles with Y-27632 treatment. *C*) Hematoxylin and eosin stain showed improved muscle regeneration with Y-27632 treatment. *D*) Oil red O stain showed slightly increased FI (arrows) with Y-27632 treatment. HO is also visible with brightfield microscopy (arrowheads). *E*) AdipoRed stain showed reduced IMCL in dKO mice with Y-27632 treatment. *F*) Immunofluorescent stain showed reduced numbers of RhoA$^+$ cells (arrows) and necrotic myofibers (arrowheads) with Y-27632 treatment. *G*) Immunofluorescent stain showed reduced numbers of CD68$^+$ inflammatory cells with Y-27632 treatment. *H*) RT-PCR of the muscle tissues revealed down-regulated expression of RhoA, BMP2/4, TNF-α, and IL-6, and up-regulated expression of PPARγ with Y-27632 treatment. *I*) The overall phenotypic change of the muscle treated with Y-27632 is summarized in the pie graph, including myofibers, HO, FI, and other (fibrosis and necrosis). It is clear that HO, fibrosis, and necrosis were reduced with Y-27632 treatment, while muscle regeneration was improved; FI was also increased, but only very slightly.

typic change in the dKO skeletal muscle treated with Y-27632 is summarized in Fig. 5*I*.

dKO cardiac muscle featured increased IMCL, fibrosis, and HO when compared to *mdx* mice

Cardiac involvement is the leading cause of early death in patients wtih DMD (63), and intramyocardial lipid accumulation in cardiac muscle has been observed in patients wtih DMD, especially in the most damaged areas of the hearts (11, 13). We hypothesized that IMCL observed in the *mdx* and dKO mice was not limited to the skeletal muscle but

would also be found in cardiac muscle and could be related to the formation of fibrosis observed in the dystrophic hearts (cardiomyopathy) of the mice.

Trichrome staining of cardiac muscles from 8-wk-old WT, *mdx*, and dKO mice was conducted to characterize ECM collagen deposition, and it revealed that fibrosis formation is generally severe in dKO mice, mild in *mdx* mice, and absent in WT mice **(Fig. 6*A*)**. Alizarin red staining of the cardiac muscle revealed occurrences of HO in the dKO mice (Fig. 6*B*), but not in the WT or *mdx* mice (data not shown). Meanwhile, we did not observe any FI in the cardiac muscles in these three
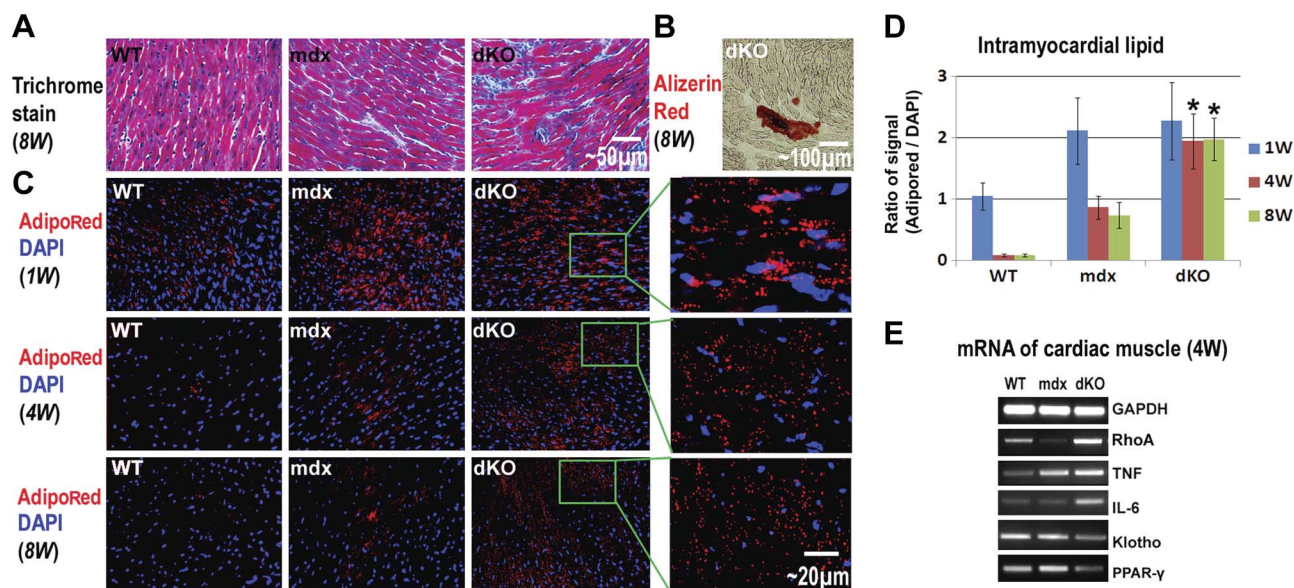
A

B

C

D

E

COLOR

Figure 6. Fibrosis formation and intramyocardial lipid accumulation in the cardiac muscles of WT, *mdx*, and dKO mice. *A*) Trichrome stain showed the progression of fibrosis formation (collagen deposition, blue) in the cardiac muscles as dKO > *mdx* > WT. *B*) Alizarin red stain revealed HO (although mild) in the cardiac muscle of dKO mice. *C*) High levels of intramyocardial lipids were observed in all three mouse models at 1 wk after birth. At 4 and 8 wk after birth, intramyocardial lipid accumulation decreased to an undetectable level in WT mice and decreased to a moderate level in *mdx* mice but still maintained a very high level in the dKO mice. *D*) Statistical analysis of the percentage of area positive for lipid accumulation in WT, *mdx*, and dKO mice of different ages. *E*) RT-PCR results showed that the expression of inflammatory factors (TNF-α and IL-6) were up-regulated in the cardiac muscles of *mdx* and dKO mice, compared with WT mice. The strongest up-regulation of TNF-α and IL-6 occurred to the dKO mice. The expression of the anti-inflammatory factor Klotho was down-regulated in the cardiac muscle of mdx and dKO mice, compared to WT mice. *P < 0.05.

mouse models (data not shown), but we did observe intramyocardial lipid accumulation in both the *mdx* and dKO mice (Fig. 6*C*, *D*).

Extensive intramyocardial lipid accumulation at 1 wk of age was observed in all 3 mouse models (Fig. 6*C*). Intramyocardial lipid accumulation in fetal WT mice is a common occurrence because, unlike adult hearts, the fetal hearts use glucose instead of fatty acids as a source of energy (64). Intramyocardial lipid accumulation was found to decrease rapidly in WT mice 1 wk after birth and became nearly undetectable at 4 wk of age (Fig. 6*C*); however, in both *mdx* and dKO mice, intramyocardial lipid accumulation was still observed at 4 wk of age, and the dKO mice exhibited more intramyocardial lipid accumulation than the *mdx* mice (Fig. 6*C*, *D*). Compared to the WT and *mdx* mice, the expression of RhoA and inflammation signaling genes (TNF-α and IL-6) were also found to be up-regulated in the dKO cardiac muscle, while the expression of the *Klotho* gene was down-regulated (Fig. 6*E*). We suggest that the activation of RhoA and inflammation signaling in dKO cardiac muscle may account for higher levels of HO, intramyocardial lipid accumulation, and fibrosis.

Systemic RhoA inactivation *via* intraperitoneal injection (IP) of Y-27632 reduced IMCL, fibrosis, and HO in dKO cardiac muscle

We hypothesized that RhoA inactivation could reduce HO, IMCL, and fibrosis in the dKO cardiac muscle. To confirm this hypothesis, Y-27632 was injected intraperi-

toneally (IP) to achieve the systemic inhibition of RhoA signaling in 3-wk-old dKO mice. As expected, after 4 wk of continuous injection. IMCL, fibrosis, and HO in the cardiac muscle decreased compared to nontreated mice (**Fig. 7***A*–*F*). Actually, involvement of RhoA/ ROCK in mediating myocardial fibrosis in type 2 diabetes has been previously demonstrated (48). Semiquantitative PCR further revealed that the expression of RhoA and inflammatory factors were down-regulated with Y-27632 administration, while the expression of Klotho and PPARγ was up-regulated (Fig. 7*G*).

F7

DISCUSSION

Heterotopic ossification (HO) and ectopic fatty infiltration (FI) have been reported in the dystrophic muscle of patients wtih DMD and related animal models (12, 14–16, 65). Our results revealed that mouse models of DMD featuring differing severities of muscular dystrophy have varied potentials for developing HO and FI, and that RhoA signaling could represent a critical mediator in the process, including progression toward HO, FI, and normal muscle regeneration. We noted that the inactivation of RhoA repressed the development of HO and IMCL and improved muscle regeneration in dKO mice. RhoA signaling was previously demonstrated to promote the osteogenic potential of MSCs, while preventing their adipogenic and myogenic potentials (37, 40). Here, we further identified a similar
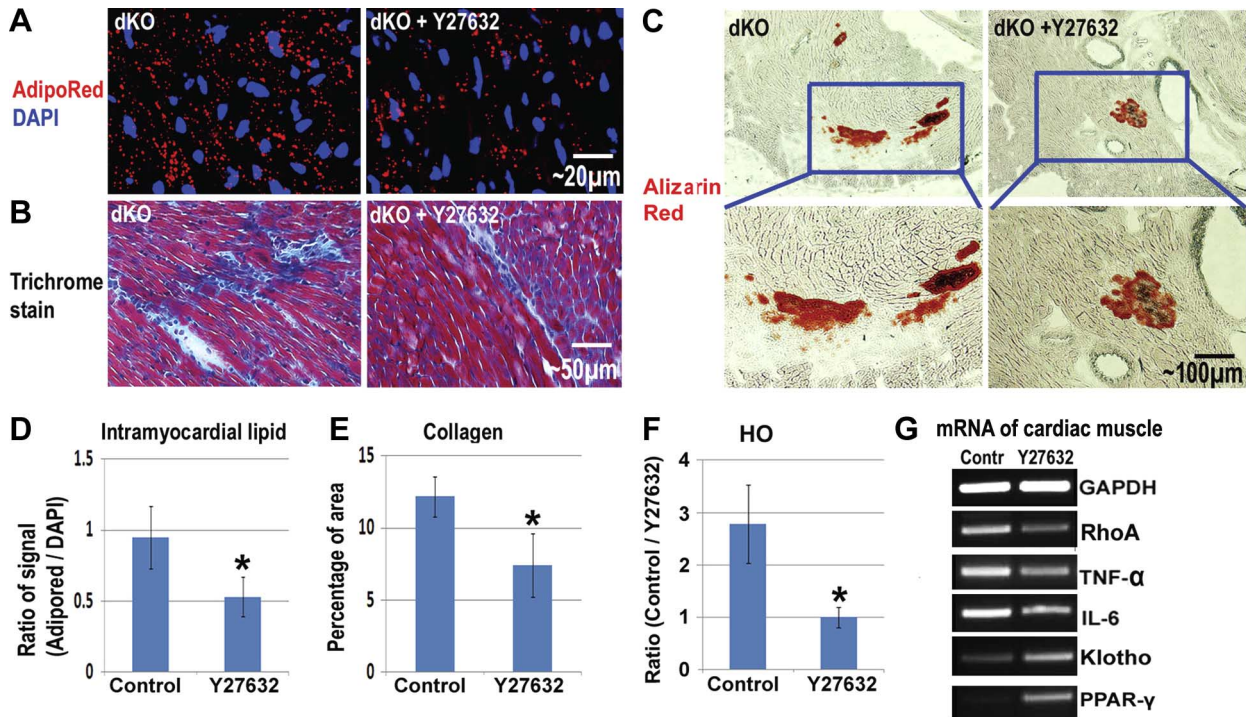
Figure 7. Reduction of intramyocardial lipid accumulation and fibrosis in the cardiac muscles of dKO mice with inactivated RhoA. *A*) AdipoRed stain showed that intramyocardial lipid accumulation in dKO mice was reduced 4 wk after the initiation of Y-27632 administration. *B*) Trichrome stain showed that fibrosis formation was reduced with Y-27632 administration. *C*) Alizarin red stain showed that HO formation in the cardiac muscles of dKO mice was reduced with Y-27632 administration. *D*) Statistical analysis of the percentage of areas positive for IMCL in dKO mice, with and without Y-27632 administration. *E*) Statistical analysis of the percentage of dKO mice positive for HO in their cardiac muscles, with and without Y-27632 administration. *F*) RT-PCR of mRNA from the cardiac muscles showed that the expression of RhoA and inflammatory factors (TNF-α and IL-6) were down-regulated with Y-27632 administration, while the expressions of Klotho and PPAR-γ were up-regulated. *Significant difference, $P < 0.05$.

role of RhoA signaling in muscle stem cells. We suggest that HO in skeletal muscle could be a cell-mediated process involving the transdifferentiation of myogenic cells into osteogenic cells in a stressful microenvironment. The potential mechanisms underlying our current results are proposed in **Fig. 8**.

Muscle stem cells from normal mice are known to possess multipotent differentiation potentials and can

F8

Figure 8. Schematic diagram of the potential mechanism involving RhoA/ROCK signaling in regulating HO, FI, and muscle regeneration in the dystrophic muscle of dKO mice. RhoA/ROCK is responsive to a variety of stresses. Multipotent stem cells, either local stem cells in the dystrophic muscle, bone-marrow-derived stem cells mobilized to the dystrophic muscle of dKO mice, or stem cells of other origins, may be stimulated to differentiate into an osteogenic lineage and may participate in HO formation by highly activated RhoA/Rock signaling, whereas normal myogenic differentiation or potential adipogenic differentiation in dKO mice were repressed by RhoA/Rock signaling. Critical HO-inducing factors, such as BMPs and inflammatory signaling, are interactive with RhoA/Rock signaling, and contribute to HO formation by stem cells or other progenitor cells. RhoA/Rock inactivation with Y-27632 has the potential to reverse the progression of differentiation of the stem cells toward HO, and improve myogenic or adipogenic differentiation. Inflammation-induced IMCL may be directly responsible for HO formation in the muscle (72).
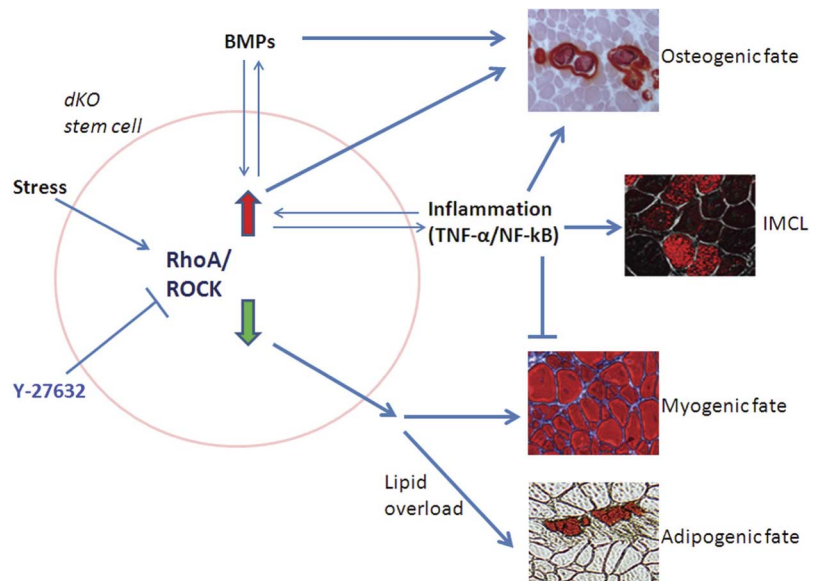
differentiate into osteogenic, chrondrogenic, adipogenic, and myogenic lineages with appropriate induction stimuli (66). In the current study, we observed that the osteogenic potential of muscle stem cells appeared to be promoted, while adipogenic and myogenic potentials appeared to be repressed in the severely dystrophic muscle of dKO mice, a process likely mediated, at least in part, by RhoA activation. RhoA activation was shown to occur in response to stresses, including mechanical stress and oxidative stress (67, 68), suggesting that RhoA activation in the dystrophic muscle of dKO mice could be related to the multiple stresses to which the skeletal muscle of dKO mice is exposed. Compared to *mdx* mice, stresses in the dystrophic muscle of dKO mice may include more myofiber damage and abnormal neuromuscular junctions created by the absence of utrophin; stronger production of profibrotic factors, such as TGF-β1; and severe inflammation caused by extensive muscle degeneration and an abnormally high fat-to-skeletal muscle ratio.

Inactivation of RhoA signaling could be beneficial for improving the severe myopathological phenotype present in dKO mice. Interestingly, RhoA signaling was found to be increased in the spinal cord of an intermediate spinal muscular atrophy (SMA) mouse model, and the inactivation of RhoA signaling with Y-27632 improved the survival of these SMA mice (69). Our results showed that RhoA inactivation in dKO mice led to a less severe dystrophic muscle phenotype that more closely resembled the phenotype observed in *mdx* mice. RhoA signaling has been found to interact with inflammatory signaling and acts as a proinflammatory factor (46, 70). In our current study, we found the level of inflammation to be higher in dKO mice compared to *mdx* mice. By inactivating RhoA with Y-27632, we observed that TNF-α and IL-6 were down-regulated, while Klotho and PPAR-γ were up-regulated in both dKO muscle stem cells and skeletal muscle tissues, indicating a repression of inflammation (59). Therefore, we suggest that the improved muscle phenotype of dKO mice with RhoA inactivation is at least partially due to a reduction in inflammation. Moreover, the up-regulation of PPARγ expression *via* RhoA inactivation could also improve the metabolism of fatty acids in dystrophic muscle since PPARγ was previously reported to increase free fatty acid (FFA) disposal in skeletal muscle through oxidation augmentation, resulting in the reduction of IMCL (71). PPARγ activation in muscle has also been reported to prevent IMCL normally observed in both fat-fed wild-type mice, as well as in the muscles of obese diabetic patients (61, 62). Thus, the up-regulation of PPARγ *via* RhoA inactivation in dKO muscle improved fat metabolism by promoting the uptake of lipids by fat cells and not by muscle cells. Since obesity, inflammation, and IMCL have also been commonly observed in human DMD, we suggest that DMD should also be investigated for the prevention of IMCL by reducing obesity, inflammation, and metabolic abnormalities.

Previous researchers have demonstrated that intramyocardial lipid accumulation is potentially involved with cardiac dysfunction in the dystrophic heart. Cardiac failure is the leading cause for early death of patients wtih DMD (63), and it has been reported that intramyocardial lipid accumulation occurs in the damaged areas of cardiac muscle in patients wtih DMD (11); however, research is sparse regarding the mechanisms and prevention of intramyocardial lipid accumulation. Compared with *mdx* mice, the dKO mouse model exhibits a more severe abnormal cardiac phenotype (*i.e.*, fibrosis formation) and is considered to be an important model for studying DMD-associated cardiomyopathy (14, 19, 20). Our results showed that, when comparing the cardiac muscles of WT, *mdx*, and dKO mice, the severity of intramyocardial lipid accumulation appeared to be closely related to progressive cardiac muscle degeneration. More importantly, our results indicate that intramyocardial lipid accumulation can be reduced by inactivating RhoA, an effect potentially associated with repressed systematic inflammation.

In summary, our results indicated that RhoA signaling could play a major role in regulating the processes of HO, FI, IMCL, and muscle regeneration in the dystrophic skeletal muscle of mice, and consequently, RhoA inactivation may represent a therapeutic target to improve the muscle histopathology associated with DMD. Moreover, RhoA signaling may also serve as a potential target for repressing the development of HO in cases of trauma, neurological injury, and genetic abnormalities. The status of RhoA activation in human patients wtih DMD and the potential effect of RhoA inactivation are, therefore, very promising but require further investigation. FJ

REFERENCES

1. Cipriano, C. A., Pill, S. G., and Keenan, M. A. (2009) Heterotopic ossification following traumatic brain injury and spinal cord injury. *J. Am. Acad. Orthop. Surg.* **17,** 689–697
2. Marcus, R. L., Addison, O., Kidde, J. P., Dibble, L. E., and Lastayo, P. C. (2010) Skeletal muscle fat infiltration: impact of age, inactivity, and exercise. *J. Nutr. Health Aging* **14,** 362–366
3. Miljkovic-Gacic, I., Wang, X., Kammerer, C. M., Gordon, C. L., Bunker, C. H., Kuller, L. H., Patrick, A. L., Wheeler, V. W., Evans, R. W., and Zmuda, J. M. (2008) Fat infiltration in muscle: new evidence for familial clustering and associations with diabetes. *Obesity* **16,** 1854–1860
4. Savage, D. B., Petersen, K. F., and Shulman, G. I. (2007) Disordered lipid metabolism and the pathogenesis of insulin resistance. *Physiol. Rev.* **87,** 507–520
5. Hulver, M. W., and Dohm, G. L. (2004) The molecular mechanism linking muscle fat accumulation to insulin resistance. *Proc. Nutr. Soc.* **63,** 375–380
6. Schulze, P. C. (2009) Myocardial lipid accumulation and lipotoxicity in heart failure. *J. Lipid Res.* **50,** 2137–2138
7. Axelsen, L. N., Lademann, J. B., Petersen, J. S., Holstein-Rathlou, N. H., Ploug, T., Prats, C., Pedersen, H. D., and Kjolbye, A. L. (2010) Cardiac and metabolic changes in long-term high fructose-fat fed rats with severe obesity and extensive

intramyocardial lipid accumulation. *Am. J. Physiol. Regul. Integr. Comp. Physiol.* **298,** R1560–R1570

8. Ruberg, F. L. (2007) Myocardial lipid accumulation in the diabetic heart. *Circulation* **116,** 1110–1112

9. Sharma, S., Adrogue, J. V., Golfman, L., Uray, I., Lemm, J., Youker, K., Noon, G. P., Frazier, O. H., and Taegtmeyer, H. (2004) Intramyocardial lipid accumulation in the failing human heart resembles the lipotoxic rat heart. *FASEB J.* **18,** 1692–1700

10. Momose, M., Iguchi, N., Imamura, K., Usui, H., Ueda, T., Miyamoto, K., and Inaba, S. (2001) Depressed myocardial fatty acid metabolism in patients with muscular dystrophy. *Neuromusc. Disord.* **11,** 464–469

11. Saini-Chohan, H. K., Mitchell, R. W., Vaz, F. M., Zelinski, T., and Hatch, G. M. (2012) Delineating the role of alterations in lipid metabolism to the pathogenesis of inherited skeletal and cardiac muscle disorders: Thematic Review Series: Genetics of Human Lipid Diseases. *J. Lipid Res.* **53,** 4–27

12. Ionasescu, V., Monaco, L., Sandra, A., Ionasescu, R., Burmeister, L., Deprosse, C., and Stern, L. Z. (1981) Alterations in lipid incorporation in Duchenne muscular dystrophy. Studies of fresh and cultured muscle. *J. Neurol. Sci.* **50,** 249–251

13. Tahallah, N., Brunelle, A., De La Porte, S., and Laprevote, O. (2008) Lipid mapping in human dystrophic muscle by cluster-time-of-flight secondary ion mass spectrometry imaging. *J. Lipid Res.* **49,** 438–454

14. Duan, D. (2006) Challenges and opportunities in dystrophin-deficient cardiomyopathy gene therapy. *Hum. Mol. Genet.* **15**(Spec. 2), R253–R261

15. Kikkawa, N., Ohno, T., Nagata, Y., Shiozuka, M., Kogure, T., and Matsuda, R. (2009) Ectopic calcification is caused by elevated levels of serum inorganic phosphate in *mdx* mice. *Cell Struct. Funct.* **34,** 77–88

16. Nguyen, F., Cherel, Y., Guigand, L., Goubault-Leroux, I., and Wyers, M. (2002) Muscle lesions associated with dystrophin deficiency in neonatal golden retriever puppies. *J. Comp. Pathol.* **126,** 100–108

17. Starkey, J. D., Yamamoto, M., Yamamoto, S., and Goldhamer, D. J. (2011) Skeletal muscle satellite cells are committed to myogenesis and do not spontaneously adopt nonmyogenic fates. *J. Histochem. Cytochem.* **59,** 33–46

18. Sicinski, P., Geng, Y., Ryder-Cook, A. S., Barnard, E. A., Darlison, M. G., and Barnard, P. J. (1989) The molecular basis of muscular dystrophy in the *mdx* mouse: a point mutation. *Science* **244,** 1578–1580

19. Grady, R. M., Teng, H., Nichol, M. C., Cunningham, J. C., Wilkinson, R. S., and Sanes, J. R. (1997) Skeletal and cardiac myopathies in mice lacking utrophin and dystrophin: a model for Duchenne muscular dystrophy. *Cell* **90,** 729–738

20. Deconinck, A. E., Rafael, J. A., Skinner, J. A., Brown, S. C., Potter, A. C., Metzinger, L., Watt, D. J., Dickson, J. G., Tinsley, J. M., and Davies, K. E. (1997) Utrophin-dystrophin-deficient mice as a model for Duchenne muscular dystrophy. *Cell* **90,** 717–727

21. Isaac, C., Wright, A., Usas, A., Li, H., Tang, Y., Mu, X., Greco, N., Dong, Q., Vo, N., Kang, J., Wang, B., and Huard, J. (2013) Dystrophin and utrophin "double knockout" dystrophic mice exhibit a spectrum of degenerative musculoskeletal abnormalities. *J. Orthop. Res.* **31,** 343–349

22. Muntoni, F., Fisher, I., Morgan, J. E., and Abraham, D. (2002) Steroids in Duchenne muscular dystrophy: from clinical trials to genomic research. *Neuromusc. Disord.* **12**(Suppl. 1), S162–S165

23. Mavrogenis, A. F., Soucacos, P. N., and Papagelopoulos, P. J. (2011) Heterotopic ossification revisited. *Orthopedics* **34,** 177

24. Neal, B., Rodgers, A., Dunn, L., and Fransen, M. (2000) Non-steroidal anti-inflammatory drugs for preventing heterotopic bone formation after hip arthroplasty. *Cochrane Database Syst. Rev.*, CD001160

25. Dahners, L. E., and Mullis, B. H. (2004) Effects of nonsteroidal anti-inflammatory drugs on bone formation and soft-tissue healing. *J. Am. Acad. Orthop. Surg.* **12,** 139–143

26. Vasileiadis, G. I., Sioutis, I. C., Mavrogenis, A. F., Vlasis, K., Babis, G. C., and Papagelopoulos, P. J. (2011) COX-2 inhibitors for the prevention of heterotopic ossification after THA. *Orthopedics* **34,** 467

27. Banovac, K., Williams, J. M., Patrick, L. D., and Levi, A. (2004) Prevention of heterotopic ossification after spinal cord injury with COX-2 selective inhibitor (rofecoxib). *Spinal Cord* **42,** 707–710

28. Joe, A. W., Yi, L., Natarajan, A., Le Grand, F., So, L., Wang, J., Rudnicki, M. A., and Rossi, F. M. (2010) Muscle injury activates resident fibro/adipogenic progenitors that facilitate myogenesis. *Nat. Cell Biol.* **12,** 153–163

29. Cox, F. M., Reijnierse, M., van Rijswijk, C. S., Wintzen, A. R., Verschuuren, J. J., and Badrising, U. A. (2011) Magnetic resonance imaging of skeletal muscles in sporadic inclusion body myositis. *Rheumatology* **50,** 1153–1161

30. Mei, M., Zhao, L., Li, Q., Chen, Y., Huang, A., Varghese, Z., Moorhead, J. F., Zhang, S., Powis, S. H., and Ruan, X. Z. (2011) Inflammatory stress exacerbates ectopic lipid deposition in C57BL/6J mice. *Lipids Health Dis.* **10,** 110

31. Hotamisligil, G. S., Shargill, N. S., and Spiegelman, B. M. (1993) Adipose expression of tumor necrosis factor-alpha: direct role in obesity-linked insulin resistance. *Science* **259,** 87–91

32. Messina, S., Altavilla, D., Aguennouz, M., Seminara, P., Minutoli, L., Monici, M. C., Bitto, A., Mazzeo, A., Marini, H., Squadrito, F., and Vita, G. (2006) Lipid peroxidation inhibition blunts nuclear factor-kappaB activation, reduces skeletal muscle degeneration, and enhances muscle function in *mdx* mice. *Am. J. Pathol.* **168,** 918–926

33. Langen, R. C., Schols, A. M., Kelders, M. C., Wouters, E. F., and Janssen-Heininger, Y. M. (2001) Inflammatory cytokines inhibit myogenic differentiation through activation of nuclear factor-κB. *FASEB J.* **15,** 1169–1180

34. Lu, A., Proto, J. D., Guo, L., Tang, Y., Lavasani, M., Tilstra, J. S., Niedernhofer, L. J., Wang, B., Guttridge, D. C., Robbins, P. D., and Huard, J. (2012) NF-κB negatively impacts the myogenic potential of muscle-derived stem cells. *Mol. Ther.* **20,** 661–668

35. Monici, M. C., Aguennouz, M., Mazzeo, A., Messina, C., and Vita, G. (2003) Activation of nuclear factor-κB in inflammatory myopathies and Duchenne muscular dystrophy. *Neurology* **60,** 993–997

36. Ridley, A. J. (2001) Rho GTPases and cell migration. *J. Cell Sci.* **114,** 2713–2722

37. McBeath, R., Pirone, D. M., Nelson, C. M., Bhadriraju, K., and Chen, C. S. (2004) Cell shape, cytoskeletal tension, and RhoA regulate stem cell lineage commitment. *Dev. Cell* **6,** 483–495

38. Khatiwala, C. B., Kim, P. D., Peyton, S. R., and Putnam, A. J. (2009) ECM compliance regulates osteogenesis by influencing MAPK signaling downstream of RhoA and ROCK. *J. Bone. Miner. Res.* **24,** 886–898

39. Meyers, V. E., Zayzafoon, M., Douglas, J. T., and McDonald, J. M. (2005) RhoA and cytoskeletal disruption mediate reduced osteoblastogenesis and enhanced adipogenesis of human mesenchymal stem cells in modeled microgravity. *J. Bone Miner. Res.* **20,** 1858–1866

40. Wang, Y. K., Yu, X., Cohen, D. M., Wozniak, M. A., Yang, M. T., Gao, L., Eyckmans, J., and Chen, C. S. (2012) Bone morphogenetic protein-2-induced signaling and osteogenesis is regulated by cell shape, RhoA/ROCK, and cytoskeletal tension. *Stem Cells Dev.* **21,** 1176–1186

41. Fromigue, O., Hay, E., Modrowski, D., Bouvet, S., Jacquel, A., Auberger, P., and Marie, P. J. (2006) RhoA GTPase inactivation by statins induces osteosarcoma cell apoptosis by inhibiting p42/p44-MAPKs-Bcl-2 signaling independently of BMP-2 and cell differentiation. *Cell Death Differ.* **13,** 1845–1856

42. Hosoyama, T., Ishiguro, N., Yamanouchi, K., and Nishihara, M. (2009) Degenerative muscle fiber accelerates adipogenesis of intramuscular cells via RhoA signaling pathway. *Differentiation* **77,** 350–359

43. Santos, A., Bakker, A. D., de Blieck-Hogervorst, J. M., and Klein-Nulend, J. (2010) WNT5A induces osteogenic differentiation of human adipose stem cells via rho-associated kinase ROCK. *Cytotherapy* **12,** 924–932

44. Goto, K., Chiba, Y., Sakai, H., and Misawa, M. (2009) Tumor necrosis factor-alpha (TNF-alpha) induces upregulation of RhoA via NF-κB activation in cultured human bronchial smooth muscle cells. *J. Pharmacol. Sci.* **110,** 437–444

45. Slice, L. W., Bui, L., Mak, C., and Walsh, J. H. (2000) Differential regulation of COX-2 transcription by Ras- and Rho-family of GTPases. *Biochem. Biophys. Res. Commun.* **276,** 406–410

46. Nakayama, Y., Komuro, R., Yamamoto, A., Miyata, Y., Tanaka, M., Matsuda, M., Fukuhara, A., and Shimomura, I. (2009) RhoA

induces expression of inflammatory cytokine in adipocytes. *Biochem. Biophys. Res. Commun.* **379,** 288–292

47. Zhou, Y., Huang, X., Hecker, L., Kurundkar, D., Kurundkar, A., Liu, H., Jin, T. H., Desai, L., Bernard, K., and Thannickal, V. J. (2013) Inhibition of mechanosensitive signaling in myofibroblasts ameliorates experimental pulmonary fibrosis. *J. Clin. Invest.* **123,** 1096–1108

48. Zhou, H., Li, Y. J., Wang, M., Zhang, L. H., Guo, B. Y., Zhao, Z. S., Meng, F. L., Deng, Y. G., and Wang, R. Y. (2011) Involvement of RhoA/ROCK in myocardial fibrosis in a rat model of type 2 diabetes. *Acta Pharmacol. Sin.* **32,** 999–1008

49. Charrasse, S., Comunale, F., Grumbach, Y., Poulat, F., Blangy, A., and Gauthier-Rouviere, C. (2006) RhoA GTPase regulates M-cadherin activity and myoblast fusion. *Mol. Biol. Cell* **17,** 749–759

50. Castellani, L., Salvati, E., Alema, S., and Falcone, G. (2006) Fine regulation of RhoA and Rock is required for skeletal muscle differentiation. *J. Biol. Chem.* **281,** 15249–15257

51. Beqaj, S., Jakkaraju, S., Mattingly, R. R., Pan, D., and Schuger, L. (2002) High RhoA activity maintains the undifferentiated mesenchymal cell phenotype, whereas RhoA down-regulation by laminin-2 induces smooth muscle myogenesis. *J. Cell Biol.* **156,** 893–903

52. Gharaibeh, B., Lu, A., Tebbets, J., Zheng, B., Feduska, J., Crisan, M., Peault, B., Cummins, J., and Huard, J. (2008) Isolation of a slowly adhering cell fraction containing stem cells from murine skeletal muscle by the preplate technique. *Nat. Protoc.* **3,** 1501–1509

53. Thibaud, J. L., Monnet, A., Bertoldi, D., Barthelemy, I., Blot, S., and Carlier, P. G. (2007) Characterization of dystrophic muscle in golden retriever muscular dystrophy dogs by nuclear magnetic resonance imaging. *Neuromusc. Disord.* **17,** 575–584

54. Valentine, B. A., Cooper, B. J., Cummings, J. F., and de Lahunta, A. (1990) Canine X-linked muscular dystrophy: morphologic lesions. *J. Neurol. Sci.* **97,** 1–23

55. Greenberg, A. S., Coleman, R. A., Kraemer, F. B., McManaman, J. L., Obin, M. S., Puri, V., Yan, Q. W., Miyoshi, H., and Mashek, D. G. (2011) The role of lipid droplets in metabolic disease in rodents and humans. *J. Clin. Invest.* **121,** 2102–2110

56. Lounev, V. Y., Ramachandran, R., Wosczyna, M. N., Yamamoto, M., Maidment, A. D., Shore, E. M., Glaser, D. L., Goldhamer, D. J., and Kaplan, F. S. (2009) Identification of progenitor cells that contribute to heterotopic skeletogenesis. *J. Bone Joint Surg. Am.* **91,** 652–663

57. Arking, D. E., Krebsova, A., Macek, M., Sr., Macek, M., Jr., Arking, A., Mian, I. S., Fried, L., Hamosh, A., Dey, S., McIntosh, I., and Dietz, H. C. (2002) Association of human aging with a functional variant of klotho. *Proc. Natl. Acad. Sci. U. S. A.* **99,** 856–861

58. Salisbury, E., Rodenberg, E., Sonnet, C., Hipp, J., Gannon, F. H., Vadakkan, T. J., Dickinson, M. E., Olmsted-Davis, E. A., and Davis, A. R. (2011) Sensory nerve induced inflammation contributes to heterotopic ossification. *J. Cell. Biochem.* **112,** 2748–2758

59. Straus, D. S., and Glass, C. K. (2007) Anti-inflammatory actions of PPAR ligands: new insights on cellular and molecular mechanisms. *Trends Immunol.* **28,** 551–558

60. Holness, C. L., and Simmons, D. L. (1993) Molecular cloning of CD68, a human macrophage marker related to lysosomal glycoproteins. *Blood* **81,** 1607–1613

61. Amin, R. H., Mathews, S. T., Camp, H. S., Ding, L., and Leff, T. (2010) Selective activation of PPARgamma in skeletal muscle induces endogenous production of adiponectin and protects mice from diet-induced insulin resistance. *Am. J. Physiol. Endocrinol. Metab.* **298,** E28–E37

62. Ye, J. M., Doyle, P. J., Iglesias, M. A., Watson, D. G., Cooney, G. J., and Kraegen, E. W. (2001) Peroxisome proliferator-activated receptor (PPAR)-α activation lowers muscle lipids and improves insulin sensitivity in high fat-fed rats: comparison with PPAR-γ activation. *Diabetes* **50,** 411–417

63. Finsterer, J., and Stollberger, C. (2003) The heart in human dystrophinopathies. *Cardiology* **99,** 1–19

64. Lehman, J. J., and Kelly, D. P. (2002) Transcriptional activation of energy metabolic switches in the developing and hypertrophied heart. *Clin. Exp. Pharmacol. Physiol.* **29,** 339–345

65. Ahmad, N., Bygrave, M., De Zordo, T., Fenster, A., and Lee, T. Y. (2010) Detecting degenerative changes in myotonic murine models of Duchenne muscular dystrophy using high-frequency ultrasound. *J. Ultrasound. Med.* **29,** 367–375

66. Qu-Petersen, Z., Deasy, B., Jankowski, R., Ikezawa, M., Cummins, J., Pruchnic, R., Mytinger, J., Cao, B., Gates, C., Wernig, A., and Huard, J. (2002) Identification of a novel population of muscle stem cells in mice: potential for muscle regeneration. *J. Cell Biol.* **157,** 851–864

67. Smith, P. G., Roy, C., Zhang, Y. N., and Chauduri, S. (2003) Mechanical stress increases RhoA activation in airway smooth muscle cells. *Am. J. Respir. Cell Mol. Biol.* **28,** 436–442

68. Aghajanian, A., Wittchen, E. S., Campbell, S. L., and Burridge, K. (2009) Direct activation of RhoA by reactive oxygen species requires a redox-sensitive motif. *PLoS One* **4,** e8045

69. Bowerman, M., Beauvais, A., Anderson, C. L., and Kothary, R. (2010) Rho-kinase inactivation prolongs survival of an intermediate SMA mouse model. *Hum. Mol. Genet.* **19,** 1468–1478

70. Segain, J. P., Raingeard de la Bletiere, D., Sauzeau, V., Bourreille, A., Hilaret, G., Cario-Toumaniantz, C., Pacaud, P., Galmiche, J. P., and Loirand, G. (2003) Rho kinase blockade prevents inflammation via nuclear factor κB inhibition: evidence in Crohn's disease and experimental colitis. *Gastroenterology* **124,** 1180–1187

71. Ciaraldi, T. P., Cha, B. S., Park, K. S., Carter, L., Mudaliar, S. R., and Henry, R. R. (2002) Free fatty acid metabolism in human skeletal muscle is regulated by PPARγ and RXR agonists. *Ann. N. Y. Acad. Sci.* **967,** 66–70

72. Demer, L. L. (2002) Vascular calcification and osteoporosis: inflammatory responses to oxidized lipids. *Int. J. Epidemiol.* **31,** 737–741

AUTHOR QUERIES

AUTHOR PLEASE ANSWER ALL QUERIES 1

AQ1— Please ensure that italics are applied correctly and consistently to distinguish genes from proteins, etc., per CBE style, throughout the text.

AQ2— Fig. 2E: Arrows explained correctly? Please confirm or revise edits.